

DOCTORAL THESIS

A low-cost remote sensing system for agricultural applications

Shuib Rambat

If you have discovered material in AURA which is unlawful e.g. breaches copyright, (either yours or that of a third party) or any other law, including but not limited to those relating to patent, trademark, confidentiality, data protection, obscenity, defamation, libel, then please read our takedown policy at <http://www1.aston.ac.uk/research/aura/aura-take-down-policy/> and contact the service immediately eprints@aston.ac.uk.

**A LOW-COST REMOTE SENSING SYSTEM FOR
AGRICULTURAL APPLICATIONS**

SHUIB RAMBAT

Doctor of Philosophy



Aston University

September 2011

This copy of the thesis has been supplied on condition that anyone who consults it is understood to recognise that its copyright rests with its author and that no quotation from the thesis and no information derived from it may be published without proper acknowledgment.

Aston University

A LOW-COST REMOTE SENSING SYSTEM FOR AGRICULTURAL APPLICATIONS

Shuib Rambat

Doctor of Philosophy, 2011

ABSTRACT

This research develops a low cost remote sensing system for use in agricultural applications. The important features of the system are that it monitors the near infrared and it incorporates position and attitude measuring equipment allowing for geo-rectified images to be produced without the use of ground control points. The equipment is designed to be hand held and hence requires no structural modification to the aircraft. The portable remote sensing system consists of an inertia measurement unit (IMU), which is accelerometer based, a low-cost GPS device and a small format false colour composite digital camera. The total cost of producing such a system is below GBP 3000, which is far cheaper than equivalent existing systems. The design of the portable remote sensing device has eliminated bore sight misalignment errors from the direct geo-referencing process. A new processing technique has been introduced for the data obtained from these low-cost devices, and it is found that using this technique the image can be matched (overlaid) onto Ordnance Survey Master Maps at an accuracy compatible with precision agriculture requirements. The direct geo-referencing has also been improved by introducing an algorithm capable of correcting oblique images directly. This algorithm alters the pixels value, hence it is advised that image analysis is performed before image geo-rectification. The drawback of this research is that the low-cost GPS device experienced bad checksum errors, which resulted in missing data. The Wide Area Augmented System (WAAS) correction could not be employed because the satellites could not be locked onto whilst flying. The best GPS data were obtained from the Garmin eTrex (15 m kinematic and 2 m static) instruments which have a high-sensitivity receiver with good lock on capability. The limitation of this GPS device is the inability to effectively receive the P-Code wavelength, which is needed to gain the best accuracy when undertaking differential GPS processing. Pairing the carrier phase L1 with the pseudorange C/A-Code received, in order to determine the image coordinates by the differential technique, is still under investigation. To improve the position accuracy, it is recommended that a GPS base station should be established near the survey area, instead of using a permanent GPS base station established by the Ordnance Survey.

Keywords: Low-Cost remote sensing, Precision Agriculture, Geometric Correction and Transformation.

Acknowledgements

It would not have been possible to write this doctoral thesis without the help and support of a number of incredibly special people around me, to only some of whom it is possible to give particular mention here.

Above all, I would like to thank my wife Marthiah Hassan for her personal support and great patience since the first day we arrived in United Kingdom. My children, parents, brother and sister have given me their unequivocal support throughout these turbulent times.

This thesis would not have been possible without the help, support and patience of my supervisor, Dr. John Elgy, whose encouragement, guidance and support from the initial to the final level enabled me to develop an understanding of the low cost remote sensing system.

I would like to acknowledge the financial, academic and technical support of the Government of Malaysia and University Technology of Malaysia and its staff, particularly in the award of the Academic Scholarships that provided the necessary financial support.

I am most grateful to Dr. Mike Pooley and Dr. Tom Chilled (Skyfarm) for providing the agriculture digital camera and inertial measurement unit, which have been valuable and reliable instruments for my project.

Last, but by no means least, I would like to offer my sincere gratitude to my colleagues at Aston University who have provided moral and technical support throughout the course of this research unwavering love and support, namely Dave Hall, Bill, Rob Poole, Andy Crowcombe, Faiz Parker and also Bryan Gulliver (an aerial photographer), who have assisted in many capacities throughout my research project.

List of Contents

List of Figures	7
List of Tables.....	10
List of Acronyms	11
List of Nomenclature.....	12
1. INTRODUCTION	13
1.1 Research Motivation	13
1.3 Limitations of the Research	17
1.4 Research Design.....	17
1.5 Thesis Structure.....	18
2. LOW-COST AIRBORNE REMOTE SENSING SYSTEM AND GEOMETRIC CORRECTION	21
2.1 Background of Low-cost Airborne Remote Sensing	21
2.2 Low-Cost Airborne Remote Sensing Instruments	23
2.2.1 Low-Cost Imaging Device	27
2.2.2 Ancillary Instruments.....	37
2.2.2.1 Inertial Measurement Unit	39
2.2.2.2 Global Navigation Satellite System	40
2.3 Geometry Correction Review	44
2.4 Sources of Geometric Distortion.....	50
2.5 Summary	52
3. PROPOSED DESIGN OF LOW-COST AIRBORNE REMOTE SENSING SYSTEM	53
3.1 Literature Findings	53
3.2 Design Objective.....	54
3.3 Design Layout	55
3.4 Selection of the Devices.....	56
3.4.1 Low-cost Inertial Measurement Unit	57
3.4.2 Low-cost GPS	62
3.4.3 Low-cost Imaging Sensor	65
3.4.3.1 Generating Colour Composite Image by using Single Shot Imaging Device	66
3.5 Justification of Selected Devices	69
3.6 Expected Data Type	74
3.7 Expected Errors of Selected Devices	76
3.7.1 Low-cost IMU Error	77
3.7.2 Low-cost GPS Error.....	78
3.7.3 Low-cost Imaging Sensor Error	79
3.7.4 Data Synchronisation Errors	80
3.8 Error Optimisation	80
3.9 Summary	81

4.	DIRECT GEO-REFERENCING	82
4.1	Introduction	82
4.2	Concept of Direct Geo-referencing	82
4.3	Preparation of Data	85
4.3.1	Pre-processing	85
4.3.2	Filter	87
4.3.3	Differential GPS	90
4.4	Approximation Process for Missing Coordinate	91
4.4.1	Extraction of Navigation and Image Ancillary Data	93
4.4.2	Reconstruction of Image Geometry	95
4.4.3	Radial Distortion	96
4.5	Image Orientation	98
4.6	Map Pixels into User Coordinate System	104
4.7	Summary	111
5.	DEVELOPMENT OF SOFTWARE	112
5.1	Introduction	112
5.2	Software Structure	112
5.3	Programming Script	113
5.3.1	Image Input	113
5.3.2	Intrinsic Parameters	113
5.3.3	Extrinsic Parameters	114
5.3.4	Image Processing	114
5.3.5	Image Resample	115
5.3.6	Interface	115
5.4	Summary	116
6.	EXPERIMENTAL INVESTIGATION	117
6.1	Introduction	117
6.2	Performance Test	117
6.2.1	IMU Performance Test	118
6.2.1.1	IMU Performance Test Results	118
6.2.2	GPS Performance Test	120
6.2.2.1	GPS Performance Test Results	120
6.2.3	Imaging Sensors Performance Test	121
6.2.3.1	Imaging Sensors Performance Test Results	121
6.3	Simulation Test	122
6.3.1	Laboratory Test	122
6.3.1.1	Laboratory Test Results	130
6.3.2	On-the-road Test Drive	137
6.3.2.1	On-the-road Test Drive Results	138
6.4	Results Discussions	139
6.5	Summary	141
7.	SYSTEM VALIDATION: A FLIGHT TEST	143
7.1	Introduction	143
7.2	Data Acquisition	143
7.2.1	Test Site	145
7.2.2	Flight Missions	147
7.2.3	Remotely Sensed Data	148
7.2.4	Ancillary Data	151

7.2.5	Software	151
7.3	Installation of Test Equipment	152
7.4	Flight Test Results	155
7.5	Summary	157
8.	RESULTS AND ACCURACY ASSESSMENT DISCUSSIONS.....	161
8.1	Introduction	161
8.2	Results	161
8.2.1	Imaging Results.....	162
8.2.2	Navigation Results	164
8.2.3	Directly Geo-referencing Result	172
8.3	Accuracy Assessment Test.....	174
8.4	Summary	184
9.	CONCLUSIONS AND RECOMMENDATIONS	186
9.1	Review of Research Study	186
9.2	Conclusions	188
9.3	Recommendations	190
	References:	193
	Appendix A: List of Available Sensors	215
	Appendix B: Chronological History of Aerial Photography and Remote Sensing..	219
	Appendix C: Image Captured	235
	Appendix D: IMU Data (Process Data)	240
	Appendix E: GPS DATA	245
	Appendix F: Corrected Images	249
	Appendix G: Microsoft Visual Studio (Visual Basic) Programming Scripts Listing	252

List of Figures

Figure 2.1: The process of gathering information using airborne remote sensing.....	22
Figure 2.2: Layout for instrument installation.	23
Figure 2.3: First unmanned vehicle for airborne remote sensing.	26
Figure 2.4: Electromagnetic spectrum a) Electromagnetic spectrum range from radio to gamma rays while b) electromagnetic spectrum used in remote sensing applications and their imaging systems; c) show the visible (Blue, Green, Red) and Infrared electromagnetic spectrum used for NDVI and SAVI calculation.	28
Figure 2.5: The ADPS based on Kodak DCS 460CIR digital frame camera which is produced by Geotechnologies of Bath Spa University.	31
Figure 2.6 : The Multispectral Digital Camera produced by Tetracam.	32
Figure 2.7: The Airborne Multispectral Scanner produced by SensyTech.....	33
Figure 2.8: (a) GPS components and (b) the location of GPS monitoring stations. ..	42
Figure 2.9: Definition of body coordinate system of Euler angles ϕ , θ , ψ	45
Figure 2.10: Definition of image coordinate system of Euler angles ω , ϕ , κ	47
Figure 2.11: Definition of misalignment in IMU and GPS integration.	51
Figure 3.1: Layout of cabin crew positions for replacing fixed installation	56
Figure 3.2: Electromechanical ('A') and Micro Controller ('B') assembled together on interface board.....	58
Figure 3.3: Mechanisation of micro-machined IMU accelerometer.....	59
Figure 3.4: Relationship between force, mass and acceleration.	61
Figure 3.5: Coriolis accelerometer concept	62
Figure 3.6: ADC compartment.....	66
Figure 3.7 : Device that been embedded into single sensor imaging for generating colour composite images. (a) the rotating filter wheel and (b) the beam splitter with colour separated prism.	67
Figure 3.8 : The architecture of single shot imaging device.....	68
Figure 3.9 : The Bayer mosaic filter	68
Figure 3.10: Typical errors in low-cost IMU	78
Figure 4.1: Flowchart depicting the geo-referencing process.....	84
Figure 4.2: Flowchart of the preparation process.....	86
Figure 4.3: Flowchart of the filter working procedure.....	88
Figure 4.4: Spread sheet showing the process of filtering	88
Figure 4.5: Difference between filtering method.....	89
Figure 4.6: Approximation process.....	91
Figure 4.7: Extraction of navigation data.....	94
Figure 4.8: Extraction of ancillary data from imagery.....	95
Figure 4.9: Camera projection, inset taken from portable device showing platform axes in flight direction.....	96
Figure 4.10: Example of automatic calibration.....	97
Figure 4.11: Geometry obtained from camera projection. (a) geometry of camera, (b) plane of tilting image and horizontal-image plane and (c) conversion from tilt image plane to horizontal-image plane.	100

Figure 4.12: (a) Projected image using simple rotation matrix as equations (4.5), (4.6); b) Projected image using projectivity condition, different angle of roll and pitch taken into account, as equations (4.10), (4.11).	101
Figure 4.13: Geometry of oblique image.	102
Figure 4.14: Establishment of trigonometric triangulation.	103
Figure 4.15: Relationship between image coordinate system and the local coordinate system.	105
Figure 4.16: Coordinates for the four corners of the image that refers to local coordinate system.	107
Figure 4.17: Mapping pixels into local coordinate system. (a) red box is image area plot, blue box area shifted after rotating image in roll and pitch directions. (b) Rotated image in yaw direction (blue), coordinates in black used to create world file format to geo-reference image into user coordinate system.	108
Figure 4.18: Image rotated in roll, pitch, then yaw direction. Later, coordinates of four corners computed. Coordinates in black used to create world file format to geo-reference image into user coordinate system.	109
Figure 5.1: Keyboard entry form for extrinsic parameter	114
Figure 5.2: Selecting image processing task.	114
Figure 5.3: User interface.	115
Figure 6.1: Observed angles (Roll, Pitch and Yaw) during performance test.	119
Figure 6.2: Blurring and unfocused imagery caused by untallied movement between platform speed (aircraft) and imaging shutter.	122
Figure 6.3: The simulation rig and bracket with dummy camera	123
Figure 6.4: Position of control points (a) image of control points captured by sensor, (b) actual control points after digitise and c) digitising equipment.	124
Figure 6.5: Sample of accuracy determination on the laboratory test product.	125
Figure 6.6: Calibration process for determining the intrinsic parameters. (a) Images used in the calibration process and (b) their view angle in 3D.	129
Figure 6.7: Single image technique for determining the intrinsic parameters. Top left is the image, bottom left is the photo browse and on the right is the product after processing.	130
Figure 6.8: Pincushion distortion in image taken from laboratory test.	131
Figure 6.9: Laboratory test results.	134
Figure 6.10: GPS and IMU devices for test drive	137
Figure 6.11: Trajectory plot of test drive	138
Figure 7. 1: Sites assigned for flight tests.	146
Figure 7. 2: Aircraft used for flight test	153
Figure 7.3: Preparation of devices ready for system validation test drive.	154
Figure 7.4: Graphs showing behaviour of GPS data obtained from wireless and Garmin76 GPS, with camera shot position.	156
Figure 7.5: Roll and pitch obtained from IMU device, yaw data extracted from GPS data	157
Figure 8.1: Image sample from the third test, (a) before, and (b) after pincushion correction.	163
Figure 8.2: Trajectory of flight test in Malling, East Kent on July 25, 2008.	166
Figure 8.3: (a) Part of GPS data processing report by Total Trimble Control Software (b) Part of Rinex ascii format.	167
Figure 8.4: Smoothing techniques to minimise random errors	170
Figure 8.5: IMU data determination problem	170

Figure 8.6: Image (a) shows for topographical reference lines, while image (b) shows topographical reference lines are only available in one half of the image.	175
Figure 8.7: Updating reference map process till assessing direct geo-referencing accuracy.....	177
Figure 8.8: Image showing poor georectification and possible errors in map content	181
Figure 8.9: Further example of large error.....	182
Figure 8.10: Well rectified image	183

List of Tables

Table 2.1:Major regions of electromagnetic spectrum.	29
Table 2.2: Previous studies on integration of IMU/GPS.....	38
Table 2.3: Performance difference between IMUs	39
Table 2.4: Frequencies and observation type.....	41
Table 2.5: Constellation Description for GPS	44
Table 2.6: Sources of Geometric Distortion.	52
Table 3.1: Estimated cost of proposed low-cost airborne remote sensing system.....	55
Table 3.2: Specification of ADC single shot CMOS imaging device.	70
Table 3.3: List of data protocols available for GPS	76
Table 3.4: Typical errors occurring during measurement process.....	77
Table 3.5: Summary of GPS Error Sources	79
Table 4.1: Lens distortion equation.....	97
Table 4.2: Sample of .TFW format	110
Table 6.1: Overall errors of rotation angle (roll, pitch and yaw).....	119
Table 6.2: Accuracy of Garmin76.....	120
Table 6.3: Sample of RMSE for the laboratory product.	126
Table 6.4: IMU data from simulation test.....	132
Table 6 5: Intrinsic parameters obtained from the calibration process	135
Table 6.6: Comparison of the rotation angles gather through extraction and IMU device.....	136
Table 6.7: Leap-frog test	139
Table 7. 1: Flight missions: Field data.....	148
Table 7.2: Optimal pixel sizes for applications.....	149
Table 7.3: Top high resolution camera with pixel size	150
Table 7.4: Specification of imaging sensor (Agricultural Digital Camera).....	150
Table 7.5: Final data obtained from imaging sensor, GPS and IMU devices.....	158
Table 8.1: Before and after image orientation using oblique algorithm.	171
Table 8.2 : List of images before and after direct geo-referencing.....	173
Table 8.3: Summary of images before and after direct geo-referencing.....	178

List of Acronyms

ADC	- agriculture digital camera
ARINC	- Airlines Electronic Engineering Committee 1982
ASCII	- American standard code for information interchange
Camera	- analogue camera
DGPS	- differential global positioning system
EGNOS	- European geostationary navigation overlay service
GLONASS	- global navigation system
GPS	- global positioning system
IMU	- inertial measurement unit
MEMs	- micro-electro mechanical system
NAVSTAR	- Navigation Signal Timing and Ranging Global Positioning System
UART	- universal asynchronous receiver/transmitter
WAAS	- wide area augmentation system
VNIR	- visible near infrared
CASI	- compact airborne spectrographic imager
CHRIS	- compact high resolution imaging spectrometer
LCRSS	- low-cost Remote Sensing System
RTCM SC104	- radio Commission for Maritime Services Special Committee 104

List of Nomenclature

C_b^n	connection matrix of the body coordinate system and navigation coordinate systems
R_z	rotation about z axis
R_y	rotation about y axis
R_x	rotation about x axis
ψ	angle in yaw between body frame and navigation frame
θ	angle in pitch between body frame and navigation frame
ϕ	angle in roll between body frame and navigation frame
r^n	transformation of navigation coordinate system
r^b	transformation of body coordinate system
C_n^b	connection matrix of body coordinate system and navigation coordinate system
C_E^B	connection matrix of body coordinate system and earth coordinate system
κ	angle in yaw between body frame and earth frame
ω	angle in roll between body frame and earth frame
φ	angle in pitch between body frame and earth frame
r^B	transformation of body coordinate system (aircraft)
r^E	transformation of earth coordinate system
T_b^B	transformation conversion between body coordinate system in IMU and body coordinate system
T_n^E	transformation conversion between earth coordinate system and navigation coordinate system
R_{BINS}^M	rotation matrix between body and mapping frame
R_{ENU}^{ECEF}	rotation matrix between earth centre fixed frame and earth north up
$R_{\omega\phi\kappa}$	rotation matrix of roll, pitch and yaw between body frame and earth frame
$r_{M,i}$	3D object coordinates in mapping frame
$r_{M,IMU}$	3D coordinates in mapping frame, provided by IMU/GPS
R_C^{BINS}	boresight matrix between IMU body and camera frame C
$r_{c,f}$	image coordinate of object in camera frame C
b_{BINS}	boresight offset vector
s	scale
t	time-dependent

1. INTRODUCTION

1.1 Research Motivation

The motivation for this research was triggered by the ambition to assist the Government of Malaysia in seeking an alternative way to manage agriculture. Improvement in the agriculture sector was the main topic in the 9th Malaysian Planning agenda., where the Government of Malaysia has allocated MYR 6.96 billion (Ministry of Agriculture Malaysia, 2006) to enhance the sector by introducing high-technology systems. This high technology includes remote sensing systems, geo-information systems, bio-diversity technology and fertilisers.

Remote sensing systems were selected for inclusion in order to provide the main spatial data stream in agricultural areas because of their capability for wide and frequent coverage. In particular airborne remote sensing systems the image analysis technique, which analyses the electromagnetic spectrum, particularly the near infrared part is valuable, for example, the output could enable the assessment to be made of the fertiliser requirements for each square metre of paddy fields even at the early stages of paddy growth. At the early stage, it is important to monitor and run frequent assessments in order to ensure that the paddy plants are healthy, since they are then vulnerable to damage from bacteria, insects and rodents.

Generally, the best platform for undertaking frequent monitoring and rapid assessment is an airborne remote sensing system. This system is preferred as the main data capturing tool, because it gives wide area coverage with high resolution

data (< 1 metre) when compared to data captured from satellite remote sensing systems. More importantly, airborne remote sensing system has the distinct advantage over the use of satellite in that it can be repeated frequently and whenever needed.

However, to establish an airborne remote sensing system is very expensive, time consuming and involves expensive safety procedures associated with the modification to the aircraft required for installation of the remote sensing instruments. For example, Nikulainen et al. (2002) took twelve months to modify the Short SC7 Skyvan turboprop aircraft to carry remote sensing instruments, while Gulliver (2008) quoted £15K as required to modify a Cessna 152 door panel for mounting an imaging sensor.

These expensive modification costs can be reduced by introducing alternative techniques for mounting the imaging sensor to the aircraft. For example, the imaging sensor can be mounted on the wing of the aircraft, attached to the nose of the aircraft, embedded on the inspection panel floor, or attached to the aisle window by using a mounting bracket. This latter will be discussed in Chapter 2.

The second main problem in imaging the earth's surface from an airborne remote sensing system is the geometric correction. In agricultural areas it is often difficult to identify an adequate number of ground control points to enable an image to be corrected (Pooley, 2007). However, the geometry of the image can be corrected if the attitude and position of the imaging sensor are known (Moffit and Mikhail, 1980). These can be obtained by measuring the movement of the imaging device by

installing a Global Navigation Satellite System (GNSS) receiver and Inertial Measurement Unit (IMU) on the imaging sensor. Read and Graham (2002) observe that GNSS and IMU are essential for aerial mapping today.

The implementation of these devices has been carried out successfully by a number of researchers, including Toth (2002), Cramer (2001), Pinto and Forlani (2002) and Schwarz et al. (1993). However, these researchers have focused only on high accuracy devices, which are very expensive and unaffordable for individual farmers or small companies. Zhang and Xiao (2003) found that it is not possible to correct the image geometry for devices which are cheap and simple because of the following problems:

- 1) Signal fluctuation in the receiving and transmitting process,
- 2) Competency of embedded software, and
- 3) Duration of operational time the devices can work and give results to the required accuracy.

These problems may cause system pauses, jamming, inaccuracies, terminations and other sorts of discontinuity in the data capturing process which affect the accuracy of the end product.

In addition, since the existing processing techniques and procedures successful when using the high accuracy devices, there is little incentive to develop technology for lower accuracy systems. For instance, Chiang et al. (2003) found that the existing techniques such as Kalman filtering perform adequately only under certain predefined dynamic models, and Hide and Moore (2005) found that the Kalman filter smoothing is rarely considered in the case of low-accuracy devices because the

signal fluctuation is unpredictable. El-Sheimy et al. (2006) have introduced a fuzzy logic solution, while Schmitz et al. (2001) adopted a rigorous method solution for curing the fluctuation problem. However, the results that they obtained were not very convincing when applied to low-accuracy device problems.

Hsiao et al., (2006) presents a method of integrating the image sensor with an inclinometer, altimeter and gyro-compass as an alternative to the use of GNSS, IMU and separate sensing developed for this research. They quote the development of their system as very inexpensive at a cost of \$1300. However as the sensor and IMU were provided by Skyfarm, an agricultural consultancy, free of charge for the use of this project it considered more useful to investigate this area rather than emulate the work of Hsiao et al.

1.2 Research Objectives

The main research objective is to develop a low cost portable remote sensing system to assist the Government of Malaysia to monitor and manage the agriculture, especially the paddy fields. The low cost remote sensing system should be cheap, easy to install and suitable for use on the small aircraft, such as the Cessna 152. Specifically, this research is going;

- 1) To develop a portable remote sensing system which requires no modification to the aircraft which can be: loaded into a small engine aircraft, flown to the target location, and is able to capture an appropriate image.
- 2) To develop an algorithm for assisting the geometric correction of the captured image, by means of a direct geo-referencing method.

- 3) To test the portable remote sensing in real time condition.
- 4) To analyse the accuracy of the resulting geo-rectified images.

1.3 Limitations of the Research

The main constraint of this research study was the limited finance to support the development of the low cost portable remote sensing system and hence, the choice of possible instruments was limited. The constraints on the research project, therefore including the following.

- 1) The use of an Agriculture Digital Camera (ADC) manufacture by the Tetracam Company, and loaned by Mike Pooley of Skyfarm, for the imaging sensor for this research. This has been used for capturing agricultural activities ranging from the early stage of plant growth, cultivating the soil, sowing the seeds, through to monitoring plant development and harvesting.
- 2) The navigation sensor system for use in conjunction with imaging sensor included an IMU loaned by Dr. Tom Chidley, together with a Garmin 76, a Garmin eTrex and a wireless GPS is a personal instruments.

1.4 Research Design

It should be noted that this research is primarily based on experimentation. The experiments begin by reviewing the loaned instruments through manufacturer's manuals and websites. Ideally the instruments should meet four main criteria: 1) low-cost, 2) flexibility, 3) simplicity, and 4) sufficient precision for the geometric correction. Cost was most important because the aim of the research is to develop a low-cost remote sensing system. These instruments should have the flexibility that

enables them to be attached to each other, and also be simple to operate and capture the information they measure.

Secondly, these instruments were tested through laboratory and field investigation for response to various types of movement; both slow and steady, and rapid and sudden. The measurements gave an idea of the occurrence of systematic, random and gross errors. Based on the information, a suitable solution would be obtained.

The third experiment was to prove that the instruments could be used to acquire real flight data, and to verify that the solutions obtained from the laboratory investigation were applicable to real flight data. The verification was undertaken in qualitative and quantitative analysis modes. The qualitative analysis was used to verify that the data obtained had a sufficient level of accuracy, while the quantitative analysis is used to ensure the research goal had been achieved.

1.5 Thesis Structure

Following this Introduction, Chapter 2 is devoted to a literature review on airborne remote sensing systems. It discusses the background of low-cost airborne remote sensing systems, low-cost airborne remote sensing instruments and their ancillary equipment, and reviews the geometric correction process, sources of geometric distortion and the algorithm for the geometric correction solution. The background study also investigates the platforms that can be used for low-cost airborne remote sensing. The geometric correction process is focused on a direct geo-referencing method. The source of geometric distortion gives an initial picture which can be used as a guideline for developing a direct geo-referencing algorithm.

Chapter 3 discusses the proposed design of the low-cost airborne remote sensing system. It begins with the design objective, design layout, and moves on to the selection of instrumentation, the data types, the expectation of error of the selected devices and error optimisation. The research objective, identified that the main cost-reduction that could be achieved by implementing a portable system with no structural modification to the aircraft. The characteristics of the selected device suited to the proposed design constraints are discussed in detail. The data types that can be obtained from the selected devices may indicate how to acquired data where can be reduced. Based on the expected data types, the expected error from the selected device can be predicted and hence the error optimisation procedure can be established. The outcome from this chapter provides an input to the Chapter 4.

Chapter 4 is dedicated to explaining the direct geo-referencing process. It covers the concept of direct geo-referencing, data preparation, image orientation and mapping pixels into a user coordinate system. The concept of direct geo-referencing is explored to provide possible approaches for the implementation of direct geo-referencing. Under data preparation, the initial processing of GNSS and IMU data, for infilling the missing data and the extraction of the navigation and the ancillary data, is explained in detail. The reconstruction of image geometry, focuses on camera lens distortion, lens misalignment and principle distance and the resolution of errors associated with roll, pitch and heading. The method scaling and aligning the entire dataset to the local coordinate system is described. The mathematical equation algorithm developed, which includes the tilt and oblique solutions for direct geo-referencing, is explained in detail. The algorithm developed is an input to the next

chapter, which develops the software for managing the low-cost airborne remote sensing data.

Chapter 5 is devoted to discussing the software developed as an enabling tool for the direct image geo-referencing. The software structure consists of 1) input parameter, 2) intrinsic parameter, 3) extrinsic parameter, 4) image processing, and 5) discussion.

Chapter 6 investigates the available instruments and their performance. The investigation is divided into three parts: performance test, simulation test and investigation results. The performance test discusses the performance of each instrument in terms of system endurance, system halting and system failure. The simulation is undertaken to investigate and predict the output and error sources of each of the instruments.

Chapter 7 is devoted to discussing how system validation was achieved through flight testing. The flight test was the only way to validate the system in a real agricultural monitoring environment. The chapter includes the test site, data acquisition, flight mission, data obtained, installation of equipment and some results.

Chapter 8 is devoted to discussion. It begins with a summary and critiques the imagery data obtained in Chapter 7, and then evaluates the overall capability of the developed system.

Based on the previous discussions, conclusions and recommendations for future work are given in Chapter 9.

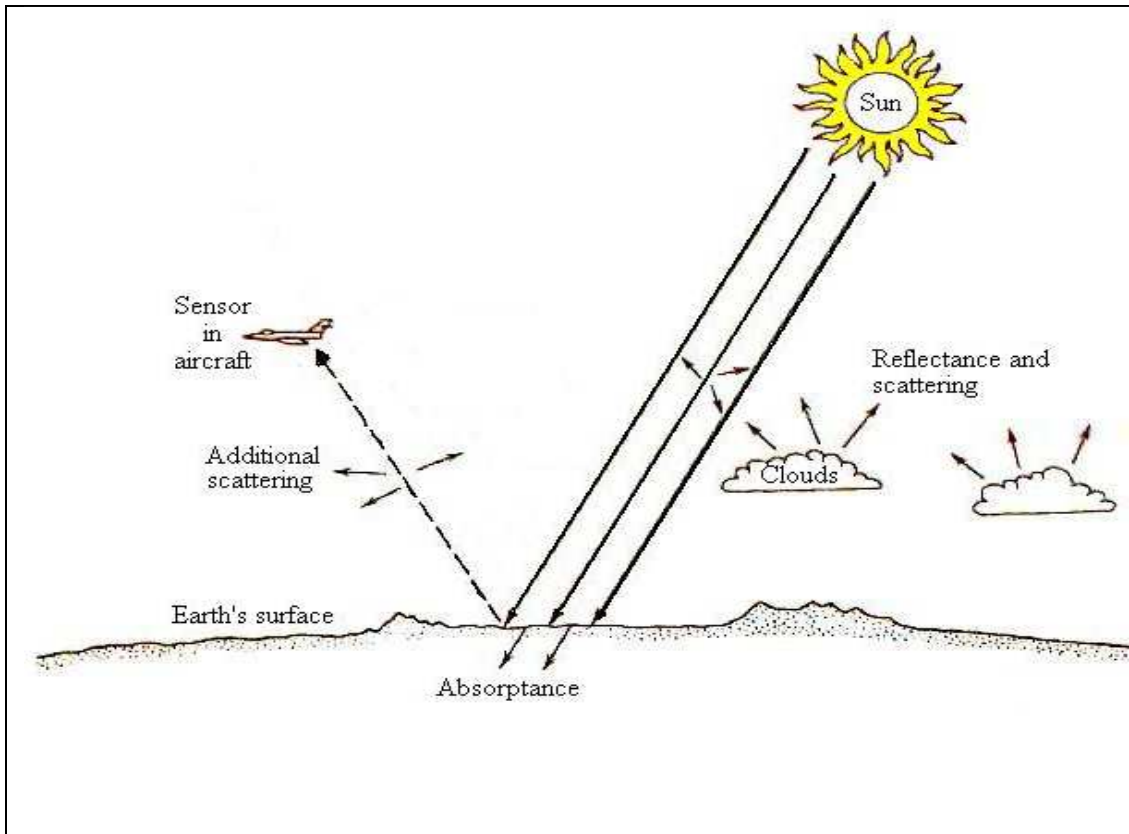
2. LOW-COST AIRBORNE REMOTE SENSING SYSTEM AND GEOMETRIC CORRECTION

2.1 Background of Low-cost Airborne Remote Sensing

Remote sensing is a technique of acquiring information about the earth surface which includes natural and man-made objects, area, or phenomenon without having direct contact with the object, area or phenomenon being investigated (Lillesand and Kiefer, 2000; Duggal, 2009) by means of the electromagnetic spectrum. The electromagnetic spectrum ranges from radio, microwave, infrared, visible, ultraviolet, x-ray to gamma rays that are produced by solar energy or the remote sensing instrument itself. Figure 2.1 illustrates the process of collecting information by using airborne remote sensing where the sun is the electromagnetic source.

Even though the range of the electromagnetic spectrum is very wide, the electromagnetic spectra available to be used for sensing the earth's surfaces is limited. Some wavelength of the electromagnetic spectra can be sensed by using photographic devices but the remainder need special instruments for their capture. The selected device can be mounted in an aircrafts when is referred to as airborne, or a spacecraft it is referred to as spaceborne. The choice of platform depends on their design purpose. The airborne remote sensing option has been used widely in aerial geomatic applications. Aerial geomatics is employed for gathering information about the earth surfaces when high spatial resolution is required. Examples of such applications are gathering information about high density areas such as Cities, inspecting construction site or monitoring the development of a highway.

Spaceborne remote sensing is used more for small scale mapping and studying inaccessible terrain or large areas such as deserts (Aerial survey, 2005). Various types of device can be used for acquiring information about the earth's surfaces either through airborne or spaceborne remote sensing.



Source: Modified from Paine and Kiser, 2003.

Figure 2.1: The process of gathering information using airborne remote sensing.

In airborne remote sensing, the off-the-shelf market offers an extensive range of devices, which include thermal radiometers, high spatial resolution spectrometers, cosine Collector Spectro radiometers or Sun Photometers, Multi-angular radiometers, Charge Couple Device (CCD), video imagery instruments, Lidar and/or range-finders, radar and passive microwave instruments, GPS units and CDI's (Course Deviation Indicators), and Cameras (Dabney and Deering, 1998). However, the device selection is dependent on project requirements, budget allocations and device

reliability. For example in low-cost airborne remote sensing, the main constraints will be the budget allocations.

2.2 Low-Cost Airborne Remote Sensing Instruments

Interest in low-cost airborne remote sensing has been stimulated by the Instrument Incubator Program (IIP) under the technological development of innovative earth science initiative funded by NASA in 2001 (Steitz, 2001). The objective of the initiative was to invest in new and innovative technologies that could lead to smaller, less expensive and more efficient flight instruments for obtaining reliable information of the earth's surface. The current established airborne remote sensing instruments such as the airborne hyperspectral sensor, the airborne thematic mapper and laser scanning devices, are quite large and need a lot of aircraft space for operations, which involves very high cost. Figure 2.2 depicts an example of airborne remote sensing instruments and their layout on board an aircraft.



Figure 2.2: Layout for instrument installation.

In this research study, the incentive for designing a low-cost airborne remote sensing system has been driven mainly by the cost factor of conventional airborne remote

sensing systems. The most costly part in developing an airborne remote sensing system is the need for a large aircraft due to power and space requirements (Roberts et al., 2000), modifying the aircraft, and obtaining an authorisation certificate from the aviation authority for the modification. The cost of developing such an airborne remote sensing system is billions of dollars, but with a low-cost airborne remote sensing system, the cost can be reduced to a range of a thousand to a million of dollars (Roberts et al., 2000).

With a view to reducing the aircraft modification cost, several innovation platforms have been introduced. One example is the satellite-based small cheap instrument for low-cost remote sensing systems developed by the University of Surrey, through its technology transfer company, Surrey Satellite Technology Limited (SSTL) (Fouquet and Sweeting, 1995). The low-cost remote sensing system was loaded with a CCD camera which orbits the earth at a range of 600 to 800 km. The system covers an area of about 75x55 km (narrow band) to 2550x1880 km (wide band).

A tethered balloon can also be employed as an alternative to reduce the aircraft modification cost. Its applications have been demonstrated by: Piwowar (1993) in aerial imaging; Storvold et al. (1998) in monitoring the temperature, wind, and water vapour profiles through the atmospheric boundary layer in the Arctic; Stamness and Storvold (1999) in measuring cloud micro-physical and radioactive properties; Siebert et al. (2003) in fine-scale measurements of metrological and microphysical properties; and, Vierling et al. (2006) who used tethered balloon in studying basic remote sensing questions and linking landscape level trace gas fluxes with spatially and temporally appropriate spectral observations.

There are examples of research work on tethered balloons which have been used in remote sensing science dating to the birth of aerial remote sensing itself. In 1858 Gaspard Felix Tournachon manually collected an aerial photograph near Paris while aboard a tethered hot air balloon. Numerous aerial photographic surveys using manned tethered balloons followed in the 1860s, establishing this method as a viable means for collecting airborne data for municipal, military, aesthetic and scientific purposes (Newhall, 1969).

Another platform, which can be used as an alternative to a plane, is the kite. The first photograph taken using a kite was demonstrated by Musee Arthur Batutin 1889 over Labruguierein, France (Estes and Hemphill, 2006). Some other researchers involved in this area are: De Moraes (2001) and Murray et al. (2001) who researched the use of a kite as a portable, low cost, and high quality alternative to current aerial photography methods; and Aber et al. (2002), who demonstrated the use of a kite for acquiring large-scale, high resolution and multiview-angle imagery from unmanned small-format aerial photography.

The Unmanned Aerial Vehicle (UAV) concept was first introduced by Julius Neubranner in 1903, who designed and patented a breast-mounted aerial camera for carrier pigeons (Figure 2.3). Weighing only 70 g the camera took automatic exposures at 30-second intervals along the flight line followed by a pigeon (Baumann, 2001).



Source: Baumann, 2001

Figure 2.3: First unmanned vehicle for airborne remote sensing.

The unmanned vehicle as a remote sensing platform has been demonstrated by several researchers (to name just a few) such as: Stombaugh and Mueller (2006), who developed a low-cost remote sensing system by using a UAV as a platform for monitoring agricultural fields; Schinstock and Ham (2005) patented a prototype UAV remote sensing system to be used for environmental study; and, Swain et al. (2007) who employed a radio-controlled helicopter as an alternative platform for low-cost remote sensing for monitoring agricultural fields.

However, the low-cost remote sensing platforms mentioned above can only be used with the approval of the local aviation authority (Graham, 2010) as each country has its own regulations. To void the authority problem of obtaining official authorisation, some researchers have invested in low-cost remote sensing instruments for use in light aircraft. Pioneering work by Graham and Read in 1986, is a good example of implementing the ultralight aircraft as a low-cost remote sensing platform. In 1985, Vooren and Offermans demonstrated the application of ultralight aircraft for low-cost, large-scale stereoscopic aerial photography.

The use of light aircraft as the remote sensing platform has been documented by Graham and Read (1986) and Read and Graham (2002) and indeed, a workshop on low-cost remote sensing instruments to be embedded in a single engine light aircraft was held at the University of Maryland on 6 October 1997 (Dabney and Deering, 1998). The workshop discussed experiences with light aircraft equipped with various types of spectral regime such as optical, lidar, thermal, microwave, and radar sensors together with ancillary equipment.

2.2.1 Low-Cost Imaging Device

The imaging device usually collects several wave bands within the electromagnetic spectrum. A camera, for instance, usually captures/collects the three primary colours: blue, green and red. A multispectral sensor is able to capture more than three discrete bands which can provide more information about crop health and vigor than one can detect with one's own eyes. In them, the more bands that the sensor can detect the more information that can be obtained. However, the more bands the sensor can detect the more expensive the sensor will be. Therefore, for the design of a low cost remote sensing system for agricultural monitoring, a knowledge and understanding of the interaction of the electromagnetic spectrum with the earth's surfaces is very useful. For example, the near-infrared (or NIR) is able to provide more sensitive information about canopy health than the visible bands of blue, green and red. Figure 2.4 illustrates the components of the electromagnetic spectrum required for monitoring agricultural regimes and especially in calculating the Normalised Difference Vegetation Index (NDVI) and Soil Adjusted Vegetation

Index (SAVI). While, Table 2.1 lists the major regions of electromagnetic spectra and their remote sensing applications in general terms.

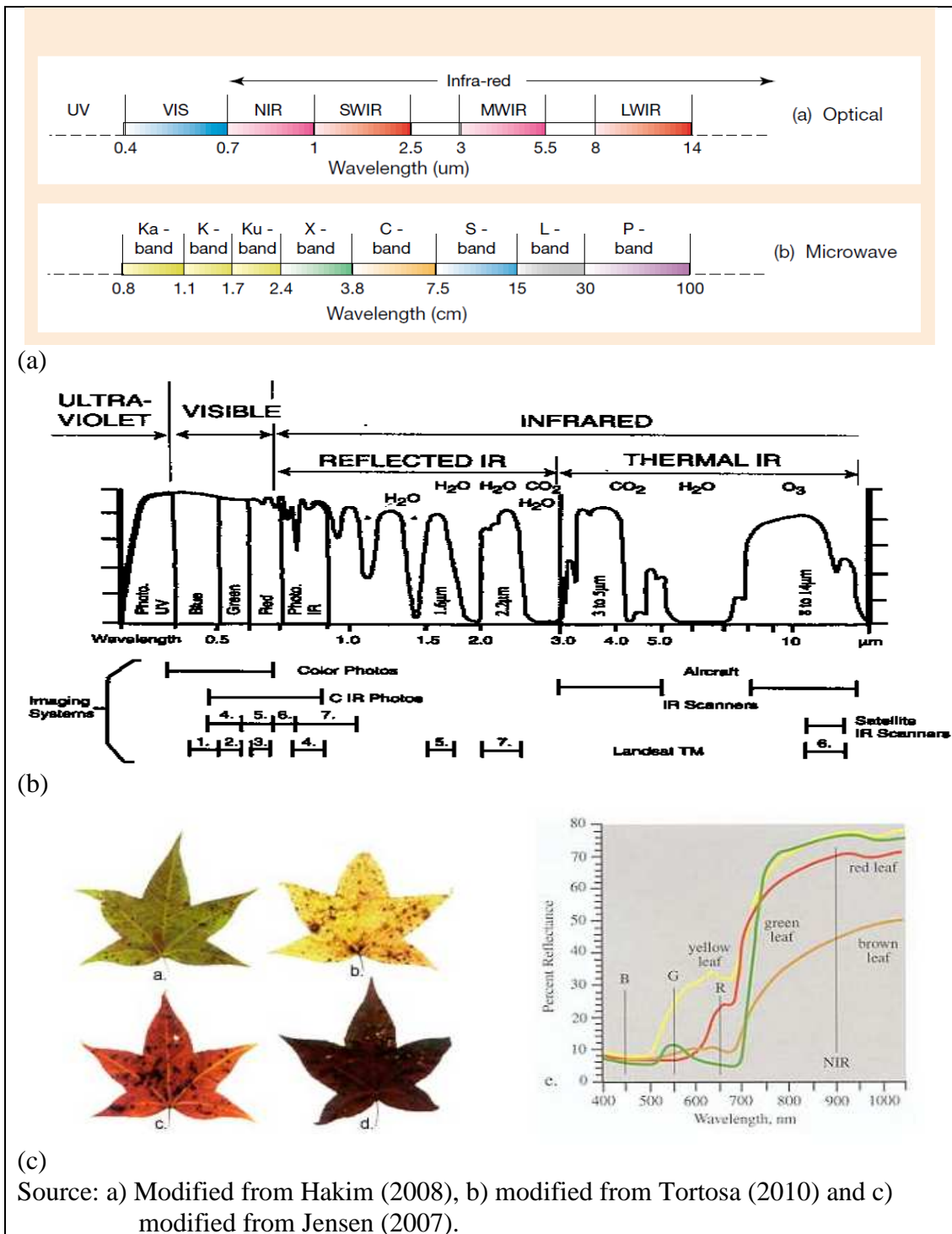


Figure 2.4: Electromagnetic spectrum a) Electromagnetic spectrum range from radio to gamma rays while b) electromagnetic spectrum used in remote sensing applications and their imaging systems; c) show the visible (Blue, Green, Red) and Infrared electromagnetic spectrum used for NDVI and SAVI calculation.

Table 2.1: Major regions of electromagnetic spectrum.



Source: Pidwirny (2006)

The use of remote sensing imaging devices for agricultural applications has been established since 1970. Sensors fall into two different categories, which are photographic sensors (Heller, 1970) and non-photographic sensors (Hotler et al., 1970). These imaging devices have been used to aid agricultural planning, development and administration (Luney and Dill, 1970). The photographic sensors such as aerial cameras provide black and white panchromatic, black and white infrared, Ektachrome infrared and colour photographs. The non-photographic sensors, such as radar, passive microwave, infrared and multispectral sensors, which are

based on the capture of distinct electromagnetic spectrum wavebands, provide images that contains a wide range of spectral regimes. At the early stage of remote sensing development, the sizes of these devices were large, had a high power consumption, and required appropriate space for their installation.

However, these imaging devices had gone through a period of innovation which has led to smaller, less expensive, and more efficient flight instruments. The innovative effort has been triggered by NASA under their Instrument Incubator Program, with total funds made available for these investigations averaging nearly USD\$1 million per year for three years or a total of approximately USD\$29.5 million (Steitz, 2001). Due to this incentive, a wide range of low-cost imaging devices are currently available for installation on single engined light aircraft.

Off-the-shelf, low-cost airborne imaging devices include the small-format digital camera, the medium-format digital camera, the large-format digital camera and the digital video camera. Unfortunately, there are only two types of imager applicable for light single engine aircraft, which are the small-format digital camera and the digital video camera. The other systems are too complicated and too large to be installed onboard a light single engine aircraft (Dare, 2005).

The most popular small format digital camera for agricultural use is the Kodak's DCS 4XX series, which includes DCS 420 GPS-C, DCS 420 GPS-IR, DCS 420 GPS-M, DCS 420CIR and DCS 460CIR, which were first introduced in 1994 and 1996 (McGarvey, 2004) . These digital cameras are ideal for environmental and law enforcement that required forestry and vegetation analysis. The pixels size for these

cameras is 1012x1524, except for the DCS 460CIR which has a 2036x3060 pixel size (McGarvey, 2004). The Kodak's DCS series has contributed significantly to the development of Aerial Digital Photographic System (ADPS) for mapping or monitoring applications. For example; Geotechnologies of Bath Spa University had developed the ADPS system based on DCS 420 and DCS 460; Technical University of Delft in Netherlands has carried out a pilot studies on the DCS 200 and DCS 460 mounted on a helicopter; the University of Calgary in Canada also developed a system similar to the ADPS, based on the DCS 420; and, the University of Florida in America has been working with DCS 420 for collecting land cover samples (Petrie, 2003). These examples show that Kodak's DCS series have proved successful for remote sensing tasks and small area mapping (Warner et al., 1996). Figure 2.5 shows the example of ADPS based on Kodak's DCS series developed by Geotechnologies of Bath Spa University (Petrie, 2002 and 2003).



Source: Petrie (2002 & 2003)

Figure 2.5: The ADPS based on Kodak DCS 460CIR digital frame camera which is produced by Geotechnologies of Bath Spa University.

Tetracam is another manufacturer that produces imaging device for agricultural applications. The products that they produce are known as the Multi-spectral Camera for Agriculture and the Agriculture Digital Camera. These two products have been used widely by individual farmers and crop consultants, as well as large organisations such as AG Canada, the U.S Department of Agriculture and universities in America (Petrie, 2003). Both imaging devices have a 1280 x 1020 pixel size and are equipped with a Bayer mosaic filter. The Bayer mosaic filter enables captured images to be seen on the screen fitted to the back of the camera and stored on a flash card. The imaging devices are also equipped with a USB port and a serial port to allow it to be connected to a laptop computer and a GPS device (Tetracam, 2010). Figure 2.6 illustrates the imaging device produce by Tetracam.



Source: Tetracam (2010)

Figure 2.6 : The Multispectral Digital Camera produced by Tetracam.

SensyTech (formerly known as Daedalus Enterprises) is another well known company that produced multispectral and line-scan imagers in the early 1980s (Petrie, 2003). Their current product includes digital frame cameras which are based

on Kodak's MegaPlus Monochrome (Black and White) series digital camera that include: MegaPlus 1.0, MegaPlus 1.4i, MegaPlus 1.6i, MegaPlus 4.2i, MegaPlus 6.3i and Megaplus 16.8i each with different size of CCD array. The SensyTech's AA456 Airborne Digital Camera is base on MegaPlus 4.2i and is equipped with a camera mount, a system control unit with built-in GPS, and an operator control and display unit for use in airborne mapping. An upgraded version of the AA456, the AA497 Airborne Multi-spectral Digital Camera is fitted with coloured optical filters for generating the multispectral image by using rotating colour filter wheels and an Inertial Measurement Unit for providing attitude data. SensyTech collaborated with ERIM International in developing the software for registration and rectification that enables the production of separate band images or colour or false-colour composite images (Petrie, 2003). Figure 2.7 demonstrate the SensyTech Airborne Multispectral Digital Camera.



Source: Imaging Group (2010)

Figure 2.7: The Airborne Multispectral Scanner produced by SensyTech.

In addition to the manufacturing companies above, RedLake (formerly known as DuncanTech) is another well known company that is involved in manufacturing small format digital cameras that use a beam splitter, with three CCD arrays to collect simultaneously the three individual band images (Petrie, 2003). This multispectral camera has overcome the limitations of the two systems mentioned above, where the true colour or false colour images were being generated either by using a Bayer mosaic filter, an alternative mosaic filter screen and subsequent interpolation, or through the use of sequential images via a rotating wheel. Some examples of Redlake products are; MS2100, MS2150, MS3100, MS4000, and MS 4100. The pixel size for these multispectral cameras ranges from 494 x 656 to 1080 x 1920 pixels. These multispectral cameras can be integrated with an electronic control unit, a GPS set and flight control and navigation software (Petrie, 2003). For example an integrated system called Agri-View, developed by Airborne Data Systems from Minnesota, was based on the MS3100 or the MS4100. Spectronics from Australia has developed the Integrated Spectronics Airborne Acquisition Camera System, that combines the MS3100 or MS4100 with a control unit and connections to an Applanix POS/AV unit and the Furgo Omnistar DGPS system, and as well as providing its own image data acquisition and processing software (Petrie, 2003).

Instead of the small format imaging devices which have been discussed above, there are several types of imaging sensors that can be used as low-cost data acquisition devices. Examples of these are, line scanner imaging, hyperspectral scanner, laser scanning, thermal imaging and polarimetric microwave systems. The line scanner developed by Redlake known as MS2200 is able to provide data in four bands: near

infrared, red, green and blue as reported by Dare (2005). Whilst, Bochert et al., (2000) have developed a low-cost line scanner, which is able to provide 2048 x 2048 pixels for the green, red and near infrared bands.

In the field of hyperspectral scanners, a company from Finland called SPECIM has manufactured various types of hyperspectral scanner which are small, easy to install, easy to transport, have high performance, stable operation, good spatial accuracy and spectral resolution, and are reliable data, low maintenance, and efficient data collector (SPECIM, 2008). For example, the AISA Airborne Hyperspectral Sensor System called AisaEAGLE, provides very near infrared in the range of 400-970nm, with 512 or 1024 spatial pixels and up to 488 spectral bands and weighs 6.5 kg.

RIEGL, an Austrian company (REGL, 2008) has developed four types of Airborne Laser Scanning device known as LMS-Q560, REIGL VQ-480, LMS-Q240 and LMS-Q160, which can be installed in twin-engine aircraft, single engine aircraft, helicopters or unmanned airborne vehicles. These instruments weighs between 4.6 to 20 kg and provide near infrared data with various types of measuring option, such as time-of-flight measurement, echo-signal digitization, wave form analysis, first return signal, last return signal, or alteration signal.

FLIR system is one of the manufacturers who has invented a compact thermal imaging cameras (FLIR, 2008). An example of the compact thermal camera is ThermalCam P620, which has 640 x 480 pixel resolution with high thermal sensitivity (0.06°C) that provides a precision of $\pm 0.2^{\circ}\text{C}$. This camera operates in the

same manner as a typical digital video camera, with data being stored on a computer hard disk through a Firewire (IEEE1394) connection (Dare, 2005).

Colliander (2007) has developed a Polarimetric Microwave Radiometer for remote sensing applications. The Polarimetric Microwave Radiometer operates at 36.5 GHz and uses a direct cross-correlation technique. It has a radiometric resolution of about 0.2 K for the orthogonal polarisations. This instrument is used to measure microwave emissions from rough surfaces such as the ocean.

The installation of the low-cost imaging devices referred to above in small single engine light aircraft, enables the study of the fields by remote sensing techniques at a much lower cost. There is evidence that the various types of low-cost imaging device which can be installed onboard together cover almost the entire electromagnetic spectrum, even though some of the imaging device need little modification. For example, Wood, et al., (2003) modified Kodak's DCS 420 by an embedding optical band-pass filter in front of the 18mm optics to centre the red waveband at 640 nm and the near infrared waveband at 840 nm made to evaluate vegetation indices investigations.

The selection of a low-cost imaging device, however, depends totally on budget allocation, project needs and device reliability. This research study, focused on budget allocation and reliability of the low-cost remote sensing system, and the Tetracam Agriculture Digital Camera was selected because this camera was loaned by Skyfarm without a fee.

2.2.2 Ancillary Instruments

The most important ancillary instruments in airborne remote sensing systems are the navigation devices. There are various types of traditional navigation systems such as altimeter, gyroscope, inclinometer, and compass. However, the now well established method in navigating airborne remote sensing aircraft is the integration of an Inertial Measurement Unit (IMU) and a Global Positioning System (GPS). The integration of IMU and GPS in airborne applications work was published by Schwarz in 1995. This made a substantial contribution on the principles of IMU and GPS in airborne environments. In 1997, Cramer conducted tests for analogue frame cameras and digital line scanner sensors which been integrated with IMU and GPS, and found that the accuracies are high enough for almost all mapping applications. Lithopoulos (1999) reported the possibility of commercial IMU and GPS integration systems for high-end applications.

Since the initial work done by Schwarz, the focus of integrating the IMU and GPS has been on the extensive testing in airborne sensor environments, such as multi-line pushbroom airborne cameras (Neukum, 1999), digital airborne cameras (Wegmann et al., 2004), laser scanners (Nagai et al., 2004; Talaya et al., 2004), analogue frame cameras and digital line scanners (Cramer, 1997). Some work on integrating IMU and GPS for mapping has been described by Talaya et al. (2004), Wegmann et al., (2004), Nagai et al. (2004), Baumker and Heimes (2002), Seara (2002), Gruen and Zhang (2001), Mostafa (2001), Jacobsen (2000) and Cramer (1997). Table 2.2 summaries published work on the integration of IMU and GPS. An accuracy of <0.6 cm can be achieved by the integration of aerotriangulation, IMU and GPS while direct orientation gives 0.30 m to 1 m mapping accuracy. It has been reported by

several researchers that mapping accuracies fall between 0.03 m to 1.0 m (in RMS), with respect to the accuracy of IMU, GPS, imaging device and camera resolution (Grejner-Brzezinska and Toth, 1998).

Table 2.2: Previous studies on integration of IMU/GPS

Researcher	Accuracy of IMU				Corrected Coordinate (RMS)		Technique Applied
	Roll (Deg)	Pitch (Deg)	Yaw (Deg)	Position (m)	X (cm)	Y (cm)	
Niu et al. (2006)	0.5	0.5	0.5				
Wegmann et al., (2004)	<0.005	<0.005	<0.008	<0.1	5.0	5.0	Combination AT, IMU & GPS
Nagai et al. (2004)	0.1	0.1	0.1	0.4	3.0	6.0	Combination AT, IMU & GPS
Baumker&Heimes (2002)	<0.005	<0.005	<0.025	-	30	43	DO (Laboratory Test)
Seara (2002)	0.013	0.013	0.035	0.05	17.0	100.0	DO
Heipke et al. (2002)	0.005	0.005	0.008	0.1	5.0	5.0	Combination AT, IMU & GPS
Gruen (2001)	0.005	0.005	0.005	0.02	7.9	7.9	DO
Mostafa et al. (2001)	0.005	0.005	0.008	0.1	0.8	0.5	DO
Jacobsen (2000)	0.005	0.005	0.008	0.1	30	30	Check on systematic error on IMU
Cramer (1997)	0.002	0.002	0.001	0.15	13	15	DO

Note: AT = Aerotriangulation, DO = Direct Orientation

Niu et al. (2006) using IMU based on accelerometer, others using gyroscopes and accelerometers IMU.

2.2.2.1 Inertial Measurement Unit

Off-the-shelf, there are various types of low-cost IMU devices ranging from navigation grade to consumer grade IMU. The difference between them is the accuracies they produce. A study of IMU performance has been carried out by several researchers, including Schwarz and El-Sheimy (1999), Greenspan (1995) and Gebre-Egziabher et al. (2001). Table 2.3 shows the performance difference between different IMUs.

Table 2.3: Performance difference between IMUs



Source: Shin, 2001.

Originally, the IMU device was based on a combination of gyroscope (angular rate) and accelerometer (force). The development of an IMU device based on gyroscope and accelerometer measurements is very complex and expensive, especially with regard to the gyroscope. Thus, through advanced technology investment an IMU based on a linear accelerometer has been developed. Merhav (1982) found that the linear accelerometer based IMU is essentially drift-free and the dynamical errors due to angular rate and force are very small. This invention has been enhanced by Hulsing (1998), who employed the single coriolis inertial rate to measure the angular rate and used the linear acceleration to measure the force. This invention has been a corner stone for inventing smaller and cheaper IMU devices through Micro-

Mechanical Electronic Manufacturing System (MEMS). Ahn and Lee (2003) have been interested in estimating the altitude of the sun-pointing mode satellite by using gyroless IMU, Pamadi and Ohlmeyer (2004) have worked on assessing the GPS for guiding a spinning projectile by using an accelerometer-only IMU, and Niu et al. (2006) have carried out research on direct geo-referencing terrestrial imagery by using an IMU based on a linear accelerometer. Park et al. (2005) have introduced a scheme for improving the performance of a gyroscope-free IMU.

The accelerometer-based IMU has become popular as the price has become cheaper, where it is around USD\$5 to USD\$30 (Niu et al., 2006) and the size has reduced to that of small coins. This type of device has opened up the choices available for selecting the most appropriate device according to budget allocation, project needs and the reliability of the device.

2.2.2.2 Global Navigation Satellite System

Low-cost GNSS were invented for recreation, road navigation and other activities which do not need a very good accuracy. There are various off-the-shelf low-cost GNSS brands and some examples are Garmin recreation products, such as Garmin eTrex, Garmin 76 and Garmin 12 XL; Magellan have a product called Triton 200, Thales Explorist and Magellan Marine GPS. In GNSS wireless (Bluetooth) products, there are various types of Holux wireless device such as Holux M-1200, Holux M-1000 and GPslim240 and from GlobalSat there are GlobalSat BT-359, BT-335 and 5843 RDS TMC. Regardless of types, brands or qualities, the low-cost GNSS uses the same principle for receiving and transmitting the GNSS signals.

Global Navigation Satellite System (GNSS) is a term used to describe a navigation network system for determining the coordinates of a location. There are three navigation networks in use; NAVISTAR, GLONASS and Galileo. All of them use radio signals to communicate within the system which consists of three major segments known as the control segment, the space segment and the user segment. Each of the segments has a receiver to transmit, receive or transmit and receive radio signals with a dedicated frequency. In the control and space segments, there is receiver able to transmit, receive or transmit and receive six types of frequencies known as C1, C2, L1, L2, P1 and P2 (see Table 2.4).

Table 2.4: Frequencies and observation type

f1	f2	Observation type	Units
L1	L2	Carrier phase	cycles
C1	C2	C/A code pseudorange	metres
P1	P2	P-Code pseudoranges	metres
S1	S2	Signal-to-noise ratio	decibels
D1	D2	Doppler frequencies	Hz

The control segment is used to track the satellites constantly and make sure that they are operating correctly and has a very precise radar to check their altitude, position and speed. Subsequently, the data are used to calculate the ephemeris constants and clock adjustments transmitted to the satellites in the space segment. The satellites in turn use these updates in the signals that they send to the user. Figure 2.8 shows the GPS components.



(a)

Source: Motorola, 1997.



(b)

Source: NASA, 2006.

Figure 2.8: (a) GPS components and (b) the location of GPS monitoring stations.

In the user segment, receiving the frequencies depends totally on the type of receiver used. For example, the military receiver is capable of receiving Y code which consists of P1 and P2 together with L1 (1575.42 MHz) and L2 (1227.60 MHz) frequencies. L1 and L2 are used to calculate the differential GPS for better accuracy. For the layman, there are single frequency and dual frequency receivers able to receive C/A code which consists of C1 or C2, or C1 and C2. The single frequency receiver will receive C/A code which consists of C1 or C2, or C1 and C2 together with either L1 or L2. A dual frequency receiver will receive C/A code which consists of C1 or C2, or C1 and C2 together with L1 and L2. In a dual frequency receiver, a technique called squaring, cross-correlation or P-W correlation is used to obtain full L2 wavelength for achieving better accuracy (Hassan, 2004).

Generally, NAVSTAR, GLONASS and GALILEO use a common principle for determining the local position (see El-Rabbany (2002) for details of process for translating signals to position). All have an identical Ground Control segment with applications for land, sea and air. The navigation networks have slightly different constellations of receivers in the Space segment where relates to satellite geometry, orbit, orbit period and the radio frequency signals. Table 2.5 shows the constellation description for all three GPS network.

Table 2.5: Constellation Description for GPS



Source: European Space Agency (2007) and Space and Tech (2001)

2.3 Geometry Correction Review

It should be noted that the geometry correction carried out in this research study is based on a parametric method which leads to direct geo-referencing. In the parametric method, the extra information needed to geo-rectify the image is the attitude, position and intrinsic parameter of the imaging sensor. This information is used to reconstruct the system's trajectory; in this case, it is the airborne remote sensing system. The reconstruction relates the imaging sensor to the platform, earth and map projection. The main idea behind the reconstruction of the sensor system's

trajectory is to place the image in its real position at the time of acquisition. As a result, each image pixel is moved to its adjusted position and the appearance of the image is thus less distorted. This technique has limited reliance on ground control and has potential for automation (Roy et al., 1997).

The reconstruction of the sensor system's trajectory requires all the relevant devices to be at one common coordinate reference, because the coordinate systems employed by each device do not comply with the coordinate system and angles used in photogrammetry. The IMU coordinate system refers to the body coordinate system, where the IMU has been strapped down to the body of the aircraft as illustrated in Figure 2.9. The mathematical equation to connect the body coordinate system with navigation coordinate system is given in 2.1.



Figure 2.9: Definition of body coordinate system of Euler angles ϕ , θ , ψ

$$\begin{aligned}
 C_b^n &= R_z(\psi) \cdot R_y(\theta) \cdot R_x(\phi) & (2.1) \\
 &= \begin{bmatrix} \cos \psi & -\sin \psi & 0 \\ \sin \psi & \cos \psi & 0 \\ 0 & 0 & 1 \end{bmatrix} \cdot \begin{bmatrix} \cos \theta & 0 & \sin \theta \\ 0 & 1 & 0 \\ -\sin \theta & 0 & \cos \theta \end{bmatrix} \cdot \begin{bmatrix} 1 & 0 & 0 \\ 0 & \cos \phi & -\sin \phi \\ 0 & \sin \phi & \cos \phi \end{bmatrix}
 \end{aligned}$$

where;

C_b^n = connection matrix of the body and navigation coordinate systems

R_z = rotation about z axis

R_y = rotation about y axis

R_x = rotation about x axis

ψ = angle of yaw

θ = angle of pitch

ϕ = angle of roll

Therefore, the transformation from body coordinate system into navigation coordinate system can be given as:

$$r^n = C_b^n \cdot r^b \quad (2.2)$$

where;

C_b^n = connection matrix of the body and navigation coordinate systems

r^n = transformation coefficient in navigation coordinate system

r^b = transformation coefficient in body coordinate system

and the inverse transformation is performed by:

$$r^b = C_n^b \cdot r^n = (C_b^n)^{-1} \cdot r^n \quad (2.3)$$

where;

C_b^n = connection matrix of the body and navigation coordinate systems

C_n^b = connection matrix of the navigation and body coordinate systems

r^n = transformation coefficient in navigation coordinate system

r^b = transformation coefficient in body coordinate system

On the imaging side, the image obtained is referred to the earth coordinate system with rotation angles referred to the body coordinate, since the camera is strapped down to the body of the aircraft, as illustrated in Figure 2.10. The mathematical equation to connect between body coordinate system with navigation coordinate system is given in 2.4.

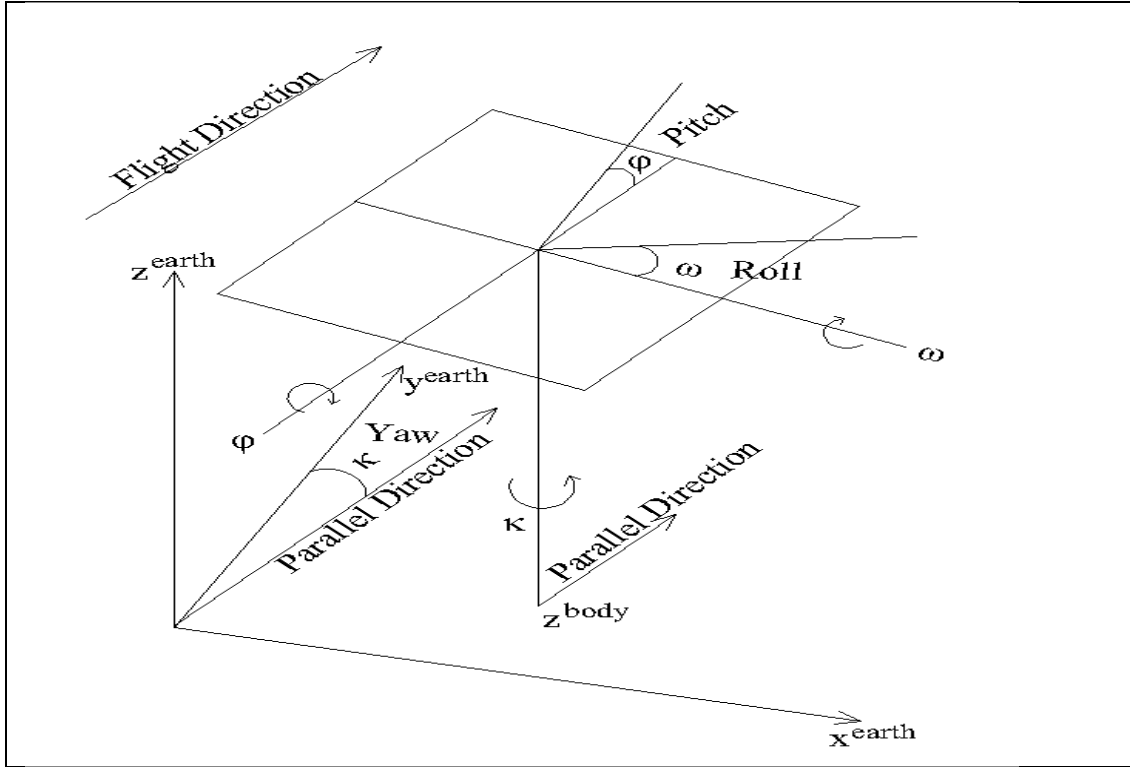


Figure 2.10: Definition of image coordinate system of Euler angles ω ϕ κ

$$C_E^B = R_z(\kappa) \cdot R_y(\omega) \cdot R_x(\phi) \quad (2.4)$$

$$= \begin{bmatrix} \cos \kappa & \sin \kappa & 0 \\ -\sin \kappa & \cos \kappa & 0 \\ 0 & 0 & 1 \end{bmatrix} \cdot \begin{bmatrix} 1 & 0 & 0 \\ 0 & \cos \omega & \sin \omega \\ 0 & -\sin \omega & \cos \omega \end{bmatrix} \cdot \begin{bmatrix} \cos \phi & 0 & -\sin \phi \\ 0 & 1 & 0 \\ \sin \phi & 0 & \cos \phi \end{bmatrix}$$

where

C_E^B = connection matrix of the earth and body coordinate systems

R_z = rotation about z axis

R_y = rotation about y axis

R_x = rotation about x axis

κ = angle of yaw

ϕ = angle of pitch

ω = angle of roll

Therefore, the transformation from image coordinate system into earth coordinate system can be given as:

$$r^B = C_E^B \cdot r^E \quad (2.5)$$

C_E^B = connection matrix of the earth and body coordinate systems

r^B = transformation coefficient in body coordinate system

r^E = transformation coefficient in earth coordinate system

and the inverse transformation is performed by:

$$r^E = C_B^E \cdot r^B = (C_E^B)^{-1} \cdot r^B \quad (2.6)$$

C_E^B = connection matrix of the body and navigation coordinate systems
 r^E = transformation coefficient in earth coordinate system
 r^B = transformation coefficient in body coordinate system

From equations (2.1) to (2.6), it is seen that both systems have one coordinate system in common, which is the body coordinate system. However, the orientation of the body coordinate system in the IMU is referred to East-North-Up (ENU), while the body coordinate system in the image is referred to Earth-Centre-Fixed Cartesian Frame (ECEF). These two systems are not the same, and thus an additional transformation is needed to convert the body coordinate system in IMU and the image body coordinate system in image – this is given in equation 2.7.

$$T_b^B = \begin{bmatrix} 1 & 0 & 0 \\ 0 & -1 & 0 \\ 0 & 0 & -1 \end{bmatrix} \quad (2.7)$$

where;

T_b^B = transformation conversion between body coordinate system in IMU and body coordinate system.

Equation 2.7 has been developed at the University of Hanover (Jacobsen, 1996) called BLUH. There is another transformation equation developed at the University of Stuttgart (INPHO GmbH, 1999) called PATB, as follows:

$$T_b^B = \begin{bmatrix} -1 & 0 & 0 \\ 0 & 1 & 0 \\ 0 & 0 & -1 \end{bmatrix} \quad (2.8)$$

where;

T_b^B = transformation conversion between body coordinate system in IMU and body coordinate system.

Finally, the common body coordinate system can be converted into the navigation coordinate system by equation 2.9.

$$T_n^E = \begin{bmatrix} 0 & 1 & 0 \\ 1 & 0 & 0 \\ 0 & 0 & -1 \end{bmatrix} \quad (2.9)$$

where;

T_n^E = transformation conversion between earth coordinate system and navigation coordinate system.

Equations 2.1 to 2.9 can be found in Skaloud (1999), Baumker and Heimes (2002) and Fiani and Pistillo (2004). These equations can be modified for tightly-coupled or single step IMU and GPS direct geo-referencing, the equation for which appears in Grejner-Brzezinska (1999), Mostafa and Schwarz (2001), Pinto and Forlani (2002), Grejner-Brzezinska and Toth (2004), Schwarz and El-Sheimy (2004) and Niu et al., (2006) and is as follows:

$$R_{BINS}^M(t) = R_{ENU}^{ECEF}(t) \cdot R_{\omega\phi\kappa}(t) = \begin{bmatrix} -\sin\lambda & -\sin\phi\cos\lambda & \cos\phi\cos\lambda \\ \cos\lambda & -\sin\phi\sin\lambda & \cos\phi\sin\lambda \\ 0 & \cos\phi & \sin\lambda \end{bmatrix} \cdot R_{\omega\phi\kappa} \quad (2.10)$$

$$r_{M,i} = r_{M,IMU}(t) + R_{BINS}^M(t)(s \cdot R_C^{BINS} \cdot r_{C,j} + b_{BINS}) \quad (2.11)$$

where;

$r_{M,i}$ = 3D object coordinates in mapping frame

$r_{M,IMU}(t)$ = time-dependent 3D IMU coordinates in mapping frame, provided by IMU/GPS

$r_{C,f}$ = image coordinate of object in camera frame C

R_C^{BINS} =boresight matrix between IMU body and camera frame C

$R_{BINS}^M(t)$ =time-dependent rotation matrix between body and mapping frames (measured by IMU)

S =scale factor

b_{IMU} =boresight offset vector

λ, ϕ = longitude and latitude measured by GPS

In order to enhance the quality of the geo-referenced image, the direct geo-referencing method has been combined with the traditional method known as aerotriangulation, as reported by Haala et al. (1998, 2000), Mostafa (2002) and Wegmann (2002). Aerotriangulation has been introduced in order to reduce some of the GPS and boresight misalignment problems.

2.4 Sources of Geometric Distortion

In this research study, three sources of geometric distortion were expected, as reported by Skaloud (1999) and Baumker and Heimes (2002) namely: 1) IMU distortion; 2) GPS distortion; and, 3) intrinsic image distortion. The IMU distortion is mainly caused by misalignment between the IMU and camera frame is referred to as boresight. This misalignment will cause coordinates shifting and angular error, which can be determined by calibration, and subsequently an adjustment is made based on the calibration data. Several researchers (eg. Mostafa et al. (2001), Toth (2002), Grejner-Brzezinska and Toth (2004) and Skaloud and Lichti (2006)) have introduced a technique to reduce the misalignment problem, such as the use of least squares (Skaloud and Schaer, 2003) and comparing with aerotriangulation (Grejner-Brzezinska, 2000). Figure 2.11 shows the definition of misalignments.



Figure 2.11: Definition of misalignment in IMU and GPS integration.

The GPS distortion will cause a shift in aircraft position and attitude, which can be minimised by implementing the differential GPS technique (Baroni and Kuga, 2005).

The intrinsic image distortion, such as relief distortion and lens distortion, are other sources of geometric error. These distortions affect the scale and the appearance of the image: for example, a straight road might appear as a curved path in the image. The fundamental approach to mitigate image distortion is by reconstruction of the geometrical plane. Table 2.6 summarises the sources of geometric distortion in this research study.

Table 2.6: Sources of Geometric Distortion.

Source of distortion	Distortion	Effect on Image (distortion)
IMU	Misalignment between IMU and camera frame, effect on shift and angular ($\Delta roll$, $\Delta pitch$, Δyaw)	Scale, Relief distortion, Tangential distortion, Skew
GPS	Platform position and attitude, cause shift and attitude (ΔX , ΔY , ΔZ , $\Delta roll$, $\Delta pitch$, Δyaw)	
Camera calibration	Interior orientation parameters (focal length, principal point, distortion parameters: lens & tilt)	
Miscellaneous distortion	Image coordinate measurement Impact of camera window in pressurised cabin Camera rigidity Topography of earth's surface	

2.5 Summary

This chapter begins with the background low-cost airborne remote sensing systems, and includes discussions of the electromagnetic spectrum, the platform and previous developments. This followed by a brief discussion on low-cost airborne remote sensing instruments, which include optical systems, lidar systems, thermal systems, microwave, radar and the ancillary equipment, namely IMU and GPS. The integration of low-cost airborne remote sensing systems with ancillary data which leads to direct geo-referencing, is given in the next section, before a review of geometric correction by the direct geo-referencing technique. The source of geometric distortion gives a general idea about what to expect in the integrating process. The next chapter will discuss the proposed design of the low-cost remote sensing system for agricultural applications.

3. PROPOSED DESIGN OF LOW-COST AIRBORNE REMOTE SENSING SYSTEM

“Low-cost technology is not a low-cost data, but it means comparatively cheap to build, install and fly...”
(Mascall and Dare, 2005)

3.1 Literature Findings

From the literature review in Chapter 2, it was found:

- 1) The best platform to carry the low-cost airborne remote sensing instrument is a single engined aircraft as it is cheap to hire and easy to find.
- 2) With a low budget, digital camera is the best device for obtaining multispectral.
- 3) An IMU based on a linear accelerometer or gyro-free IMU is able as appropriate motion monitoring system.
- 4) Low-cost GPS equipped with WAAS facilities gives accurate position measurements.
- 5) Boresight misalignment contributes to an additional error to the direct geo-referencing process.
- 6) The algorithm used to solve the geometric issues via direct geo-referencing method is focused on vertical and tilt images. A traditional method (bundle adjustment and triangulation) is selected for processing the oblique image.

These six major issues will be addressed in this chapter and solutions developed. It begins by introducing the design objective and is followed by the design layout for the low cost remote sensing system, which presents an alternative to platforms

currently available. Subsequently, the devices selected for the proposed system are described. The characteristic of each of the devices is explained in detail together with justification and rationalisation for their selection. Since the system is new to airborne remote sensing, there is very little information on using it for airborne remote sensing applications, and consequently the quality of the data from the receiver is unknown. The expected errors of the selected devices and their minimisation are also discussed in this chapter. Based on the discussions within this chapter, a mathematical model is developed and discussed in Chapter 4.

3.2 Design Objective

The main objective of the proposed design is to reduce the cost of airborne remote sensing through the introduction of a portable system requiring no structural modification to the aircraft. The application of the portable remote sensing instrument has been driven by the potentially low-price compared to the satellite originating remote sensing system such as Daedalus, CASI, and CHRIS. Appendix A lists most of the imaging sensors used in airborne remote sensing systems.

The project objective is achievable with advanced technology in the manufacturing sector, which is able to reduce the size and complexity of the equipment. The advances in Micro-Electro Mechanical Systems (MEMs) technology using machine-based micro-fabrication techniques to assemble the small mechanical or electronic parts of the instruments, enables material and labour costs to be reduced and hence the production of high quality but cheaper equipment. The total expected cost of the proposed design is listed in Table 3.1.

Table 3.1: Estimated cost of proposed low-cost airborne remote sensing system

Item	Cost £
IMU (Non-Gyro IMU)	800.00
Low-cost GPS	100.00
Agriculture Digital Camera	1000.00
Cessna single engined aircraft (Charter) @ £185 per hour	100.00
Software for processing	100.00
Total (all costs in GBP)	2100.00

Note: The prices are based on receipts and company quotation.

3.3 Design Layout

As the objective of this design is to propose a portable remote sensing system, which is light, and easy to install, it needs a layout plan to explain how this portable system is going to work. Ideally, the portable system should have a pilot and a single operator to handle the instrument. However, for this research study, two operators are needed: 1) navigator who points the imaging device at the target object, and 2) data manager for the whole system. Figure 3.1 shows the proposed design of the low-cost remote sensing system for the research project.

Theoretically, the equipment of a low-cost remote sensing system should simply consist of a navigation system and an imaging device. As normal navigation system is used to track the location and the attitude of the platform, whereas in the portable equipment, it is used to locate the position and the attitude of the imaging device. This is a significant change, and has been employed in order to avoid boresight misalignment, as discussed in Chapter 2.

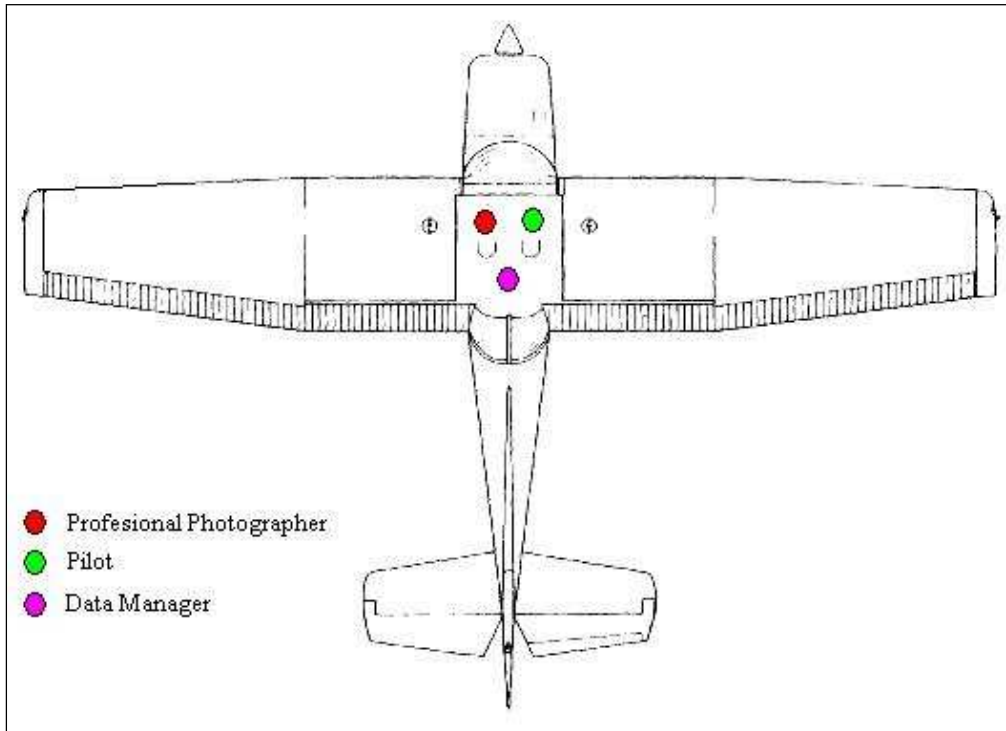


Figure 3.1: Layout of cabin crew positions for replacing fixed installation

3.4 Selection of the Devices

The portable remote sensing system needs to be small, light and easy to carry but able to give an equal level of quality to the current low-cost imaging devices. With the plug and play generation, an electronic engineer is no longer required to connect remote sensing sensors to computers when building bespoke systems. Generally, the airborne remote sensing system requires:

- 1) an imaging device for image acquisition;
- 2) a navigation device to measure attitude and position of imaging device;
- 3) a data storage device.

All these devices can be connected to each other through fire-wire cables or wireless connections, such as Bluetooth, which enables the data to be transferred at high speed without the need of additional support hardware.

3.4.1 Low-cost Inertial Measurement Unit

The low-cost IMU which has been identified for inclusion in this proposed design is a non-gyroscope linear accelerometer device. This device is preferable because it is fast, essentially drift-free and the dynamic errors due to force and angular rate are reduced to small values (Merhav, 1982). Secondly, this device is far cheaper than IMUs with gyroscopes and accelerometer, and it is small, which enables it to be attached to the imaging device.

Specifically, the eGyro-XP (PCFlightSystems) IMU has been selected. In it, there are three solid-state electronic gyroscope equivalents, three solid-state accelerometers and a micro-controller. The ‘gyroscopes’ sense the rate of rotation of the moving body (imaging device) around the roll, pitch and yaw axes. The accelerometers sense the acceleration of the moving body (imaging device) along these axes and also sense the orientation relative to the earth. The micro-controller converts the gyroscope and accelerometer signals into digital signals.

All these components are wire bonded onto an electromechanical circuit board. The electromechanical circuit is a board contains: 1) mechanical parts (gyroscope and accelerometer); and, 2) electronic parts (integrated circuit and micro-controller). Figure 3.2 shows the electromechanical circuits fixed on the interface board. Each of the electromechanical circuits is arranged with regard to the axes of the moving body. X-direction is a wing direction moving up and down, Y-direction is nose direction moving up and down and Z-direction is the heading direction.

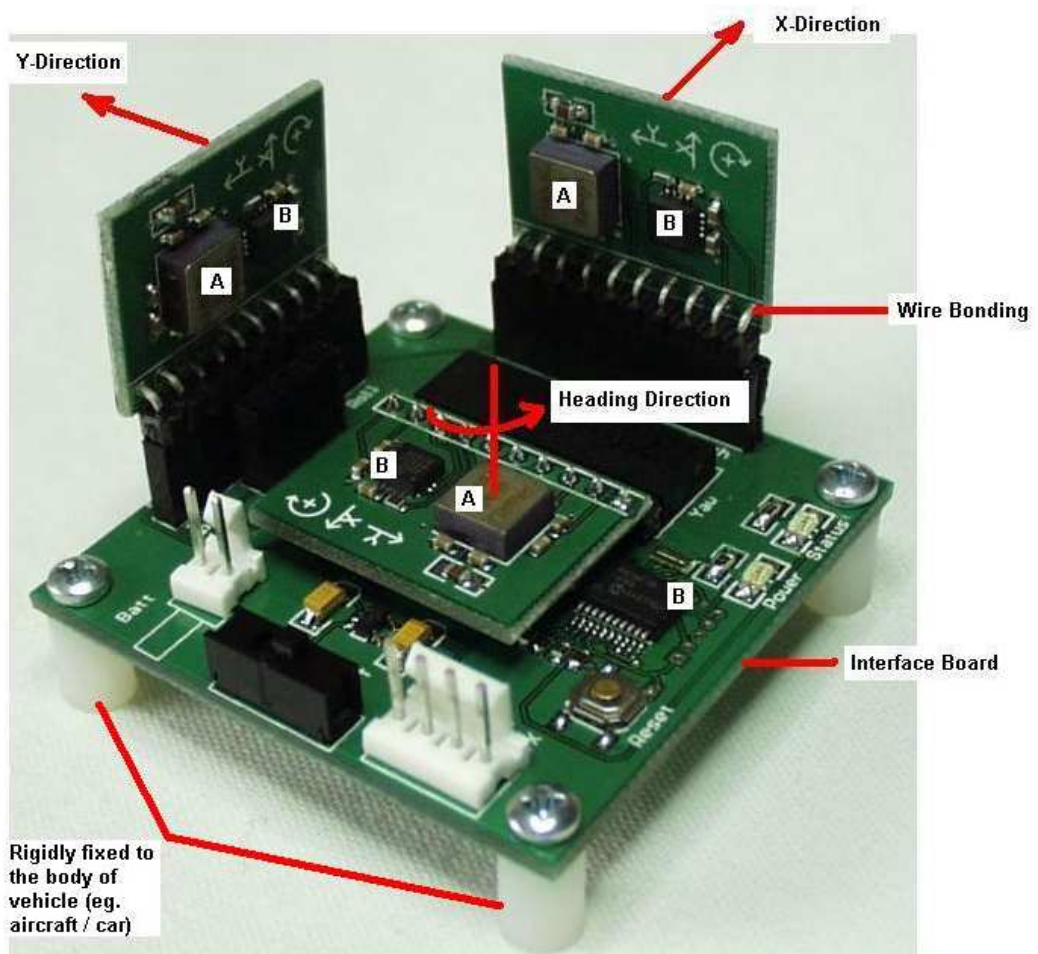


Figure 3.2: Electromechanical ('A') and Micro Controller ('B') assembled together on interface board.

A. Mechanical Part

The mechanical part contains vibration mechanical elements (proof-mass) to simulate the body (imaging device) acceleration. This acceleration is measured by an electrodes sensing element, which is placed on both sides of the proof-mass (see Figure 3.3). These sensing electrodes are connected to micro processors on a circuit board in integrated circuit units (ICs) to process the force and angular rate data before transmission to a data storage device. The IMU has been designed with a lateral comb on both sides, surrounded by a silicon frame boundary, banded to a glass substrate. There is also a suspension beam on the four corners of the mass, which functions as a spring to return the mass to its original position when it is in

stationary. The frame acts like a damper and limits the proof mass from outrange acceleration. The mechanical system is manufactured using micro-fabrication technology (using micro-machined silicon) and mounted on a nonconductive material such as glass.

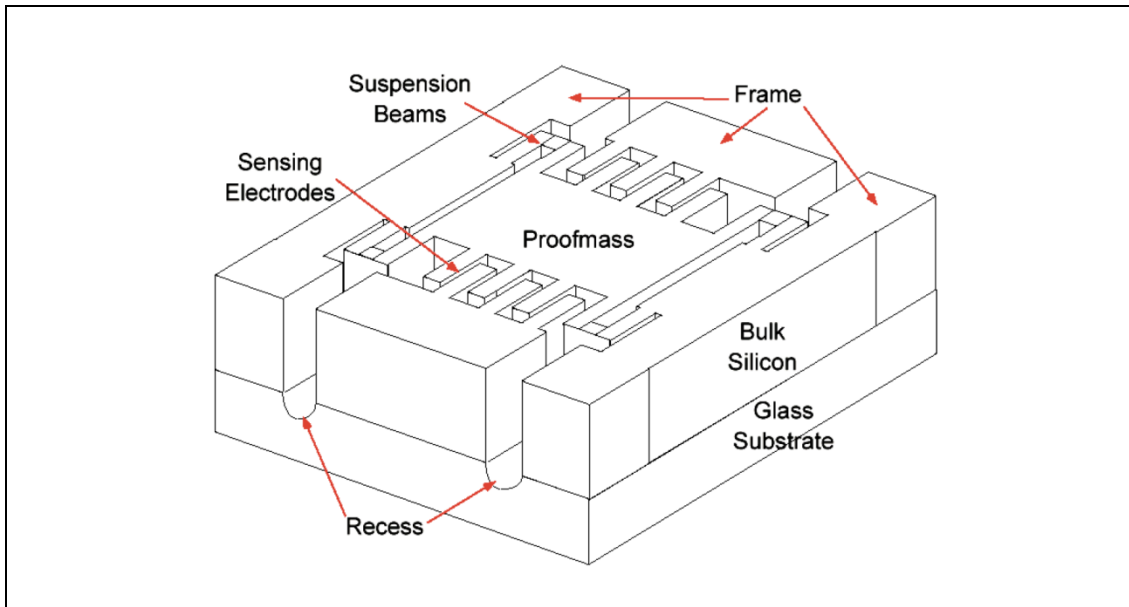


Figure 3.3: Mechanisation of micro-machined IMU accelerometer

The ‘gyroscope’ measures angular rate by using the Coriolis acceleration¹ concepts introduced by Hulsing (1998). It is based on the energy disturbance caused by Coriolis acceleration. In most cases, an electric power supply, such as a battery, is used to generate the energy (magnetic) field. These energy fields create a potential difference between the proof-mass and the sensing electrodes. Any change in movement by the freely moving mass will disturb the magnetic field. This

¹ Coriolis acceleration, named after the French scientist and engineer, G. G. de Coriolis (1792–1843), is an apparent acceleration arising in a rotating reference frame and is proportional to the rate of rotation (Figure 2.5) (Nasiri, 2000).

disturbance will be recorded by an on-board microchip on the interface board, which interprets the disturbance of the electric signal and translates the signals into an angle of movement. The translation is developed from the corresponding inertial force equation (3.1) as follows:

$$f = ma \quad 3.1$$

where,

f = force (known parameter, calculated from $x = f/k$)

m = mass (known parameter)

a = acceleration

x = mass displacement

k = gap constant

This force acts on and displaces the mass a distance $x = f/k$, where k is the gap constant between sensing electrodes and the mass (see Figure 3.4). The sensor's output is related either to the mass displacement or to the internal force required to accelerate the mass, both of which are proportional to the applied acceleration. The equation (3.1) is then multiplied by the Coriolis equation (Figure 3.5) to produce the Coriolis force. The multiplication result is shown in equation (3.2).

$$f = 2mVx\Omega \quad 3.2$$

where,

f = Coriolis force

m = mass (known parameter)

Ω = angular velocity

V = velocity of particle (easting, northing or up/down axis)

The rotation angle (roll, pitch and yaw) has now been derived from this equation (3.2) in terms of the angular velocity which is related to the angular rate multiplied by the rotation angle, as in equation (3.3):

$$\Omega = w\varphi \quad 3.3$$

where,
 w = angular rate
 φ = rotation angle (roll, pitch or yaw)

Since each axis has its own mechanical device, V can be eliminated and the equation for determining the rotation angle is:

$$\varphi = \frac{f}{2mw} \quad 3.4$$

where,
 φ = rotation angle (roll, pitch or yaw)
 f = Coriolis force
 m = mass
 w = angular rate

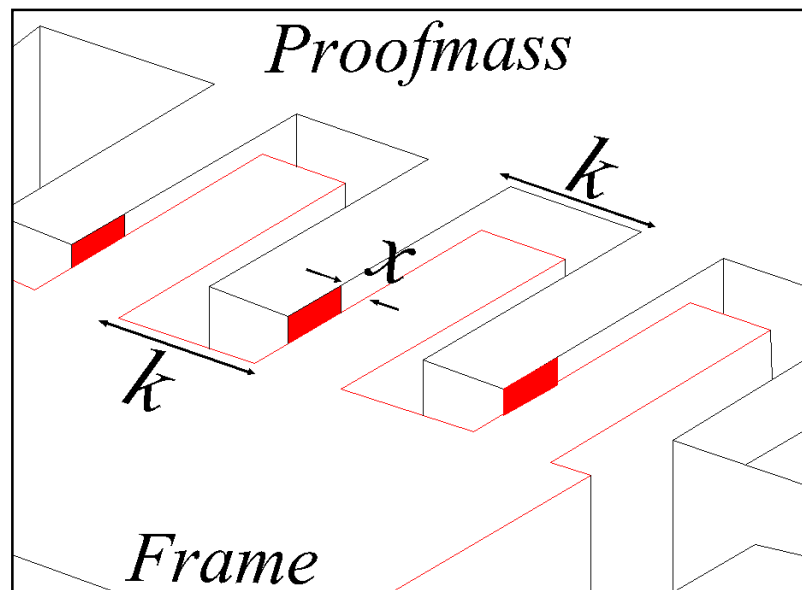


Figure 3.4: Relationship between force, mass and acceleration.



Figure 3.5: Coriolis accelerometer concept

B. Micro-Controller

The micro-controller is a microelectronic semiconductor device which places the transistors, resistors, capacitors and all the connecting wiring onto a single crystal (or 'chip') made of semiconductor material such as silicon and germanium. A micro-controller can be classified as a medium to process analogue, digital or mixed signals. While operating, the micro-controller changes the signal in some manner, such as converting the signal into some other format, such as a digital signal or modifying it in some other way. These digital signals are then processed using algorithms and sent over a serial communication cable to the data logger.

3.4.2 Low-cost GPS

Three low-cost GPS devices were selected for locating the imaging device, namely 1) Garmin 76 GPS, 2) Garmin eTrex GPS and 3) Holux wireless GPS. All of these GPSs are equipped with Wide Area Augmented System (WAAS) which promises ± 3

metres of positioning accuracy. This can be an alternative solution for a low-cost GPS receiver to obtain differential GPS data. The WAAS has been developed by the Federal Aviation Administration to enable small aircraft to have better safety during landing and takeoff. The term WAAS is used in the United States, in Europe it is called European Geostationary Navigation Overlay Service (EGNOS) and in Japan the term Multi-Functional Satellite Augmentation System is used. These three systems are compatible to each other and the generic term SBAS (Satellite Based Augmentation Systems) is used by the International Civil Aviation Organisation (Kohne and Wobner, 2009). In this thesis, the term SBAS is used for all these system.

The importance of SBAS is its capability for improving the GPS vertical and horizontal positional data. The SBAS consists of geostationary satellites and ground reference stations. The latter receive GPS signals and determine if any errors exist. If there is judged to be an error, the correction is computed and sent to the geostationary satellites via a ground uplink system at the reference stations. Finally, the geostationary satellites transmit the correction to the individual receiver. This correction can only be received by a receiver with the SBAS capability.

Garmin 76 GPS

One of the selected GPSs is Garmin 76 GPS, and as it has SBAS capability, it has the capacity for differential GPS measurements. The accuracy claimed by the manufacturer is ± 15 metres without differential GPS, $\pm 3-5$ metres with differential GPS and less than ± 3 metres with SBAS correction. It has 12 channels which means it is able to lock on to up to 12 satellites at a time with a fast update rate of 1/second.

Interfacing can be made via NMEA 0183 and RTCM SC-104 differential GPS to a data logger, such as personal data assistant, laptop or field electronic book. It also has an external antenna, which is small and can be attached to any small space within the aircraft. From the internet review, it can be said that this device is rugged, accurate (2 metres with external antenna), full function and easy to operate (Garmin, 2001; Mehaffey and Yeazel, 2004).

Garmin eTrex

The main reason for selecting this GPS is its high-sensitivity. The high-sensitivity enabled the position to be located quickly, precisely (2 metres accuracy at best) and is able to maintain its GPS location even in heavy cover and deep canyons. It is also SBAS capable which enables better accuracy. The track-log is very good compared to the Garmin 76 GPS, and therefore the travel print can be traced-back more easily. The manufacturer claims an accuracy of ± 15 metres without differential GPS, $\pm 3-5$ metres with differential GPS and less than ± 3 metres with SBAS correction. It has 12 channels which means it is able to lock onto up to 12 satellites at a time with fast update rate at 1/second. Interfacing can be made via NMEA 0183, RTCM SC104 differential GPS and proprietary Garmin eTrex to a data logger such as a personal data assistant, laptop or field electronic book.

Holux wireless GPS

The main advantage of using this GPS is that it does not need to be tethered by cable or wire to connect with the data logger, and provides real time navigation for location based services. It is also SBAS capable, which ensure that it is able to obtain high level of accuracy. The manufacturer claims that the accuracy is ± 10 metre without

differential GPS, $\pm 1-5$ metre with differential GPS and less than ± 7 metre with SBAS correction. It has 20 channels which means it is able to lock on to up to 20 satellites at a time with fast update rate at 1 Hz/second. Interfacing can be made via NMEA 0183 protocol and SiRF binary code to a data logger such as personal data assistant, laptop or field electronic book with Bluetooth enabled.

3.4.3 Low-cost Imaging Sensor

The low-cost imaging sensor selected for this study is known as the Agriculture Digital Camera (ADC) illustrated in Figure 3.6. The camera has been purposely designed for the study of agricultural vegetation canopies by farmers, agronomists, crop consultants, viticulturists and agricultural engineers. The study of vegetation canopies is useful in precision agriculture for differentiating, monitoring or planning the crop management. It has a 1.3 megapixels digital camera with three bands; red, green and near infrared. The ADC is a single lens camera featuring a Motorola CMOS (Complementary Metal Oxide Semiconductors) areal array that generates 1280 x 1024 pixels when equipped with a Bayer mosaic filter. The resulting colour image can be seen directly on tiny screen fitted to the back of the camera and is stored on a flash card (Petrie, 2003). The output image can be stored in two types of format which are; JPEG (Joint Photographic Experts Group) and raw data format with .DCA extension. The true colour composite image is stored in JPEG format while the monochrome (black-and-white) image is stored in raw data format with .DCA extension. The image format is interchangeable by using appropriate software such as PixelWrench and Briv32, which are included in the imaging packages. These software are able to extract NDVI, SAVI, IPVI and NIR/G index data in grayscale or colorized format.

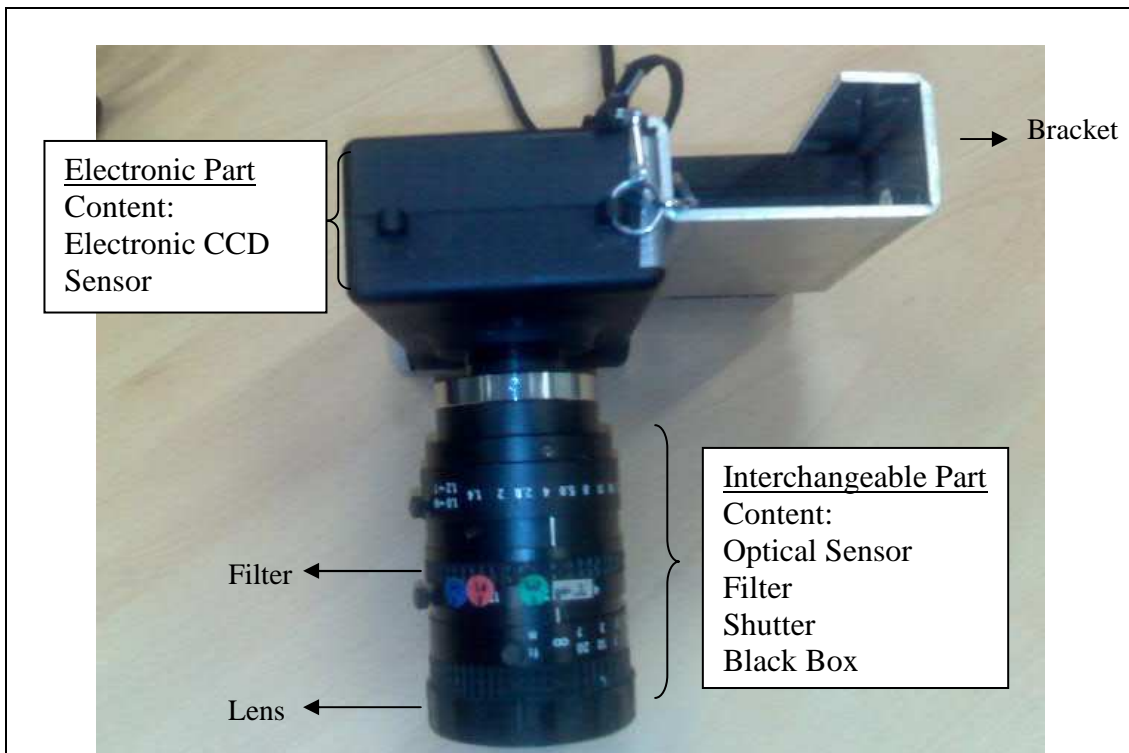


Figure 3.6: ADC compartment

3.4.3.1 Generating Colour Composite Image by using Single Shot Imaging Device

There are three methods used in single sensor imaging for generating colour images which are; mosaic filter, rotating filter wheels and beam splitter. The rotating filter wheel and beam splitter have been used by the Airborne Multispectral Digital Camera and Redlake Multispectral camera respectively.

The rotating filter wheel method (see Figure 3.7a) will generate two to five separate colour images with between 80% to 98% overlap. These images need to be rectified in order to register the individual images into their exact position for creating the final colour composite images. The advantage of this method is that the user can obtain either separate colour images or colour composites.

The beam splitter method (Figure 3.7b) splits the spectral bands through the beam splitter and colour separating prism that are located immediately behind the lens. As a final result, the user can obtain separate colour images or colour composites.

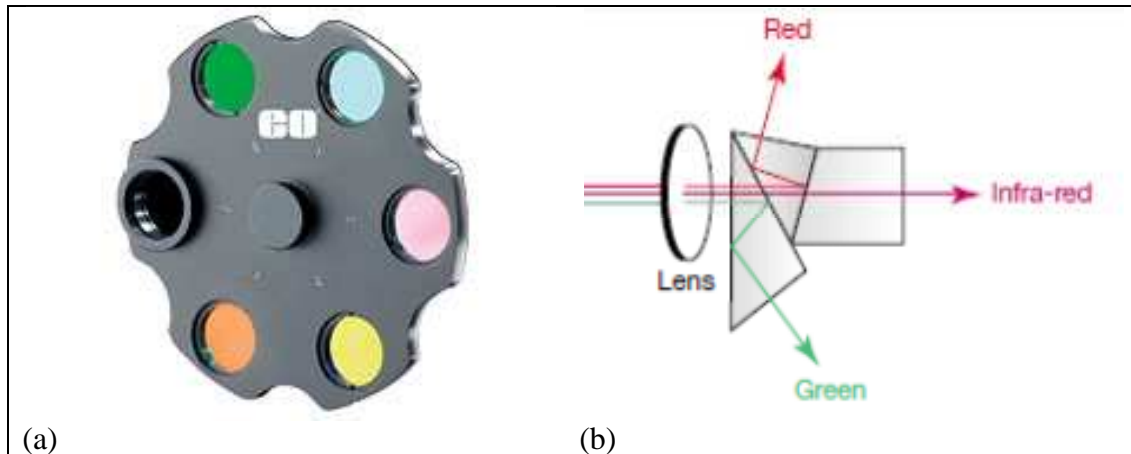


Figure 3.7 : Device that been embedded into single sensor imaging for generating colour composite images. (a) the rotating filter wheel and (b) the beam splitter with colour separated prism.

The mosaic filter or Bayer mosaic filter is the most popular method for generating colour composite images using a single sensor imaging device such as ADC and Kodak's DCS series. The Bayer mosaic filter comprises an RGB filter mask applied to a standard grey or monochrome sensor. It is placed either in front of the sensor chip beneath a micro lens, as illustrated in Figure 3.8, or in some systems the filter is inserted behind the lens in the optical path (Wrotniak, 2004). The mosaic filter is made up of a two-dimensional array of photosensitive detectors. On each element of the array only red, green or near-infrared waveband are captured (in-case of ADC device). This filter mosaic red (R), green (G) and near infrared (NIR) are then recorded in alternating rows of RG and GNIR. There are twice as many green filters as red and near infrared. Figure 3.9 shows the arrangement of Red, Green and near infrared resulting from the use of the Bayer mosaic filter. Details discussions on mosaic filter have been given by Lukac (2008).



Figure 3.8 : The architecture of single shot imaging device.

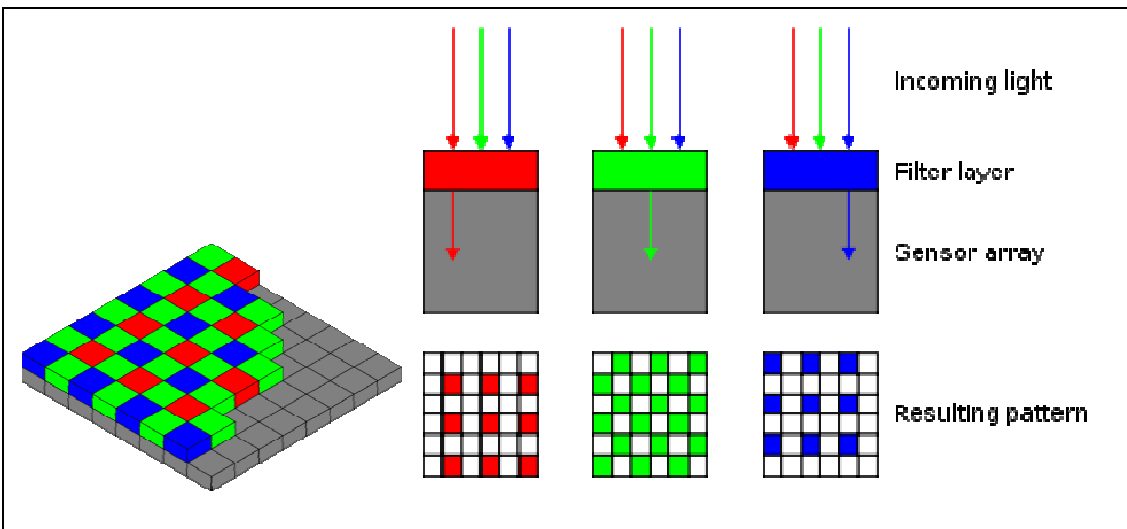


Figure 3.9 : The Bayer mosaic filter

To produce the final colour image, each element on the array photosensitive detectors should have a red, green and near infrared. An interpolation technique such as nearer neighbor, BiLinear, BiCubic, Spline, Laplacian and adaptive interpolation can be applied for this purpose. In this research project, the interpolation technique

is not being discussed because it is achieved using specific software which comes with the single shot imaging device packages.

The specific software not only processes the colour images but also the monochromatic images or black-and-white images. Using the ADC sensor the monochromatic images can be obtained by setting the digital imaging device into monochromatic mode. Subsequently, the filters (red, green and near infrared) produce a grayscale value proportional to the amount of red, green and near infrared light reaching the photosensitive detectors. The images taken in monochromatic mode are stored in raw digital format and specific software is required to open them. The raw files contain the image pixels and image metadata, such as camera model, serial number, shutter speed, aperture, focal length, navigation data and some other additional information that is recorded during the image acquisition process. All the recorded data (colour images or raw images) can be saved to a compact flash card, so that it can be downloaded later for processing purposes or saved directly to a portable computer through data streaming. In most single shot imaging devices, including the ADC, the captured image is labelled with the date and time of acquisition, as this information is important in any remote sensing system (Mascall and Dare, 2005).

3.5 Justification of Selected Devices

The foremost consideration with respect to the selected devices is the image resolution. Image resolution describes the detail apparent in an image and depends on the pixel resolution and the spatial resolution of the imaging sensor. Dabney and Deering (1998) have found that an effective imaging sensor for use in a low-cost remote sensing system should have a minimum image size of 1.3 mega pixels.

However, the spatial resolution determines the ideal size of an object to be discernible in the image with that particular size of pixel. The spatial resolution depends primarily on the Instantaneous Field of View (IFOV). In this research study the specification of the single shot digital imaging device used is shown in Table 3.2.

Table 3.2: Specification of ADC single shot CMOS imaging device.



Source: Swain et al., 2007.

From the specification information in Table 3.2, the approximate ground resolution (GR) or ground sample distance (GSD) at 1000 feet (304.8 metres) can be obtained as follows:

Step 1: Conversion pixels to mm;

$$\text{Width (mm)} = \frac{7.7}{1280} = 0.006 \text{ mm} \approx 6 \text{ micron / pixel} \quad (3.5)$$

$$\text{Height (mm)} = \frac{6.1}{1024} = 0.006 \text{ mm} \approx 6 \text{ micron / pixel} \quad (3.6)$$

Step 2: Calculation of Instantaneous Field of View (IFOV) angle:

$$\frac{1}{2} \text{ IFOV} = \text{Tan}^{-1} \left[\frac{0.006 * 640}{8.5} \right] \quad (3.7)$$

$$\frac{1}{2} \text{ IFOV} = \text{Tan}^{-1} [0.45176470]$$

$$\frac{1}{2} \text{ IFOV} \approx 26^\circ \approx 0.42432048 \text{ rad}$$

$$\therefore \text{ IFOV} \approx 52^\circ$$

Step 3: Calculation of GR or GSD

GR or GSD refers to the smallest size on the ground that can be apparent on the image and it can be determined as:

$$\begin{aligned} \text{GSD(m)} &= \frac{(304.8 * \text{Tan} (0.42432048))}{640} \quad (3.8) \\ &= 0.2151529 \text{ metres} \end{aligned}$$

or it can also be calculated by using (Neumann, 2008; Comer et al., 1998);

$$\begin{aligned} \text{GSD(m)} &= \left(\frac{304.8}{0.0085} * 0.000006 \right) \quad (3.9) \\ &= 0.2151529 \text{ metres} \end{aligned}$$

The correlation between GSD and map scale can be interpreted by equation 3.10 (Comer et al., 1998), whereby;

$$GSD(m) = resolving_capability_x_Map_Scale \quad (3.10)$$

then the scale is;

$$Scale = \frac{GSD}{resolving_capability} \quad (3.11)$$

$$Scale = \frac{215mm}{0.1mm} = 2150$$

The value of resolving capability of human eye can be taken as 0.1mm (Koh, 2007) or 0.3mm (Comer et al., 1998). The resolving capability is considered as the smallest pixel or dot that can be seen by the human eye on the output (either on screen or paper) for the particular image. Equation 3.10 is similar to equation 3.12 which has been introduced by Foster (1985) if 3×10^{-4} metres (0.3mm) is consider as the resolving capability of the human eye.

$$P_m \leq 3 \times 10^{-4} S_m \quad (3.12)$$

$$0.21 = 0.0003 \times Map_Scale$$

$$\therefore Map_Scale = \frac{0.21}{0.0003} \approx 700$$

but if the resolving capability of the human eye is 0.1mm then the map scale would be 2100. Therefore, it can be said that the smallest scale for that particular image is 1:2100 while the largest scale for that image will be 1:700.

For future reference:

P_m is pixel size of image data

S_m is the map scale

However, although, the scale become an irrelevant factor when dealing with the digital images (Comer et al., 1998), because digital images are not photos, it can be an indicator for the quality reproduced images.

The second constraint of the ADC imaging device is the CMOS micro lens that is located above the photosensitive detectors along the optical path. The problem of the CMOS micro lens is that it might result optical crosstalk. Optical crosstalk is where an image sensor degrades the colour separation when light entering at angles other than orthogonal, passes through a filter and is partially be absorbed by the adjacent pixel rather than one vertically the lens below the lens (Agranov et.al., 2003). As a result the particular pixel might have poor colour separation. However, this may be a minor problem because in remote sensing the determination of object in an image is done by analysing a group of pixels. Furthermore, it is unlikely that a single pixel represents a single object.

The third constraint on the selected devices is the capability of the low-cost IMU to measure the angle on the nominally horizontal axes. It is noticeable that the maximum angle this axes can be tilted is ± 3 degrees to produce a vertical image, as mentioned in Moffit and Mikhail (1980). The advantage of the vertical image is that it can be readily converted to create a map, because the radial distortion is minimum and the relief distortion is minimum at the centre of the image and increases in an outward direction from the centre.

The final constraint on the selected devices is the capability of the low-cost GPS to measure the position of the location. The best accuracy which can be achieved by the low-cost GPS is ± 1 to 2 metres with the use of the Wide Area Augmentation System (WAAS) (see European Space Agency, 2006). Since all the GPS devices selected have WAAS capability, it therefore justified their choice..

In this study, it is estimated that the final accuracy of the end product will be ± 3 metres, of which the major errors will be due to the low-cost GPS which has an accuracy of 2 metres, followed by the pixels size, which is 0.2 metres at a flying height above 304.8 metres (1000 feet). This accuracy is adequate in precision agriculture and moreover, it is much better than the satellite imagery data such as LandSat, TiungSat and Micro-Satellite which produce ± 30 to 80 metres accuracy. However, the accuracy cannot be achieved if the systematic and random errors in the selective devices have not been minimised appropriately. Examples of these systematic errors are lag in data delivery, shutter actuations and GNSS output frequency, while random errors are unpredictable events that occur during the acquisition process. These errors can be identified through experimental investigation- see Chapter 6.

3.6 Expected Data Type

It was anticipated that the imaging device data would be in raster data format, the IMU device would provide ASCII data format according to ARINC 705, whilst GPS devices would provide ASCII-based NMEA 0183 data format and binary data written in ASCII-based RINEX data format.

The imaging device stores the acquired images in DCA (Digital Camera Format), which is a compressed file that can be un-compressed and transferred to Bitmap format. An alternative data format for the IMU is 'raw signal' data which can be obtained by using an oscilloscope device. Obtaining IMU data by using this device (oscilloscope) is not included in this thesis.

There is no other alternative for storing GPS data, as low-cost GPS devices are restricted to NMEA 0183 data format (output). Fortunately, research by Hill et al., (2002), shows that GPS raw data can be retrieved by using a force algorithm such as embedded in the GRINGO software, even though success is not guaranteed. This software enables the GPS raw data to be stored in RINEX format. The GPS data (in RINEX format) is used for differential processing.

It very important to determine which data format is required for each task as some tasks cannot be performed if the data format does not match the required processing requirement format. For example, GPS with NMEA 0183 data format is not compatible for differential processing. Table 3.2 lists the data protocols and their message types.

Table 3.3: List of data protocols available for GPS



(Source: Yan, 2006)

3.7 Expected Errors of Selected Devices

Error has been classified as the imperfection of the measurement (Paine and Kiser, 2003) and can be caused by technical aspects, the working conditions, the operation or the instrument itself. For example, a personal computer such as laptop, is not able to work properly under high pressure conditions, and some researcher have experienced problems where it was not possible to unable lock onto a GPS signal for this reason. The GPS signal can also be obstructed by parts of the aircraft body. The causes error are minimised by setting up an appropriate procedure or sequence during measurement process, but this does not guarantee that the measurements are

free from error. Based on previous research, there are several typical errors which are common in the devices selected, which can be grouped as illustrated in Table 3.4.

Table 3.4: Typical errors occurring during measurement process

Instrument(s)	Typical Error
Low-Cost IMU	Biases
	Scale factor
	Noise
GPS	Satellite Clocks
	Orbit Errors
	Ionosphere
	Troposphere
	Receiver Noise
	Multipath
ADC Sensor	Lens distortion
	Relief distortion

3.7.1 Low-cost IMU Error

The errors typical of a low-cost IMU are known as: 1) bias, 2) scale factor, and 3) noise. These errors can be expected to accrue in the navigation data due to the dynamic noise of the accelerometer output (Ding and Wang, 2005) and can be revealed by a self-determination test process. In this method, the instrument is placed under conditions where the instrument's errors are zero. At the end of the test, output values plotted on a graph and the likely errors identified. Figure 3.10 illustrates typical errors in the low-cost IMU instrument.

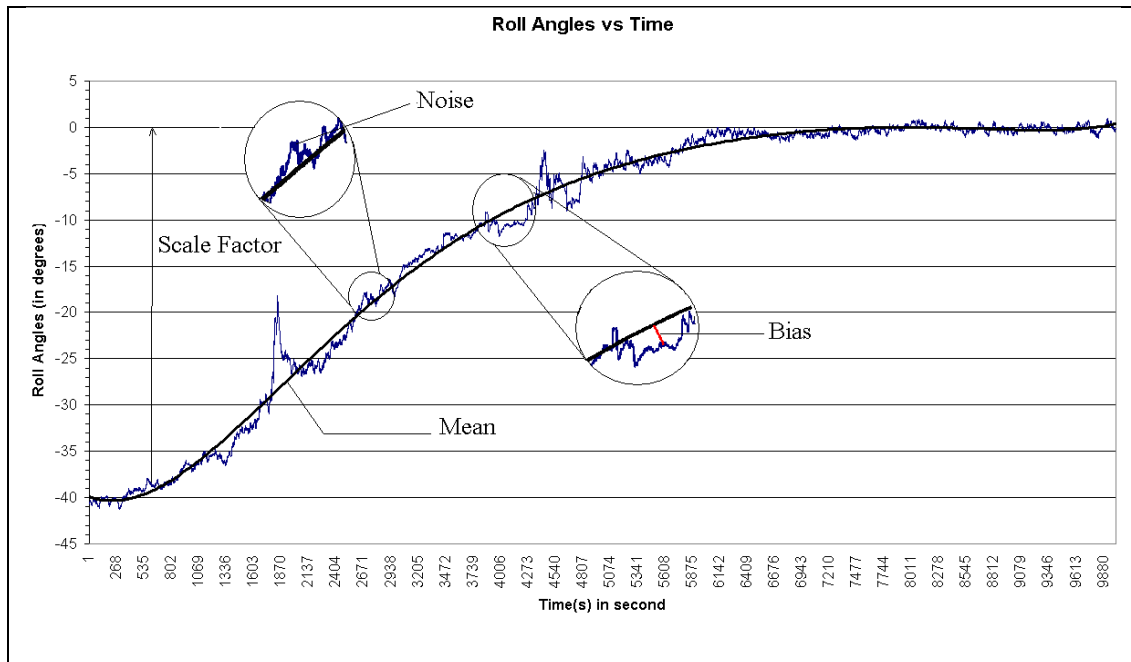


Figure 3.10: Typical errors in low-cost IMU

3.7.2 Low-cost GPS Error

Investigations on GPS error have been carried out since the first receiver was invented. Most researchers, for example, agreed that the GPS contains errors mainly caused by: 1) ionosphere and troposphere delays; 2) receiver clock; 3) ephemeris orbit; 4) multipath; 5) number of satellites; 6) satellite geometry; 7) selective availability (removed in 2000); 8) antenna bias, and 9) processing algorithm used.

Table 3.4 summarises the main GPS error sources. Some can be reduced by processing techniques, such as the differential technique, and some are not applicable. It is assumed that the three selected low-cost GPS receivers have a similar pattern of error since they share the same navigation satellites, and further explanation of these errors will be discussed in Chapter 6.

Table 3.5: Summary of GPS Error Sources



Source: Trimble (2007)

3.7.3 Low-cost Imaging Sensor Error

The imaging sensor error may be due to a variety of factors, including one or more of the following: 1) perspective error, 2) motion scanning error, 3) stability of platform, 4) terrain relief, 5) radial distortion, 6) the microlens and 7) curvature and rotation of the earth. Some of these errors can be cancelled out in the appropriate equations, some can be ignored because the error is not significant, and some need further considerations. These errors are treated as either systematic or random. Systematic error correction is carried out if the displacement's parameter can be determined. If this is not possible, the error will be treated as random and the nature of the error is studied to determine if there is any pattern which enables adjustment or reduction.

3.7.4 Data Synchronisation Errors

An integration error occurs when combining two sets of data captured from different devices, such as IMU and GPS, which may result in missing data. There are several factors which cause missing data, such as during signal outages, receiver power failure or when the minimum interval recorded does not meet specific requirements. In this study, the IMU output is integrated with the GPS velocity data. This is calculated from the difference of two positions obtained by the Differential Global Positioning (DGPS) technique at Δt , where Δt is the time difference between the two positions.

The combination of drift, scale factor, random fluctuation and bias in the IMU is known as cohesion error. Even though the estimated position produced by the IMU is deemed of appropriate accuracy, the internal cohesion error of the IMU device has to be compensated for this can only be achieved if it is known. Therefore, a laboratory investigation was undertaken to investigate the internal cohesion error of the IMU device and all other devices used in this study (see Chapter 6).

3.8 Error Optimisation

Error optimisation is aimed at minimising the unwanted signals which influence the IMU and GPS observation data. For instance, the dither spike and noise in the IMU and GPS data, has to be removed from the observation data. Since all the errors in the IMU and GPS data (as mentioned in the previous section) are accumulated from different error sources, it is therefore difficult to trace and correct the error of each individual source. The most effective way to minimise the error is by using a modelling and estimating method.

It is frequent in modelling to employ a statistical approach, because this gives a measure of the quality of the observation. Based on the resulting indication, the IMU and GPS errors are estimated, and these values are used to compensate the raw data. The most popular modelling and estimating method is known as Kalman Filtering.

3.9 Summary

This chapter has given an overall idea of the low-cost remote sensing system for use in an agricultural environment. Then, an alternative to the low-cost remote sensing system, based on portable devices has been set out. These proposed portable devices have been discussed and the justification for the devices selected has been put forward. Furthermore, the expected errors, which may occur during the acquisition process have been identified and the error optimisation procedure has also been discussed in detail. The estimation of these expected errors will be discussed in Chapter 6.

4. DIRECT GEO-REFERENCING

4.1 Introduction

This chapter reveals the technique of direct geo-referencing of digital imagery. It begins with the introduction of the concept of direct geo-referencing, which together with the necessary instruments. The preparation of data has been emphasised as very important, since synchronisation of both intrinsic and extrinsic parameters is crucial input data. Subsequently, the data obtained needs to be cleaned of noise, bias and scale factors. The clean data are then used to estimate any positional information lost due to bad data or signal loss. Next, these data are extracted from the file data to be matched with the image ancillary data. Finally, the reconstruction of the image geometry begins. This starts with minimising the radial distortion which enables the reduction of lens and relief distortion. The image orientation algorithm is then used to correct the orientation of the image before mapping the image it into the user coordinate system

4.2 Concept of Direct Geo-referencing

Geo-referencing can be defined as a process of gaining information about the origin of an image captured from the imagery sensor. The information can be attained by;

- 1) comparing recognisable objects in the image with ground control points; or
- 2) by measuring the position, attitude, velocity and time during the image acquisition.

The velocity is required to interpolate any missing or erroneous data. Gaining the information from the second technique is called direct geo-referencing, and it needs a

navigation device to be installed on-board the platform. This device for example a combined Inertial Measurement Unit (IMU) and Global Positioning System (GPS), is used to measure the exterior orientation parameter. In particular, the exterior orientation gives the initial position and the attitude information of the image centre, while the velocity data is required to interpolate any missing or erroneous data lost during the acquisition process.

As well as the exterior orientation, direct geo-referencing requires the interior orientation parameters of focal length, principal point, lens characteristic, and image scale (Moffit and Mikhail, 1980), together with the pixel resolution, instantaneous field of view angle, ground spatial resolution and altitude. This additional information is used to correlate the relation between image and ground position. Figure 4.1 depicts the representation of direct geo-referencing without the aid of aero-triangulation. In direct geo-referencing, the navigation data (motion data and position data) needs to be reduced to minimise the error then these data will be used as an input parameter together with the principal point, focal length and pixel information to correct the image.

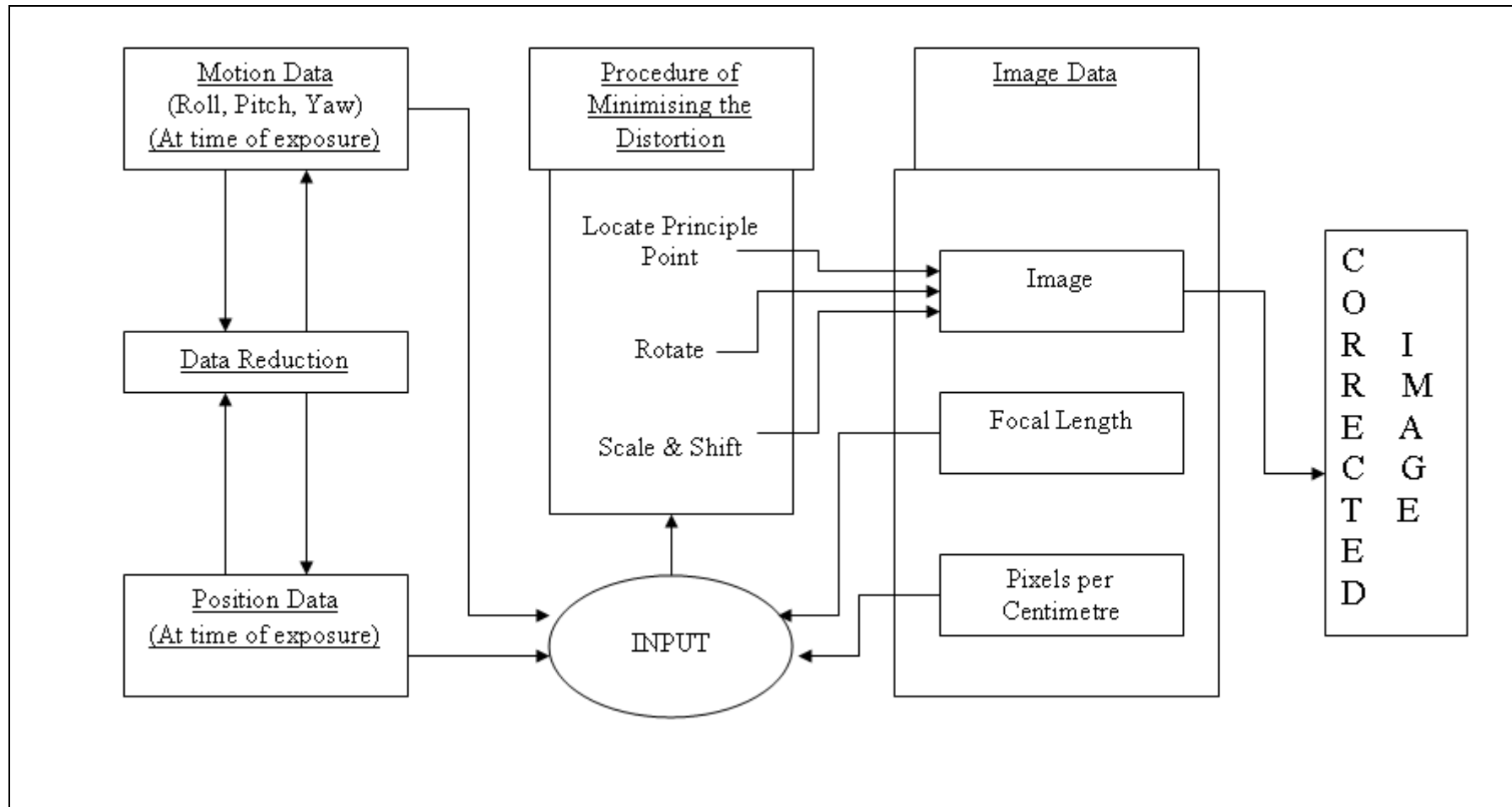


Figure 4.1: Flowchart depicting the geo-referencing process

4.3 Preparation of Data

Data obtained from the navigation device and the imagery sensor has to be ready for the minimisation process before they can be used for the direct geo-referencing process. Since the IMU and GPS data are mixed in one file they need to be separated, and are then uploaded into a spreadsheet for initial preparation, such as converting the roll, pitch and yaw angles into radians. Subsequently, the standard deviation of the roll, pitch and yaw angle are calculated, the latitude and longitude position information extracted from the GPS data, the latitude and longitude (WGS84) converted into the British National Grid reference system, and the synchronisation between image data and navigation data determined. Figure 4.2 illustrates the preparation process for direct geo-referencing.

4.3.1 Pre-processing

The goal of pre-processing is to minimise random errors, especially bias and noise.

There are three steps to be taken:

- 1) Filtering the IMU data: the most effective technique for reducing the random error is by filtering out the incoming high frequency signals (Skaloud, 1999).
- 2) For the GPS, the best technique to minimise the bias and noise in the GPS signal is by using the Differential GPS technique.
- 3) The final output can be improved by a process of approximation and revision technique.

The output from this pre-processing process will provide an input for the direct geo-referencing. Since there will be several sets of data detained at the same time (IMU, GPS and Imagery), a time synchronisation technique is therefore employed.

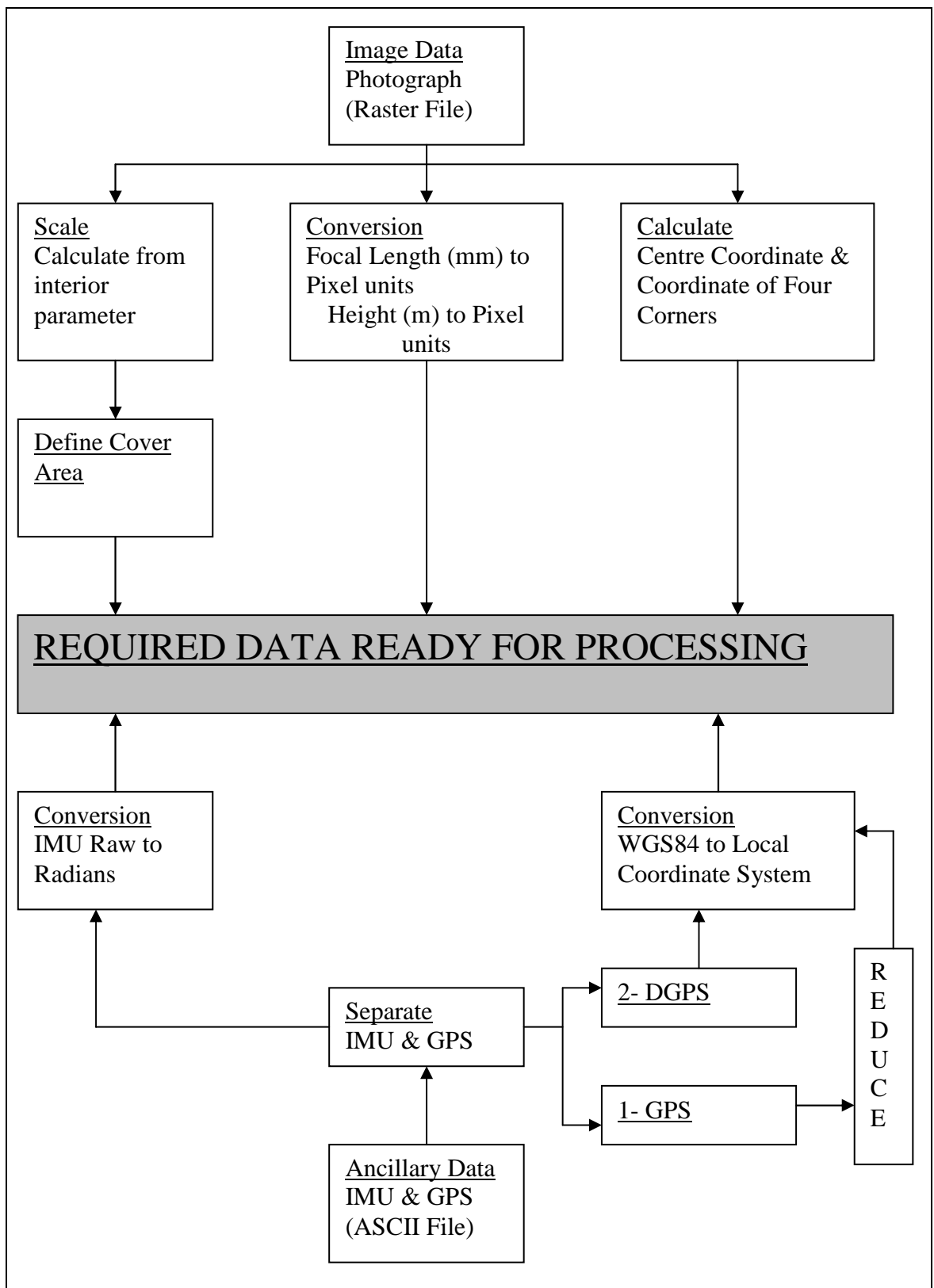


Figure 4.2: Flowchart of the preparation process

4.3.2 Filter

Filtering is the most suitable tool for isolating an error from the data stream. In filtering, a cut-off value is set and any data beyond this cut-off value will be isolated from the data stream. For instance, in mean filtering, the mean value plus a selected interval used as a cut-off value whereby any observation data outside this range will be eliminated and replaced with a new value.

Skaloud (1999) set the cut-off value as $\text{mean} + \sigma_{\text{IMU}}$, whereby IMU data 10% higher than this cut-off value was given a new value (mean value). Zhou (2006) used the bandwidth as the cut-off value, whereby the bandwidth is the difference between the high frequencies and the low frequencies, and any signal exceeding this value was given a new value. In fact, the filter can be designed to suit the IMU device, for instance El-Shimey et al., (2004) designed a federate filter to minimise error in the Honeywell IMU device.

In this study, the main constraint of the IMU data was the fluctuation of the IMU signals, which resulted in a yo-yo pattern in one-second data. To overcome this problem, the IMU data have been segmented into groups. Ideally each of the groups should contain values which are $\pm 2\%$ of the original data. For example, if the data is 75 then the group would not contain any value which exceeds the maximum value of 77 or falls below a minimum value of 74. However, if a data value did not fall within the bounds set for a group then it would be considered as missing data and an interpolation procedure applied to determine an appropriate value for the missing data. Figure 4.3 shows the flowchart of the working procedure to minimise the biases in the IMU data. Figure 4.4 illustrates the implementation of the minimising procedure using a spread sheet.

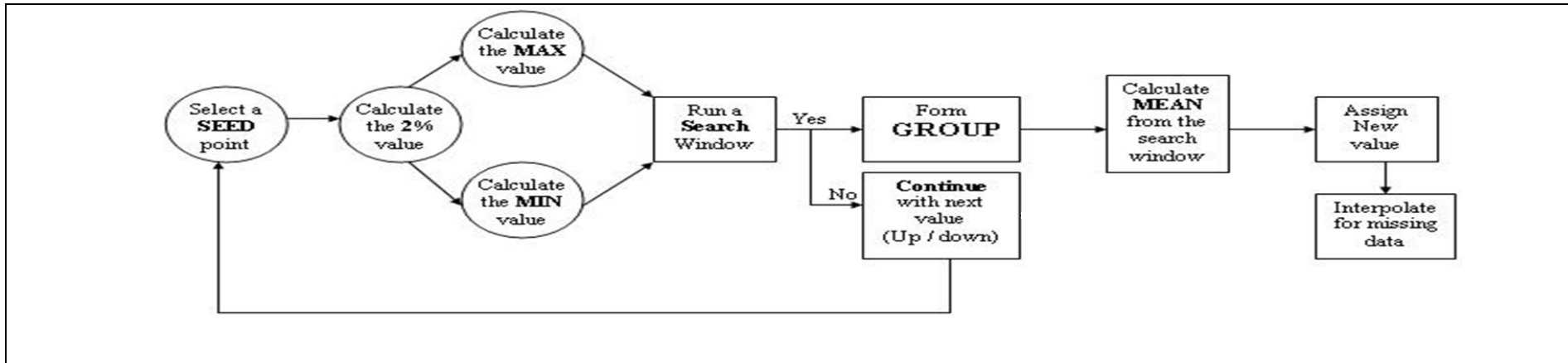


Figure 4.3: Flowchart of the filter working procedure

18907	131719	-62.954	-1.054	247.046					
18908	131719	-62.254	-0.254	247.246					
18909	131719	-64.654	0.554	245.946					
18910	131719	-64.154	1.054	244.946					
18911	131719	-61.354	1.754	243.246	-64.404	0.804	245.446		
18912	131719	-63.754	2.654	240.146	-64.747	1.794	243.400	Max	-67.681
18913	131719	-66.554	3.054	237.046	-65.090	2.784	241.353	"2%"	-1.32707
18914	131719	-63.954	3.654	237.546	-65.434	3.774	239.306	Min	-65.027
18915	131719	-66.354	5.454	235.846	-65.777	4.764	237.260	Mean	5.443
18916	131719	-65.754	5.854	234.846	-66.120	5.754	235.213		0.804
18917	131719	-66.254	5.954	234.946					245.446
18918	131720	-71.754	6.354	232.546					
18919	131720	-71.654	6.254	231.546					

SEED POINT → -66.354 5.454 235.846

Missing Data →

Assign Value →

Search Window →

Figure 4.4: Spread sheet showing the process of filtering

An interval of $\pm 2\%$ was used to ensure that each of the faction contains small dispersion, whereby the small dispersion means that the IMU data has been tightly clustered and large dispersion means that the IMU data is widely scattered. The dispersion can be expressed as;

$$s^2 = \frac{1}{n-1} \sum (x_i - \bar{x})^2 \quad (4.1)$$

where;

- s^2 = sample variance
- n = sample size
- x_i = current IMU data
- \bar{x} = mean of IMU data

This technique has been compared with alternative methods for smoothing dynamic data, such as the moving average and polynomial method as in Figure 4.5. It is found that the polynomial technique tries to average the IMU data in order to create a smooth curve. The moving average has created a wide-gap between the original data and the adjusted data, while in the $\pm 2\%$ method the “yo-yo” has been removed and replaced by new values because it does not belongs to any nearest members in that particular epoch.

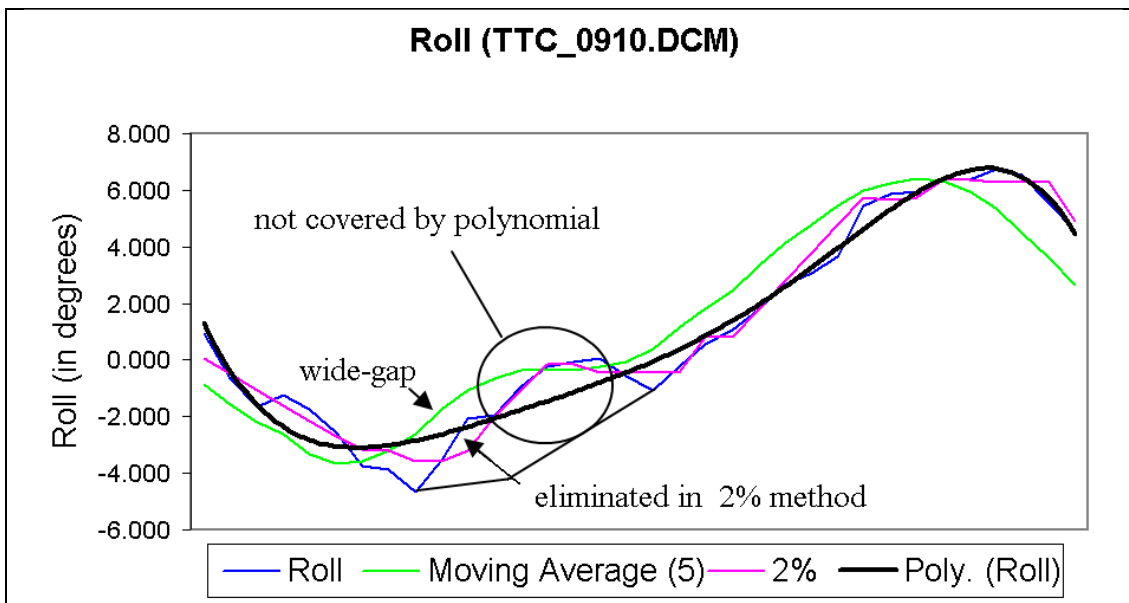


Figure 4.5: Difference between filtering method

4.3.3 Differential GPS

One of the advantages of using the WAAS GPS receiver is that the coordinates given are formed in DGPS fix mode when the WAAS satellites (35, 47, 33, 37 and 39) appear in the orbit. The coordinates from the DGPS fix mode are considered as accurate, which means no further reduction process is needed. In the Garmin 76, the coordinate from the DGPS fix mode is coded as 2 in \$GPGGA NMEA 1813 code, for example. The red column indicates that the coordinates are in DGPS fix mode, if not this column would read 0 (invalid) or 1 (GPS fix).

```
$GPGGA,162422,5106.22,N,42.7275,E,2,10,1.5,738.9,M,47,M, , *41
```

On occasions where the WAAS satellites are not visible at the ephemeris orbit (GPS on fix mode) the DGPS coordinate can be obtained by using post processing software such as GRINGO, Trimble Geomatics Office (Trimble), SKI-Pro (Leica) and Javad. The particular software chosen should support the data format obtained from the GPS receiver, as some of the handheld GPS receivers, such as Garmin 76, Garmin eTrex, Garmin 12 and Garmin 12XL, do not store the pseudo-range and carrier phase like geodetic receivers (Schwieger, 2003). However, this information can be accessed by decoding the Garmin Communications Protocol (Hill et al., 2002).

In the case of GPS fix mode being flagged 0 (invalid), an external data source such as an inertial measurement unit should be used to estimate the current position. Later, this position can be verified or improved with the updated coordinates from the GPS. Besides, the inertial data for the approximation process, estimating the current position also needs the velocity and time information.

4.4 Approximation Process for Missing Coordinate

The objective of the approximation process is to estimate the current position where there are 'missing' coordinates. In this study, the 'missing' coordinates are computed by either interpolation or extrapolation. The computation takes into account the initial base value which should be as accurate as possible, being determined by WAAS or post-processing DGPS. From this starting point, the 'missing' coordinates are computed. Figure 4.6 illustrates the approximation process to determine the missing coordinates.

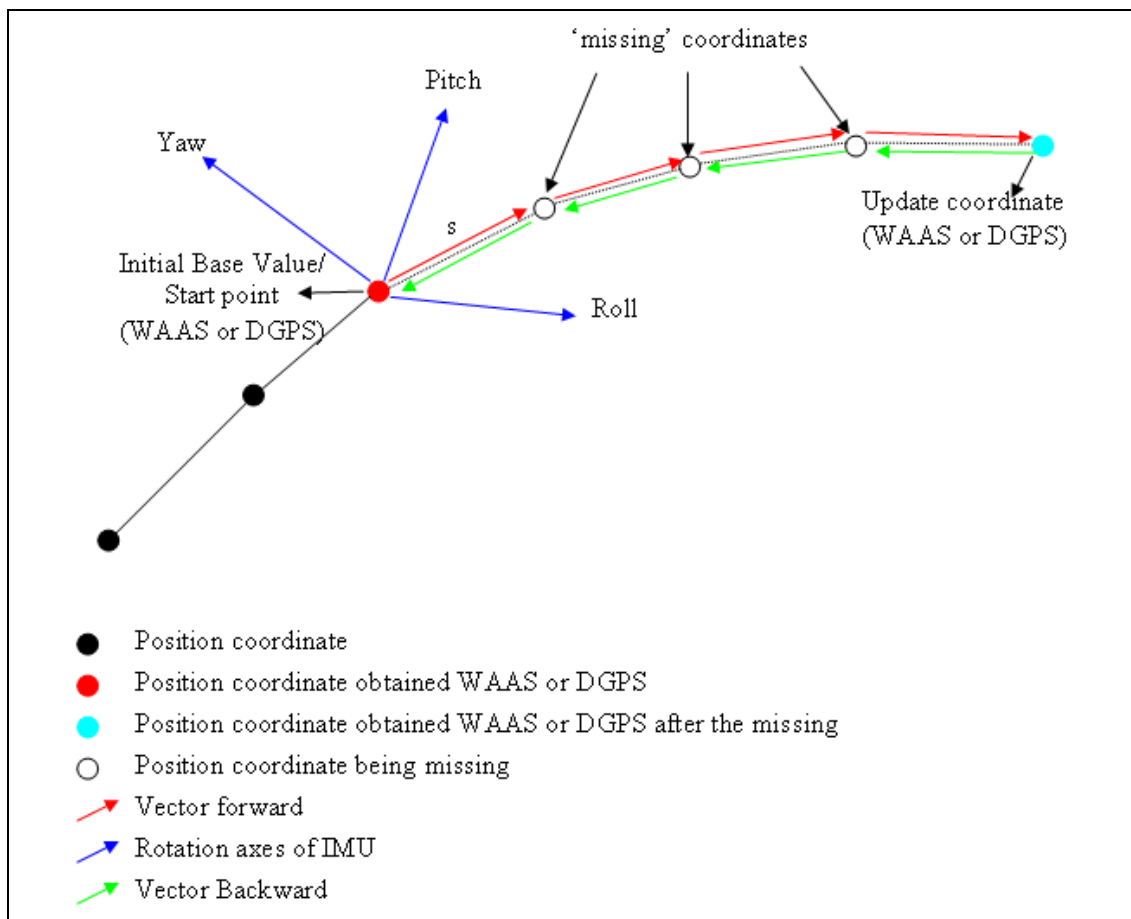


Figure 4.6: Approximation process

It is obvious from Figure 4.6 that the ‘missing’ coordinates can be determined if the vector ‘s’ is known. This can be computed if the speed and the time of travel of the vehicle are known. If the GPS receiver is on board the vehicle then the velocity and travel time of the vehicle can be extracted from the NMEA data coded as;

\$GPVTG,360.0,T,348.7,M,005.5,N,010.2,K*41

The yellow column is the ground speed in knots while the red column is the ground speed in kilometres per hour.

By using the relationship between measured speed, time and distance the vector ‘s’ can be determined. By rotating the vector ‘s’ according to the rotation angle provided by the IMU device, the final coordinates for the ‘missing’ coordinates are computed by using Equation (4.2) as follows;

$$L_{(t+1)} = s \cdot R + L_{(t)} \quad (4.2)$$

in matrix form

$$\begin{bmatrix} L1 \\ L2 \end{bmatrix}_{t+1} = s \begin{bmatrix} \sin \theta \\ \cos \theta \end{bmatrix} + \begin{bmatrix} L1 \\ L2 \end{bmatrix}_t$$

where;

$L_{(t+1)}$ = missing position in X, Y or Z

s = distance obtain for conversion of speed and time

R = rotation from IMU device

$L_{(t)}$ = known position from initial base value

The ‘missing’ coordinates are improved by using updated information from the GPS receiver to model the error through statistical modelling or by smoothing the error with forward and backward determination.

4.4.1 Extraction of Navigation and Image Ancillary Data

Direct geo-referencing needs an input from the interior orientation, exterior orientation and image ancillary data. This information has to be extracted from the data logger and pre-processed before it can be used for the direct geo-referencing task. Figure 4.7 depicts the extraction of the navigation data.

The image ancillary data can be obtained from the image header or header file, which contains information about image size, shutter speed, focal length, date and time taken. The ancillary data are really important for geometry correction of the single imagery. Figure 4.8 illustrates the information obtained from the image header.

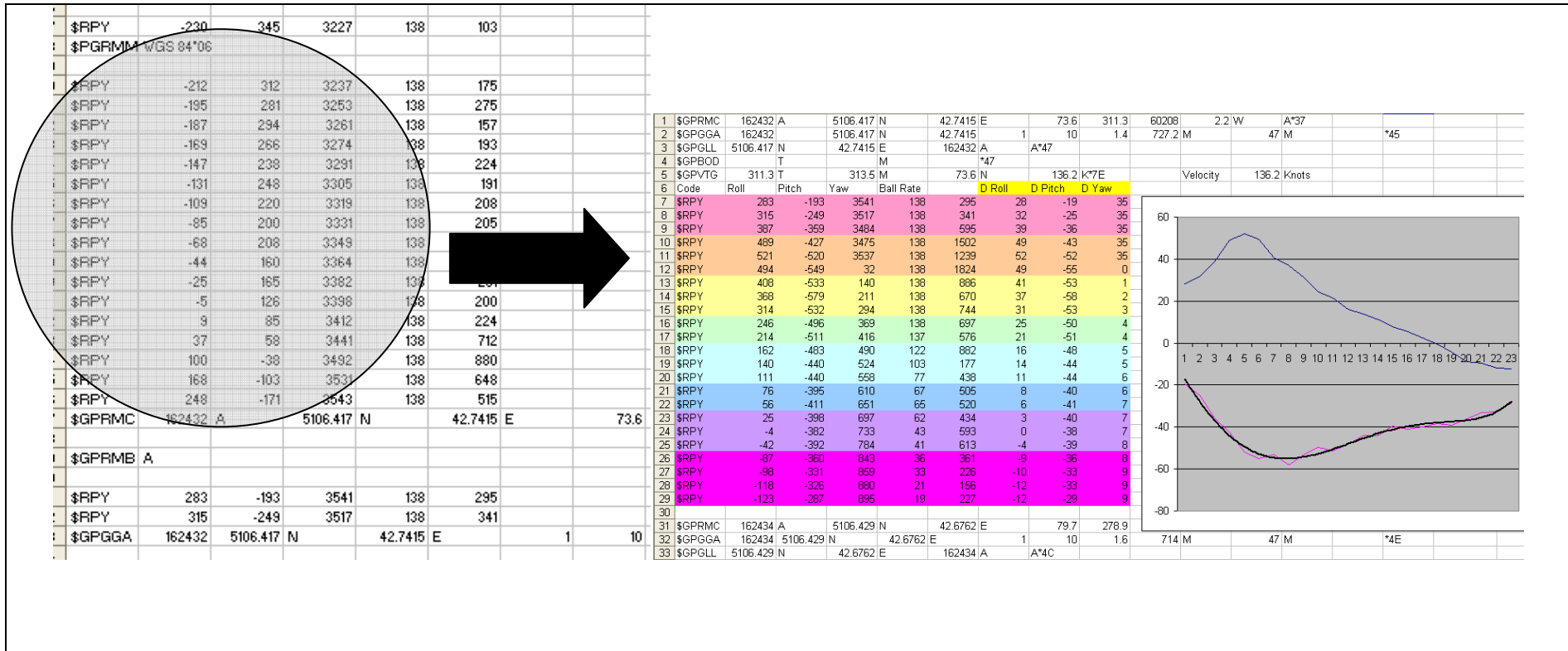


Figure 4.7: Extraction of navigation data

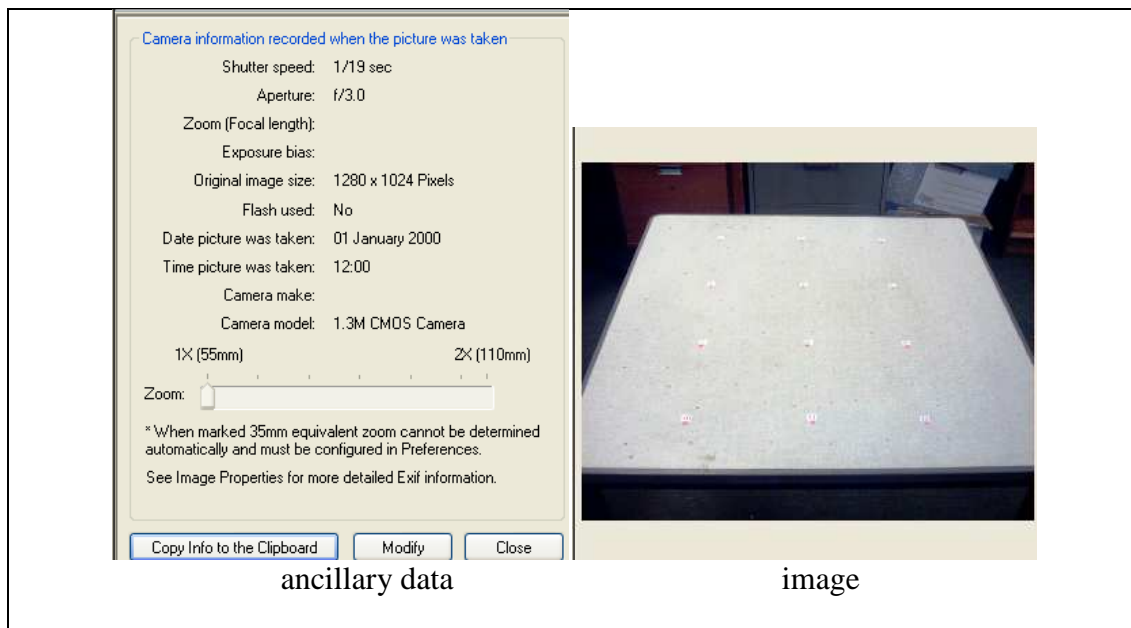


Figure 4.8: Extraction of ancillary data from imagery

4.4.2 Reconstruction of Image Geometry

The main objective of the reconstruction process is to revolve a tilted image into a horizontal-plane image and thereby enable direct measurements to be obtained from the image. The reconstruction begins with developing the camera projection (as shown in Figure 4.9). The camera projections can express the relationship between an object and its image, which lie on a straight line passing through the perspective centre. The reconstruction process based on this relationship involves interior and exterior parameters such as focal length, flying height, spatial resolution, pixel resolution and tilting angles, such as 1) radial distortion, 2) sensor orientation and 3) relief distortion.

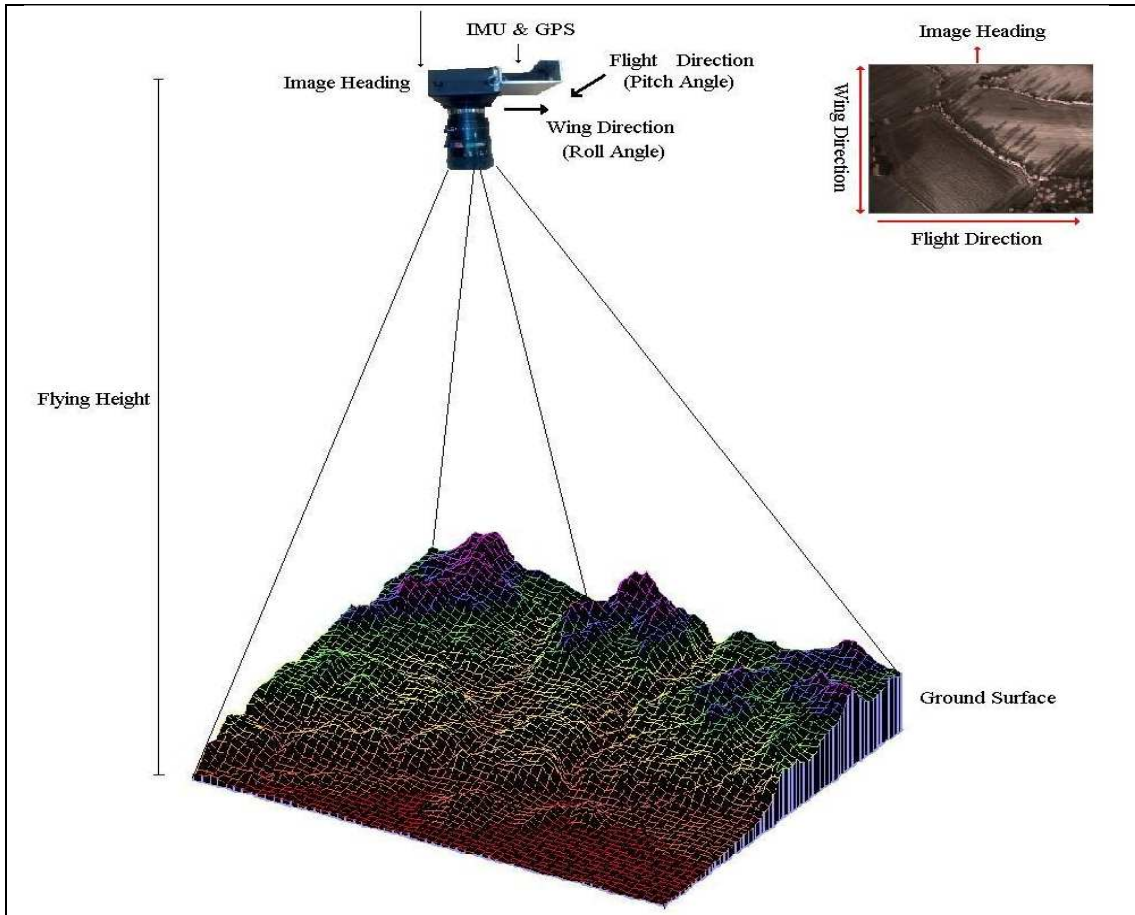


Figure 4.9: Camera projection, inset taken from portable device showing platform axes in flight direction.

4.4.3 Radial Distortion

Traditionally, all lens sensors are laboratory-calibrated at regular intervals. However, since the CMOS-based sensors are not professional metric devices and are small format sensors, their calibration raises some issues. Some of these issues mentioned in Toth (2002) are the long-term stability of the parameters and the way in which the calibration should be or can be performed (for example, collimators built for calibrating large-format aerial cameras cannot properly handle the small sensor size).

These issues have led to automatic calibration techniques, indeed the calibrations are well understood and widely used (Robson and Shortis, 1998). Table 4.1 lists the

popular equations which have been used to correct radial error, but in automatic calibration the equations in row 1 are preferable.

Table 4.1: Lens distortion equation

Method	Equation
1) Radial distortion	$\delta_x = k_1 r^2 x$ $\delta_y = k_1 r^2 y$
2) Radial distortion	$\delta_x = k_1 r^2 x + k_2 r^4 x$ $\delta_y = k_1 r^2 y + k_2 r^4 y$
3) Radial & Tangential distortion	$\delta_x = k_1 r^2 x + k_2 (r^2 + 2x^2) + k_3 2xy$ $\delta_y = k_1 r^2 y + k_3 (r^2 + 2y^2) + k_2 2xy$
4) Radial distortion	$\delta_x = rx(k_0 + k_1 r^2 + k_2 r^4)$ $\delta_y = ry(k_0 + k_1 r^2 + k_2 r^4)$

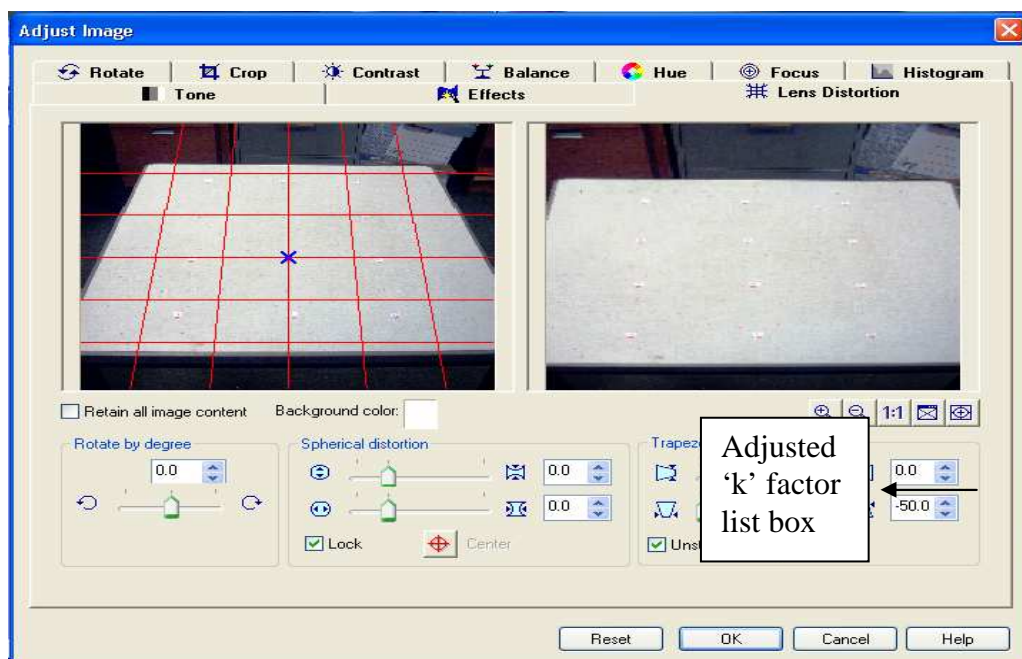
where;

δ_x, δ_y = correction value

k_1, k_2, k_3, \dots = distortion coefficient

x and y = image coordinate $r^2 = x^2 + y^2$

In automatic calibration, the factor 'k' is designed to be flexible and can take any number within a range set by the program (see Figure 4.10 for an example). The choice of the 'k' value is determined by visual interpretation.



Note: Snapshot from Ulead Photo Explorer

Figure 4.10: Example of automatic calibration

4.5 Image Orientation

It should be noted that the aim of image orientation in this study is to reconstruct the image geometry. There are two types of images to deal with; 1) tilt image, and 2) oblique image. Tilt image relates to images taken with the optical axis unintentionally tilted slightly from the vertical, while an oblique image is one taken with the camera axis strongly tilted (Moffit and Mikhail, 1980). These two cases need to be considered when projecting the image onto the horizontal-plane, as discussed below.

1) Projecting tilt imagery onto horizontal-plane.

The idea of projecting the tilt image onto the horizontal plane is to minimise the radial distortion at the periphery of the image (measured outward from the image centre). This can be done by computing the potential position of a pixel (P) in the horizontal plane (P') shown as in Figure 4.11. A simple sine-cosine formula can be used for this purpose. For instance,

$$XP' = XP \times \cos(\text{Tilt}) \quad (4.3)$$

$$YP' = YP \times \cos(\text{Tilt}) \quad (4.4)$$

where;

XP' distance of O and P' on X direction in horizontal plane

YP' distance of O and P' on Y direction in horizontal plane

XP distance of O and P on X direction in image plane

YP distance of O and P on Y direction in image plane

Tilt is pitch rotation in Y direction and Tilt is roll rotation in X direction.

However, theory shows that the rotation in one axis affects the direction of the following axes, and thus moves the pixel. For example, rotation in the X direction will move the pixel towards the Y and Z directions. These conditions can be formulated as follows;

	X rotation	Y rotation	Z rotation
XP'	X	$X*\text{Cos}(\text{Pitch})-Z*\text{Sin}(\text{Pitch})$	$X*\text{Cos}(\text{Yaw})+Y*\text{Sin}(\text{Yaw})$
YP'	$Y*\text{Cos}(\text{Roll})+Z*\text{Sin}(\text{Roll})$	Y	$-X*\text{Sin}(\text{Yaw})+Y*\text{Cos}(\text{Yaw})$
ZP'	$-Y*\text{Sin}(\text{Roll})+Z*\text{Cos}(\text{Roll})$	$X*\text{Sin}(\text{Roll})+Z*\text{Cos}(\text{Roll})$	Z

where;

XP' distance of O and P' on X direction in horizontal plane
 YP' distance of O and P' on Y direction in horizontal plane
 ZP' distance of O and P' on Z direction in horizontal plane
 XP distance of O and P on X direction in image plane
 YP distance of O and P on Y direction in image plane
 ZP' distance of O and P' on Z direction in image plane
 Roll, Pitch and Yaw are the rotation angles

In the case where the Z coordinates are not available (for example, Z coordinate obtained from low accuracy GPS), $-Z*\text{Sin}(\text{Pitch})$ and $Z*\text{Cos}(\text{Roll})$ have to be removed from the equations above, giving:

$$XP' = X + X*\text{Cos}(\text{Pitch}) + X*\text{Cos}(\text{Yaw}) + Y*\text{Sin}(\text{Yaw}) \quad (4.5)$$

$$YP' = Y + Y*\text{Cos}(\text{Roll}) - X*\text{Sin}(\text{Yaw}) + Y*\text{Cos}(\text{Yaw}) \quad (4.6)$$

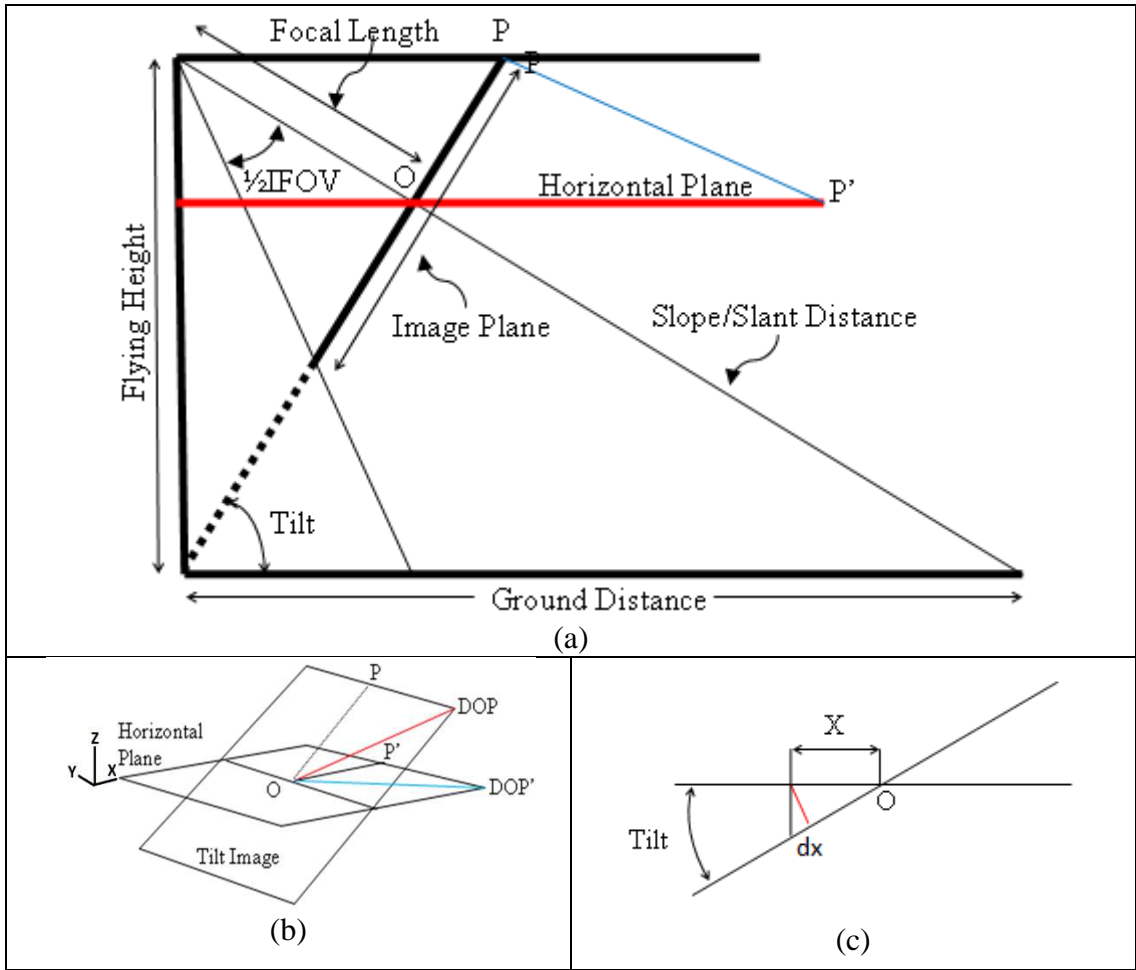


Figure 4.11: Geometry obtained from camera projection. (a) geometry of camera, (b) plane of tilting image and horizontal-image plane and (c) conversion from tilt image plane to horizontal-image plane.

Unfortunately, equations (4.5) and (4.6) are not capable of orientating the image into the horizontal position, especially when the rotation angle is large. Figure 4.12(a) shows distortion occurring when using equations (4.5) and (4.6). To overcome this problem, a ratio between distance OP and OP' (Figure 4.11) has been used. The distance of OP and OP' can be computed as follows;

$$DOP = \sqrt{(XP)^2 + (YP)^2} \quad (4.7)$$

$$DOP' = \sqrt{\left(\frac{XP}{\cos(\text{Roll})}\right)^2 + \left(\frac{YP}{\cos(\text{Pitch})}\right)^2} \quad (4.8)$$

Therefore; $ratio, k = \frac{DOP}{DOP'}$; replace multiplicative parameters, X and Y with **k**, then;

$$XP' = X + k * \text{Cos}(\text{Pitch}) + k * \text{Cos}(\text{Yaw}) + k * \text{Sin}(\text{Yaw}) \quad (4.10)$$

$$YP' = Y + k * \text{Cos}(\text{Roll}) - k * \text{Sin}(\text{Yaw}) + k * \text{Cos}(\text{Yaw}) \quad (4.11)$$

By using equations (4.10) and (4.11) the image orientation is rotated into horizontal-position. Figure 4.12(b) shows the results obtained from equations (4.10) and (4.11). Subsequently, the corrected image can be scaled according to the ratio of the focal length and flying height. If the optical axis is unintentionally tilted then the image is oblique and has to be orientated by using an appropriate algorithm.

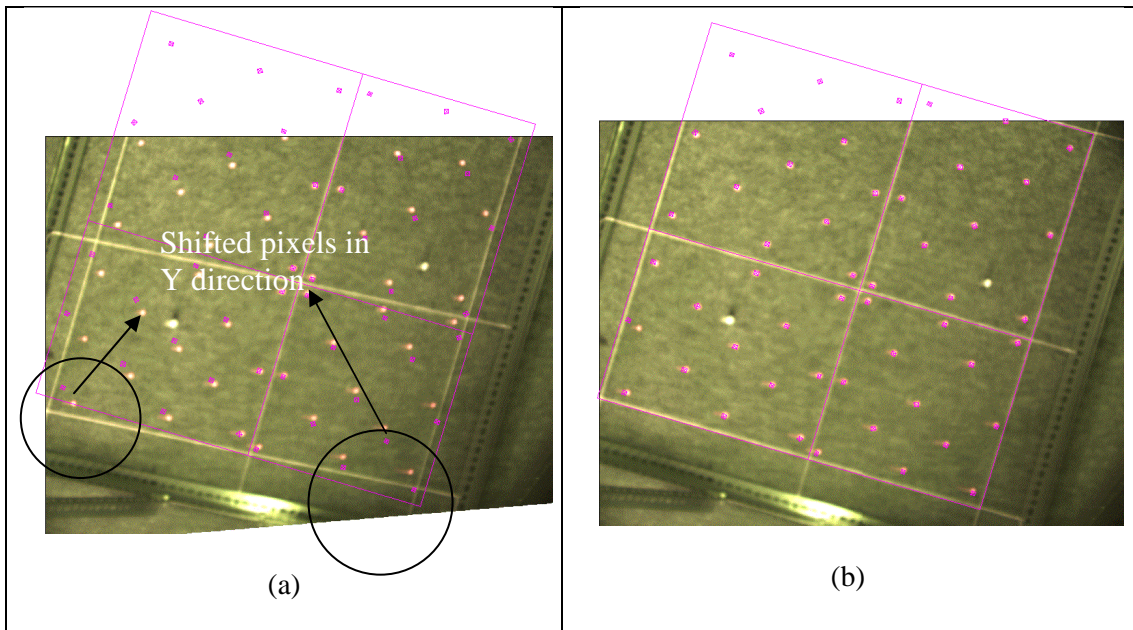


Figure 4.12: (a) Projected image using the simple rotation matrix expressed as equations (4.5), (4.6); (b) Projected image using equations (4.10), (4.11).

2) Projecting oblique image onto horizontal-plane

In the case mentioned above, when the optical axis of the camera lens is strongly tilted from the vertical axis then the image has to be treated as oblique. Oblique imagery can be projected onto the horizontal plane by reconstructing the image geometry via intrinsic and extrinsic parameters. Figure 4.13 depicts the geometry of the oblique image.

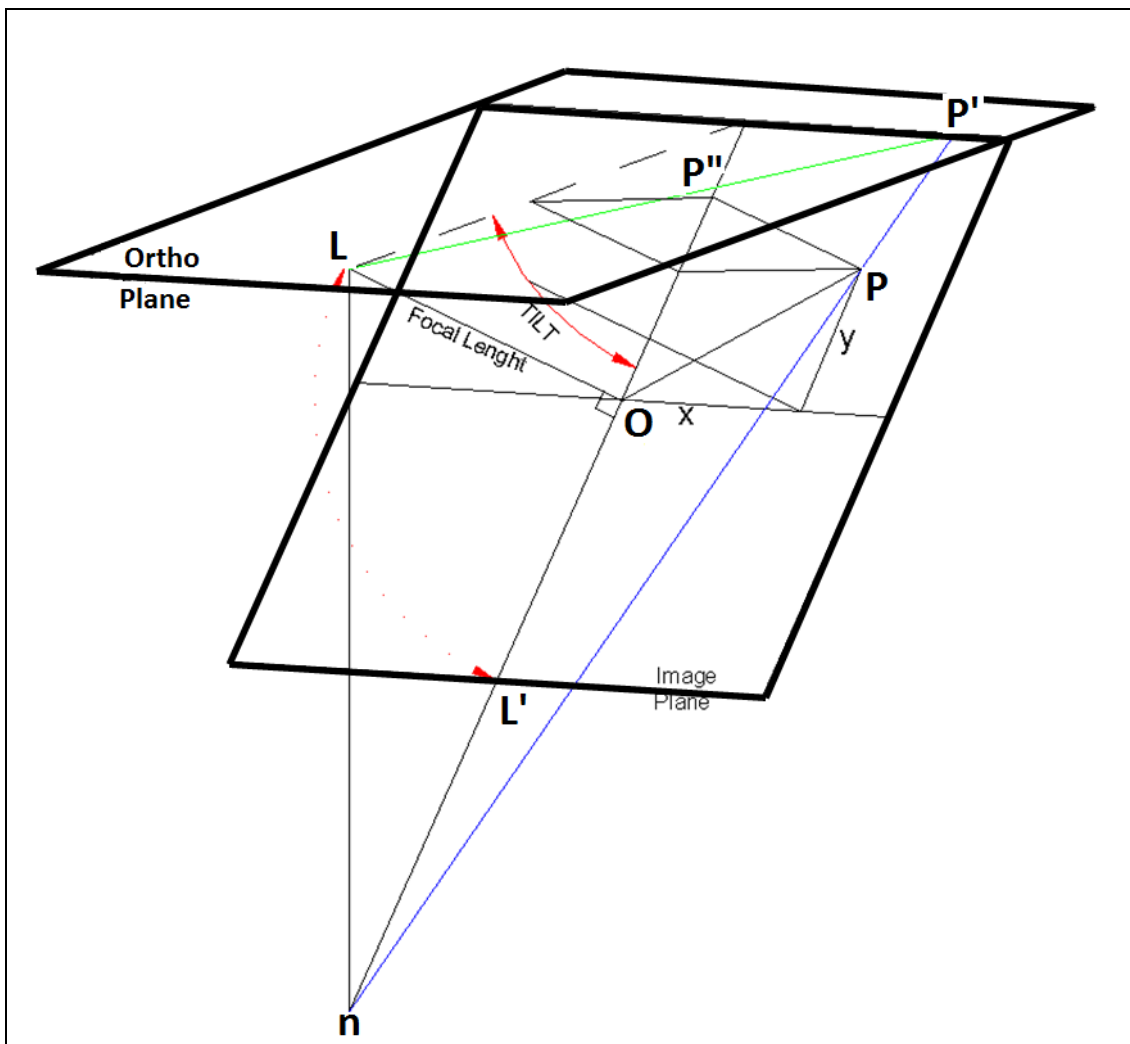


Figure 4.13: Geometry of oblique image.

In Figure 4.13, it is assumed that one end of the image coincides with the ortho-plane. L is an exposure station with a distance of OL from the image centre. The P position can be traced by projecting the line of nP to the horizontal-plane (P'). Due to the condition of collinearity, the image of P should be somewhere on line LP'. To

compute the coordinate P in the ortho-plane (P''), a trigonometric triangulation has to be undertaken and Figure 4.14 illustrates graphical construction for this.

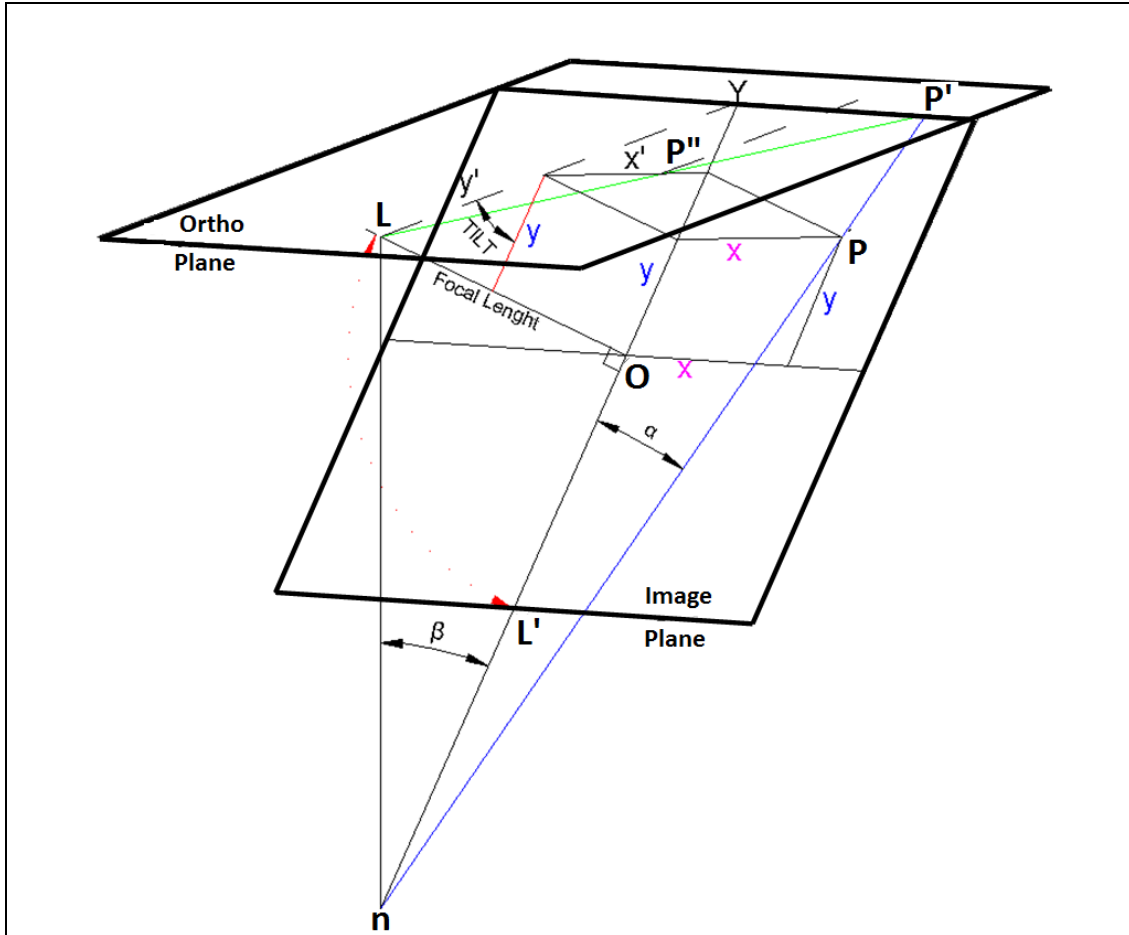


Figure 4.14: Establishment of trigonometric triangulation.

From Figure 4.14, let P'' be the position of P in the ortho-plane, then

$$x' = y' \tan(\angle YLP') \quad (4.12)$$

$$y' = \frac{y}{\cos(\text{TILT})} \quad (4.13)$$

It is also known that $\beta = 90 - \text{TILT}$, therefore nO is

$$nO = \frac{\text{FocalLength}}{\tan(\beta)} \quad (4.14)$$

and;

$$\alpha = \tan^{-1}\left(\frac{x}{nO + y}\right) \quad (4.15)$$

Then,

$$YP' = nY * \tan(\alpha) \quad (4.16)$$

and;

$$\angle YLP' = \tan^{-1}\left(\frac{YP'}{LY}\right) \quad (4.17)$$

where;

$$LY = \frac{\text{FocalLength}}{\cos(90 - \text{TILT})} \quad (4.18)$$

Equations (4.12) to (4.18) have been used to compute the new position of all pixels in the image on the horizontal-plane. Please note that all computations are done in pixel unit. The conversion from pixels metric to metric units is based on the *pixels per cm*. For example, if an image has been scanned at resolution of 28 pixels per cm, then a 1024x1024 pixel image can be transformed to 36 x 36 cm. If the image scale is 1: 1000, then 1 cm (in photo) = 1000 cm (on ground) and the image covers an area of 36000 x 36000 cm square. Later, each pixel in an image can be mapped into the user coordinate system.

4.6 Map Pixels into User Coordinate System

The objective of mapping the image pixels into a user coordinate system is to enable direct measurements to be taken. There are two techniques for mapping the pixel image into a user coordinate system, which are;

- 1) Based on the coordinates of the image centre, compute the coordinates of the four corners. The resulting image then needs to be orientated to reconstruct the image geometry. Please note that all computations should be in metric units.
- 2) Reconstruct the image geometry according to the attitude information, and then compute the coordinates of the four corners based on the coordinates of the image centre. The computations of the geometric image reconstruction

can be in pixel units, and during the calculations for the coordinates of the four corners the conversion between pixel and metric units can take place.

However, both techniques need the image to be mapped onto the local coordinate system. Figure 4.15 illustrates the relationship between the image coordinate system and the local coordinate system.

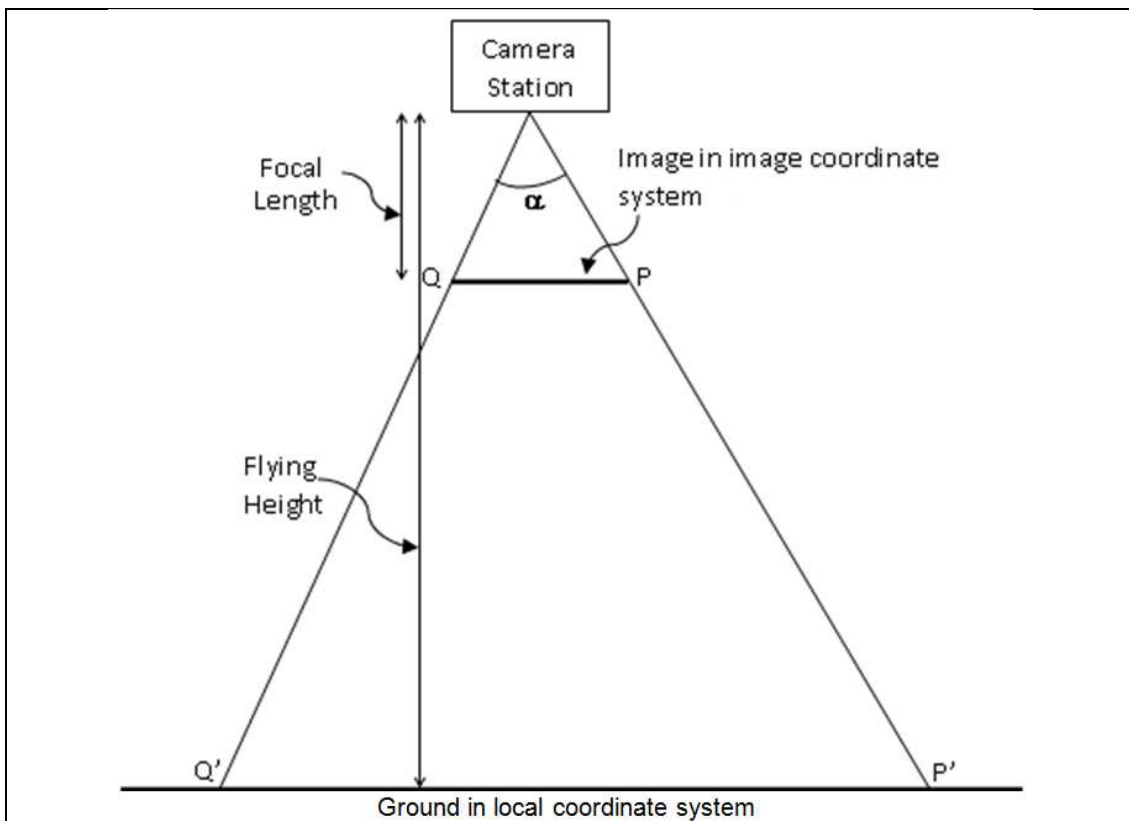


Figure 4.15: Relationship between image coordinate system and the local coordinate system.

Figure 4.15 shows that P is representing P' in the image, and therefore the coordinates of P' can be computed as;

$$XP' = \text{Focal Length} \times \tan\left(\frac{\alpha}{2}\right) \quad (4.19)$$

Where α is the field of view and is equal for both axes, then $XP' = YP'$.

The α value is normally given by the instrument manufacturer. However, if the α value is unknown it can be calculated as follows:

- 1) If image width and image height can be determined, for example by using photomodeler software, then α will be;

$$\alpha = 2 \tan^{-1} \left(\frac{\text{Width}}{\text{Focal length}} \right) \dots \dots \dots \text{in X direction} \quad (4.20)$$

$$\alpha = 2 \tan^{-1} \left(\frac{\text{Height}}{\text{Focal length}} \right) \dots \dots \dots \text{in Y direction} \quad (4.21)$$

- 2) If the magnification is known, then α will be;

$$\alpha = 2 \tan^{-1} \left(\frac{\text{FH}}{\text{Focal length}} \times M \right) \dots \dots \dots \text{in X direction} \quad (4.22)$$

$$\alpha = 2 \tan^{-1} \left(\frac{\text{FH}}{\text{Focal length}} \times M \right) \dots \dots \dots \text{in Y direction} \quad (4.23)$$

By knowing the field of view (α), the four corners of the image can be determined into local coordinate system. For example, assume that the width and height of the image are known to be 4.8 mm and 6.4 mm as obtained from photomodeler software, and the focal length is 8.5 mm, given by the manufacturer, then;

$$\frac{\alpha}{2} = \tan^{-1} \left(\frac{4.8}{8.5} \right) \dots \dots \dots \text{in X direction}$$

$$\frac{\alpha}{2} \approx 29^\circ$$

$$\frac{\alpha}{2} = 2 \tan^{-1} \left(\frac{6.4}{8.5} \right) \dots \dots \dots \text{in Y direction}$$

$$\frac{\alpha}{2} = 37^\circ$$

If the camera station is 1000 metre North and 1000 metre East with a flying height of 380 metres, then the coordinates of the four corners can be determined as illustrated in Figure 4.16. The difference in longitude departure (ΔD) and difference in latitude (ΔL) can be calculated as;

$$\Delta D = FH \times \tan\left(\frac{\alpha}{2}\right)$$

$$\Delta D = 380 \times \tan(29)$$

$$\Delta D = 214.588 \text{ metres}$$

$$\Delta L = FH \times \tan\left(\frac{\alpha}{2}\right)$$

$$\Delta L = 380 \times \tan^{-1}(37)$$

$$\Delta L = 286.118 \text{ metres}$$

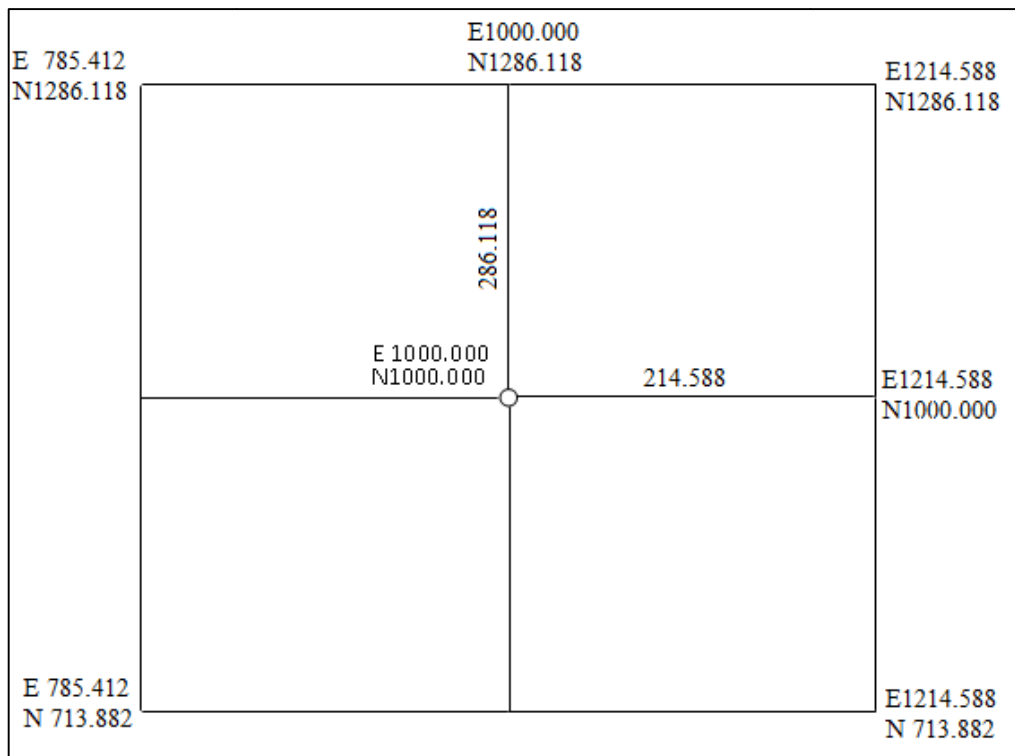


Figure 4.16: Coordinates for the four corners of the image that refers to local coordinate system.

The calculated coordinates, as shown in Figure 4.16 are correct if the Y direction is equal to the north direction. However if it is not, the image needs to be rotated according to the yaw. Figure 4.17 shows the process of how the image is mapped into local coordinate system.

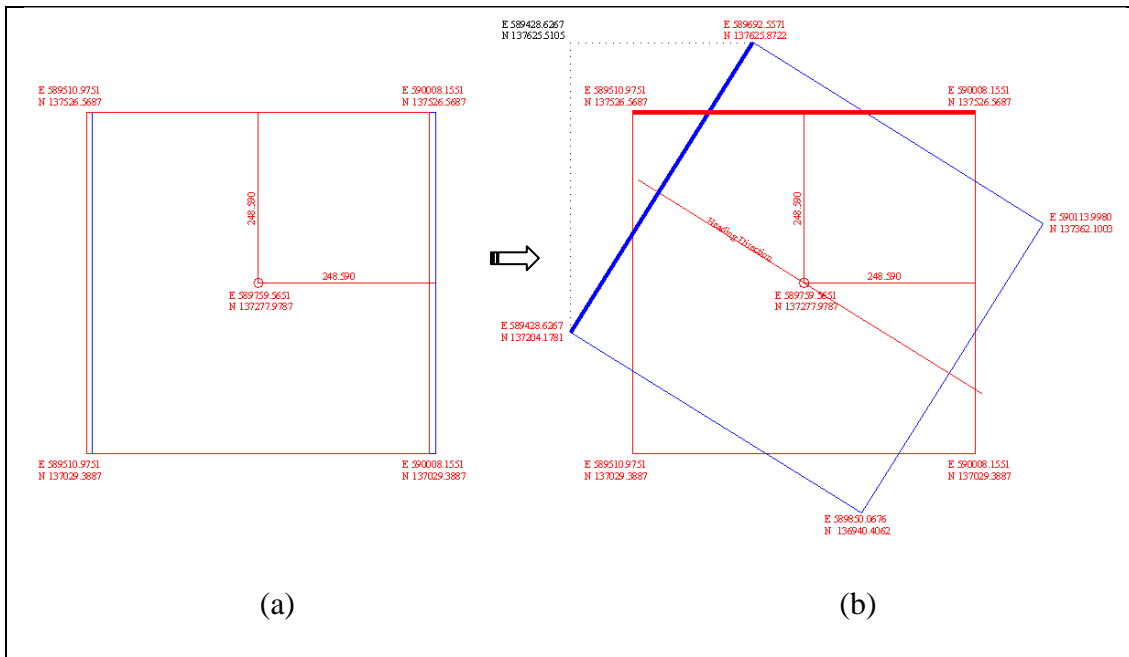


Figure 4.17: Mapping pixels into local coordinate system. (a) red box is image area plot, blue box area shifted after rotating image in roll and pitch directions. (b) Rotated image in yaw direction (blue), coordinates in black used to create world file format to georeference image into user coordinate system.

An alternative to mapping the image into the local coordinate system is by determining the orientation of the image before calculating the coordinates of the four corners. The advantage of this technique is that there is an opportunity to check the position of the image by comparing the orientated image with google earth (URL: <http://www.google.com/earth/index.html>) or ready map obtained from British Ordnance Survey. Figure 4.18 shows the process of mapping the image into local coordinate system by this latter method.

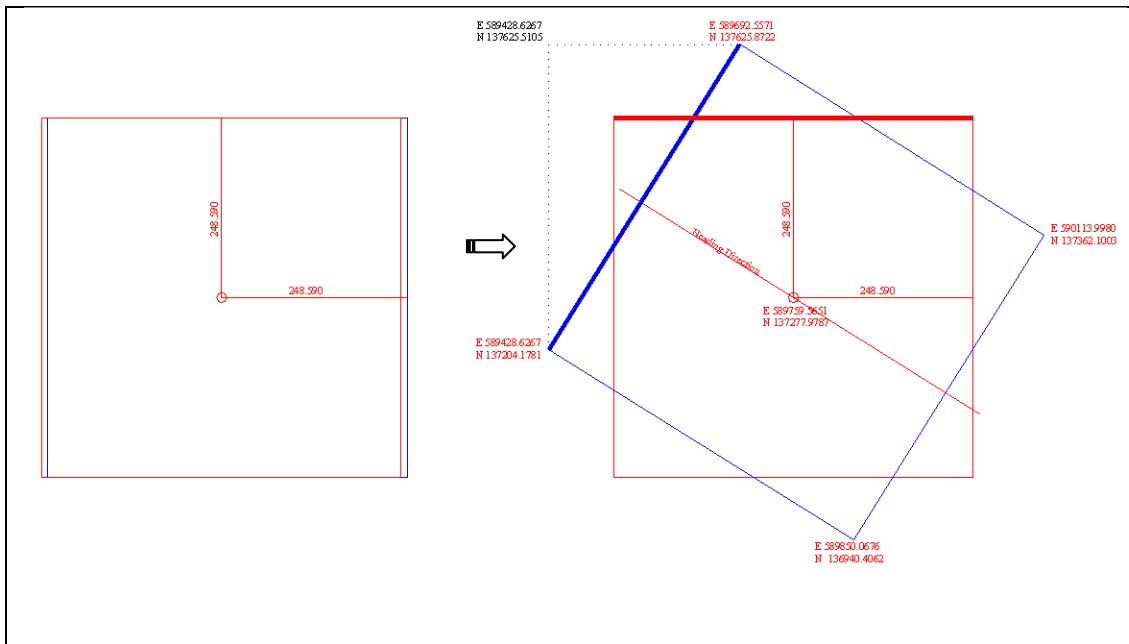


Figure 4.18: Image rotated in roll, pitch, then yaw direction. Later, coordinates of four corners are computed. Coordinates in black used to create world file format to geo-reference image into user coordinate system.

The process of mapping the image into the local coordinate system can be done either mathematical or graphical. The mathematical method needs well organise documentation whereby every single step documented. The graphical method is achieved with suitable software, such as AutoCad. The graphical method is tedious in that it requires reconstructing the geometry of the image.

Once the geocorrection has been achieved, the coordinates are transferred into “World File” format to enable the image to be used directly without repeating the same registration process having to be repeated.

World File

World file is a small-standardised support file employed by some software such as ESRI for images in Arcview (Luijten, 2003) to geo-reference a digital image to a user coordinate system. For example, an image with .TIF format has a world file with .TFW extension, which acts as a support file. The .TFW contains initial information such as pixel size, image origin and origin coordinates, and can be created by any software which can produce ASCII data format. Table 4.2 shows an example the .TFW format and the content information.

Table 4.2: Sample of .TFW format

+6.00	<i>Line1</i>
-0.00	<i>Line2</i>
-0.00	<i>Line3</i>
-6.00	<i>Line4</i>
589428.6267	<i>Line5</i>
137625.5105	<i>Line6</i>

Note: *Line1* to *Line 6* are not included in the .TFW format. It is only the annotation to describe the contents of that particular line as listed below:

Line 1 - Cell size in "X" direction

Line 2 - Insertion point in "X" direction

Line 3 - Insertion point in "Y" direction

Line 4 - Cell size in "Y" direction

Line 5 - Easting value of insertion point "X"

Line 6 - Northing value of insertion point "Y"

Additional remarks: sign on line 4 shows if insertion point is upper left or lower left corner. Positive means "Y" values are increasing upwards and therefore registration must start at bottom or lower corner. Vice-versa for negative sign.

4.7 Summary

This chapter has covered the fundamentals of direct geo-referencing, which include the concept of direct geo-referencing, data preparation, pre-processing, extraction of navigation information, image reconstruction and finally mapping the digital image onto the user coordinate system. It begins by describing the concept of direct geo-referencing and the information needed to carry out the process. The information obtained from the imaging and navigational devices need ‘curing’ before pre-processing tasks are undertaken. The discussion of the pre-processing tasks is limited to filtering, differential GPS and approximation processes. Subsequently, the particular data required for reconstructing the image geometry, and includes correcting radial distortion and image orientation, is extracted and applied. Finally, a discussion on transferring the pixels coordinates into the user coordinate system has been presented. The process of writing the mathematical equations developed in this chapter is described in Chapter 5.

5. DEVELOPMENT OF SOFTWARE

5.1 Introduction

The objective of software development in this study is to assist the direct geo-referencing process. The input to this software is raster and text data. Raster data are obtained during the image acquisition process, while text data are from the IMU, GPS and other extrinsic processed data, such as the initial coordinates and the flying height. The intrinsic parameters of the image, such as pixel resolution and image size, are obtained by using the visual basic .net customised programming scripts. The specifications for the various devices, such as digital screen size, lens focal length and band channel, are given by the manufacturer, and the software structure has been designed based on this information. The programming script lists the detail of each task, such as input image, input extrinsic data, extracting the image intrinsic data, processing and resampling tasks, and each of the command lines has been labelled for easy identification.

5.2 Software Structure

The software has been structured as follows:

- 1) **Image Input.** Since there are various types of image format the focus is on raster images that can be recognised by the visual basic .net programming language.
- 2) **Intrinsic Parameters.** The intrinsic parameters of an image can be extracted by using a ready-made command in the visual basic software.

- 3) **Extrinsic Parameters.** The extrinsic parameters for the direct geo-referencing are entered by using a form created for the purpose.
- 4) **Processing.** The processing task will be triggered by selecting the appropriate application process from the pull-down menu.
- 5) **Resampling.** The resampling process used the image warping technique to alter the image pixels.

5.3 Programming Script

The programming script is written in visual studio 2009 .net programming language with visual basic .net as the main source. Some of the script is adopted or modified from Internet forums such as VB.net forum and CNET forum. A complete script of the programme development is given in Appendix G.

5.3.1 Image Input

The programming script used for selecting the raster file to be processed uses standard a visual basic framework for calling the file. Below is the programming script to input the image file with default extensions from visual basic framework. A programming script used for extracting the default extensions from the image file is given in Appendix G.

5.3.2 Intrinsic Parameters

The program to extract the intrinsic parameters of the image is given in Appendix G.

5.3.3 Extrinsic Parameters

The extrinsic parameters are imported into the program by keyboard entry. A multiple Tab control dialog box was designed to able the import process, see Figure 5.1.

Figure 5.1: Keyboard entry form for extrinsic parameter

5.3.4 Image Processing

The image processing script is based on a pull-down selection menu where the user is able to select the process needed. Figure 5.2 illustrates the dialog box for choosing the application and the programming script is given in Appendix G.

Figure 5.2: Selecting image processing task.

5.3.5 Image Resampling

A programming script used for image resampling is based on warping technique where the pixels are altered individually and is provided in Appendix G. Since altering pixels individually may cause the image size to expand, and as it is important to maintain the original size (rectangular or square), any pixels extending beyond the original frame are removed. The reason for discarding the coverage beyond the image size is to reduce the image distortion because these pixels which are distant from the image centre suffered severe distortion when compared with those nearest to the centre of the image. This resulting image makes the mapping of the pixels to the user coordinate system a simpler and more direct process.

5.3.6 Interface

Figure 5.3 shows the user interface, developed in the visual basic .net programming language, to make the process of moving from task to task simple.

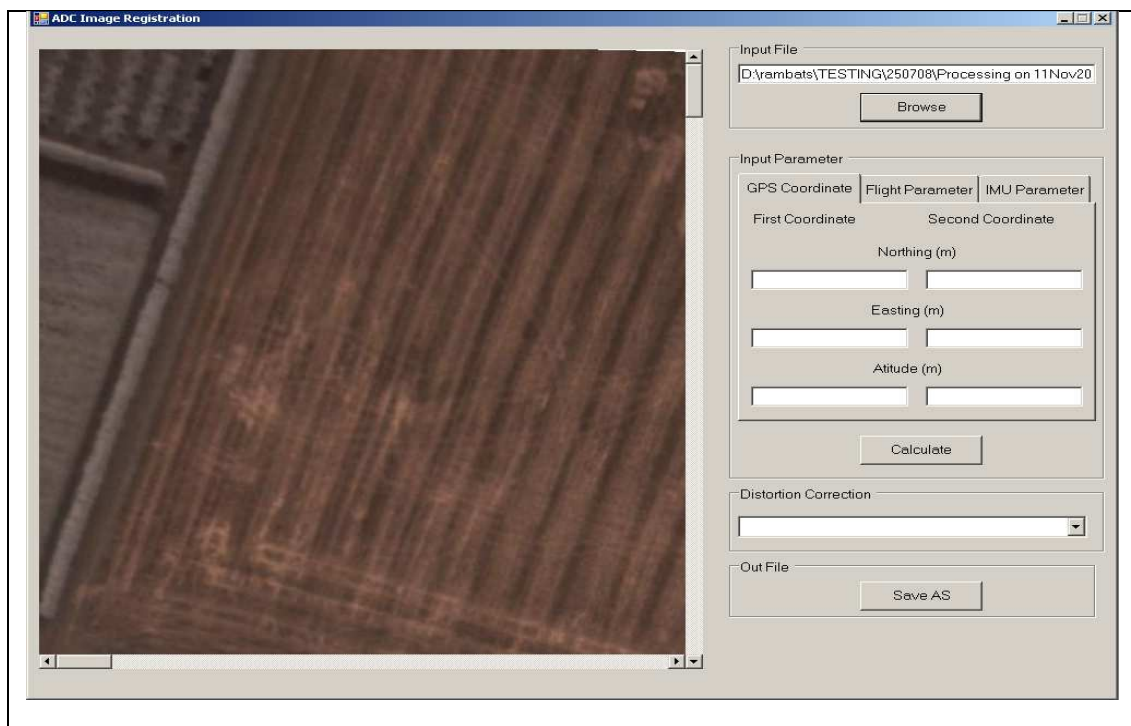


Figure 5.3: User interface.

5.4 Summary

This chapter has outlined the programmes developed for the direct geo-referencing process. The various operations are managed by an interface for easy browsing from task to task. The software product is used for direct geo-referencing task described in Chapters 6 and 7.

6. EXPERIMENTAL INVESTIGATION

6.1 Introduction

As an initial investigation into the suitability of the IMU, a laboratory test was undertaken. In addition, to ensure that the instruments met the requirements of the Low Cost Remote Sensing System (LCRSS), three types of test were set up. The first was a performance test to examine the performance of the instruments. The second was a simulation test to ensure that the instruments provided sufficient data for the image geo-rectification process. The third test was a test-drive to evaluate the data quality. Finally, all the instruments were installed in a light aircraft for the final test to evaluate the full portable remote sensing system (see Chapter 7). The laboratory investigation included designing, analysing and determining an appropriate test for the system.

6.2 Performance Test

Performance testing is a rigorous evaluation of usability, capability and approximate accuracy of the instrument. In this study, all the instruments (sensor, GPS and IMU) were tested independently to identify and remove gross or systematic errors. The performance test was necessary since all the instruments were new (first time of use) to the LCRSS application (Cramer, 2005). In addition, the instruments (especially the IMU/GPS) contained random errors such as acceleration biases and noise (El-Sheimy et al, 2006; George and Sukkarieh, 2005) which need to be minimised.

6.2.1 IMU Performance Test

The IMU performance test was carried out to determine the characteristic behaviour of the IMU. In this test, the IMU was attached statically to a survey-pole on the ground surface. The roll, pitch and yaw data were obtained from the IMU for three hours which was sufficient to sense any drift which occurred in the IMU. El-Sheimy (1996) allocated the same time (three hours) for testing the IMU/GPS performance on a flight-run. At the end of this test, it was expected that:

- 1) The characteristic of each epoch, either homogeneous or heterogeneous, could be obtained.
- 2) The quality of each epoch measurement could be established.
- 3) The approximate accuracy of the IMU could be obtained and compared with the manufacturer's claimed accuracy.

6.2.1.1 IMU Performance Test Results

The IMU performance test yielded 7200 epochs in the two and half hours period of observation were analysed because the first 30 min is a warm up period to let the IMU become stable (El-Sheimy, 1996). For the first 30 min of two and half hours, the mean values were 0.056, 0.030 and 150.189 degrees for the rotation angle in roll, pitch and yaw, respectively. The mean value remained the same for the next one hour of observation, but improved in accuracy in the last one hour. However, the standard deviations for the first 30 min, 1 hour and the last 1 hour were nearly the same. The RMS fell between 0.001 to 0.003 degrees which is unexpected for the rate grade gyroscope, as El-Sheimy et. al., (2006) found that gyroscope to be the most erroneous gyro device compared to tactical and inertial grade gyros. Table 6.1 summarises the mean, standard deviation and RMS for the roll, pitch and yaw

rotations. Figure 6.1 shows the observation angles (Roll, Pitch and Yaw) during the performance test.

Table 6.1: Overall errors of rotation angle (roll, pitch and yaw)

Observed Overall Errors			
	Mean	Standard Deviation	DRMS
First 30 minutes			
Roll (degrees)	0.056	0.344	0.002
Pitch (degrees)	0.030	0.490	0.003
Yaw (degrees)	150.189	133.432	1.370
1st hour			
Roll (degrees)	0.057	0.371	0.002
Pitch (degrees)	0.038	0.461	0.002
Yaw (degrees)	177.851	104.063	0.994
2nd hour			
Roll (degrees)	0.029	0.401	0.001
Pitch (degrees)	0.042	0.626	0.002
Yaw (degrees)	179.001	127.563	0.750

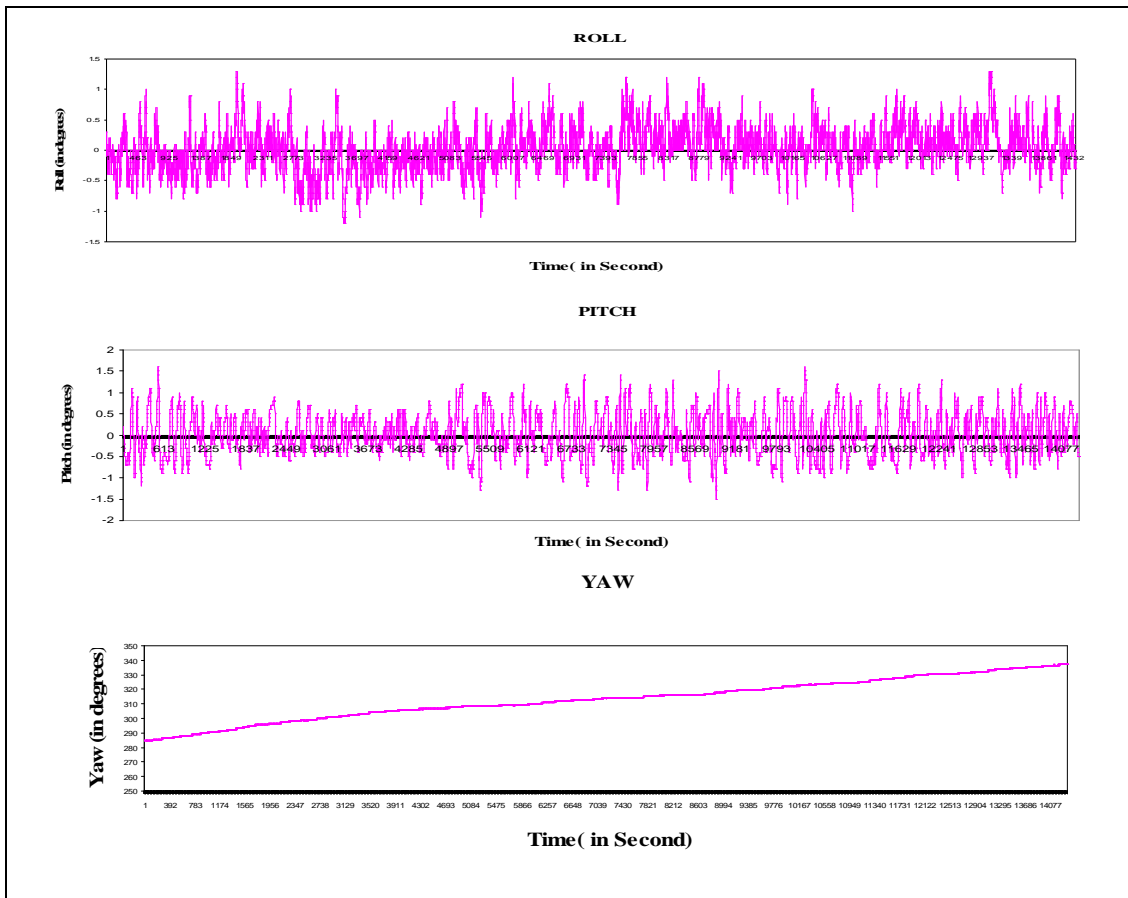


Figure 6.1: Observed angles (Roll, Pitch and Yaw) during performance test.

6.2.2 GPS Performance Test

GPS performance test was carried out to identify the positioning accuracy, satellite availability and battery life span. In this test, the GPS instrument was placed statically in a single position for three hours. All the information from the GPS receiver was recorded in the Personal Data Assistant (PDA). These data were written in ASCII format in a file data. At the end of the test, the standard deviation of the GPS was obtained. This standard deviation was to be an initial input for the error modelling process in the assimilation procedure of IMU and GPS data.

6.2.2.1 GPS Performance Test Results

This performance test revealed that the Garmin 76 is capable of producing position accuracy in the range of ± 0.005 degrees to ± 0.006 degrees in northing and easting directions. The height above the ellipsoid reference was about ± 6.002 m which was not really suitable to determine height for a single point; however, this particular accuracy might be sufficient for determining the altitude of the flying aircraft. Table 6.2 shows the residual mean, standard deviation and RMSE for the GPS Garmin 76. It is also notable that the WAAS satellite (35, 47, 33, 37 and 39) did not exist during the time of the observations. This means that the chances of having DGPS coordinates was very high, with 95 per cent of the positions determined by the DGPS method.

Table 6.2: Accuracy of Garmin 76

	Residual Mean	Standard Deviation	RMSE
North (\pm second)	3.1×10^{-10}	0.001	0.005
East (\pm second)	8.5×10^{-12}	0.001	0.006
Height (\pm metre)	0.368	0.049	6.220
Velocity (ms^{-1})	0.000	0.000	0.0000

6.2.3 Imaging Sensors Performance Test

The sensor performance test was done by fitting the sensor on the test rig (see section 6.3.1) built in a ratio of 1:1000 to the real flying height, whereby 1 metre height of the rig was equal to 1000 metres of real flying height. Then the sensor was rotated to create unpredictable movement to determine the best speed for flying and the fastest exposure the sensor can make. Seeing objects through moving glass (lens) will cause high temporal frequency, which occurs when there is relative movement between camera and scene or if the brightness of lighting changes. In this research, the main cause of temporal frequency will be the relative movement between camera (flight speed) and scene. To overcome this issue, the camera shutter should be set at the optimum level to allow enough light onto the imaging sensor to both allow adequate exposure time, and reduce the temporal effects. It can be said that the camera shutter is inversely proportional to the flight speed as shown by equation 6.1.

$$\frac{1}{ShutterSpeed} \propto Flight\ speed \quad (6.1)$$

6.2.3.1 Imaging Sensors Performance Test Results

In this performance test, 104 images were captured from the simulation platform. During the capture period, the platform was rotated to provide various different angles and movements: slow, rapid and fast. It was found that it is very difficult to capture good quality images while moving, because the speed of the moving platform (aircraft) should tally with the shutter of the imaging sensor, otherwise it results in blurring and unfocused imagery, as shown in Figure 6.2.

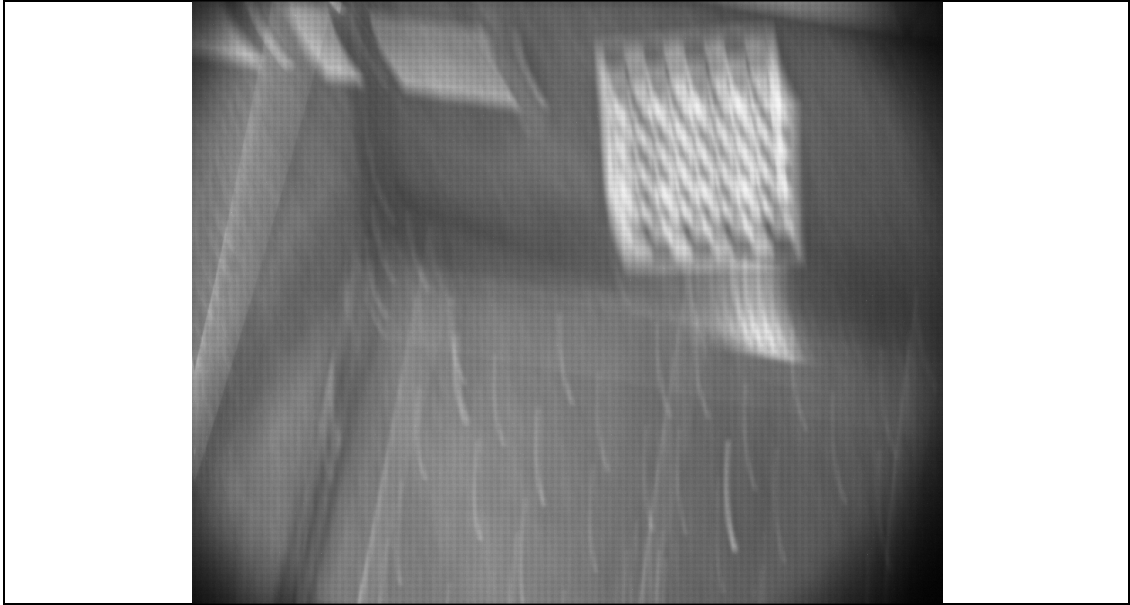


Figure 6.2: Blurring and unfocused imagery caused by untallied movement between platform speed (aircraft) and imaging shutter.

6.3 Simulation Test

The main objective of the simulation test was to use the rotation angles to orientate the image into its true geometric position. Secondly, the simulation test was used to evaluate the frequency of capture of the GPS and IMU data. From the simulation test, the quality, the capability and the sensitivity of the navigation instruments on the image could be determined. For the main objective, the laboratory test drive was set up and for the second the on-the-road test drive was performed.

6.3.1 Laboratory Test

In the laboratory test, a simulation platform was built to a scale of 1:1000, with a designed bracket, control points and pivoting system. The bracket had flexible movement in roll, pitch and yaw. The twirling system moved the bracket up and down in roll and pitch directions, and the rotary motor was used to simulate the yaw movement.

A. Platform/Rig

The platform was designed to simulate the instantaneous position of an airborne system during the data acquisition process. This platform was built with an ‘A’ shaped frame. The platform base size was 1 metre x 1 metre and platform height was 3 metres. On the top of the platform was captured of parallel bars on which to hang the bracket containing the sensor and the IMU device. The gap between the bracket and parallel bars was designed with 45 degrees of clearance to simulate the roll and pitch movement. The rotary motor to simulate yaw movement was attached inside the bracket while the roll and pitch were simulated by pulling a string attached to linear actuators. Figure 6.3 shows the simulator platform/rig.

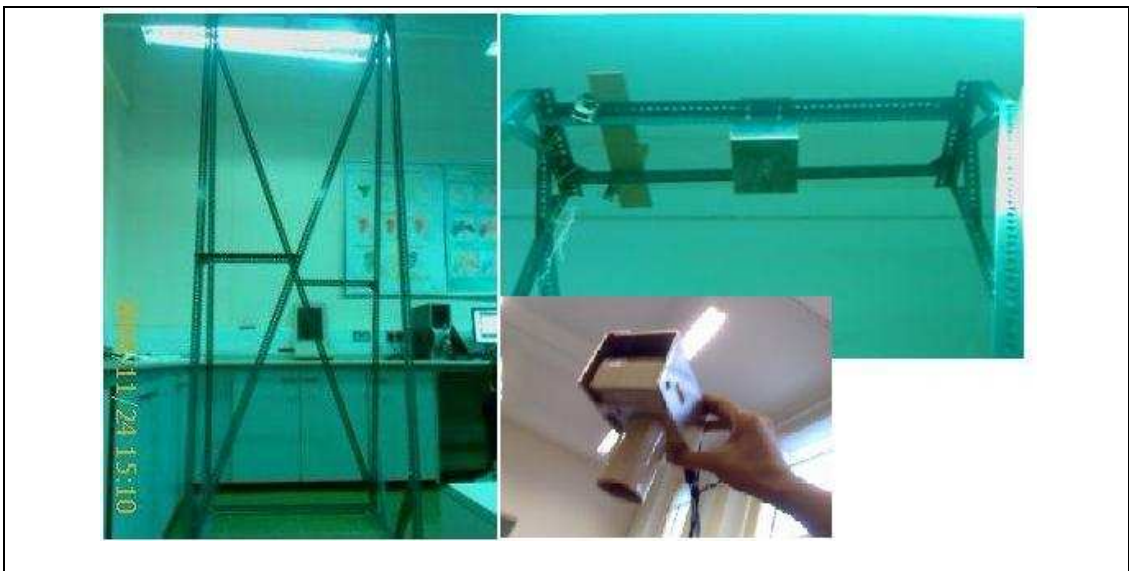


Figure 6.3: The simulation rig and bracket with dummy camera

B. Control Points

A control model was used for calibration purposes. In this investigation, fifty-one stickers 2.5 mm x 2.5 mm square were placed beneath the rig and acted as well-distributed control points. The position of each square was transferred onto a transparency and by using the digitising table the position of the squares was

converted into digital form. Figure 6.4a shows an image of the control points and Figure 6.4b depicts the control points in vector form after digitising.

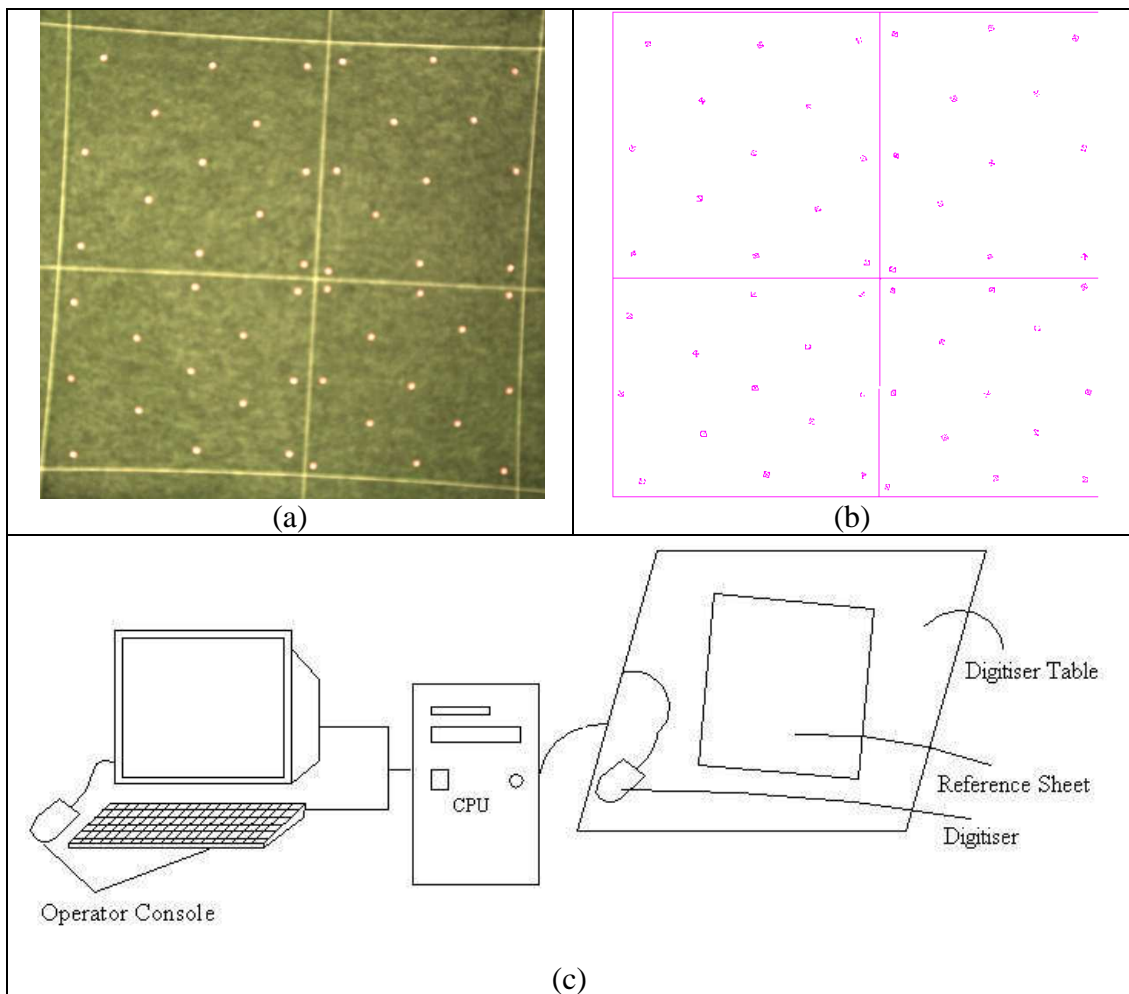


Figure 6.4: Position of control points (a) image of control points captured by sensor, (b) actual control points after digitise and c) digitising equipment

C. Root Mean Square Error (RMSE)

To determine the accuracy for the laboratory test, the test image was overlaid onto the digitised control points in vector format. The differences between the control points (in image and digitise) were measured. Based on these measurements the root mean square error (RMSE) was produced to show the quality of lens distortion algorithm, tilt algorithm and oblique algorithm. Figure 6.5 shows the difference between extracted reference points from the test image and reference points from the

digitised control points, while Table 6.3 shows an example of determining the RMSE for each of the particular laboratory test images. The laboratory experiment was measured quantitatively to ensure the algorithm is suitable for low cost remote sensing images.

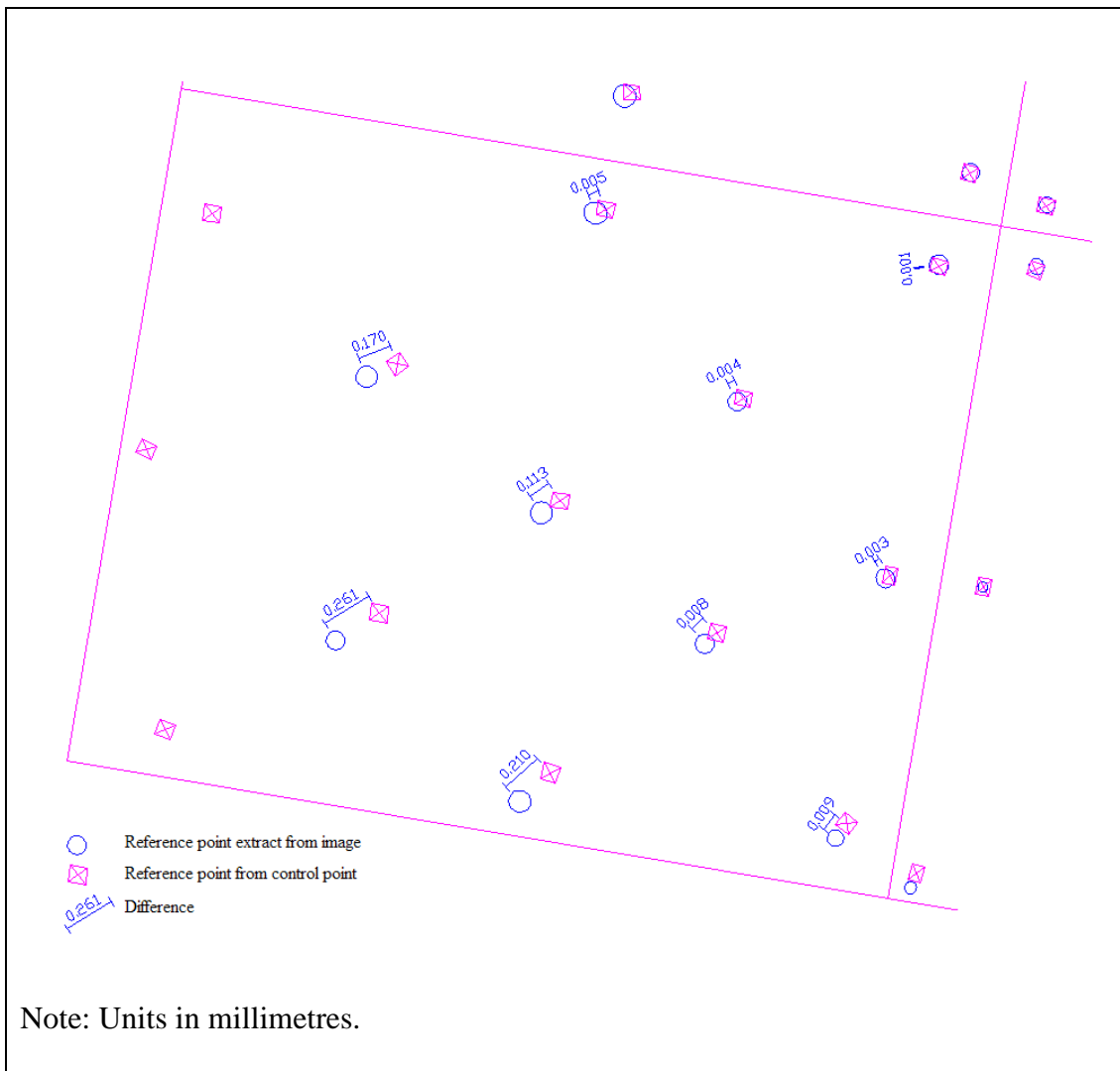


Figure 6.5: Sample of accuracy determination on the laboratory test product.

Table 6.3: Sample of RMSE for the laboratory product.

ID POINT	REF. X	REF. Y	ORI. X	ORI. Y	LNS. X	LNS. Y	TILT. X	TILT. Y	OBLI. X	OBLI. Y	SQ ORI. X	SQ ORI. Y	SQ LNS. X	SQ LNS. Y	SQ TILT. X	SQ TILT. Y	SQ OBLI. X	SQ OBLI. Y
ID01	-0.3	0.4	20.2	-12.3							408.0	151.3						
ID02	-0.1	0.4	4.4	-2.5	-1.6	-1.2	-1.2	5.5	-2.7	3.3	19.4	6.3	2.6	1.4	1.4	30.3	7.3	10.9
ID03	0.0	0.4	-0.1	0.6	-2.2	-1.6	-2.7	-6.5	-1.8	2.8	0.0	0.4	4.8	2.6	7.3	42.3	3.2	7.8
ID04	0.1	0.4	-0.4	1.5	-2.7	-1.3	-3.2	-10.8	-1.4	3.3	0.2	2.3	7.3	1.7	10.2	116.6	2.0	10.9
ID05	0.2	0.4	1.8	2.9	-0.9	-1.4	-2.4	-21.8	-0.3	2.1	3.2	8.4	0.8	2.0	5.8	475.2	0.1	4.4
ID06	0.4	0.3	3.4	3.0	-0.4	-1.1	-2.2	-31.1	2.0	1.7	11.6	9.0	0.2	1.2	4.8	967.2	4.0	2.9
ID07	0.3	0.2	2.5	1.4	-1.4	-3.5	-3.0	-27.6	0.2	-1.2	6.3	2.0	2.0	12.3	9.0	761.8	0.0	1.4
ID08	0.2	0.3	0.3	1.7	-1.3	-3.2	-2.3	-17.4	0.5	0.6	0.1	2.9	1.7	10.2	5.3	302.8	0.3	0.4
ID09	-0.1	0.3	0.4	0.2	-1.9	-1.9	-1.8	0.9	-2.1	1.5	0.2	0.0	3.6	3.6	3.2	0.8	4.4	2.3
ID10	-0.2	0.3	8.2	-3.3	-0.6	-1.6	-0.1	13.6	-2.5	1.9	67.2	10.9	0.4	2.6	0.0	185.0	6.2	3.6
ID11	-0.3	0.3																
ID12	-0.2	0.2	2.2	-0.5	-1.5	-1.5	-1.2	9.0	-3.1	1.1	4.8	0.3	2.3	2.3	1.4	81.0	9.6	1.2
ID13	0.0	0.2	-1.0	0.2	-0.9	-2.8	-1.2	-4.9	-0.7	-0.6	1.0	0.0	0.8	7.8	1.4	24.0	0.5	0.4
ID14	0.1	0.2	-0.4	0.2	-0.2	-3.3	-0.7	-9.1	0.5	-0.8	0.2	0.0	0.0	10.9	0.5	82.8	0.3	0.6
ID15	0.2	0.2	1.2	-0.5	-1.0	-4.3	-2.2	-21.1	1.2	-1.3	1.4	0.3	1.0	18.5	4.8	445.2	1.4	1.7
ID16	0.3	0.2	4.1	-0.1	-1.5	-3.5	-3.4	-31.5	1.0	-2.2	16.8	0.0	2.3	12.3	11.6	992.3	1.0	4.8
ID17	0.1	0.1	0.1	-1.0	0.1	-3.3	-0.8	-12.8	1.1	-1.9	0.0	1.0	0.0	10.9	0.6	163.8	1.2	3.6
ID18	-0.1	0.1	-0.3	0.2	-0.9	-1.7	-0.8	3.1	-1.4	-0.1	0.1	0.0	0.8	2.9	0.6	9.6	2.0	0.0
ID19	-0.3	0.2	7.9	-0.6	-0.2	-1.1	0.7	17.3	-2.5	0.8	62.4	0.4	0.0	1.2	0.5	299.3	6.3	0.6
ID20	-0.4	0.1																
ID21	-0.2	0.1	3.4	1.2	-0.6	-0.9	-0.3	12.4	-2.3	0.0	11.6	1.4	0.4	0.8	0.1	153.8	5.3	0.0
ID22	0.0	0.0	-0.5	-0.8	0.0	-1.9	-0.4	-1.2	-0.4	-1.6	0.3	0.6	0.0	3.6	0.2	1.4	0.2	2.6
ID23	0.0	0.0	-0.8	-0.8	0.0	-1.4	-0.6	-3.6	-0.2	-1.3	0.6	0.6	0.0	2.0	0.4	13.0	0.0	1.7
ID24	0.2	0.0	0.6	-1.7	-0.7	-1.4	-1.9	-15.3	0.1	-1.6	0.4	2.9	0.5	2.0	3.6	234.1	0.0	2.6

ID25	0.3	0.0	3.7	-3.5	-1.5	-2.9	-3.1	-27.8	2.0	-2.3	13.7	12.3	2.3	8.4	9.6	772.8	4.0	5.3
ID26	0.3	-0.1	3.0	-3.7	-1.6	-2.2	-3.5	-26.4	1.6	-1.8	9.0	13.7	2.6	4.8	12.3	697.0	2.6	3.2
ID27	0.2	0.0	0.3	-2.5	-0.8	-1.2	-1.9	-14.3	-0.3	-1.7	0.1	6.3	0.6	1.4	3.6	204.5	0.1	2.9
ID28	0.0	0.0	-0.5	-2.0	-0.2	-2.0	-0.4	-3.6	-0.4	-2.4	0.3	4.0	0.0	4.0	0.2	13.0	0.2	5.8
ID29	0.0	0.0	0.1	-1.3	0.1	-1.9	-0.1	0.2	-0.5	-2.1	0.0	1.7	0.0	3.6	0.0	0.0	0.2	4.4
ID30	-0.2	0.0	4.9	1.0	0.1	-0.7	0.9	14.1	-1.8	-0.7	24.0	1.0	0.0	0.5	0.8	198.8	3.2	0.5
ID31	-0.4	0.0																
ID32	-0.3	-0.1	15.9	5.4							252.8	29.2						
ID33	-0.1	-0.1	3.2	0.8	0.3	-0.7	0.6	9.4	-1.3	-1.6	10.2	0.6	0.1	0.5	0.4	88.4	1.7	2.6
ID34	0.1	-0.1	-0.6	-2.7	-1.2	-1.5	-2.0	-7.4	-1.4	-2.7	0.4	7.3	1.4	2.3	4.0	54.8	2.0	7.3
ID35	0.2	-0.1	1.2	-3.8	-1.6	-1.7	-2.9	-19.2	0.4	-1.3	1.4	14.4	2.6	2.9	8.4	368.6	0.2	1.7
ID36	0.3	-0.2	1.9	-3.1	-1.5	-2.4	-3.0	-23.8	1.5	-3.3	3.6	9.6	2.3	5.8	9.0	566.4	2.3	10.9
ID37	0.1	-0.2	0.5	-2.8	-1.5	-1.6	-2.4	-11.3	-1.5	-3.8	0.3	7.8	2.3	2.6	5.8	127.7	2.3	14.4
ID38	0.0	-0.2	0.8	-0.6	-1.1	-1.1	-1.4	0.3	-2.0	-2.8	0.6	0.4	1.2	1.2	2.0	0.1	4.0	7.8
ID39	-0.1	-0.2	2.8	1.1	0.2	-0.1	0.2	4.5	-1.0	-2.1	7.8	1.2	0.0	0.0	0.0	20.3	1.0	4.4
ID40	-0.2	-0.1	9.7	5.3	1.9	1.4	2.6	18.8	-0.9	-0.1	94.1	28.1	3.6	2.0	6.8	353.4	0.8	0.0
ID41	-0.3	-0.2																
ID42	-0.4	-0.1	-95.1	95.0							9044.0	9025.0						
ID43	-0.1	-0.2	6.5	4.7	1.0	1.2	1.3	12.9	-1.1	-1.0	42.3	22.1	1.0	1.4	1.7	166.4	1.2	1.0
ID44	0.1	-0.3	0.6	0.3	-1.9	-0.9	-2.5	-4.5	-2.5	-3.3	0.4	0.1	3.6	0.8	6.3	20.3	6.3	10.9
ID45	0.2	-0.3	0.3	-1.9	-2.1	-2.1	-3.7	-16.4	-2.3	-4.6	0.1	3.6	4.4	4.4	13.7	269.0	5.3	21.2
ID46	0.3	-0.4	0.8	1.8							0.6	3.2						
ID47	0.1	-0.3	0.8	2.1							0.6	4.4						
ID48	0.0	-0.3	3.9	6.9	-1.4	1.5	-1.6	6.1	-2.7	-1.7	15.2	47.6	2.0	2.3	2.6	37.2	7.3	2.9
ID49	-0.1	-0.3	6.3	6.7	0.5	1.7	0.5	9.0	-1.3	-1.3	39.7	44.9	0.3	2.9	0.3	81.0	1.7	1.7
ID50	-0.2	-0.3	16.0	13.3	4.4	5.1	5.2	23.8	1.6	2.0	256.0	176.9	19.4	26.0	27.0	566.4	2.6	4.0
ID51	-0.4	-0.3																
TOTAL err (value in mm)			44.2	105.5	-28.3	-56.0	-48.9	208.5	-28.7	-32.1	10432.9	9666.3	80.9	190.3	187.1	9988.2	104.0	177.2
Sample Number			45.0	45.0	41.0	41.0	41.0	41.0	41.0	41.0	231.8	214.8	2.0	4.6	4.6	243.6	2.5	4.3
RMSE (value in mm)											15	15	1	2	2	16	2	2

D. Determination of Intrinsic Parameters

Instead of qualitative measurement, the laboratory test was also used to measure quantitatively measure the laboratory product, in order to assess the consistency of the observation made by the low cost remote sensing device (IMU and imaging device). Before measuring the consistency, the imaging device was calibrated by using well established software, photomodeler scanner version 6.6 (Photomodeler, 2011). The calibration gave the intrinsic parameters of the imaging device. These parameters were compared with the intrinsic parameters obtained the from single image approach. Later, the rotation of the camera was extracted and compared with the rotation given by the IMU device.

In the calibration process, six images, is the minimum requirement for camera calibration by photomodeler software, were selected namely; LAB14020602, LAB14020617, LAB14020608, LAB14020672, LAB14020614 and LAB14020698. These images had been selected because the combination of these images enable photomodeler to process the calibration task where other combinations had failed. In the calibration process, the reference points on each image were matched to each other manually, because the laboratory images did not have an identical control point compatible with the calibration grid provided by photomodeler. Figure 6.6 shows the images and the 3D view after the calibration process.

For the single image, the intrinsic parameters can be obtained by matching the reference points in the laboratory image with the reference points from digitised control points, which had been imported through the autocad exchange format or .dxf

format. This process enabled the intrinsic parameters such as focal length, roll, pitch and yaw to be produced. Figure 6.7 shows an example image and the 3D view after the processing process. Results from calibration and single image processing can be compared to evaluate the low cost remote sensing device, especially the IMU and the imaging device.

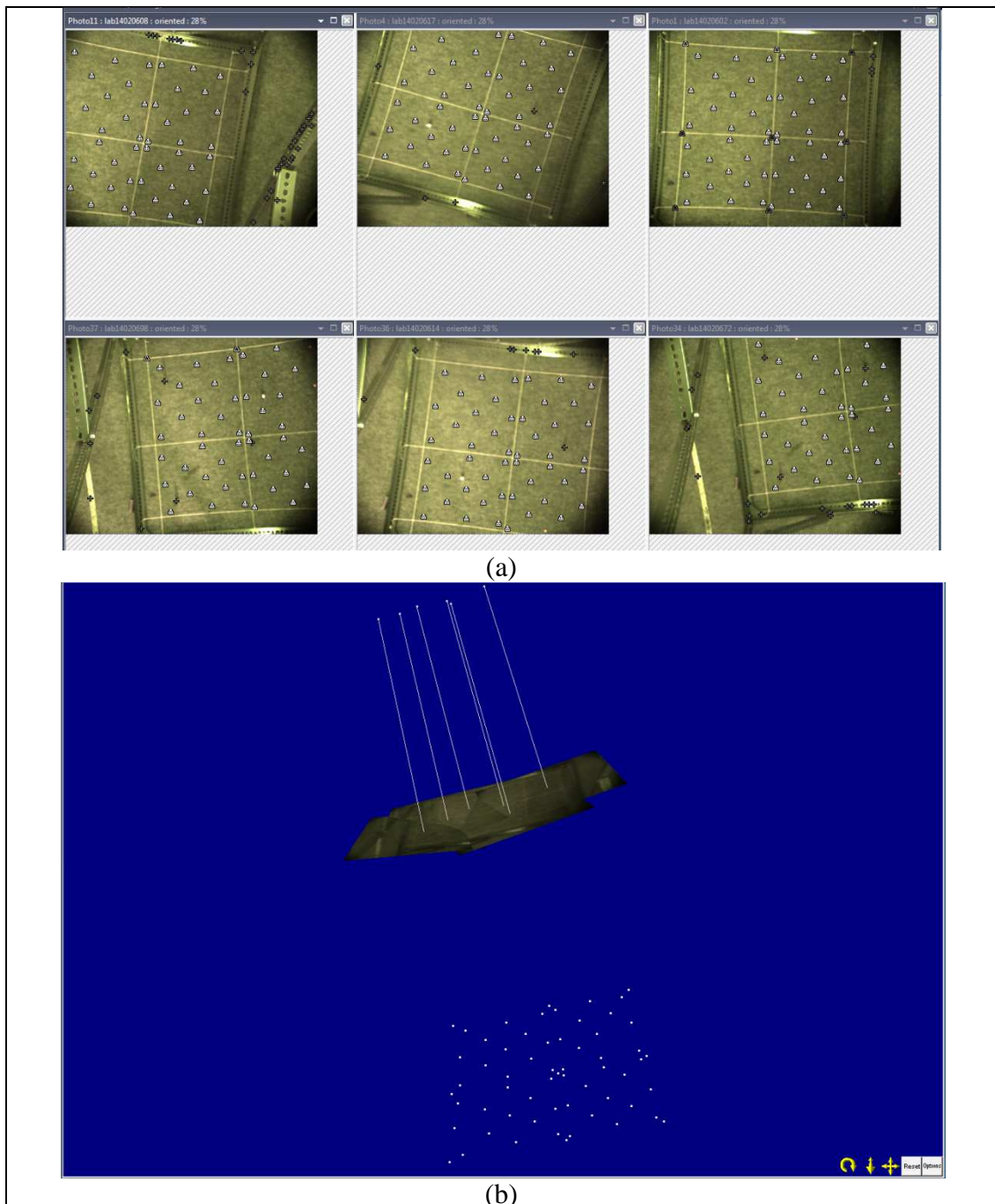


Figure 6.6: Calibration process for determining the intrinsic parameters. (a) Images used in the calibration process and (b) their view angle in 3D.

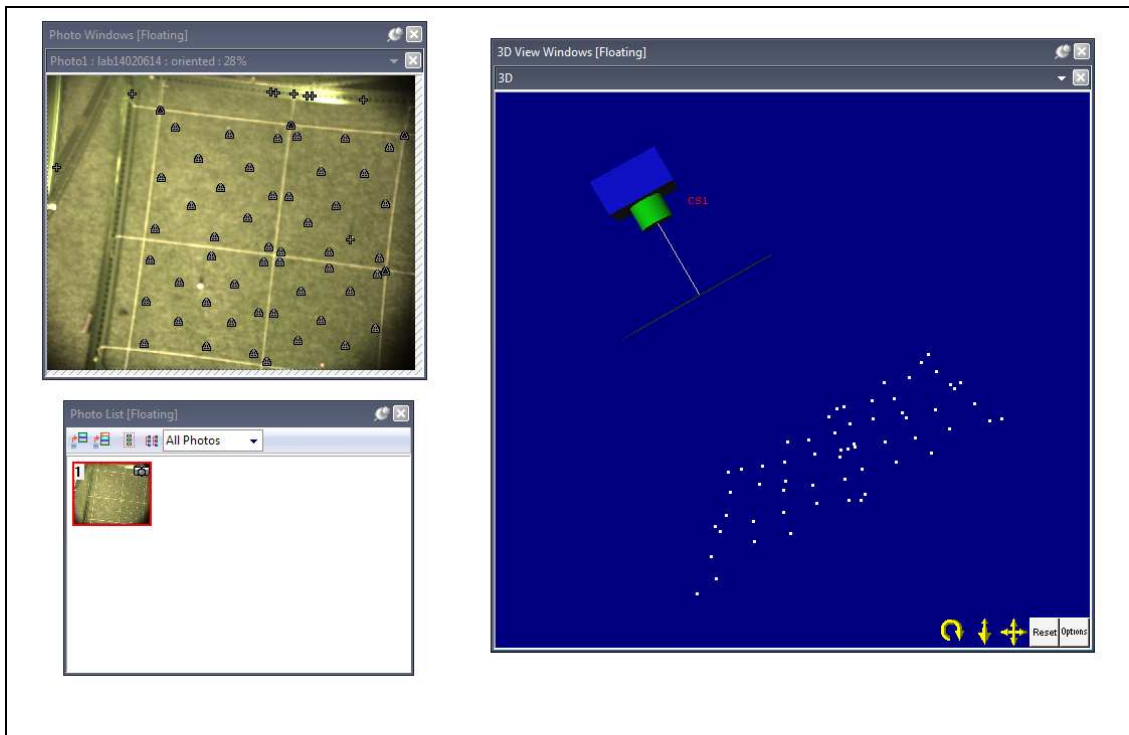


Figure 6.7: Single image technique for determining the intrinsic parameters. Top left is the image, bottom left is the photo browse and on the right is the product after processing.

6.3.1.1 Laboratory Test Results

Qualitative Test

The simulation test revealed that the imaging sensor might have suffered from lens distortion, for example pincushion distortion as illustrate in Figure 6.8. By using the lens distortion algorithm as described in Chapter 4, the pincushion distortion could be removed. Its application, showed that the algorithm used for correcting the lens distortion performed very well. In the qualitative test, the laboratory results had shown significant accuracy for the geometric correction task. The accuracy of the geometric correction was in the range of ± 01 mm to ± 16 mm, depending on the method of correction applied to the images. For instance, the vertical imagery needed only the lens distortion correction, in other words the vertical imagery can be used instantly if the lens is in perfect conditions. The tilt imagery can be considered

as a special case of oblique image, as these images can be corrected by using the oblique algorithm. It was also found that the tilt algorithm was able to correct the vertical imagery. Unfortunately, the implementation of the tilt algorithm on tilt imagery was not successful. Discussions on the failure of the tilt algorithm to correct the tilt images will be presented in Section 6.4.

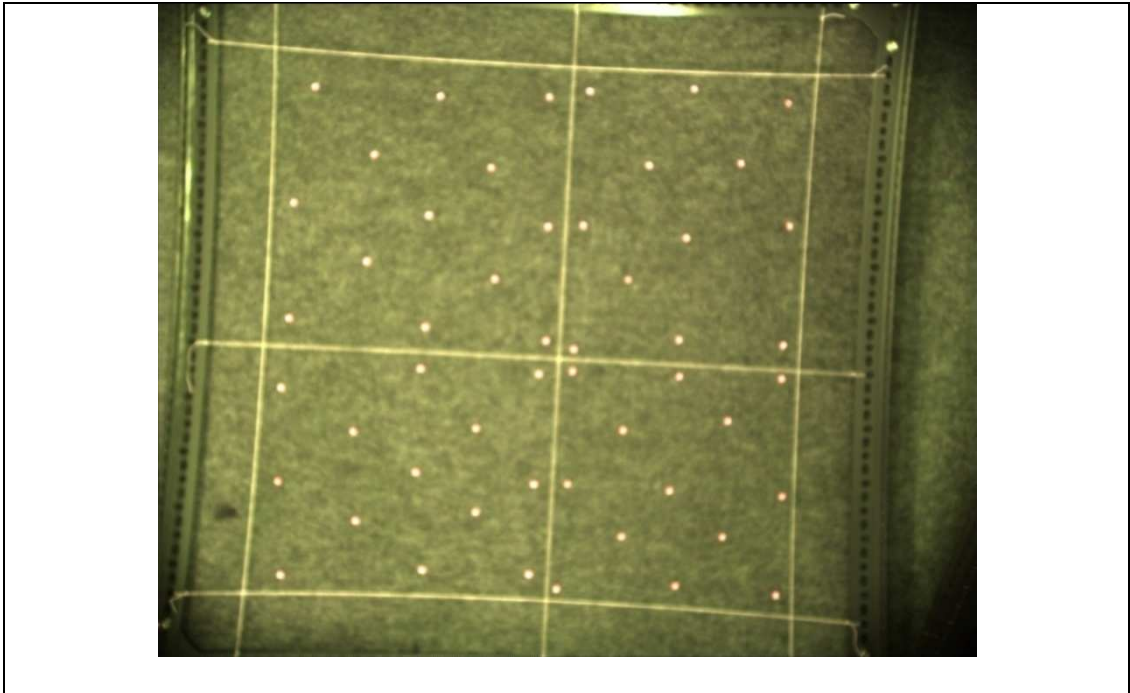



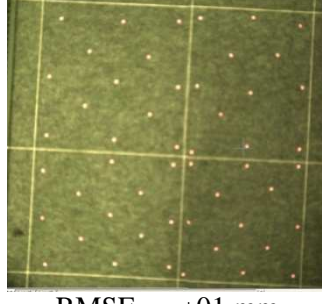

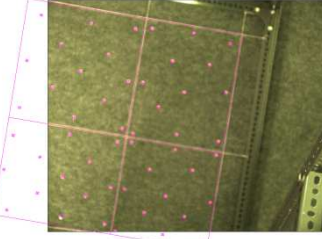
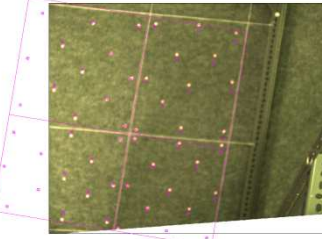
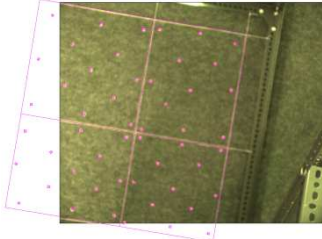

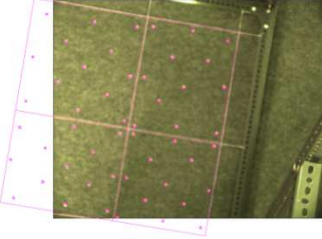
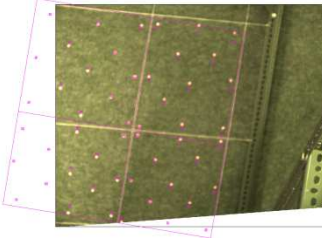
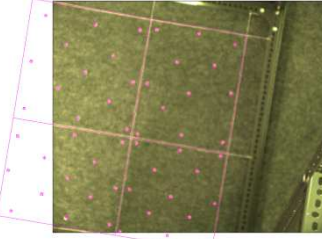


Figure 6.8: Pincushion distortion in image taken from laboratory test

For the oblique algorithm, it was found that the performance was acceptable within the range of ± 01 mm to ± 03 mm. It also revealed that the oblique algorithm was able to correct vertical and tilt images. It is presumed that in a real test a good result can be obtained from these low cost remotes sensing sensors. Figure 6.9 shows the image corrected by using different types of correction algorithm and Table 6.4 shows the IMU data collected from the laboratory test. The results will be discussed further in section 6.4.

Table 6.4: IMU data from simulation test

ID Data	SEC	Roll			Pitch			Time		
		Deg	Min	Sec	Deg	Min	Sec	Hour	Min	Sec
LAB14020602	64	0	6	30	0	4	0	12	13	4
LAB14020603	121	4	33	0	0	21	30	12	14	1
LAB14020606	288	0	22	0	0	49	0	12	16	48
LAB14020608	357	4	20	30	3	15	30	12	17	57
LAB14020609	483	0	49	30	-3	37	0	12	20	3
LAB14020610	527	0	8	0	0	33	0	12	20	47
LAB14020611	582	0	5	0	0	20	30	12	21	42
LAB14020612	631	0	45	0	0	35	30	12	22	31
LAB14020613	734	0	11	0	0	7	30	12	24	14
LAB14020614	780	-3	51	30	0	53	0	12	25	0
LAB14020616	840	-2	35	0	0	3	0	12	26	0
LAB14020617	900	4	47	0	1	39	30	12	27	0
LAB14020619	960	2	21	30	2	5	0	12	27	0
LAB14020620	1020	-2	56	30	0	23	0	12	29	0
LAB14020621	1090	-2	55	30	0	31	30	12	30	10
LAB14020628	1416	1	27	0	-1	50	0	12	35	36
LAB14020629	1457	2	27	30	0	1	0	12	36	17
LAB14020633	1656	-3	55	30	-1	39	30	12	39	36
LAB14020634	1709	-17	11	0	0	6	0	12	40	29
LAB14020646	2580	2	37	30	-2	19	0	12	55	0
LAB14020647	2614	1	14	30	-2	3	0	12	55	34
LAB14020651	2741	0	35	0	0	18	30	12	57	41
LAB14020654	2815	1	11	0	0	40	30	12	58	55
LAB14020656	2851	-5	58	0	-1	1	0	12	59	31
LAB14020657	2874	10	20	0	0	48	30	12	59	54
LAB14020668	3171	-2	22	0	4	23	0	1	4	51
LAB14020672	3275	-6	18	30	0	2	0	1	6	35
LAB14020675	3347	-11	7	30	4	14	0	1	7	47
LAB14020677	3412	-5	34	30	-4	16	0	1	8	52
LAB14020678	3435	-2	9	0	0	16	0	1	9	15
LAB14020679	3455	-4	28	0	0	19	30	1	9	35
LAB14020685	3589	-4	52	0	0	39	30	1	11	49
LAB14020687	3639	-1	10	30	2	21	0	1	12	39
LAB14020688	3666	0	34	0	0	28	30	1	13	6
LAB14020695	3813	0	29	30	-4	2	30	1	15	33
LAB14020698	3884	-11	11	30	0	35	30	1	16	44
LAB14020699	3923	1	34	0	0	48	0	1	17	23

IMAGE ID / ROTATION ANGLE	ORIGINAL / UNCORRECTED	AFTER LENS DISTORTION	CORRECTED USING TILT ALGORITHM	CORRECTED USING OBLIQUE ALGORITHM
LAB14020602 ROLL = 0° 06' 30" PITCH = 0° 04' 00"	 RMSE _X = ±04 mm RMSE _Y = ±05 mm	 RMSE _X = ±02 mm RMSE _Y = ±03 mm	 RMSE _X = ±02 mm RMSE _Y = ±03 mm	 RMSE _X = ±01 mm RMSE _Y = ±02 mm
LAB14020608 ROLL = 4° 20' 30" PITCH = 3° 15' 30"	 RMSE _X = ±15 mm RMSE _Y = ±15 mm	 RMSE _X = ±02 mm RMSE _Y = ±02 mm	 RMSE _X = ±02 mm RMSE _Y = ±16 mm	 RMSE _X = ±02 mm RMSE _Y = ±02 mm
LAB14020614 ROLL = -3° 51' 30" PITCH = 0° 53' 00"	 RMSE _X = ±15 mm RMSE _Y = ±15 mm	 RMSE _X = ±02 mm RMSE _Y = ±02 mm	 RMSE _X = ±03 mm RMSE _Y = ±16 mm	 RMSE _X = ±01 mm RMSE _Y = ±02 mm

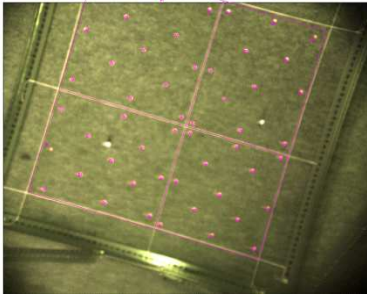
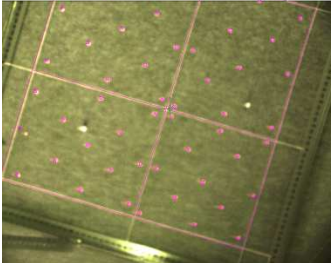
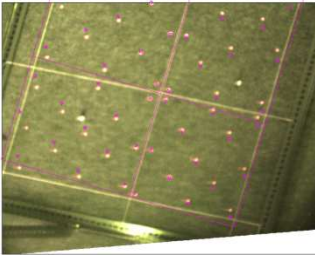
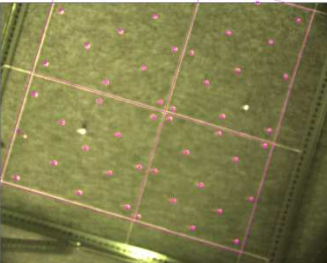
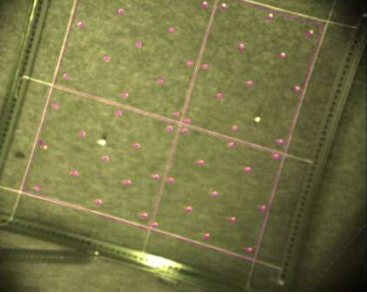
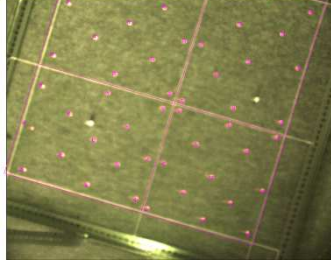
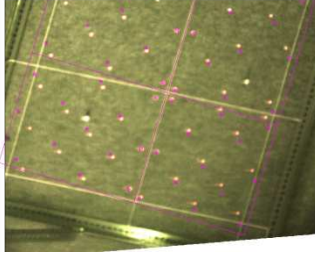
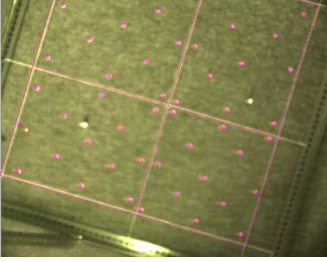
<p>LAB14020617</p> <p>ROLL = $4^{\circ} 47' 00''$</p> <p>PITCH = $1^{\circ} 39' 30''$</p>	 <p>RMSE_X = ± 02 mm RMSE_Y = ± 04 mm</p>	 <p>RMSE_X = ± 02 mm RMSE_Y = ± 02 mm</p>	 <p>RMSE_X = ± 02 mm RMSE_Y = ± 19 mm</p>	 <p>RMSE_X = ± 02 mm RMSE_Y = ± 03 mm</p>
<p>LAB14020698</p> <p>ROLL = $-11^{\circ} 11' 30''$</p> <p>PITCH = $0^{\circ} 35' 30''$</p>	 <p>RMSE_X = ± 02 mm RMSE_Y = ± 04 mm</p>	 <p>RMSE_X = ± 03 mm RMSE_Y = ± 04 mm</p>	 <p>RMSE_X = ± 08 mm RMSE_Y = ± 20 mm</p>	 <p>RMSE_X = ± 02 mm RMSE_Y = ± 03 mm</p>

Figure 6.9: Laboratory test results.

Quantitative Test

The quantitative test has found that not all images can be used for field calibration. In this study, it was found that only six images was suitable for field calibration out of the thirty six (36) images obtained. However, it shows that the field calibration was able to attain the full interior orientation parameters. Table 6.5 shows the full interior orientation parameters obtained from the photomodeler software.

Table 6 5: Intrinsic parameters obtained from the calibration process

Parameters	Value
Focal Length	9.329514 mm
Xp – Principle Point x	3.317975 mm
Yp – Principle Point y	2.706496 mm
Format Width	6.008832 mm
Format Height	4.800000 mm
K1- radial distortion	-3.637e-003
K2- radial distortion	-5.704e-005
K3- radial distortion	0.000e+000
P1 - decentering	-2.329e-003
P2 - decentering	3.155e-003

The quantitative test also revealed that eighteen (18) out of the thirty six (36) images could not be processed by the photomodeler software using the single image technique. The difference in roll and pitch between extraction from the software and the IMU device fall in the range of -8.2 to 10.8 degrees in roll and -12.5 to 7.8 degrees in pitch. Table 6.6 show the comparisons of rotation angles between extraction and the IMU device.

The focal length obtained from the photomodeler software fall in range of 0.1 to 9.6 mm with one of the test image (LAB14020621) giving a focal length that is similar to manufacturer's value which is 8.5mm.

Table 6.6: Comparison of the rotation angles gather through extraction and IMU device

ID DATA	Focal Length	PP (X)	PP(Y)	Format Width	Format Height	ROLL	PITCH	Roll	Pitch	Diff. Roll	Diff. Pitch
LAB14020602	0.3	3.0	2.4	6.0	4.8	0.0	0.0	0.1	0.1	-0.1	-0.1
LAB14020603	4.1	3.0	2.4	6.0	4.8	1.7	2.8	4.6	0.4	-2.9	2.4
LAB14020606	UNABLE TO BE PROCESSED							0.4	0.8		
LAB14020608	0.2	3.0	2.4	6.0	4.8	0.1	-0.2	4.3	3.3	-4.3	-3.4
LAB14020609	6.1	3.0	2.4	6.0	4.8	9.8	-7.0	0.8	-2.4	8.9	-4.6
LAB14020610	UNABLE TO BE PROCESSED							0.1	0.6		
LAB14020611	0.2	3.0	2.4	6.0	4.8	0.0	-0.2	0.1	0.3	0.0	-0.5
LAB14020612	UNABLE TO BE PROCESSED							0.8	0.6		
LAB14020613	UNABLE TO BE PROCESSED							0.2	0.1		
LAB14020614	UNABLE TO BE PROCESSED							-2.1	0.9		
LAB14020616	UNABLE TO BE PROCESSED							-1.4	0.1		
LAB14020617	9.6	3.0	2.4	6.0	4.8	-3.4	-0.2	4.8	1.7	-8.2	-1.9
LAB14020619	UNABLE TO BE PROCESSED							2.4	2.1		
LAB14020620	1.2	3.0	2.4	6.0	4.8	-0.2	0.9	-1.1	0.4	0.9	0.5
LAB14020621	8.5	3.0	2.4	6.0	4.8	-2.2	-3.4	-1.1	0.5	-1.1	-3.9
LAB14020628	UNABLE TO BE PROCESSED							1.5	-0.2		
LAB14020629	UNABLE TO BE PROCESSED							2.5	0.0		
LAB14020633	UNABLE TO BE PROCESSED							-2.1	-0.3		
LAB14020634	UNABLE TO BE PROCESSED							-16.8	0.1		
LAB14020646	UNABLE TO BE PROCESSED							2.6	-1.7		
LAB14020647	0.2	3.0	2.4	6.0	4.8	-0.1	0.1	1.2	-2.0	-1.4	2.0
LAB14020651	UNABLE TO BE PROCESSED							0.6	0.3		
LAB14020654	UNABLE TO BE PROCESSED							1.2	0.7		
LAB14020656	UNABLE TO BE PROCESSED							-4.0	-1.0		
LAB14020657	8.0	3.0	2.4	6.1	4.8	15.0	2.5	10.3	0.8	4.7	1.7
LAB14020668	UNABLE TO BE PROCESSED							-1.6	4.4		
LAB14020672	6.1	3.0	2.4	6.0	4.8	-2.3	7.8	-5.7	0.0	3.4	7.8
LAB14020675	5.1	3.0	2.4	6.0	4.8	-2.1	4.0	-10.9	4.2	8.8	-0.2
LAB14020677	0.1	3.0	2.4	6.0	4.8	0.0	0.0	-4.4	-3.7	4.4	3.8
LAB14020678	UNABLE TO BE PROCESSED							-1.9	0.3		
LAB14020679	5.5	3.0	2.4	6.0	4.8	4.6	-7.4	-3.5	0.3	8.1	-7.7
LAB14020685	UNABLE TO BE PROCESSED							-3.1	0.7		
LAB14020687	UNABLE TO BE PROCESSED							-0.8	2.4		
LAB14020688	6.3	3.0	2.4	6.0	4.8	6.1	-12.0	0.6	0.5	5.5	-12.5
LAB14020695	2.3	3.0	2.4	6.0	4.8	-1.1	1.8	0.5	-4.0	-1.5	5.8
LAB14020698	0.9	3.0	2.4	6.1	4.8	0.0	0.9	-10.8	0.6	10.8	0.3
LAB14020699	UNABLE TO BE PROCESSED							1.6	0.8		

Note: ROLL and PITCH is obtained from image extraction, Roll and Pitch is obtained from IMU device, Diff. Roll and Diff. Pitch is the different in roll and pitch between angles obtained from image extraction and IMU device.

The chip format for the imaging sensor obtained from the photomodeler software is 6.8 x 4.8 mm which is consistent for all test images. It shows that the established photomodeler software is unable to give consistent results (especially the focal length) for these low cost remote sensing images. These issues will be discussed further in section 6.6.

6.3.2 On-the-road Test Drive

The objective of the on-the-road test drive was to evaluate the ability of the GPS (Garmin 76) receiver to receive the GPS signal when the vehicle speed varied. This investigation was used to determine the optimum speed of the light aircraft to be used for image acquisition. In the on-the-road test drive, the navigation units containing the GPS receiver and IMU unit were loaded into the vehicle, which was driven at speeds varying from 10 to 70 mph for the test duration of three hours. At the end of the test, a series of GPS and IMU data was obtained. All the navigation information was recorded by a personal data assistant. Figure 6.10 shows the navigation equipment loaded in the land vehicle.



Figure 6.10: GPS and IMU devices for test drive

6.3.2.1 On-the-road Test Drive Results

The on-the-road test drive confirmed that the WAAS satellites were available, whereby all the GPS coordinates could be obtained using the differential method, which is recognised as the best technique to obtain GPS data. The reference position had an error of ± 0.04 seconds of arc in both directions (North and West). This means the error would be ± 1.300 metres for northing and ± 0.786 metres for easting in the OSTN02 coordinate system. The conversion from WGS84 to OSTN02 was made by using the Grid InQuest software provided by Ordnance Survey of Great Britain. Analysis had shown that the Garmin 76 GPS was sufficient for precision agriculture applications (Searcy, 2003). In addition, a plot of the trajectory (Figure 6.11) showed no missing data occurred during the test. It had been expected that during the validation test (Chapter 7) the same results could be obtained.

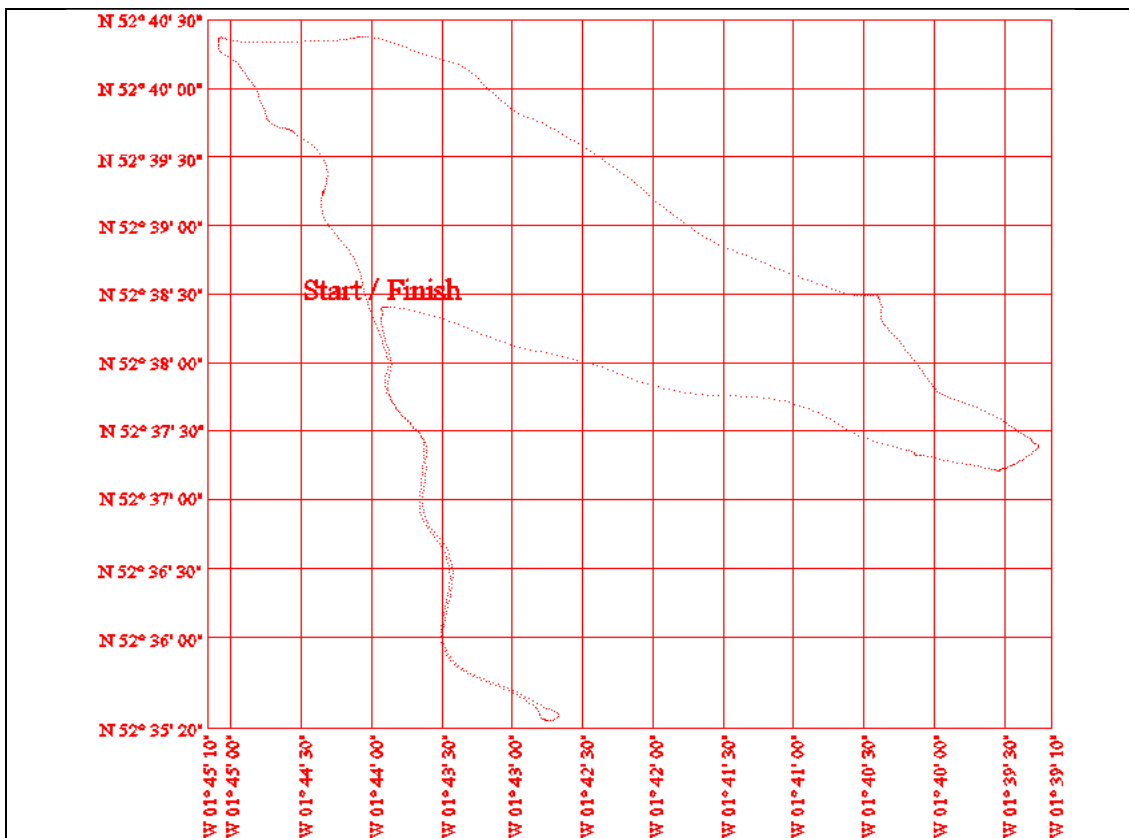


Figure 6.11: Trajectory plot of test drive

The IMU had shown an acceptable difference (error) in both axes (roll and pitch), but a distinct difference in yaw axis was found. However, it was noticeable that this error was much better than what was claimed by the manufacturer. Therefore, it can be said that the selected IMU device had adequate accuracy for use as a navigation tool. Table 6.7 shows the difference of IMU and GPS at the reference station, before and after the on-the-road test drive.

Table 6.7: Leap-frog test

	Time	12:59:22	13:30:16	13/09/2007	
	Item	Before	After	Diff	Units
	Roll	-3.5000	-3.5833	0.0083	degrees
	Pitch	1.6667	2.0000	-0.0333	degrees
	Yaw	2758.0000	2181.0833	5.7692	degrees
\$GPGGA	West	1°48.6101'	1°48.6109'	-0.0480	sec
	North	52°39.2459'	52°39.2452'	0.0420	sec
\$GPGLL	West	1°48.6101'	1°48.6108'	-0.0420	sec
	North	52°39.2458'	52°39.2453'	0.0330	sec

6.4 Results Discussions

The investigation results show the pattern of the errors in the GPS, the IMU and the imaging sensor. The error pattern was analysed in order to assess the competency of the instruments for use in the portable remote sensing system. By pinpointing the pattern of errors in the individual instruments, the correct procedure could be determined in order to mitigate the errors. The most important thing was to ensure that all the instruments were capable of delivering the information needed for the research.

The IMU performance test show good accuracy, as claimed by the manufacturer with ≈ 0.5 degrees in roll and pitch orientation, but it gives a poor result with ≈ 130 degrees in yaw direction. The GPS gives good results with an accuracy of ± 0.005 and ± 0.006 degrees in the north and south directions and ± 6.002 metre for height. The GPS simulation test showed that an accuracy of ± 1.300 m can be achieved, since it was discovered that most of the position was determined by the WAAS capability.

The simulation test has shown that the IMU could produce an accuracy of ± 2 mm to ± 16 mm when the tilt algorithm was employed and ± 4 mm and ± 3 using the oblique algorithm. However, following testing, it was found that the tilt algorithm is only suitable for vertical images (with tilt angle less than ± 3 degrees). This is because the tilt algorithm formula orientated the image by using the image centre as the pivot point, whereas for tilt image the orientation axis should be at the photo nadir point. Employing the oblique algorithm overcame the tilt algorithm problem and was used in the real applications.

The established software (photomodeler) is unable to work with the low cost remote sensing imaging device. A publish article from the photomodeler website in 2008, state that the application of this software is limited to imaging devices that have 11 megapixels and above, in order to run the field calibration (Photomodeler, 2008). The field calibration enabled full interior calibration to be obtained at a high level of accuracy. Even though the quantitative test was able to obtain the full interior calibration, the accuracy is not good enough. Remondino and Fraser (2006) found that it is not always possible to perform field-calibration for practical projects,

because the network geometries that are optimal for scene reconstruction are different from those (network geometries) that support comprehensive camera calibration. Therefore, it is better to pre-calibrate the camera rather than performing a field-calibration simultaneously with the object reconstruction. Since, the selected software was not able to give consistent results for the laboratory test, the manufactures values (as in section 7.2.3) were used for the direct georeferencing, whilst the RMS value was used to evaluate the accuracy of the low-cost remote sensing system rather than making a comparison with other particularly software. The low-cost remote sensing system required further testing to assess the accuracy of the system via real-data acquisition. This is described in Chapter 7.

6.5 Summary

This chapter has discussed the experimental investigation for the selected devices. Two types of experiments were carried out: 1) performance test and 2) simulation test. The main focus of the performance test was to verify the accuracy of the devices. This accuracy would be an initial input for filtering the IMU data. While for GPS this performance test gave an idea of the accuracy to be expected from the Garmin 76, for the imaging sensor it gave a warning of action necessary during the data acquisition process.

The simulation test focused on the dynamic accuracy with respect to position, direct geo-reference accuracy, and stability of the IMU and GPS devices. Two types of test were carried out: 1) laboratory test, and 2) on-the-road test drive. In the laboratory test, the accuracy of direct geo-referencing using IMU data was evaluated. In the test

drive mode, the dynamic capability was assessed. Finally, the experimental investigation results were presented and will be discussed in Chapter 9.

7. SYSTEM VALIDATION: A FLIGHT TEST

7.1 Introduction

Chapter 6 showed that the system has good performance, especially the low-cost GPS, Garmin 76, which records 100% differential data, while the IMU data provides the capability for orientating the images. The oblique algorithm works well for vertical images and that a tilt image can be regarded as a special case of oblique.

This chapter will demonstrate how the system was tested in a real world situation aboard a light aircraft and, importantly, it will confirm that the data processing technique, discussed in Chapter 4, is adequate to solve the geo-rectification problem. As the equipment has been designed for use with respect to agriculture, the flight test was carried out for data acquisition in a known designated area of agricultural fields. Data acquisition included determination of the test site, planning the flight mission and obtaining the image data and ancillary data. These data were then processed as discussed in Chapter 4, and the accuracy of the final results, which was a geocoded image was evaluated. The discussions on results follow in Chapter 8.

7.2 Data Acquisition

Data acquisition took place on 30 January, 7 February and 25 July, 2008. The first attempt was unsuccessful because of technical failure, whereby the data logging software could not store the volume of data captured from the IMU and GPS devices. The second attempt seemed to work very well in the field and on the processing desk, but unfortunately, the accuracy obtained did not meet expectations, and thus

the third test was carried out. In all attempts, the procedure and main instruments remained unchanged, except that an additional GPS and new logging software were included and the number of crew members onboard increased. There were three crew members: 1) pilot, 2) navigator and 3) data manager. The pilot flew the aircraft to the test site and controlled the aircraft (turning, banking and gliding) during the acquisition process. The navigator pointed the imaging device at the target objects, whilst the operator managed the logging system.

Before acquiring data, it was very important that a short briefing on the procedure was given to all crew members, since the test flight did not follow the normal of remote sensing or photogrammetry procedures. Here, the navigator would instruct the pilot to bank the aircraft about 70-90 degrees to enable a vertical position downwards towards the target object to be detected as defined by the sensor's viewfinder. The pilot had to ensure that the position was safe for this acrobatic move. In addition, the pilot had to keep providing updates on current wind speed, tracking information from the base station and maintaining a stable aircraft platform. The navigator and pilot received updates on the acquisition progress from the data manager, who controlled the data logging system. This task showed that effective communication was essential to ensure a smooth and clean process.

Since the procedure did not follow an existing method applied by photogrammetrists to get an overlap image, the light aircraft had to circle above the target area. This enabled the sensor operator to capture an over-lapping image of that particular area. The orientation of the overlap images were determined by GPS coordinates. As the

device used was portable, the position of the camera could be changed very frequently.

7.2.1 Test Site

The test site was an agricultural farming area in the south west of Kent in the UK. The farming area was selected on account of its reputation: “The Rural Economy of the Southern Counties” was mentioned by William Marshall in 1798, but it has been named the Garden of England for more than 400 years (Wainwright, 2006) and also because of the navigator’s local knowledge.

Intensive agriculture and smaller scale farms exist side-by-side here, with a total area of 374 000 hectares covered with a dense concentration of high value crops, especially soft fruits and hops, and this made the test site very interesting to the study. Figure 7.1 shows the agriculture land classification from the Kent County Landscape Information System and was obtained from Kent County Council (2008). Another factor in the choice of site was the availability of local airports and aerodromes, which have a variety of light aircraft available for hire for personal purposes: these include Rochester Airport, Kent International Airport, Headcorn Aerodrome, Bekesbourne Aerodrome and Damnys Hall Aerodrome all of which offer a variety of aviation activity.



Source: Kent County Council (2008)

Figure 7. 1: Sites assigned for flight tests.

7.2.2 Flight Missions

The flight missions were to test a new design of portable remote sensing system and the procedure adopted to manage the system, being a first of its kind. The flight missions would provide unprecedented information on the condition of the portable remote sensing system, especially on its capability and quality and most important, the limitations of the system.

For a flight mission, a single engined light aircraft, specifically a Cessna 172, with four seated cabin, opening window next to the front passenger seat and glass topped roof had been chosen. The choice of this particular aircraft was to ensure that the aerial photographer was able to capture the scene through the open window and that the GPS receiver could receive signals continuously. The flying height varied between 150 to 460 m above ground level and the data acquisition was based on a single location verified previously on the map. This meant that no distinct pattern of flight-lines would be formed. For each location, the aircraft would fly in a circle with a ground speed of 100 miles per hour before continuing to the next location. The wind speed at the time of the flight mission should not exceed 15 knots, to reduce the aircraft vibration due to cross-wind, for safe operation.

Table 7.1 shows the outline of the flight missions undertaken on January 30, February 7 and July 25, 2008. Different airfields were used due to availability of the light aircraft. The flights each took about 30-40 minutes, including the journey from the airfield to the target area.

Table 7. 1: Flight missions: Field data

Date/Time 30 January 2008	
Airport	Stappleford Aerodrome (Essex)
Weather	Bright/Sunny
Flying Duration	30 min
Aircraft Speed	105 km/hr
Average flying height above ground	2500/2000/1500/1000/500 ft
Wind Speed	8 knots
Date/Time 7 February 2008	
Airport	Headcorn Aerodrome (Kent)
Weather	Bright/Sunny
Flying Duration	30 min
Aircraft Speed	105 km/hr
Average flying height above ground	1000 ft
Wind Speed	15 knots
Date/Time 25 July 2008	
Airport	Rochester Airport (Kent)
Weather	Bright/Sunny
Flying Duration	30 min
Aircraft Speed	105 km/hr
Average flying height above ground	2000/1000/500 ft
Wind Speed	14 knots

7.2.3 Remotely Sensed Data

During the test, 21 images were captured on the 30 January, 15 on 7 February and 18 on 30 January 2008. Unfortunately, none of the images acquired on 30 January 2008 could be processed because of the technical failure of the data logger device, due to problems with jack plugs and the software itself. Seven of the images taken on 7 February 2008 were available for processing, while the other eight could not be synchronized with the IMU due to lost signals. On 25 July 2008, seven of seventeen images were available for direct geo-referencing, others could not be processed because no matching IMU data was detained.

The images mainly covered the agricultural fields, residential areas and road lines as recognised objects. The pixels resolution of each image was about 1.3 mega pixels imaged on a 7.7 x 6.1 mm digital sensor screen (Heinold, 2008). The spatial resolution of each image was 6 microns per pixel, thus the particular image was sufficient for practical handling, interpretation, mapping and fine detailing, as reported by Baltsavias (1998), see Table 7.2. According to Ferrano et al., (2010), digital images produced either by scanning the image photo or obtained directly from a digital camera, have two important common features:

- i- discrete spatial information: which means that spatial information is stored and sampled in a fixed pattern array which determines the pixel size and pixel number;
- ii- the grey values digitised on the sensors are available as analogue values even on CCD or CMOS sensors, and analogue to Digital (A/D) conversion, or vice-versa can be achieved after the image capture.

Therefore, Table 7.2 can be used as a guideline for determining the limit of applications for digital cameras.

Table 7.2: Optimal pixel sizes for applications



Source: Baltsavias, 1998.

In addition, the pixel size in microns also shows that the acquired images have equivalent quality when compared with high resolution camera images, as shown in Table 7.3.

Table 7.3: Top high resolution camera with pixel size



Source: Petrie, 2003.

The coverage of field area depends on the altitude of the platform. A 40° field of view (FOV) angle at an altitude of 500m would give coverage of approximately 0.8 x 0.8 km square, with a spatial resolution of approximately 1.2 m. This spatial resolution is sufficient for precision agriculture applications. The estimations of pixel size, spatial resolution, FOV and the coverage area can be derived from the sensor specification as listed in Table 7.4 and this specification was used in the processing tasks.

Table 7.4: Specification of imaging sensor (Agricultural Digital Camera)



(Sources: Heinold, 2008)

7.2.4 Ancillary Data

The main purpose of the ancillary data in the validation process is to facilitate the direct geo-referencing task. This task needs: IMU data to orientate the image into the geo-position; GPS coordinates to rectify the image coordinates; topographical map to assess the accuracy; GPS base reference coordinates to reduce the GPS data; image property to scale and convert pixels (unit) into metric units; and, other relevant sources, such as the average height above mean sea level detained from the Ordnance Survey or a map.

The ancillary data were collected directly from the field or gathered from a recognised agency. For instance the digital topographical maps were obtained from UK Ordnance Survey, a subsidiary of the Ordnance Survey of Great Britain. The GPS reference data were obtained from the British Isles GPS archive Facility (BIGF) operated by Nottingham University's IESSG (BIGF, 2008). Other data, such as the image properties were inclusive within the image data or obtained through the relevant website.

7.2.5 Software

The main software for orienting the image into the geo-position was developed in Visual Basic .net programming language using Microsoft Visual Studio 2005, as given in Appendix G. Other software was used for processing, analysing and displaying the acquired data: an AutoCad 3D map was used to display the reference map and in determining the image coordinates; Trimble Geomatics Office was used to process the GPS kinematic data; ArcView version 9.0 was used to analyse the final results; and, Microsoft Excel spread sheet to analyse and reduce the IMU data.

7.3 Installation of Test Equipment

Since the sensing system is intended to be portable there was no intricate installation needed. However, it is necessary to be well prepared and it is advisable for the devices to be connected and tested before takeoff, to avoid any miscommunications between devices. The connecting cables should be laid on a non-destructive path and free from photographer movement. The data logger should hold enough power for maintaining the data transferring process and it is advisable for an external power supply to be available. The data manager controlling the data logger should monitor closely the data collection process to identify and trace any inexplicable incidents. The navigator and the pilot should be informed of any odd incident so that a mistake or error may be dealt with before returning to ground. Thus, effective internal communications between navigator, data manager and pilot are needed to ensure a smooth acquisition process.

As the portable remote sensing device is assembled from a series of selected devices, it is vital to ensure that they are tightly stacked. It is preferable that a specially designed bracket is used to hold the devices together. Figure 7.2 shows the aircraft used in this research study, while Figure 7.3 shows the devices used in the validation test drive.



Figure 7. 2: Aircraft used for flight test

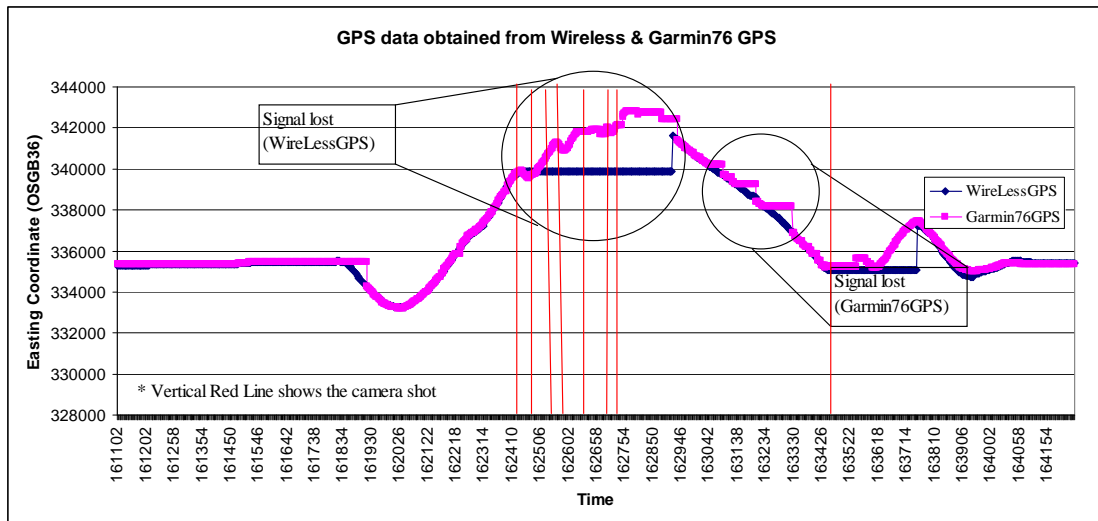


Figure 7.3: Preparation of devices ready for system validation test drive.

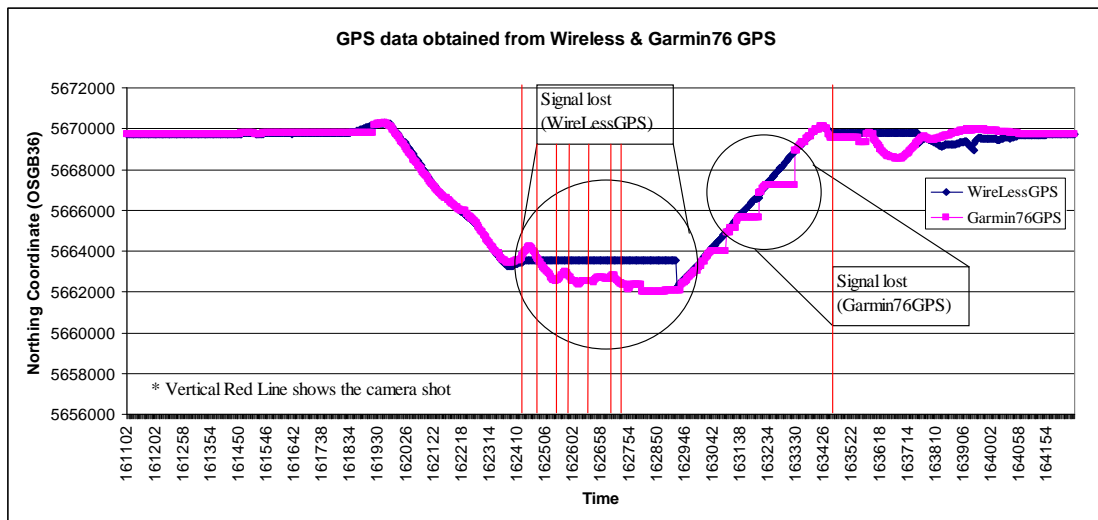
7.4 Flight Test Results

The various results obtained from the flight test were processed independently to study the behaviour of each individual device. The device behaviour study is a significant element, as the performance of each device used in the integrated IMU/GPS/image sensor system cannot be directly interpreted (in terms of mapping accuracy) unless operations and conditions are consistent (e.g. camera type and quality, image scale, image processing and operational aspects) (Skaloud, 1999). In addition, the specific operationing conditions, which have led to algorithm development, have their own relative merits. This means that there is no unique algorithm that can be applied as a universal solution, and hence they can only be referred to as guidelines (see, for instance, Abdullah and Tuttle (1999); Reid et al. (1998); Grejner-Brzezinska and Toth (1998)).

In this research study, three sets of GPS data were obtained from the flight tests: 1) Garmin 76 GPS data, 2) Garmin eTrex GPS data, and 3) Holux Bluetooth (wireless) GPS data. Garmin 76 and Wireless. The majority of the GPS data were recorded in NMEA0183 data format while Garmin eTrex GPS data were recorded in Rinex version 2.0 data format. Data recorded in NMEA0183 is considered as 'process data' via built-in software in the receivers, while data recorded in Rinex format are raw data and need to be processed. Unfortunately, data in Rinex format could not be processed due to a large number of check-sum errors (data acquired on 25 July 2008). The behaviour of Garmin 76 and wireless GPS is plotted in Figures 7.4 (a) and (b) in easting and northing coordinates, respectively.



(a)



(b)

Figure 7.4: Graphs showing behaviour of GPS data obtained from wireless and Garmin 76 GPS, with camera shot position.

In addition to GPS, the IMU data were also recorded in NMEA0183 data format which gives an output in roll, pitch, yaw and yaw rate. All the data were processed with the built-in software. Figures 7.5 (a) and (b) show the behaviour of the IMU data in roll and pitch, respectively. Later, these data (images, GPS and IMU) were matched based on the acquisition time-tag. Table 7.5 lists a sample of final data which were input in the direct geo-referencing process. These data were input to the software (developed in Chapter 5) manually in keyboard entry mode, since there was no intention to develop an automatic system as part of the research project. A

sample direct geo-referencing image is shown in Figure 6.9 in Chapter 6. In the direct geo-referencing process, the coordinates were converted into the British National Grid (OSTN02) coordinate system, which fits to the standard digital map produced by the Ordnance Survey for data analysis, as discussed in Chapter 8.

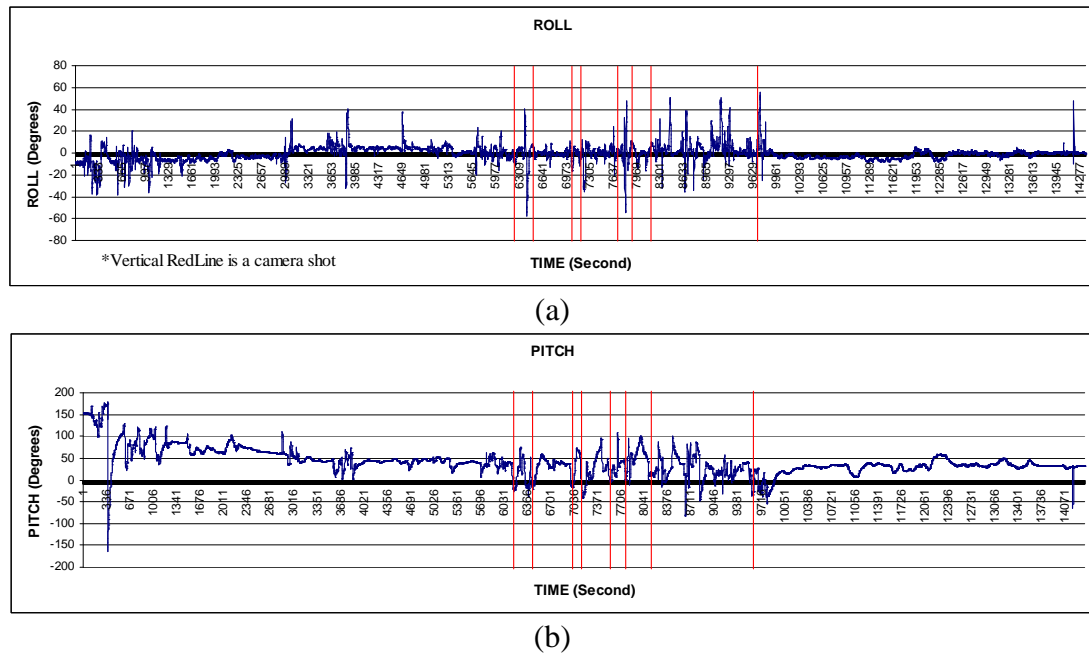








Figure 7.5: Roll and pitch obtained from IMU device, yaw data extracted from GPS data

7.5 Summary

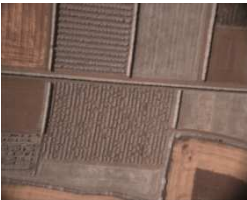





The system validation process, which focused mainly on data acquisition, test site, flight mission, installation of equipment and a sample analysis of results, has been presented in this chapter. The data acquisition, which included test site, flight mission, remotely sensed data, ancillary data and software, was a 'real-time' experience in operating the remote sensing system. The flight test results have shown the behaviour of the various devices in a real-time environment, with respect to images acquired by a small format digital camera. The accuracy of the direct geo-referencing of the images will be discussed in Chapter 8.

Table 7.5: Final data obtained from imaging sensor, GPS and IMU devices.

No	1	2	3	4	5	6
ID	TTC_0911	TTC_0912	TTC_0913	TTC_0914	TTC_0915	TTC_0916
Time Stamp	23:19:56	23:20:28	23:21:03	23:22:47	23:24:26	23:25:10
Time Different	00:02:37	00:00:32	00:00:35	00:01:44	00:01:39	00:00:44
Reduce Time	13:20:10	13:20:42	13:21:17	13:23:01	13:24:40	13:25:24
Easting (m)	570226.229	570193.997	570342.132	570229.241	572249.736	No Data
Northing (m)	156328.545	156525.364	157568.384	156398.803	155986.051	No Data
Height (m)	438.071	438.070	438.070	438.071	438.088	No Data
Roll	-4°	No DATA	-4°	-5°	0°	No Data
Pitch	3°	No DATA	-17°	-19°	20°	No Data
Yaw	57°	No DATA	-4°	2°	302°	No Data
Remarks	Vertical	Unknown	Tilt	Tilt	Tilt	Unknown
Image						




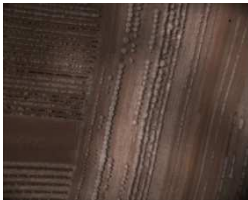

(continued)

...Table 7.5 (continued)

No	7	8	9	10	11	12
ID	TTC_0917	TTC_0918	TTC_0919	TTC_0920	TTC_0921	TTC_0922
Time Stamp	23:26:36	23:27:18	23:27:29	23:27:46	23:28:44	23:30:23
Time Different	00:01:26	00:00:42	00:00:11	00:00:17	00:00:58	00:01:39
Reduce Time	13:26:50	13:27:32	13:27:43	13:28:00	13:28:58	13:30:37
Easting (m)	No Data	No Data	No Data	569559.131	571530.155	570607.113
Northing (m)	No Data	No Data	No Data	155767.884	156952.919	157319.593
Height (m)	No Data	No Data	No Data	438.068	438.080	438.073
Roll	No Data	No Data	No Data	No Data	-12°	-6°
Pitch	No Data	No Data	No Data	No Data	-50°	36°
Yaw	No Data	No Data	No Data	No Data	258°	222°
Remarks	Unknown	Unknown	Unknown	Unknown	Oblique	Tilt
Image						

(continued)....

.....Table 7.5 (continued)

No	13	14	15	16	17	
ID	TTC_0923	TTC_0924	TTC_0925	TTC_0926	TTC_0927	INTENDED BLANK
Time Stamp	23:30:33	23:31:02	23:32:28	23:32:51	23:34:26	
Time Different	00:00:10	00:00:29	00:01:26	00:00:23	00:01:35	
Reduce Time	13:30:47	13:31:16	13:32:42	13:33:05	13:34:40	
Easting (m)	No Data	570679.741	No Data	No Data	No Data	
Northing (m)	No Data	157223.447	No Data	No Data	No Data	
Height (m)	No Data	438.073	No Data	No Data	No Data	
Roll	No Data	8°	No Data	No Data	No Data	
Pitch	No Data	2°	No Data	No Data	No Data	
Yaw	No Data	314°	No Data	No Data	No Data	
Remarks	Unknown	Tilt	Unknown	Unknown	Unknown	
Image						

8. RESULTS AND ACCURACY ASSESSMENT DISCUSSIONS

8.1 Introduction

This chapter discusses the direct geo-referencing results obtained by means of the portable remote sensing device and the assessment of each component's accuracy. These results are examined comprehensively and their significance is discussed along with device performance and reliability. The significance of each device is reflected in the final product of the direct geo-referencing image. A summary of results and their accuracy is given at the end of this chapter.

8.2 Results

Three types of data were produced by the portable remote sensing device: 1) imaging data, 2) navigation data, and 3) directly geo-referenced images. The imaging data were recorded in monochrome format instead of true colour, because monochrome has both greater sensitivity and higher spatial resolution than true colour (Videre Design, 2010; Dage-MTI, 2009). The navigation data includes GPS and IMU data recorded in ASCII data format. ASCII data format is the most satisfactory for data processing as it is interchangeable into different types of format, easy to access by computer programming, extractable and can be input to most established software. The directly geo-referenced images are produced from the navigation data and imaging data. Thus, their accuracy is dependent on the accuracy of the navigation devices as well as the accuracy of the imaging device.

8.2.1 Imaging Results

The images obtained were overlaid on relevant Ordnance Survey Master Maps. It was found that all the images were distorted, as none coincided with the topography. The most obvious distortion occurring in the image was lens distortion. Two types of lens distortion have been distinguished: 1) pincushion distortion and 2) orientation distortion (trapezium distortion), as discussed in Chapter 3. Even the image closest to vertical (TTC_0911.DCM), which has 3 degrees of roll and -4 degrees of pitch, displays lens distortion. It is clear from the images that even when they were close to vertical, the lens distortions results is significant error in geo-rectification. Figure 8.1 shows a comparison of before and after pincushion correction. See Appendix F for a complete list of the images before and after pincushion correction.

Seven of the seventeen images obtained in the third flight are suitable for further direct geo-referencing process, while the other images have coordinates, orientation data or both missing. The focus is therefore on these seven images, which are complete with their ancillary data, and the other images have been eliminated from further processing. Table 7.5 in Chapter 7 has a complete list of the images and their ancillary data.

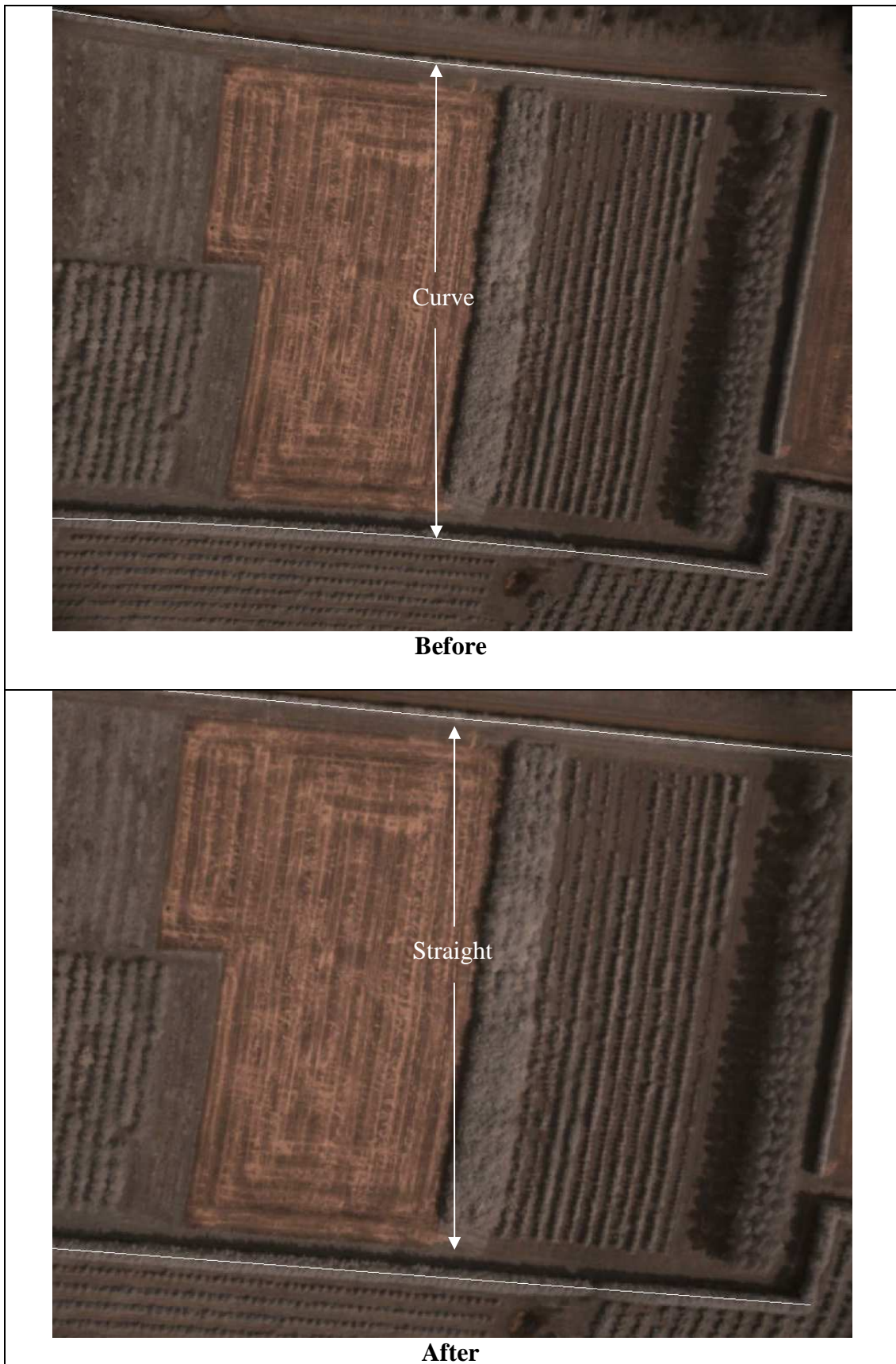


Figure 8.1: Image sample from the third test, (a) before, and (b) after pincushion correction.

8.2.2 Navigation Results

Two types of navigation data were obtained during the acquisition process, from GPS devices and IMU device. The end product of GPS devices was recorded in two types of ASCII format, NMEA 0183 and RINEX GPS data format. The NMEA 0183 data were processed by the built-in micro-processor in the device itself, while RINEX GPS data were processed using the external software GRINGO (version 2.0). The main reason for recording the GPS data in NMEA 0183 data format is because it was a ready-made end product if the WAAS satellites had been available, as discussed in Chapter 6. Recording in RINEX data format enables differential GPS data processing for comparisons with the NMEA 0183 data format. The IMU data were recorded in NMEA 0183 data format as it can be instantly used for image orientation purposes. All GPS devices were set to record to one second of data intervals to ensure that the location for every image was captured.

During the image acquisition process, it was observed that none of the WAAS satellites was broadcasting its data. This was required in order to obtain coordinates by the differential GPS method for the Garmin 76 GPS, which had been proved during the test-drive in Birmingham. The Garmin eTrex ascii file (in Rinex format) shows that the C/A and L1 wavelength code signals had been detected. It had been observed that the low-cost GPS had the capability to record all signals received from the locked satellites.

The GPS receivers exhibited different levels of data quality. The best quality GPS data were received for Garmin eTrex with its waypoint data recorded through GRINGO version 2.0. None of the GPS data could be processed using the

differential technique. The worst GPS data were received from Garmin 76 GPS, which was only able to record for a short period before the signal was completely lost. The wireless GPS from Holux shows great potential for coordinating the flight path. However, it experienced signal loss during the image acquisition process, because the GPS equipment was totally blocked by the photographer from receiving the satellites' signals.

It was also found that the RS232 cable was unable to provide smooth and reliable communication between devices, especially the Garmin 76 GPS and IMU. The longest duration of signal loss was 4052 sec for the Garmin 76 , 26 sec for the Garmin eTrex and 41 sec for wireless GPS. The occurrence of signal loss is very rapid in wireless GPS with 45 occurrences experienced, 30 with the Garmin 76 GPS and 6 with the Garmin eTrex. The latter has the shortest total period of signal loss occurrences and the Garmin 76 GPS the longest. The signal losses are caused not only by the communication cable problems but also depending on overhead obstruction. In this case, the Garmin 76 and Garmin eTrex were placed completely clear from any obstructions, while wireless GPS is placed on top of the camera, and can be easily obscured by navigator interactions and the aircraft wing during the acquisition process. Figure 8.2 shows the trajectory of the GPS track prints for the July 25th 2008 flight.

None of the GPS data could be processed using the differential method due to a lack of C/A-code and P-code signals. The NMEA 0183 is a ready-made data therefore the failure record any raw data containing carrier phase and the pseudorange data thus limits the reduction techniques for minimising random error (Yan, 2006). The

GPS data which were recorded directly to Rinex ascii file could not be corrected by the differential method because there were not enough redundant pairs to enable DGPS processing. Figure 8.3 shows part of a GPS data processing report produced by Total Trimble Control Software and the GPS data recorded by GRINGO software in Rinex ascii format.

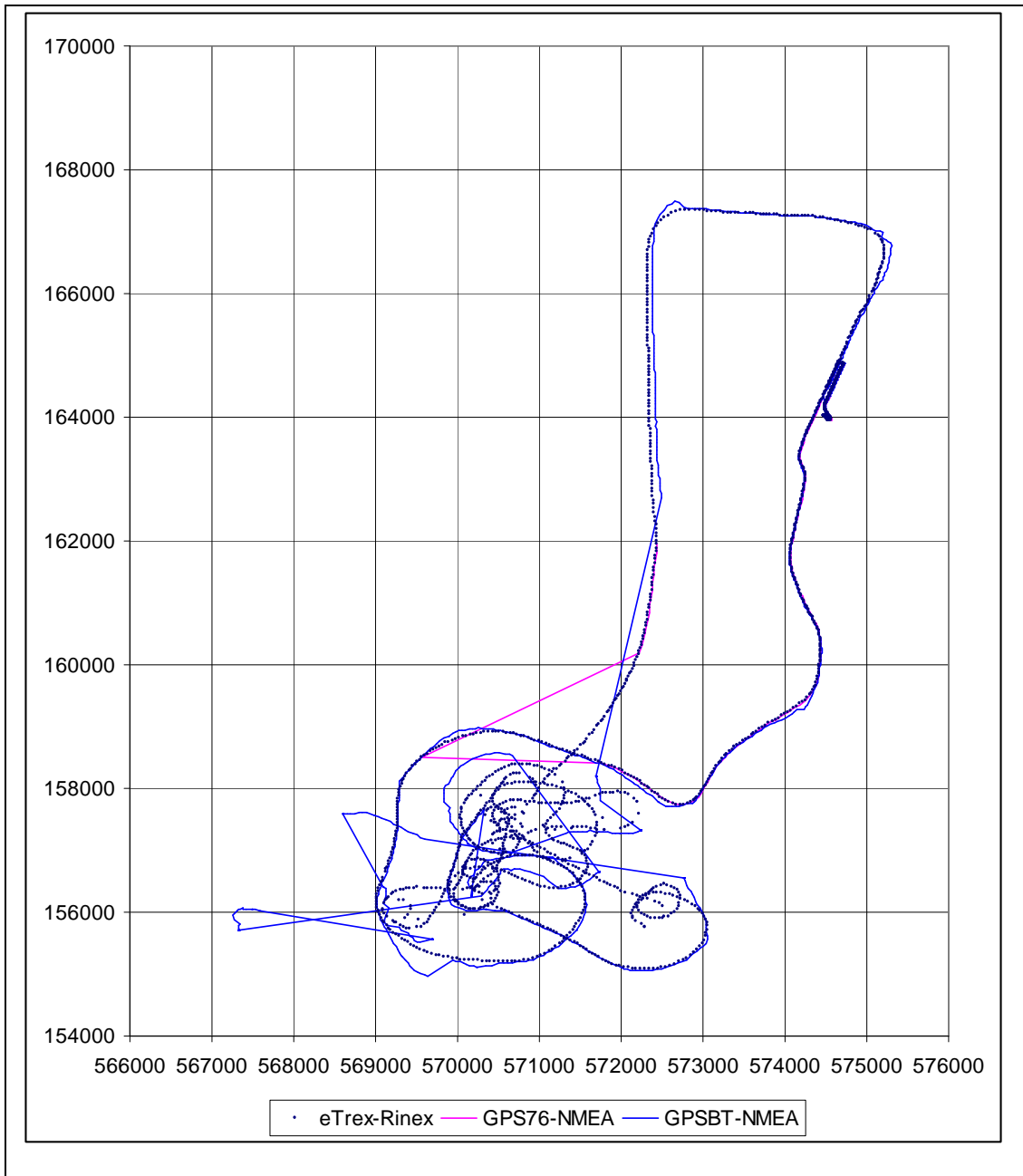


Figure 8.2: Trajectory of flight test in Malling, East Kent on July 25, 2008.

(a) WAVE Baseline Processor 3.12

* Initializing database *

base.rnx: Estimated load size: -1 bytes (-1 0 3.000 1.000 1.000)

rover-2.rnx: Estimated load size: -1 bytes (-1 0 3.000 1.000 1.000)

Load file: C:\Trimble Geomatics Office\Projects\suib\Data Files\Trimble Files\base.rnx

base.rnx: Estimated load size: 1400735 bytes (4669116 4669116 3.000 1.000 1.000)

MCNAV : No solution @ 475261.0 : Bad code observations detected

MCNAV : Disabling all observations to all SVs @ 475261.0

.....

.....

.....

.....

MCNAV : No solution @ 475265.0 : Bad code observations detected

MCNAV : Disabling all observations to all SVs @ 475265.0

MCNAV : No solution @ 475266.0 : Bad code observations detected

(b)

```
2.10      OBSERVATION DATA  GPS                RINEX VERSION / TYPE
GRINGO [2.0.0]  Aston University 25-Jul-08 13:53:14 PGM / RUN BY / DATE
[Registered Version - Serial Number : 11736]      COMMENT
My Marker                MARKER NAME
1                          MARKER NUMBER
ShuibRambat    Aston University  OBSERVER / AGENCY
80322155      GARMIN eTrex    2.14  REC # / TYPE / VERS
00000000      External      ANT # / TYPE
3991675.8681  35134.6501 4957848.5569 APPROX POSITION XYZ
[APPROX POSITION XYZ based on receiver's lat/lon& zero ht.]COMMENT
[approx lat/lon/ht = 51.3484457 0.5043033 0.000 ] COMMENT
0.0000      0.00000.0000      ANTENNA: DELTA H/E/N
1 0                WAVELENGTH FACT L1/2
2 C1 L1            # / TYPES OF OBSERV
SNR mapping        COMMENT
>1650 -> 1; >1700 -> 2; >1800 -> 3; >2000 -> 4;      COMMENT
>2400 -> 5; >3200 -> 6; >4800 -> 7; >8000 -> 8; >11200 -> 9 COMMENT
1                INTERVAL
2008 07 25 12 53 46.0000000 TIME OF FIRST OBS
1                RCV CLOCK OFFS APPL
                END OF HEADER
2    *** START MOVING ANTENNA ! ***      COMMENT
```

Figure 8.3: (a) Part of GPS data processing report by Total Trimble Control Software (b) Part of Rinex ascii format.

Interruptions to the data stream recorded by the computer were a major problem on all flights, and the best flight from this point of view was the last one undertaken on 25th July 2008. On this flight the IMU experienced data loss on 13 separate occasions, each lasting 10 to 13 seconds. It was known that the IMU had continued to work, as when data capture began again, the roll pitch and yaw were in their correct locations. They had simply not been recorded by the computer for this period. Unfortunately, these data stream interruptions coincided with when 10 images were being acquired, and they therefore lacked the attitude information necessary for geo-referencing and could not be used further in this project. Data Connect Enterprises (2008) report similar failings with the RS232 data communication cable for high speed data transfer protocol.

RS232 communication protocol states that higher frequency devices such as the IMU have a problem with the wave signal becoming rounded instead of the ideal square wave form and hence can be incorrectly interpreted by the receiving device, the laptop computer (Data Connect Enterprises, 2008). The use of the RS232 cable is therefore not recommended for the low cost airborne sensor system. However, it was all that was available at the time and the problems were only identified once the field tests has commenced.

The IMU presented its data in ARINC 075 format with a considerable amount of processing already carried out. This made further processing difficult, other than employing digital techniques to smooth and filter the data to remove noise and bias. It was found that over the one hour flight duration there were no scale factor or drift errors, as shown in Chapter 6. Drift errors occurred after approximately 2 hours of

operation. Therefore, provided the flight lasts less than one hour this should not prove a problem in data acquisition.

The IMU data have been smoothed by employing a forward and backward moving average smoothing technique to minimise random errors, with the means of the two taken as the 'true' value of the IMU data. This method could only be validated by examining the direct geo-referencing product, because there are no references to be compared with. Figure 8.4 shows the comparisons between moving average and polynomial smoothing techniques. It was discovered that the polynomial smoothing technique was best on certain occasions, such as if the IMU had a well distributed data.

Using the 2% filtering technique (see section 4.2.1) on the IMU data produced good results and readily showed the correct camera attitude at the moment the image was captured. However, there was some ambiguity in selecting the correct IMU data to match the correct image and this took some sorting out. For example, for the image taken at 13:24:53 on 25th July 2008, there were three possible groups of IMU data, which could be chosen from the green, light blue and cyan highlighted groups in Figure 8.5 (note that this group has been filtered by the 2% technique). The best way to determine the appropriate IMU data is therefore by 'trial and error', and hence shows the advantage of using the epoch analysis technique for dynamic data, whereby each epoch can be analysed independently.

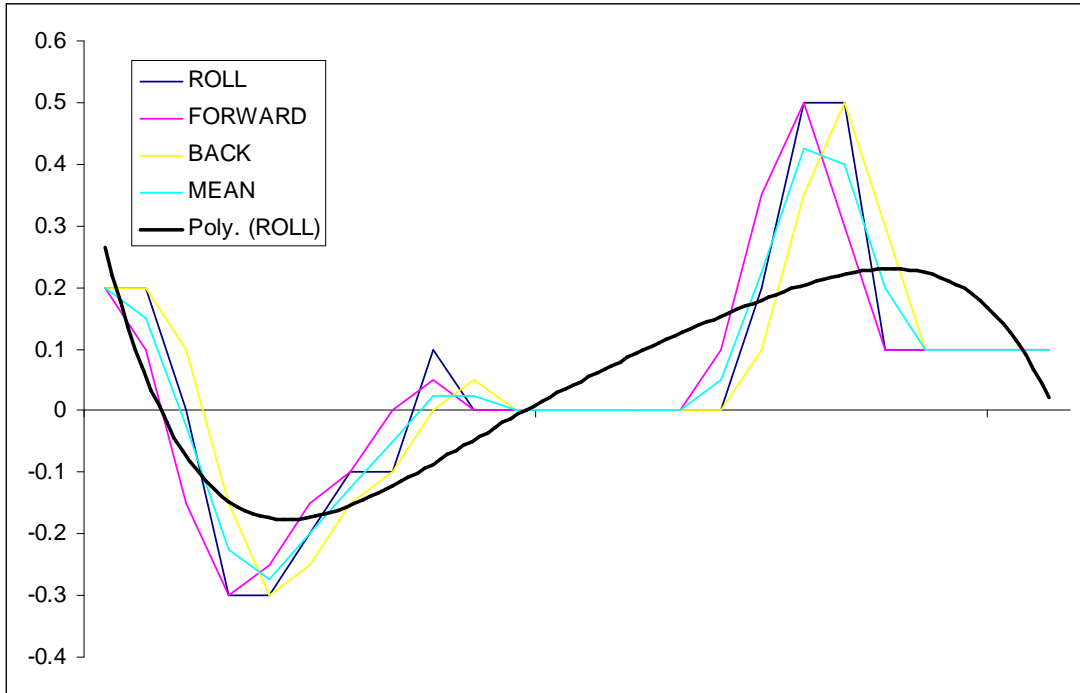


Figure 8.4: Smoothing techniques to minimise random errors

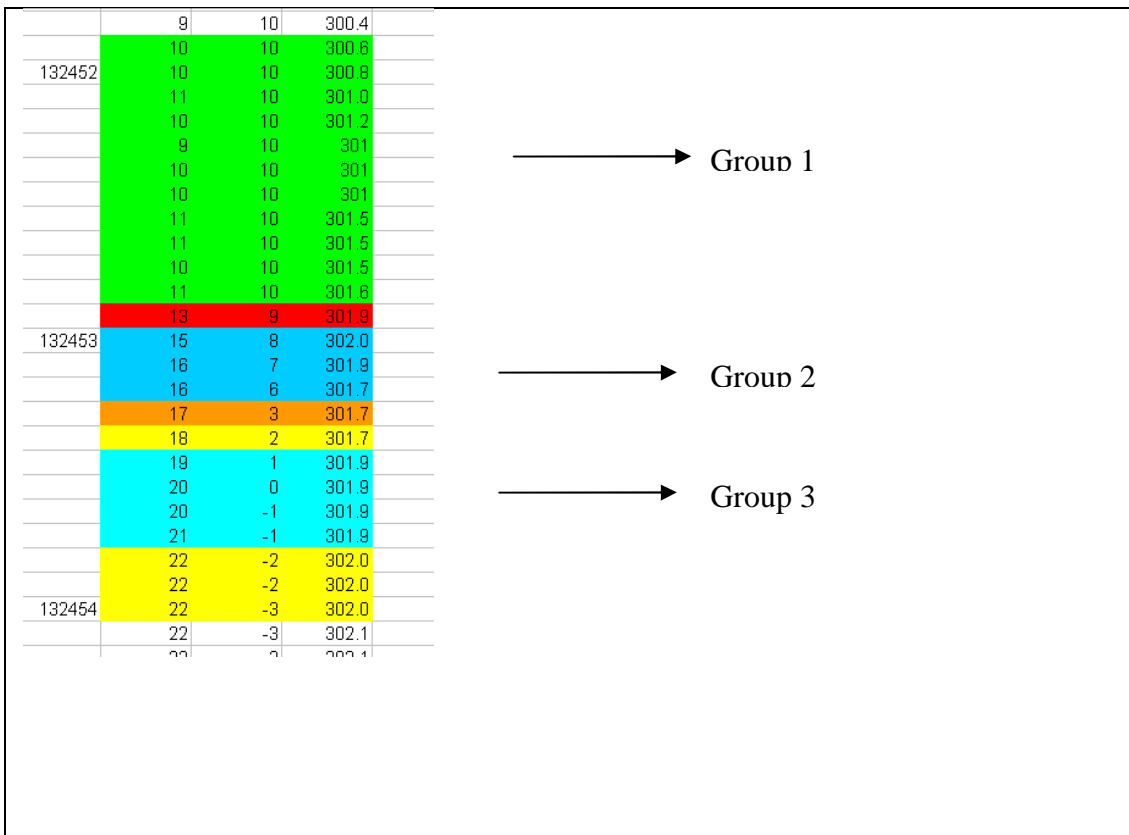
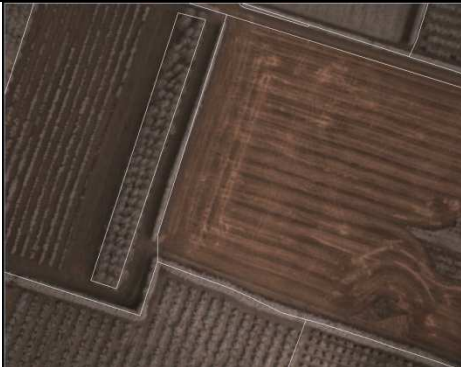


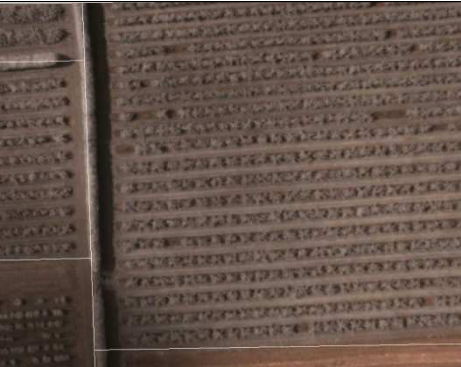

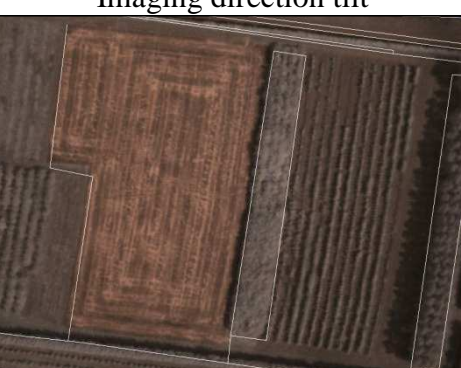


Figure 8.5: IMU data determination problem

It has been demonstrated that the MEMS IMU device, which has 0.5 degree per hour (manufacturer information) bias drift, is capable of being used as an added instrument for directly geo-referencing an image. These results indicated that orientation is not a major issue in the direct geo-referencing. This therefore depends on the GPS data, which could be evaluated through direct accuracy assessment of the geo-referencing results.

Table 8.1: Before and after image orientation using oblique algorithm.

Before image orientation	After image orientation
 <p data-bbox="400 1111 740 1144">Imaging direction vertical</p>	 <p data-bbox="963 1111 1303 1144">Imaging direction vertical</p>
 <p data-bbox="432 1514 713 1547">Imaging direction tilt</p>	 <p data-bbox="995 1514 1273 1547">Imaging direction tilt</p>
 <p data-bbox="400 1917 740 1951">Imaging direction oblique</p>	 <p data-bbox="963 1917 1303 1951">Imaging direction oblique</p>

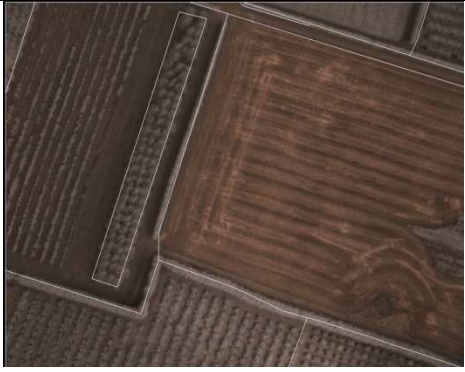
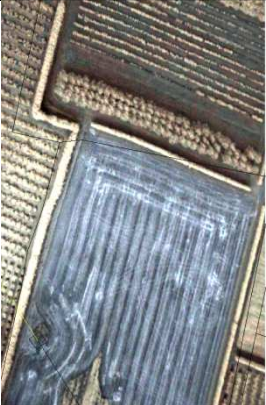
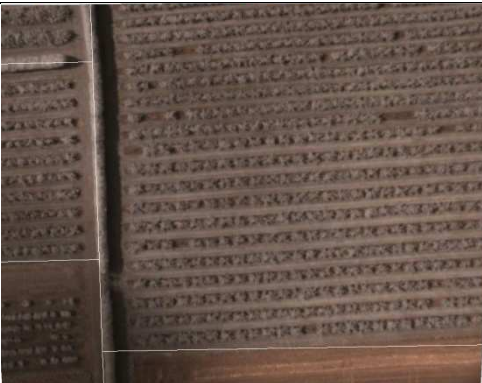
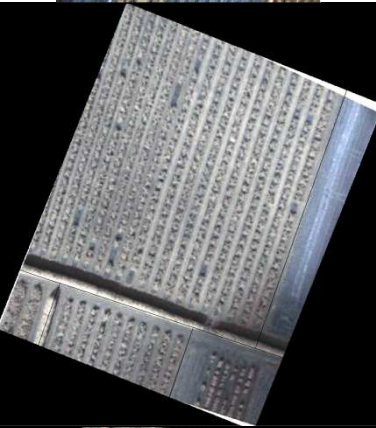


8.2.3 Directly Geo-referencing Result

Seventeen images were acquired from the flight test, but only seven had the orientation data provided by the IMU device as well as GPS position data from the Garmin eTrex (Waypoints). Of these images: one was considered vertical and could be used directly after pincushion correction; one was considered to be a tilt image; and, the remainder were considered to be oblique images, with a range of angles between -50 to 36 degrees of pitch and range of -6 to 8 degrees of roll, and needed further processing after the pincushion correction. Table 8.2 lists the three main categories of images before and after direct geo-referencing using the algorithm discussed in Chapter 4.

Practice showed that the .tif world file format works well during conversion process to enable the corrected image to be read by existing software as this format type can combine image and their coordinate's information and it is needed in ArcView (ESRI) software to display the corrected images.

When resampling the image it was decided to maintain a rectangular output image orientated to the British National Grid, with the maximum coordinates that could be derived without any null pixels. Other options exist, such as a minimum bounding rectangle, but flagging as missing any pixels not gathered by the camera. Pixel size was retained as the size of the original. As a result, an image size which has the same dimension as the input image is produced. The advantage of this was that coordinates for the four corners and the image centre can be defined with a simple mathematical equation as shown in Chapter 4.

Table 8.2 : List of images before and after direct geo-referencing.

Before direct geo-referencing	After direct geo-referencing
 <p data-bbox="475 719 673 752">Vertical Image</p>	
 <p data-bbox="504 1133 644 1178">Tilt image</p>	
 <p data-bbox="475 1541 673 1574">Oblique Image</p>	

8.3 Accuracy Assessment Test

The accuracy assessment was done by visual interpretation, due to the small area coverage and very few control points that could be identified on the Ordnance Survey reference map. The accuracy assessment was based on the disparity of linear features such as agricultural field boundaries, houses, ponds, and/or any distinct feature for which a comparison between image and the reference map could be undertaken.

For the root mean square error (RMSE) to be a useful measure of spatial accuracy, there should be a good number of ground control points randomly scattered around the image. However, in most of the corrected images there were only one or two points identifiable. For example, in figure 8.6a the hedge lines provide a linear feature which appears to define the field boundaries very well, but there is only one identifiable intersection and one angular bend. In Figure 8.6b, the identifiable points are all towards the east of the image. As the image is accurately rendered at that side, the good RMSE may give an overly optimistic impression of the accuracy of the overall rectification.

Two other points are worthy of note in Figure 8.6. In Figure 8.6b one of the recognised objects to be used as a ground control point for geo-rectification had changed position, whilst some features shown on the map were no longer present when the image was detained. Figure 8.6a shows a general problem with the areas, in that the field boundaries are mapped precisely, but the canopy of the hedges does not provide a distinct line on the ground. Table 8.3 lists the images which were successfully corrected by of direct geo-referencing.

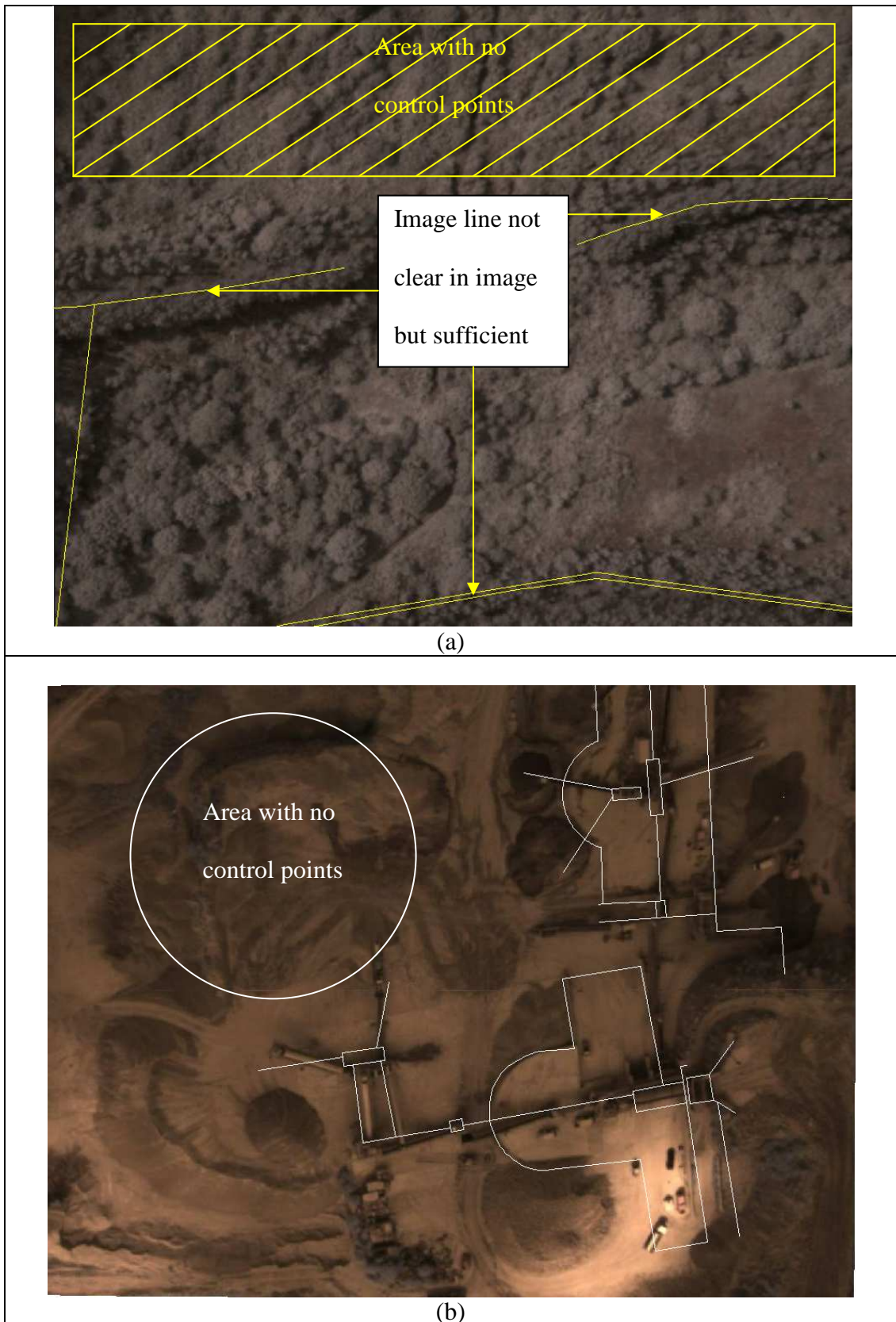


Figure 8.6: Image (a) shows few topographical reference lines, while image (b) shows topographical reference lines are only available in one half of the image.

The mastermap data obtained from the Ordnance Survey did often not show the boundaries between farming plots which were visible in the imagery. However, in many instances these boundaries were available from other sources. For example, imagery from Google earth could be downloaded and referenced to the British National Grid. Figure 8.7 shows this methodology. Note that it is fortuitous that this imagery was available and its use for checking the accuracy of the geo-rectification process was simple. However, since the date of the Google earth imagery was not known and it could not be ordered on demand, it is not possible to use it for precision farming applications.

Figure 8.8 shows an enlargement of the second row, final column of the Table 8.3, so that the spatial accuracy can be seen more clearly. The poorest of the rectified images is shown in Figure 8.9 with an error of 15m at one point, but with other parts of the image apparently more accurately registered. This large error can be ascribed to errors in measuring the height of the aircraft using the GPS. Figure 8.10 shows a more successful rectification with errors of about 1m. The lack of ground control points in this image illustrates the problem of rectifying small format images in agricultural areas.

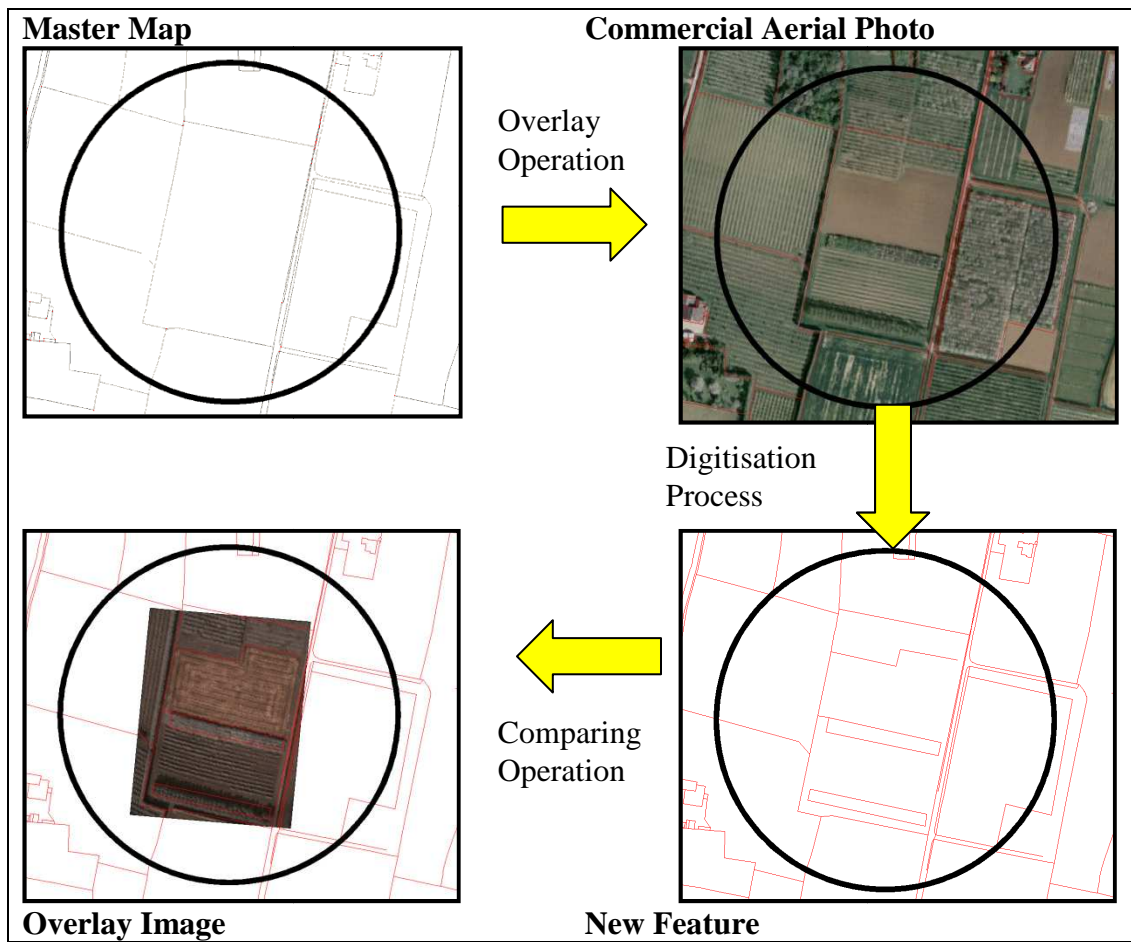


Figure 8.7: Updating reference map process till assessing direct geo-referencing accuracy.

Table 8.3: Summary of images before and after direct geo-referencing.

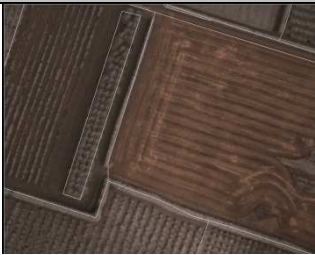
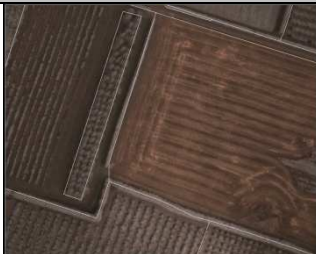
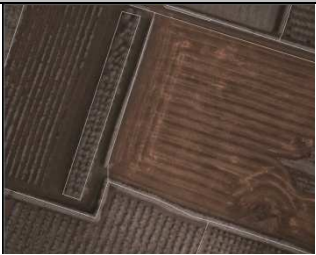
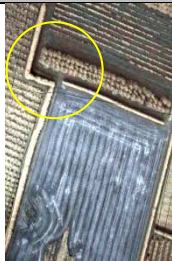

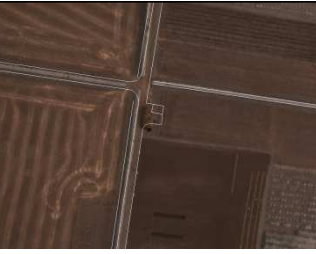






Image ID / Rotation Angle	Original Image / Uncorrected	Corrected using Tilt Algorithm	Corrected using Oblique Algorithm	Map pixels to user coordinate system
TTC_0911.DCM Roll: -4° Pitch: 3° Yaw: 57°				
TTC_0913.DCM Roll: -4° Pitch: -17° Yaw: -4°				
TTC_0914.DCM Roll: -5° Pitch: -19° Yaw: 2°				


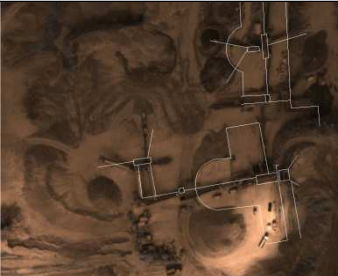
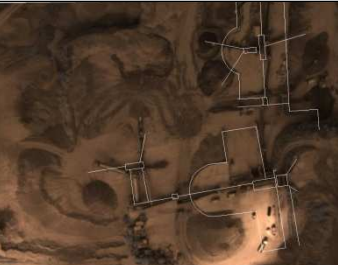





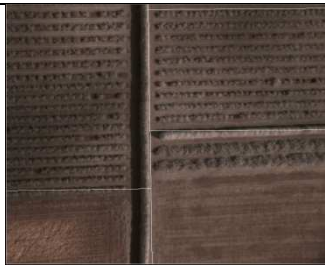
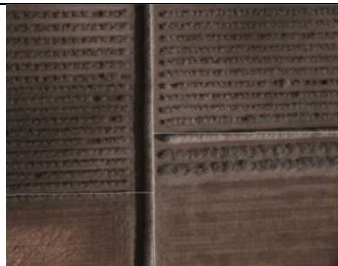

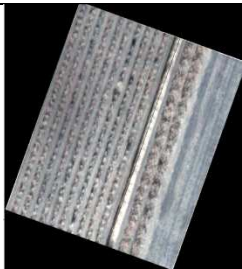
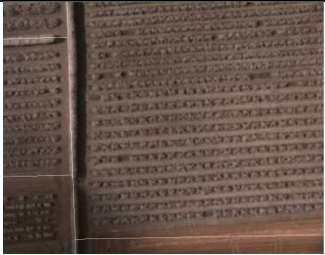

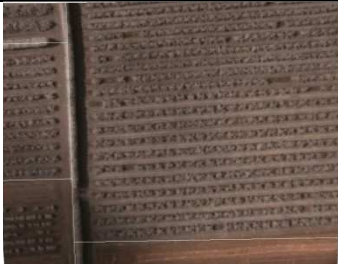
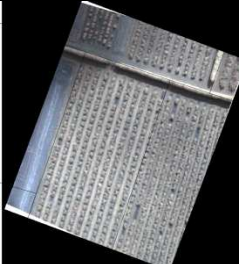
Image ID / Rotation Angle	Original Image / Uncorrected	Corrected using Tilt Algorithm	Corrected using Oblique Algorithm	Map pixels to user coordinate system
TTC_0915.DCM Roll: 15° Pitch: 7° Yaw: 302°				
TTC_0921.DCM Roll: -12° Pitch: -50° Yaw: 258°				
TTC_0922.DCM Roll: 36° Pitch: -6° Yaw: 222°				

Image ID / Rotation Angle	Original Image / Uncorrected	Corrected using Tilt Algorithm	Corrected using Oblique Algorithm	Map pixels to user coordinate system
TTC_0924.DCM Roll: 8° Pitch: 2° Yaw: 314°				

Note: Yellow circle shows mis-registration between image and OS map reference.

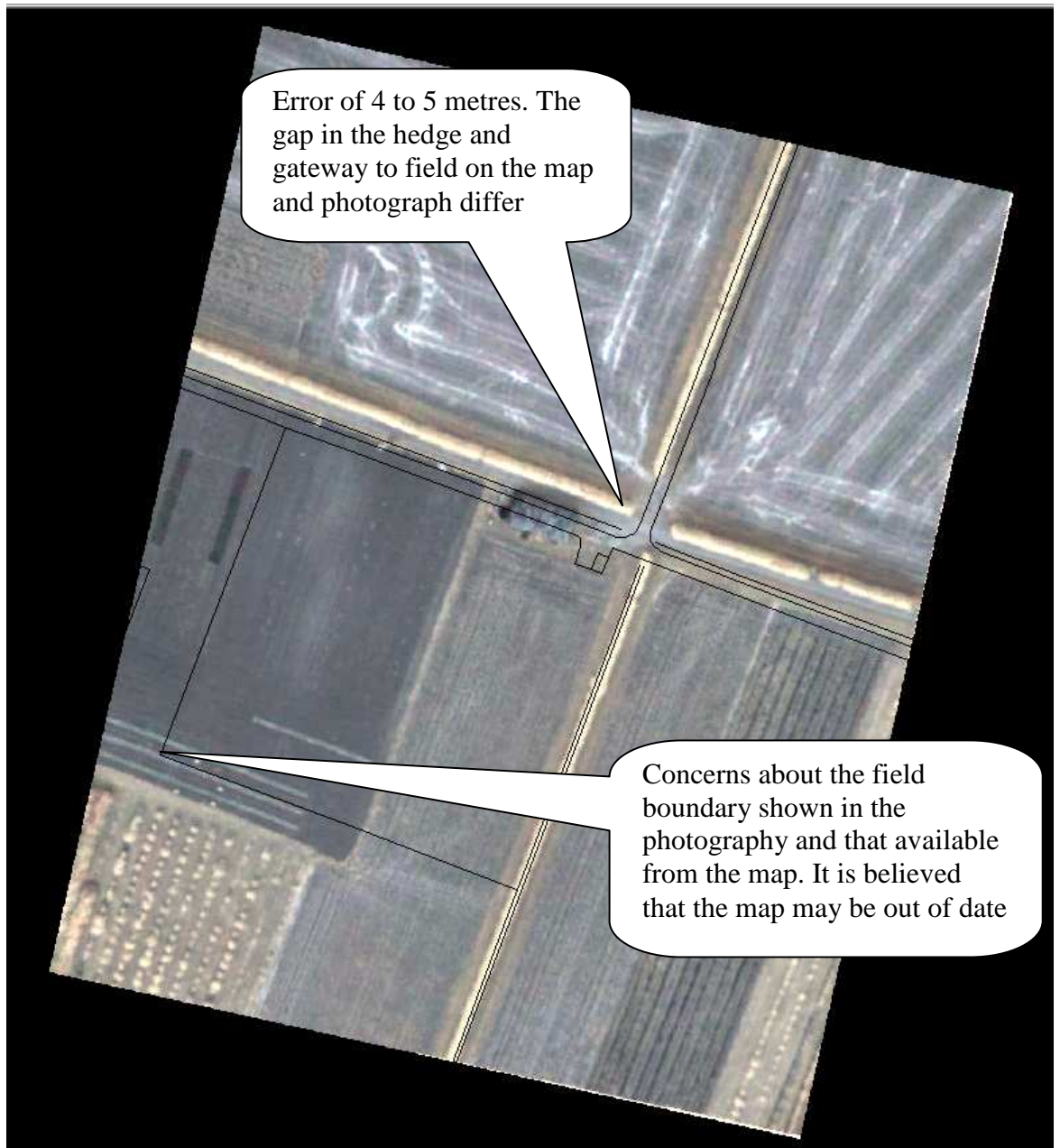


Figure 8.8: Image showing poor georectification and possible errors in map content

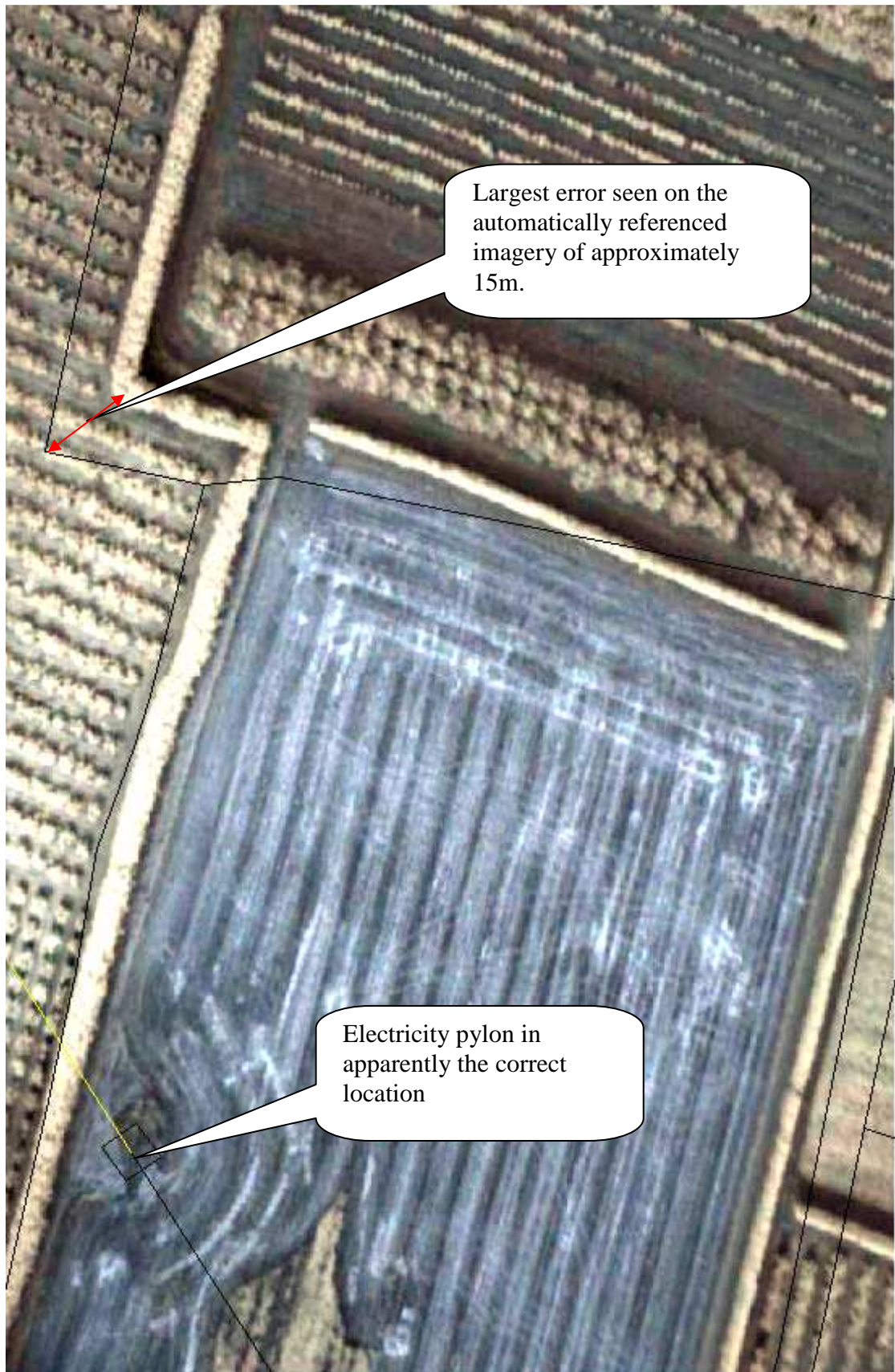


Figure 8.9: Further example of large error

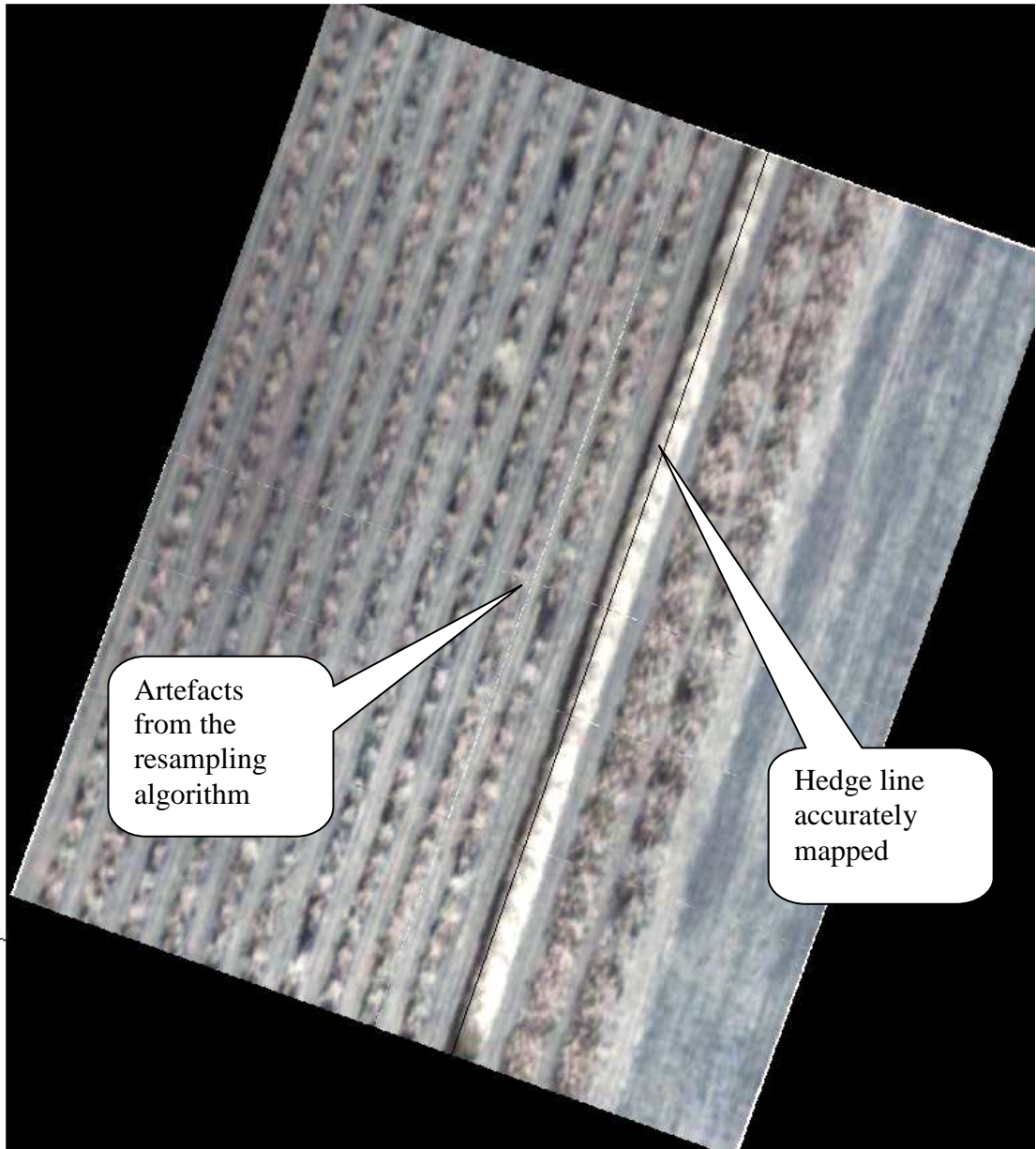


Figure 8.10: Well rectified image

8.4 Summary

The results have shown the capability of a portable remote sensing system as a low-cost device for acquiring images and then directly rectifying them into a user coordinate system. The experimental investigation in Chapter 6 helped to predict the outcome from a real test flight and thus the errors and their correction were as expected.

Unfortunately, the quality of real-flight data could not be examined quantitatively due to a lack of identifiable ground control points. As an alternative, the quality can be assessed visually by matching feature in an image with those on a reference map or publicly available image. Care is required in the use of existing Ordnance Survey Master Maps as they may well be outdated.

The IMU data can be used to orientate the image, when the GPS data is not able to detect any WAAS/EGNOS satellites. This is because the WAAS/EGNOS program is still under preliminary test therefore the availability of those satellites is not guaranteed. The use of the Sync In and Pulse per Second (PPS) signals on recreational GPS were not considered, since the standard NMEA (0183) in these GPS devices does not have a pulse per second output that can be utilised for synchronising the GPS with the data storage device.

The potential for GPS sampling frequency error was taken into account by specifying the speed at which the flight test were undertaken (about 100 km/hour). Additionally, highly sensitive recreational GPS (Garmin eTrex) were added to the flight tests to avoid or minimise the GPS lag, due to the speed at which it picked up

the first fix and was able to stay locked on the satellites. In order to minimise the multipath error, the antenna of the GPSs was placed on the front panel of the aircraft, where there were no obstructions.

Overall, the geo-corrected images met the requirements for precision agricultural use, which requires $\pm 3\text{m}$ accuracy (Searcy, 2003), but at one or two places in some photographs the error was 15m. This error was primarily due to method (affine transformation method) used for the geo-correction process. The affine transformation is best for small and flat area, and since, no digital elevation model (DEM) was introduced into the geo-correction process, the error could not be eliminated. However, the oblique algorithm was capable of directly geo-rectifying the images of small and flat areas. On the whole, the portable remote sensing system has potential to assist low-cost remote sensing, but a few modifications are still required, especially with respect to the GPS devices. Chapter 9 will discuss the conclusions which can be drawn from this research and recommendations are made at the end of the chapter on how to improve the portable remote sensing system.

9. CONCLUSIONS AND RECOMMENDATIONS

9.1 Review of Research Study

The overall objective of this research was to develop a low-cost airborne remote sensing system without the requirement of structural modification to the aircraft. To accomplish this objective, research has been undertaken which embraced: current sensing technology; the investigation and selection of the most appropriate combination of readily instruments, appropriate techniques for processing imaging from low-cost system developed for use in an agriculture environment. From the results achieved and documented in this thesis, the main objective of the research has been met, thus the following questions have been answered.

(1) What is the current status of technology available for incorporation into low-cost remote sensing systems?

Literature search and review showed that there are plenty of appropriate low-cost IMU, GPS and imaging devices readily available on the market.

(2) Can a low-cost remote sensing system be developed that will enable geometric correction of digital image by means of a direct geo-referencing method?

There are existing appropriate low-cost instruments which can be combined to produce a comprehensive low-cost airborne remote sensing system. For example, an IMU based accelerometer, purposely designed for use in the aviation field, will

provide attitude orientation data. There are high sensitivity GPSs able to lock onto 'visible' satellites for the whole duration of the image acquisition process.

(3) Is there an appropriate technique available for processing low-cost IMU and GPS data?

Investigation showed that there was no appropriate technique immediately available for processing the low-cost IMU and GPS data. Approaches such Kalman filtering, effective Kalman filter and neural networks were not suitable for low-cost IMU data because they need frequent reference updates to calculate the necessary correlation coefficients.

Therefore, an epoch analysis was introduced, whereby, each of the epochs was studied and a smoothing technique used to accommodate bias and random errors. Three types of smoothing techniques were tested: moving average, polynomial and averaging smoothing. The averaging smoothing technique gave the worst results, while the polynomial smoothing technique works very well for calibrating the IMU data. The means of forward and backward moving average produce very good results for smoothing the IMU data, which later was subsequently matched with the relevant image.

A technique for extracting the correct IMU data for the particular image from a number of possibilities has also been developed during this research study. This used the concept that an image is acquired instantaneously and not over a period of time by photographer (at least 0.02 seconds). Therefore, there is a group of data which belongs to this specific moment in time. A window searching technique was

applied to look for this particular group, and once identified, the mean value from this group was matched with easting and northing data obtained from the GPS by using time synchronisation.

(4) What is the effect of accepting (2) and (3)?

A portable low-cost airborne remote sensing system was successfully developed and tested in this research study. It was demonstrated that this system met the project objectives through the acquisition of imaging that could be used for mapping agricultural fields. The low-cost IMU component of the system also enabled the reorienting of tilt images into the vertical position.

9.2 Conclusions

From the work presented in this thesis, the following conclusions can be drawn:

1) Overall System

It can be concluded that a low-cost airborne remote sensing system has been successfully developed, and installed on a light aircraft. Imagery, GPS and IMU data have been acquired, the data processed and the images geo-rectified.

The installation procedures for the system have raised some important issues, such as effectiveness of operator communications and the arrangement of the devices various employed.

2) Instruments

From the results obtained, it is evident that although all devices were able to produce some results, the effectiveness was influenced by connection problems. Unlike when mounted in a land based vehicle, the single engined aircraft is very small and

consequently wire-cable connections may be easily disturbed and/or broken by navigator or data manager movement. Due to the high data transfer speeds involved, RS232 cabling was found unsuitable for this purpose.

The low-cost IMU device selected was able to obtain roll, pitch and yaw data of sufficient accuracy for the geometric correction. Geometric distortion of all the seven images with compatible IMU data were corrected using either by tilt or the oblique algorithm. The GPS receivers created some difficulties as the expected accuracy could not be achieved. The best accuracy was 2 to 4 m when static, but when in motion the accuracy was about 10-15 m (the same as reported by Schwieger, 2003).

The imaging device could produce a multi-spectral image with three bands: green, red and infrared. The flight images obtained were free from vignette problems, such as blurring and unfocused images, experienced during the experimental investigation. However, it was found that images suffered from pincushion distortion, as none could be matched perfectly with the reference map. This lens effect was successfully removed using an appropriate correction algorithm.

3) Data Processing

The image data obtained from the digital small format camera covered an area of between 200x 200 m and 400x400 m, depending on the aircraft height. As this area was quite small it was found that there is often a limited availability of reference point for geo-rectifying the image, especially for purely agriculture areas.

The low cost of accelerometer- based IMU produced data suitable for use as an extrinsic parameter for direct geo-referencing. Even though the accuracy claimed by the manufacturer was 0.5 degrees, with proper data processing techniques, the accuracy could be enhanced.

Epoch analysis on IMU data enables the correct data set for the image orientation to be selected. It has proved that the reducing technique in processing the low-cost device data is very important.

Any misalignment between the imaging sensor and IMU device can be reduced as the ancillary device of the portable remote sensing equipment is able to measure the orientation of the portable device directly.

9.3 Recommendations

The following recommendations for future work are proposed:

- 1) This research shows that the oblique algorithm works very well on oblique images captured by a small format digital camera. Therefore the algorithm should be tested on other types of imaging device, such as medium or large format digital cameras.
- 2) As the image warping technique employed for direct geo-referencing was found to produce good results, it should therefore be tested on geo-referencing multiple images. For a comparison, the multivision software for oblique management and analysis tool can be used to test the results (GPS World Staff, 2006). The Ricoh G700SE digital camera which has a GPS system that enables geotagging and which allows the image to be uploaded

and overlaid over Google Earth images (Ricoh, 2011), might also be useful for comparing the geo-referencing results with an established device.

- 3) It is found that the mean of forward and backward moving averages gives good smoothing results for IMU data. Thus, it should be used on other IMU data to reduce the bias and random errors.
- 4) The epoch analysis approach has shown that the signal fluctuation from the IMU device works very well, whereby images are perfectly matched with the reference map after the orientation process. Thus, this technique should be tested on IMU device such as navigation or tactical devices.
- 5) In this research, it has been found that low-cost GPS with high sensitive response, such as Garmin eTrex, are good at locking onto visible satellites. Therefore, it is recommended that high-sensitivity low-cost GPS receivers should be installed on every low-cost airborne remote sensing system.
- 6) In raw GPS data, it is found that the P-Code wavelength needed for differential processing techniques is not fully received by low-cost GPS receivers. Thus low-cost GPS should be improved to enable them to receive better P-Code wavelengths.
- 7) The track-log from the Garmin eTrex GPS shows good tracking mode, and therefore an investigation into converting track-log data to accurate positional data would be beneficial to the low-cost airborne remote sensing industry.
- 8) The boresight correction can be ignored as it is possible to measure the location of the image acquisition device directly. Therefore, it is recommended that the IMU device should be installed in the imaging device.
- 9) It is recommended that a completely integrated system which includes an IMU, a GPS and an Imaging device is designed for commercial marketing.

10) The GI-Eye camera which is small (2 x 2 x 4 cm), light and capable of recording near infrared images can be integrated with an IMU and GPS.

References:

- Abdullah, Q.A., and Tuttle, M.A., (1999). Integrated GPS-Inertial Measurement Solution as an Alternative to Aerial Triangulation: A Case Study. Proceedings ASPRS Annual Convention, Baltimore. 867-876.
- Aber, J. S., Aber, S. W., and Pavri, F., (2002). Unmanned small-format aerial photography from kites for acquiring large-scale, high-resolution, multi view-angle imagery. Percora 15, Land Satellite Information IV and International Society of Photogrammetry and Remote Sensing, Commission I, Conference, Proceedings. November, 2002, Colorado:Denver.
- Aerial survey (2005). The Oxford Companion to the Photograph. Oxford University Press. Available from: <http://www.answers.com/topic/aerial-survey> [Accessed 04 May 2010].
- Agranov, G., Berezin, V., and Tsai, R.H., (2003). Crosstalk and Microlens Study in a Color CMOS Image Sensor. IEEE Transactions on Electron Devices, Vol. 50, No. 1, January 2003. 133-136.
- Ahn, H., and Lee, S., (2003). Gyroless Attitude Estimation of The Sun-Pointing Mode Satellite. International Conference on Control, Automation and Systems, October 22-25, 2003. Korea:Gyeongju. [online]. Available from http://2003.iccas.org/Full_Paper/GyrolessAD.pdf [Accessed 27 November 2008].
- Baltsavias, E.P., (1998). Photogrammetric Scanners - Survey, Technology Development and Requirements. International Society of Photogrammetry and Remote Sensing, Commission I Symposium, 25-27 February 1998, Bangalore, India. 1-9.

- Baroni, L., and Kuga, H.K., (2005). Analysis of Navigational Algorithms for A Real Time Differential GPS System. 18th International Congress of Mechanical Engineering, November 6-11, 2005. Proceedings of Congresso Brasileiro de Engenharia Mecânica., ABCM, Ouro Preto, MG.
- Baumann, P.R., (2001). History of Remote Sensing, Photogrammetry [online]. Available from http://employees.oneonta.edu/baumanpr/geosat2/RS_History/HistoryRSPart1.htm [Accessed 28 November 2008].
- Bäumker, M., and Heimes, F.J., (2002): New Calibration and Computing Method for Direct Georeferencing of Image and Scanner Data Using the Position and Angular Data of an Hybrid Inertial Navigation System. In: Heipke, C., Jacobsen, K., and Wegmann, H., (eds.), (2002). Integrated Sensor Orientation, OEEPE Official Bundesamt für Kartographie und Geodäsie. Frankfurt: am Main, 197 – 212.
- BIGF, (2008). Homepage of The British Isles Continuous GNSS Facility. [online] Available from <http://www.bigf.ac.uk> [Accessed 28Feb 2008].
- Bochert, A., Hacker, J.M., and Ohm, K., (2000). Color Line Scanner as Imaging NDVI Sensor. Proceedings of Second EARSeL Workshop on Imaging Spectroscopy, Enschede, July 2000.
- Canada Centre of Remote Sensing, (2008). Remote Sensing Then and Now [online]. Available from http://cct.rncan.gc.ca/org/history/history1_e.php [Accessed 27 October 2008].
- Chiang, K.W., Noureldin, A., and El-Sheimy, N.(2003): Multi-sensors Integration using Neuron Computing for Land Vehicle Navigation, GPS Solutions.,Vol. 6, No. 3, pp. 209-218.

- Colliander, A., (2007). Development, Calibration and Applications of Polarimetric Microwave Radiometers for Remote Sensing. PhD Thesis. Department of Helsinki University of Technology, Finland.
- Comer, R.P., Kinn, G., Light, D., and Mondello, C., (1998). Talking Digital. Photogrammetric Engineering and Remote Sensing, Journal of The American Society for Photogrammetry and Remote Sensing. Vol. 64, No. 12, 1139-1142.
- Cramer, M., (1997). GPS/INS Integration. In: Photogrammetric Week '97. Fritsch, D., and Hobbie, D., (eds) Wichmann, Heidelberg. [online] Available from <http://www.ifp.unistuttgart.de/publications/phowo97/phowo97.en.htm>. [Accessed 27 June 2005].
- Cramer, M., (2001). Performance of GPS/Inertial Solution in Photogrammetry. In: Fritsch, D., and Spiller, R., (eds.), (2001). Photogrammetry Week '01. Heidelberg: Wichmann Verlag, 49-269. [online] Available from <http://www.ifp.uni-stuttgart.de/publications/phowo01/phowo01.en.htm>. [Accessed 27 June 2005].
- Cramer, M., (2005). Digital Airborne Cameras-Status and Future. Proceedings of International Society of Photogrammetry and Remote Sensing, Hannover Workshop 2005. High-resolution Earth Imaging for Geospatial Information. 1-8.
- Dabney, P.W., and Deering, D.W., (1998). Report on the NASA LBA-ECO: Light Aircraft Remote Sensing Instrumentation Workshop, October 6-7, 1997. University of Maryland [online]. Available at: http://www.lbaeco.org/lbaeco/invest/docs/reports/LightAirRemote/lightair_remotsens0499.PDF. [Accessed 12 December 2006].

- Dage-MTI, (2009). An international leader in the design and manufacture of high performance digital Firewire cameras and analog video cameras and monitors [online]. Available from <http://www.dagemti.com/> [Accessed 27 July 2010].
- Dare, P.M., (2005). The Use of Small Environment Research Aircraft (SERAs) for Environmental Remote Sensing. *International Journal of Geoinformatics*, 1(3). 19-26.
- Dare, P.M., (2008). Small Format Digital Sensors For Aerial Imaging Applications. *The International Archives of the Photogrammetry, Remote Sensing and Spatial Information Sciences*, Vol.XXXVII (Part B1), Beijing, 533-538.
- Data Connect Enterprise (2008). RS232 Data Reference [online]. Available from http://www.data-connect.com/RS-232_Info_page.htm. [Accessed 25 June 2008].
- De Moraes, R.M., (2001). A low-Cost Solution for Obtaining Remote Sensing Images. *Proceedings of the 14th Brazilian Symposium on Computer Graphics and Image Processing*. IEEE Computer Society. USA:Washington, DC, 405.
- Ding, M., and Wang, Q., (2005).An Integrated Navigation System of NGIMU/ GPS Using a Fuzzy Logic Adaptive Kalman Filter. *Fuzzy Systems and Knowledge Discovery*, 3613(), 812-821.
- Dunggal, S.K., (2009). *Surveying : Volume II*. 3rd edition. New Delhi, India. Tata McGraw-Hill Education Private Limited.
- El-Rabbany, A., (2002). *Introduction to GPS: The Global Positioning System*. Boston, MA: Artech House.
- El-Sheimy, N., (1996). *The Development of VISAT- A Mobile Survey System For GIS Applications*. PhD. thesis, Department of Geomatics Engineering,

- University of Calgary, Canada [online]. Available from: <http://www.geomatics.ucalgary.ca/research/publications/GradTheses.html> [Accessed 28 November 2008].
- El-Sheimy, N., Nassar S. and Noureldin A., (2004). Wavelet De-noising for IMU Alignment. *IEEE Aerospace and Electronic Systems*, V 19 (10), pp. 32-39.
- El-Sheimy, N., Chiang, K.W., and Noureldin, A., (2006). The Utilization of Artificial Neural Networks for Multisensor System Integration in Navigation and Positioning Instruments. *IEEE Transactions on Instrumentation and Measurement*, 55(5), 1606-1615.
- Estes, J.E., and Hemphill, J., (2006). Some Important Dates in the Chronological History of Aerial Photography and Remote Sensing [online]. Available from <http://www.geog.ucsb.edu/~jeff/115a/remotesensinghistory.html> [Accessed 27 October 2008]
- European Space Agency, (2006). The European Geostationary Navigation Overlay System: A Cornerstone for Galileo. Battrick, B., and Danesy, D., (eds.), The European EGNOS Project. Netherlands [online]. Available from <http://www.esa.int/esapub/sp/sp1303/sp1303toc.pdf>. [Accessed 27 October 2008]
- European Space Agency, (2007). Full Deployment and Operations: Galileo Systems [online]. Available from http://www.esa.int/esaNA/SEM5K8W797E_galileoN_0.html [Accessed 24 August 2011].
- Ferrano, G., Neumann, K-J., and Doerstel, Ch., (2010). New Quality Standards For Digital Images. *The International Archives of Photogrammetry, Remote Sensing, and Spatial Information Sciences*, Vol. 34, (Part B2), 249-253.

- Fiani, M. and Pistillo, P., (2004). A Low-cost Mms Integrating Gps, Digital Compass and A Camera To the Direct Georeferencing of Digital Images, International Society of Photogrammetry and Remote Sensing Congress, Commission 5, XXth Istanbul, Turkey. 747-752.
- FLIR, (2008). Thermal Infrared Camera Systems, Incorporation. Available from <http://www.flirt.com/> [Accessed 17 Nov 2008].
- Foster, B.C., (1985). Mapping Potential of Future Spaceborne Remote Sensing System. Proceedings of 27th Australia Survey Congress, Alice Spring. 109-117.
- Fouquet M, and Sweeting, M.N., (1996). UoSAT-12 Minisatellite for High Performance Earth Observation at Low Cost. The 47th International Astronautical Congress, Beijing, October 7-11 1996, Paper Number IAF-96-B.2.09.
- Garmin, (2001). GARMIN: GPS 76 and GPSMAP 76 [online]. Available from http://www.busse-yachtshop.de/pdf/gps76_gpsmap76.pdf [Accessed 12 September 2011].
- Gebre-Egziabher, D., Powell, J.D., and Enge, P.K., (2001). Design and Analysis of A Low-Cost Aided Dead Reckoning Navigation System. The International Conference on Integrated Navigation Systems in St. Petersburg Russia, May 2001 [online]. Available from <http://waas.stanford.edu/~wwu/gebre/papers/drsystem/drsystem.pdf> [Accessed 27 November 2008].
- George, M., and Sukkarieh, S., (2005). Tightly Coupled INS/GPS with Bias Estimation for UAV Applications. Proceedings of the 2005 Australasian Conference on Robotics & Automation. Claude Sammut (ed.). Australia:

- Sydney [online]. Available at <http://www.cse.unsw.edu.au/~acra2005/proceedings / contents.html>. [Accessed 21 May 2007].
- GPS World Staff, (2006). MultiVision USA Delivers High-Resolution Oblique Imagery to Mid-America Regional Council. [online] Available from <http://www.gpsworld.com> [Accessed 22 August 2011]
- Graham, S., (2010). From Helmand to Merseyside: Unmanned drones and the militarisation of UK policing. [online] Available from <http://www.opendemocracynet> [Accessed 20 October 2010].
- Graham, R, and Read, R.E., (1986). "Manual of Aerial Photography," Focal Press, London and Boston.
- Greenspan, R.L., (1995). Inertial Navigation Technology from 1970-1995. The Journal of the Institute of Navigation, vol. 42, no. 1, pp. 165-186.
- Grejner-Brzezinska, D.A., (2000). Direct Exterior Orientation of Airborne Imagery with GPS/INS systems: Performance Analysis, Navigation, 46(4). 261-270.
- Grejner-Brzezinska, D.A., and Toth, C.K., (1998). Airborne Remote Sensing MultiSensor System: Development, Testing and Applications. Proceedings of the GPS and Forestry Conference. Canada: British Columbia, Colona.
- Grejner-Brzezinska, D.A., and Toth, C.K., (2004). High-Accuracy Direct Aerial Platform Orientation with Tightly Coupled GPS/INS System. Columbus: Ohio State University. 1-79.
- Gruen, A., and Zhang, L., (2001). TLS Data processing modules. Proceedings of the 3rd International Seminar on New Developments in Digital Photogrammetry, Gifu, Japan, 24-27 September, 2001, pp. 69-70.
- Gulliver, B., (2008). Personal Communication (interview). The Aerial Reconnaissance Company, Kent, United Kingdom.

- Haala, N., Stallmann, D., and Cramer, M. (1998). Calibration of Directly Measured Position and Attitude by Aerotriangulation of Three-Line Airborne Imagery. The International Archives of Photogrammetry and Remote Sensing. Budapest, 32(Part 3). 23-30.
- Haala, N., Fritsch, D., Stallman, D., and Cramer, M., (2000). On The Performance of Digital Airborne Pushbroom Cameras for Photogrammetric Data Processing-A Case Study. International Archive of Photogrammetry and Remote Sensing, Vol. 33, Part B4/1, pp. 324-331.
- Hakim, G. (2008). The Electromagnetic Spectrum. Available from: <http://www.atmos.washington.edu/~hakim/301/electromagnetic-spectrum.jpg> [Accessed 05 Nov 2008].
- Hassan, A., (2004). Workshop on Global Navigation Satellite System (GNSS): Fundamentals & Enhancements 29th April 2004. Center for Technology Policy & International Studies (CENTEPIS) Universiti Teknologi Malaysia, City Campus Jalan Semarak, 54100 Kuala Lumpur. Workshop materials on CD.
- Heinold, S. (2008). Personal Communication. Actual Focal Length. Email: "Steve Heinold" steve@tetracam.com, "ShuibRambat" rambats@aston.ac.uk.
- Heipke C., Jacobsen K., Wegmann H. (2002). Analysis of the results of the OEEPE test, Integrated sensor orientation. In: Heipke C., Jacobsen K., Wegmann H. (eds.), Integrated Sensor Orientation. Proceedings of the OEEPE Workshop: Integrated Sensor Orientation, Institute for Photogrammetry and Geoinformation, University of Hannover, Hannover, Germany, pp. 31-49.

- Heller, R.C., (1970). Imaging with Photographic Sensors. In: Remote Sensing with Special Reference to Agriculture and Forestry. National Academic of Science: Washington D.C.
- Hide, C.D., and Moore , T. (2005). "GPS and Low Cost INS Integration for Positioning in the Urban Environment". Proceedings of ION GNSS 2005. California: Long Beach, September 2005. 1007-1015.
- Hill, C.J., Moore, T., and Napier, M.E., (2002): Rapid Mapping with Post-processed Data from Garmin Handheld Receivers. Proceedings of ION GPS 2002, 24-27 September 2002, USA:Portland.
- Hotler, M.R., Bair, M., Beard, J.L., Limperis, T., and Moore, R.K., (1970). Imaging with Nonphotographic Sensors. In: Remote Sensing with Special Reference to Agriculture and Forestry. National Academic of Science: Washington D.C.
- Hsiao, F.B., Liu, T.L., Chien, Y.H., Lee, M.T, and Hirst, R., 2006, "The Development of a Target-lock-on Optical Remote Sensing System for Unmanned Aerial Vehicles," The Aeronautical Journal, March 2006,.
- Hulsing, R., (1998). MEMS inertial rate and acceleration sensor. Proceedings of the 1998 National Technical Meeting of the Institute of Navigation January 21-23, 1998. Westin LongBeach Hotel, Long Beach, CA, 161-168. [online] Available from: <http://www.ion.org/search/viewabstract.cfm?jp=p&idno=625> [Accessed 22 Nov 2008].
- INPHO GmbH (1999): FAQ - PATB-GPS. In: Firmen Website unter [online]. Available from <http://www.inpho.de> [Accessed 27 November 2008].

- Imaging Group (2010). AHS-75 Airborne Hyperspectral Scanner. argonST: Environmental Remote Sensing Technology. [online] Available from <http://www.arginst.com/docs/AHS-75.pdf> [Accessed 23 August 2011]
- Jacobsen, K. (1996): User Manual Programm System BLUH. Institute for Photogrammetrie and Engineering Surveys, University Hannover, 1996. 444.
- Jacobsen K. (2000). Potential and Limitation of Direct Sensor Orientation. International Archive of Photogrammetry and Remote Sensing, Amsterdam, The Netherlands, 33 (Part B3/1). 429-435.
- Jensen, J.R., (2007). Remote Sensing of Environment: An Earth Resource Perspective. 2nd Edition, Upper Saddle River: Prentice-Hall.
- Kent County Council (2008). Kent Landscape Information [online]. Available from <http://extranet7.kent.gov.uk/klis/default.asp> [Accessed 22 Nov 2008].
- Koh, A., (2007). Airborne Geospatial Technologies-Fitness for Purpose of Use. [online]. Available from [http://rpsoc.org/documents/learning_resources/FITNESS FOR PURPOSE OF USE 1.pdf](http://rpsoc.org/documents/learning_resources/FITNESS_FOR_PURPOSE_OF_USE_1.pdf) [Accessed 23 August 2011]
- Kohne, A., and Wobner, M., (2009). The GPS System: Sources of errors in GPS. [online] Available from <http://www.kowoma.de/en/gps/erros.htm> [Accessed 22 August 2011].
- Lillesand, T.M., and Kiefer, R.W., (2000). Remote Sensing and Image Interpretation. 4th edition. United State of America. John Wiley and Sons Incorporation.
- Lithopoulos, E., (1999). A modular integrated inertial/GPS system for survey and mapping applications. In: ION GPS 99. Institute of Navigation, Nashville, TN, 1897-1900.

- Luijten, J., (2003). Grid to image conversion [online]. Available from <http://arcscripsts.esri.com>. [Accessed 22 August 2011].
- Lukac, R., (2008). Single-Sensor Imaging: Methods and Applications for Digital Camera. Canada: CRC Press/Taylor & Francis.
- Luney, P.R., and Dill, H.W., (1970). Uses, Potentialities, and Needs in Agriculture and Forestry. In: Remote Sensing with Special Reference to Agriculture and Forestry. National Academic of Science: Washington D.C.
- Mascall, S., and Dare, P.M., (2005). Small and Light: Exploring Low-Cost Remote Sensing. Position Magazine, Issue 19, October – November 2005, in editor: Jon Fairall. [online] Available from http://www.gisuser.com.au/POS/content/2005/POS19/pos19_feature/pos19_feature_2.html. [Accessed 05Nov 2008].
- McGarvey, J., (2004). The DCS Story: 17 years of Kodak Profesional digital camera systems, 1987-2004. [online] Available from http://www.nikonweb.Com/files/DCS_Story.pdf [Accessed 23 August 2011].
- Mehaffey, J., and Yeazel, J., (2004). Low Cost Receiver and Moving Map PC Software Reviews. [online] Available from <http://gpsinformation.net/main/ot-20.htm#GARMIN> RECEIVERS: [Accessed 12 September 2011].
- Merhav, S.J., (1982). A Nongyroscopic Inertial Measurement Unit. Journal of Guidance, Control and Dynamic, 5(3). 227-235.
- Ministry of Agriculture Malaysia (2006). Proliferation Mind of The 9th Malaysia Planning Agenda. Speech Collection Achieve of Ministry of Agriculture Malaysia.
- Moffitt, F., H., and Mikhail, E., M., (1980). Photogrammetry. 3rd (ed.). USA: Harper and Row Incorporation.

- Mostafa, M.M.R. (2001). Bore-sight Calibration of Integrated Inertial/Camera Systems. Proceeding of International Symposium on Kinematic Systems in Geodesy, Geomatics and Navigation – KIS 2001, Banff, Canada, June 5-8.
- Mostafa, M.M.R., (2002). Precision aircraft GPS positioning using CORS. Photogrammetry Engineering Remote Sensing, 68: 1125–1126
- Mostafa, M.M.R., and Schwarz, K.P., (2001). Digital Image Georeferencing from Multiple Camera System. International Society of Photogrammetry and Remote Sensing, 56. 1-12.
- Motorola, (1997). ONCORE Receivers and Antennas User's Guide. Motorola Incorporation, United State of America. [online] Available from <http://gpsd.berlios.de/vendor-docs/motorola/ch2.pdf>. [Accessed 27Sept 2005].
- Murray, J.C., Neal, N.J., and Labrosse, F., (2001). Intelligent Kite Aerial Platform for Site Photography. Proceedings of the 3rd Annual IEEE Conference on Automation Science and Engineering Scottsdale, AZ, USA, Sept 22-25, 2007. 548-533. [online] Available from: <http://ieeexplore.ieee.org/stamp/stamp.jsp?arnumber=04341813>. [Accessed 22 Nov 2008]
- Nagai, M., Shibasaki, R., Manandhar, D., Zhao, H., (2004). Development of digital surface and feature extraction by integrating laser scanner and CCD sensor with IMU. International Archives of Photogrammetry and Remote Sensing, XXXV (Part B5). Istanbul. [online] Available from <http://www.isprs.org/congresses/istanbul2004/comm5/papers/655.pdf>. [Accessed 05 Nov 2008]
- NASA, (2006). National Aeronautics and Space Administration: Visible Earth. A catalog of NASA images and animations of our home planet. [online] Available from <http://visibleearth.nasa.gov> [Accessed 24 August 2011]

- Nasiri, S., (2000). A Critical Review of MEMS Gyroscopes Technology and Commercialization Status, 1–8. [online] Available from <http://www.docstoc.com/docs/2399336/A-Critical-Review-of-MEMSGyroscopesTechnology-and> [Accessed 05 Nov 2008].
- Neukum, G. (1999). The Airborne HRSC-A: Performance Results and Application Potential. Photogrammetric Week '99, D. Fritsch, D. Hobbie (Eds.), Wichmann, Heidelberg, pp. 83-88.
- Neumann, K.J., (2008). Trends For Digital Aerial Mapping Cameras. International Archives of Photogrammetry and Remote Sensing, XXXVII (Part B1). Beijing. [online] Available from http://www.isprs.org/proceedings/XXXVII/congress/1_pdf/93.pdf [Accessed 23 August 2011]
- Newhall, B., (1969). Airborne camera: The world from the air and outer space. New York: Hastings House, 144.
- Nikulainen, M., Hallikainen, M., Kempainen, M., Tauriainen, S., Taskinen, H., Roschier, M., Salminen, J., Valmu, H., and Lauha, M., (2002). The airborne remote sensing platform of the Helsinki University of Technology. [online]. Helsinki University of Technology, Laboratory of Space Technology. Available from: <http://www.space.tkk.fi/research/>; [Accessed 22 Nov 2008]
- Niu, X., Hassan, T., Ellum, C., and El-Sheimy, N., (2006). Directly Georeferencing Terrestrial Imagery using MEMS-based INS/GNSS Integrated Systems. Mobile Mapping, Shaping the Change, XXIII FIG Congress, October 8-13, 2006. Germany:Munich. 1-16.
- Paine, D.P., and Kiser, J.D., (2003). Aerial Photography and Image Interpretation. 2nd (ed.), USA: John Wiley and Sons Incorporation, 9.

- Pamadi, K.B., and Ohlmeyer, E.J., (2004). Assessment of GPS Guided Spining Projectile Using an Accelerometer-Only IMU. American Institute of Aeronautics and Astronautics Guidance, Navigation and Control Conference and Exhibition, 16-19 August 2004. Rhode Island: Providence. [online] Available from: http://pdf.aiaa.org/preview/CDReadyMGNC04_855/PV2004_4881.pdf. [Accessed 22 Nov 2008]
- Park, Sungsu, Tan, Chin-Woo., and Park, Joohyuk., (2005). A scheme for improving the performance of a gyroscope-free inertial measurement unit. *Sensors and Actuators . A Physical Volume* 121, Issue 2, 30 June 2005, 410-420.
- Petrie, G., (2002). Eyes in the Sky - Guide to the Current State-of-the-Art in Terrain Imagers & Imagery: Part I - Airborne Imagery", *GI News*, Vol. 2, No. 7, p. 36-47. [online] Available from [http://web.ges.gla.ac.uk/~gpetrie/petrie\(part1\).pdf](http://web.ges.gla.ac.uk/~gpetrie/petrie(part1).pdf) [Accessed 23 August 2011]
- Petrie, G., (2003). Airborne digital frame cameras, *GeoInformatics* 7(6), October/November 2003, 18-27.
- PhotoModeler, (2011). Users Manual. EOS Syrtems. [online]. Available from <http://www.photomodeler.com>. [Accessed 22 August 2011]
- Pidwirny, M. (2006). Introduction to Geographic Information Systems. *Fundamentals of Physical Geography*, 2nd Edition. [online]. Available from <http://www.physicalgeography.net/fundamentals/2e.html>. [Accessed 28 Oct 2008].
- Pinto, L., and Forlani, G., (2002). A Single Step Calibration Procedured for IMU/GPS in Aerial Photogrammetry. *Photogrammetric Computer Vision*. International Society for Photogrammetry and Remote Sensing, Commission

- III, Symposium 2002 September 9 - 13, 2002, Austria:Graz. B-210ff – B-214ff.
- Piwowar, J.M., (1993). Aerial Imaging from A Tethered Balloon. Proceedings, 16th Canadian Symposium on Remote Sensing, Sherbrooke PQ, June 1993, 185-188.
- Pooley, M., (2007). Personal Communication. Sky-farm Ltd. Oxford, United Kingdom.
- Read, R.E., and Graham, R., (2002). Manual Aerial Survey: Primary Data Acquisition. CRC Press/Whittles Publishing: USA.
- Reid, B., Lithopoulos, E., and Hutton, J., (1998). Position and Orientation System for Direct Georeferencing (POS/DG), Proceeding ION 54th, June 1-3. California: Denver. 445-449.
- REIGL, (2008). Laser Measurement Systems Company. [online] Available from: <http://www.reigl.com> [Accessed 17 Nov 2008].
- Remondino, F., and Fraser, C., (2006). Digital Camera Calibration Methods: Considerations and Comparisons. International Society for Photogrammetry and Remote Sensing, Commission V, Symposium 'Image Engineering and Vision Metrology', September 25 - 26, 2006, Dresden. 266-272.
- Ricoh, (2011). Geo Imaging: GPS-Ready Camera Captures Location Data with Your Images. [online] Available from <http://www.ricohdc.com> [Accessed 22 August 2011].
- Roberts, A., Sherwood, R.L., and Coburn, C., (2000). Low Cost Integrated Airborne Multispectral Remote Sensing. The International Archives of Photogrammetry and Remote Sensing, Vol.XXXIII (Part B2), Amsterdam, 455-460.

- Robson, S., and Shortis, M., (1998). Practical influences of geometric and radiometric image quality provided by different digital camera systems. *Photogrammetry Record*, 16 (92), 225–247.
- Roy, D.P., Devereux, B., Grainger, B., and White, S.J., (1997). Parametric Geometric Correction of Airborne Thematic Mapper Imagery. *International Journal of Remote Sensing*, 18(9). 1865-1887.
- Sanchez, R.D., (2004). Airborne Digital Sensor System and GPS Aided Inertial Technology for Direct Geopositioning in Rough Terrain, U.S. Geological Survey Open-File Report 04-151.
- Schinstock and Ham (2005). Development of UAV remote sensing for ecosystem research. Kansas state university, news letter. [online] Available from:<http://www.k-state.edu> [Accessed 28 November 2008].
- Schmitz, M., Wübbena, G., and Bagge, A., (2001). Benefit of Rigorous Modeling of GPS in Combined AT/GPS/IMU–Bundle Block Adjustment. Presented at OEEPE Workshop on Integrated Sensor Orientation, September 17th–18th, 2001, Hannover, Germany. [online] Available from: http://www.geopp.de/download/geopp_gip_oepe_p.pdf?PHPSESSID=d7bb2c7727114ed50103cb2f26f99cba. [Accessed 28 November 2008].
- Schwarz, K.P., (1995). Integrated Airborne Navigation System for Photogrammetry. In: Fritsch, D., and Hobbie, D., (eds), *Photogrammetry Week '95*. WichmannVerlag, Germany: Heidelberg. 139-153.
- Schwarz, K.P. and El-Sheimy, N. (1999). Future Positioning and Navigation Technologies. Study performed under the Scientific Services Agreement with Batelle, Columbus Division and Topographic Engineering Center, Fort Belvoir, VA, USA.

- Schwarz, K.P., and El-Sheimy, N., (2004). Mobile mapping systems - state of the art and future trends. *International Archives of Photogrammetry, Remote Sensing and Spatial Information Sciences*, 35(Part B). 1-10.
- Schwarz, K.P., Chapmann, M.A., Cannon, M.E., Gong, P. (1993): An integrated INS/GPS approach to the georeferencing of remotely sensed data, *PE&RS* (59) 11, 1667-1674.
- Schwieger, V., (2003). Using Handheld GPS Receivers for Precise Positioning. 2nd FIG Regional Conference, 2-5 December 2003. Morocco:Marrakech. [online] Available from: http://www.fig.net/pub/morocco/proceedings/TS12/TS12_1_schwieger.pdf [Accessed 28 November 2008].
- Seara, A., (2002). Comparison Between Direct Camera Orientation Measurement and Bundle Block Adjustment Determination. In: Heipke C., Jacobsen K., Wegmann H. (eds.), *Integrated Sensor Orientation. Proceedings of the OEEPE Workshop: Integrated Sensor Orientation*, Institute for Photogrammetry and Geoinformation, University of Hannover, Hannover, Germany, 261-267. [online] Available from: <http://topo.epfl.ch/documents/EuroSDR/heipke02.pdf>. [Accessed 28 November 2008]
- Searcy, S.W., (2003). Precision Farming: A new Approach to Crop Management. Texas Agricultural Extension Service, The Texas A&M University System, College Station, Texas. USA. [online] Available from: <http://txprecag.tamu.edu/content/pub/pf-ncm.pdf> [Accessed 05 April 2007]
- Shin, E.H., (2001). Accuracy Improvement of Low Cost INS/GPS for LandApplications, M.Sc. thesis, Department of Geomatics Engineering, University of Calgary, Canada [online]. Available from:

<http://www.geomatics.ucalgary.ca/research/publications/GradTheses.html>

[Accessed 28 November 2008].

Siebert, H., Wendisch, M., Conrath, T., Teichmann, U., and Heintzenberg, J., (2003).

A New Tethered Balloon-Borne Payload for Fine-Scale Observations in The Cloudy Boundary Layer. *Boundary-Layer Meteorology*, 106. 461-482.

Skaloud, J., (1999), Optimizing Georeferencing of Airborne Survey Systems by

INS/DGPS, Ph. D. Thesis, UCGE Report 20216 University of Calgary, Alberta, Canada. [online] Available from <http://www.geomatics.ucalgary.ca/research/publications/GradTheses.html> [Accessed 5 June 2005].

Skaloud, J., and Lichti, D., (2006). Rigorous Approach to Bore-sight Self-

Calibration in Airborne Laser Scanning. *International Society of Photogrammetry and Remote Sensing, Journal of Photogrammetry & Remote Sensing*, 61(1). 47-59.

Skaloud, J. and Schaer, P., (2003). Towards A More Rigorous Bore-sight Calibration,

International Society of Photogrammetry and Remote Sensing, International Workshop on Theory Technology and Realities of Inertial/GPS/Sensor Orientation, Spain:Castelldefels. [online]. Available from: http://www.isprs.org/commission1/theory_tech_realities/pdf/p01_s2.pdf. [Accessed 28 November 2008].

Sogbanmu, E., and Hodge J., (2003). Introducing 'High Fidelity Photography. Press

Centre at Fujifilm United Kingdom. Available from: <http://www.fujifilm.co.uk/> [Accessed 19 October 2010].

Space and Tech (2001). Navstar GPS: Summary. [online] Available from [http://www](http://www.spaceandtech.com/spacedata/constellation/navstar-gps_consum.shtml)

www.spaceandtech.com/spacedata/constellation/navstar-gps_consum.shtml.

[Accessed 24 August 2011]

- SPECIM, (2008). Homepage of the company SPECIM. [online] Available from <http://www.specim.fi/> [Accessed 17 November 2008].
- Stamnes, K., and Storvold, R., (1999). Development and deployment of a powered tethered balloon system SHEBA ice station for measurements of cloud micro-physical and radioactive properties , Proceedings of the 9th Atmospheric Radiation Measurement Science team meeting, San Antonio, March 22-26, 1999. [online] Available from <http://www.arm.gov/publications/proceedings/conf09/index.stm>. [Accessed 28 November 2008].
- Steitz, D., (2001). Nasa Awards Contract for New Remote Sensing Instrument Technology [online]. Available from http://findarticles.com/p/articles/mi_pasa/is_200108/ai3604170800 [Accessed 05 Nov 2008].
- Stombaugh, T.S., and Mueller, T.G., (2006). A Low-cost Remote Sensing Platform for Agriculture in Precision Agriculture: Development and Assessment of Integrated Practices for Kentucky Producers - Phase V. A Special Grants Program under Cooperative State Research, Education, and Extension Service (CSREES) of USDA, September 2003 to September 2006. Available from: http://www.bae.uky.edu/~precag/PrecisionAg/Development_and_Assessment/phase5/contents.htm [Accessed 05 November 2008].
- Storvold, R., H.A. Eide, P. Utley, K. Stamnes, G. Adalgeirsdottir, D. Lubin, T. Svendby, B.D. Zak, R.Moritz, P. Lawson, and J.A. Moore, (1998). Boundary-layer structure obtained with a tethered balloon system obtained with a satellite data acquisition system at the SHEBA ice camp, Proceedings of the 8thARM Science team meeting, Tucson, March 23-27, 1998, 733-

738.[online] Available from: <http://www.arm.gov/publications/proceedings/conf08/index.stm>. [Accessed 28 November 2008].

Swain, K.C., Jayasuriya, H.P.W. and Salokhe, V.M., (2007). Low-Altitude Remote Sensing with Unmanned Radio-Controlled Helicopter Platforms: A Potential Substitution to Satellite-Based Systems for Precision Agriculture Adoption Under Farming Conditions in Developing Countries. [online] Available from: <http://ecommons.cornell.edu/bitstream/1813/10678/1/InvitewOverviewSwainJayasuriyaSalokhe27Sept2007.pdf>. [Accessed 28 November 2008].

Talaya, J., Alamus, R., Bosch, E., Serra, A., Kornus, W., and Baron, A., (2004). Integration of A Terrestrial Laser Scanner with GPS/IMU Orientation Sensors. International Archives of Photogrammetry and Remote Sensing, XXXV (Part B5). Istanbul.

Tetracam (2010). Agriculture Camera User's Guide. [online] Available from <http://www.tetracam.com/pdf/ADC/ADCUserManual.pdf> [Accessed 23 August 2011].

Tortosa, D. (2010). Remote Sensing Course. Available from: <http://hosting.soonet.ca/eliris/remotesensing/bl130intro.htm> [Accessed 30 March 2010].

Toth, C.K., (2002). Sensor Integration in Airborne Mapping. IEEE Transactions on Instrumentation and Measurement, 51 (6), 1367-1373.

Trimble, (2007). Homepage of the company Trimble. [online] Available from: <http://www.trimble.com>. [Accessed 1 June 2006].

Videre Design, (2010). An international company in developing and supplying the vision and robotics market with high-quality stereo and monocular cameras,

- intelligent mobile robots, and stereo software [online]. Available from <http://www.videredesign.com/> [Accessed 27 July 2010].
- Vierling, L.A., Fersdahl, M., Chen, X., Li, Z., and Zimmerman, P., (2006). The Short Wave Aerostat-Mounted Imager (SWAMI): A novel platform for acquiring remotely sensed data from a tethered balloon. *Remote Sensing of Environment* 103 (2006) 255-264.
- Vooren, A.P., and Offermans, D.M.J., (1985). An Ultralight Aircraft for Low-Cost, Large-Scale Stereoscopic Aerial Photographs. *The Association for Tropical Biology and Conservation, Biotropica*, 17(1), 84-88.
- Wainwright, M., (2006). Kent loses its Garden of England title to North Yorkshire [online]. Available from: <http://www.guardian.co.uk/uk/2006/jun01/rural-affairs.travelnews>. [Accessed 1 June 2006].
- Warner, W.S., Graham, R.W., and Read, R.E., (1996). Small format aerial photography. American Society for Photogrammetry and Remote Sensing, Bethesda: Maryland.
- Wegmann, H., (2002). Image Orientation by Combined (A)AT with GPS and IMU. Percora 15, Land Satellite Information IV and International Society of Photogrammetry and Remote Sensing, Commission I, Conference, Proceedings. November, 2002, Colorado: Denver. Co, USA.
- Wegmann, H., Heipke, C., and Jacobsen, K., (2004). Direct sensor orientation based on GPS network solutions. *International Archives of Photogrammetry and Remote Sensing*, XXXV (Part B1), Istanbul, 153-158.
- Wood, G.A., Taylor, J.C., and Godwin, R.J., (2003). Calibration Methodology for Mapping Within-field Crop Variability using Remote Sensing. *Biosystems Engineering*, 84(4), 409-423.

- Wrotniak, J.A., (2004). Infrared photography with a Digital Camera. Quest, Summer and Fall issues 2004. [online]. Available from: <http://www.wrotniak.net/photo/infrared/#WHAT> [Accessed 1 June 2006].
- Yan, T.S, (2006). GNSS Data Protocols: Choice and Implementation. Symposium on GPS/GNSS (IGNSS2006). Australia: Surfers Paradise, 17-21 July, CD-ROM proceedings.
- Zhang, K., and Xiao, B., (2003). Current status of low-cost GPS and mobile mapping systems, Proceedings of the Malaysia Geoinformation and Surveying Conference, 9-10 April, Kuching, Malaysia.
- Zhou, J.Q., (2006). Simplified Analysis of IMU Sensor Corruptions on Existing Pendulation Control System For Ship-Mounted Crane. Master's Thesis, Aerospace and Ocean Engineering Department, Virginia Polytechnic Institute and State University, Blacksburg, VA, December 2006. Available from <http://homepage.mac.com/hanspeterschaub/work/masters.html> [Accessed 05 Nov 2008].

Appendix A: List of Available Sensors

List of available sensor for airborne remote sensing used.





Aston University

Illustration removed for copyright restrictions



Illustration removed for copyright restrictions

Source: <http://hydrolab.arsusda.gov/rsbasics/acknow.php>

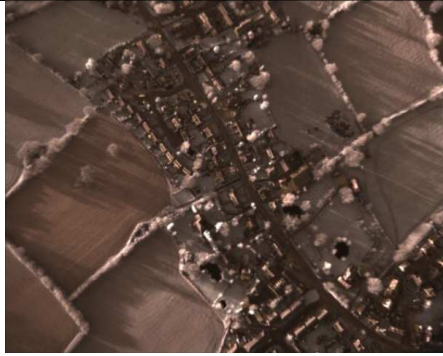
**Appendix B: Chronological History of Aerial Photography and
Remote Sensing**

Download from <http://www.geog.ussb.edu/~jeff/115a/remotesensinghistory.html>

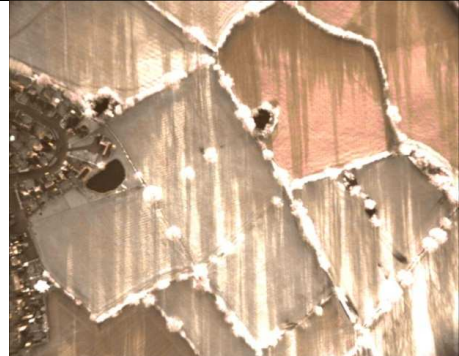
Last accessed 18/08/2011

Page removed for copyright restrictions.

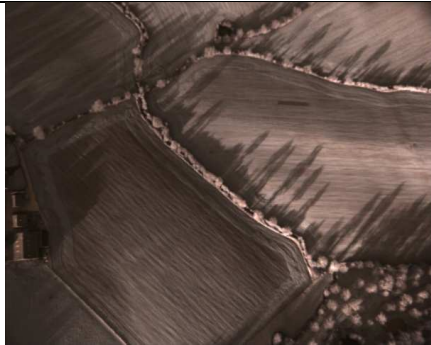
Appendix C: Image Captured



TTC_0893.DCM
February 7, 2008



TTC_0894.DCM
February 7, 2008



TTC_0895.DCM
February 7, 2008



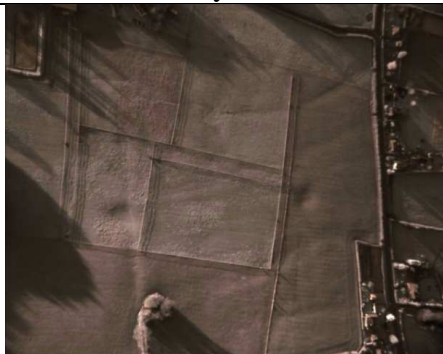
TTC_0896.DCM
February 7, 2008



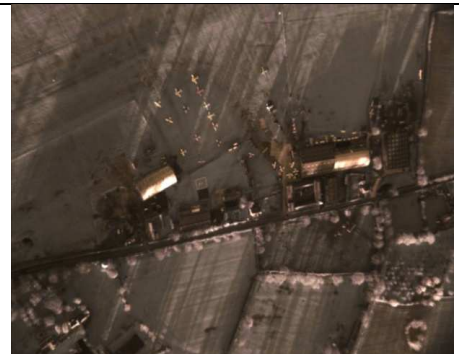
TTC_0897.DCM
February 7, 2008



TTC_0899.DCM
February 7, 2008



TTC_0900.DCM
February 7, 2008

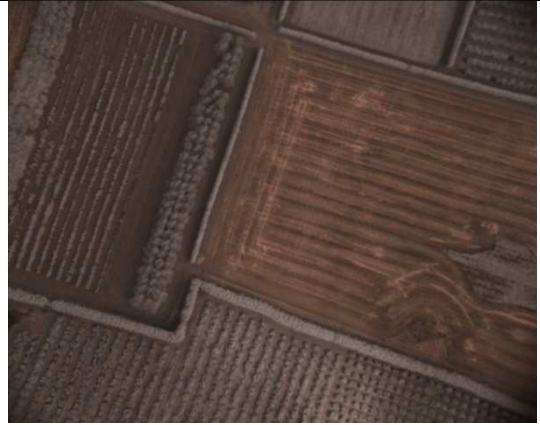


TTC_0905.DCM
February 7, 2008

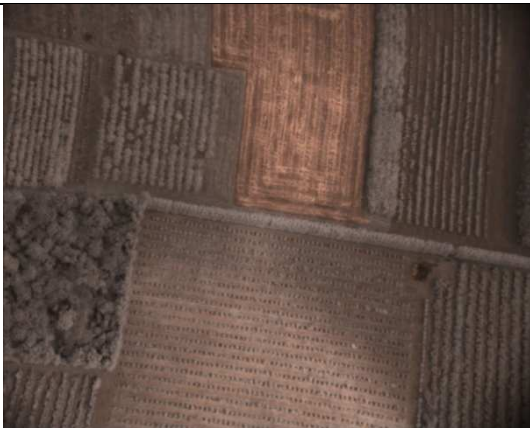
Note: All above data are unable to be corrected by using direct georeferencing method because the average height above mean sea level cannot be obtained.



TTC_0910.DCM
July 25, 2008
Unable to be corrected



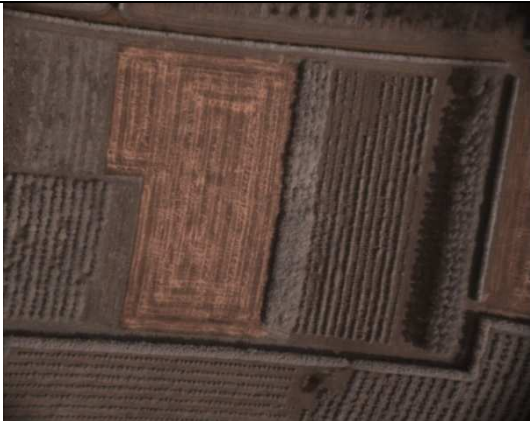
TTC_0911.DCM
July 25, 2008
Able to be corrected



TTC_0912.DCM
July 25, 2008
Unable to be corrected



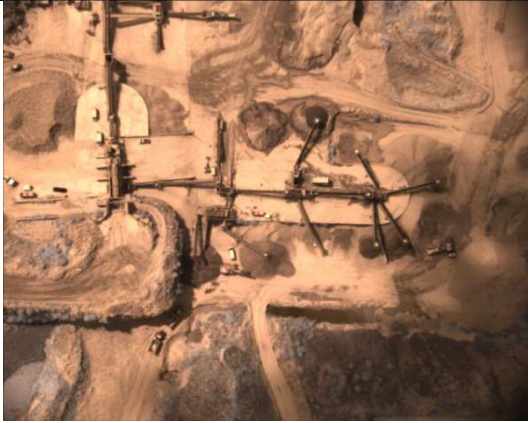
TTC_0913.DCM
July 25, 2008
Able to be corrected



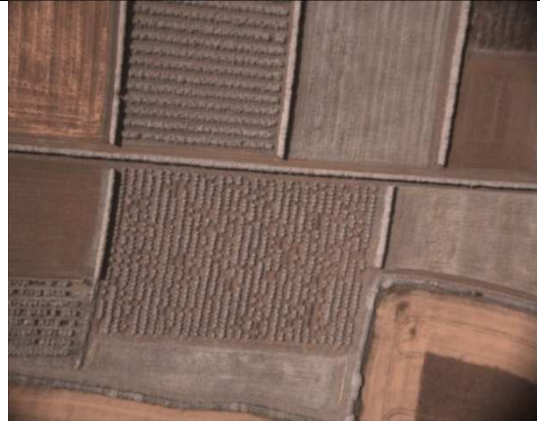
TTC_0914.DCM
July 25, 2008
Able to be corrected



TTC_0915.DCM
July 25, 2008
Able to be corrected



TTC_0916.DCM
July 25, 2008
Unable to be corrected



TTC_0917.DCM
July 25, 2008
Unable to be corrected



TTC_0918.DCM
July 25, 2008
Unable to be corrected



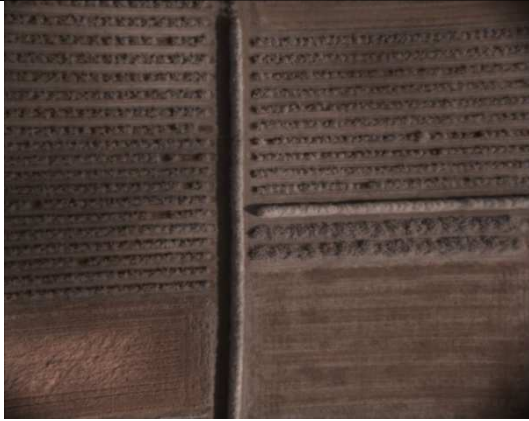
TTC_0919.DCM
July 25, 2008
Unable to be corrected



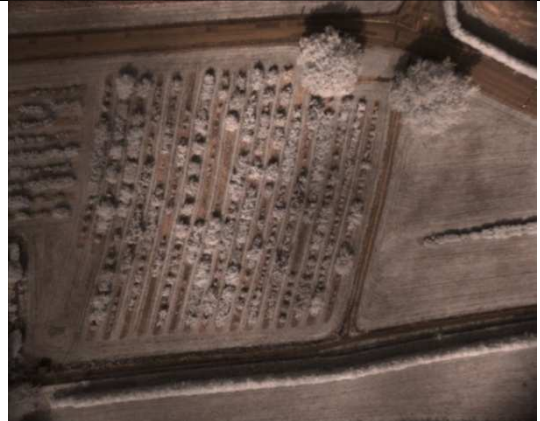
TTC_0920.DCM
July 25, 2008
Unable to be corrected



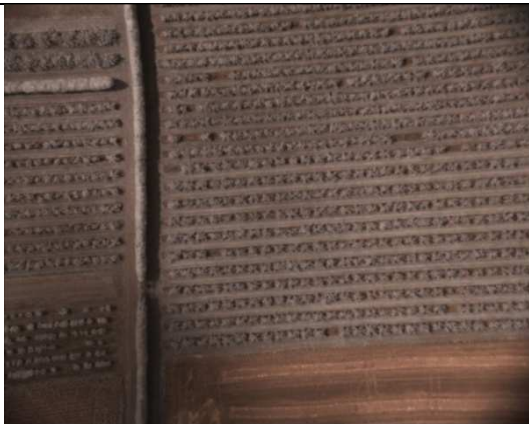
TTC_0921.DCM
July 25, 2008
Able to be corrected



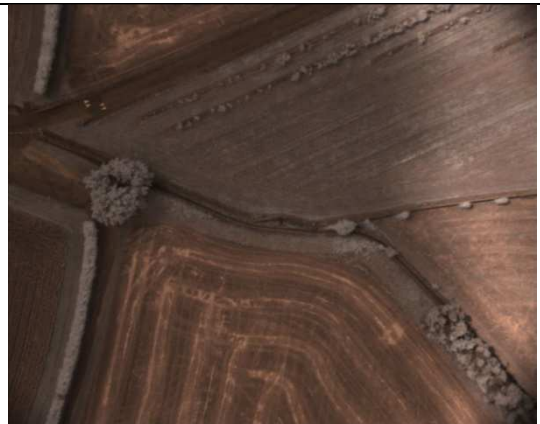
TTC_0922.DCM
July 25, 2008
Able to be corrected



TTC_0923.DCM
July 25, 2008
Unable to be corrected



TTC_0924.DCM
July 25, 2008
Able to be corrected



TTC_0925.DCM
July 25, 2008
Unable to be corrected

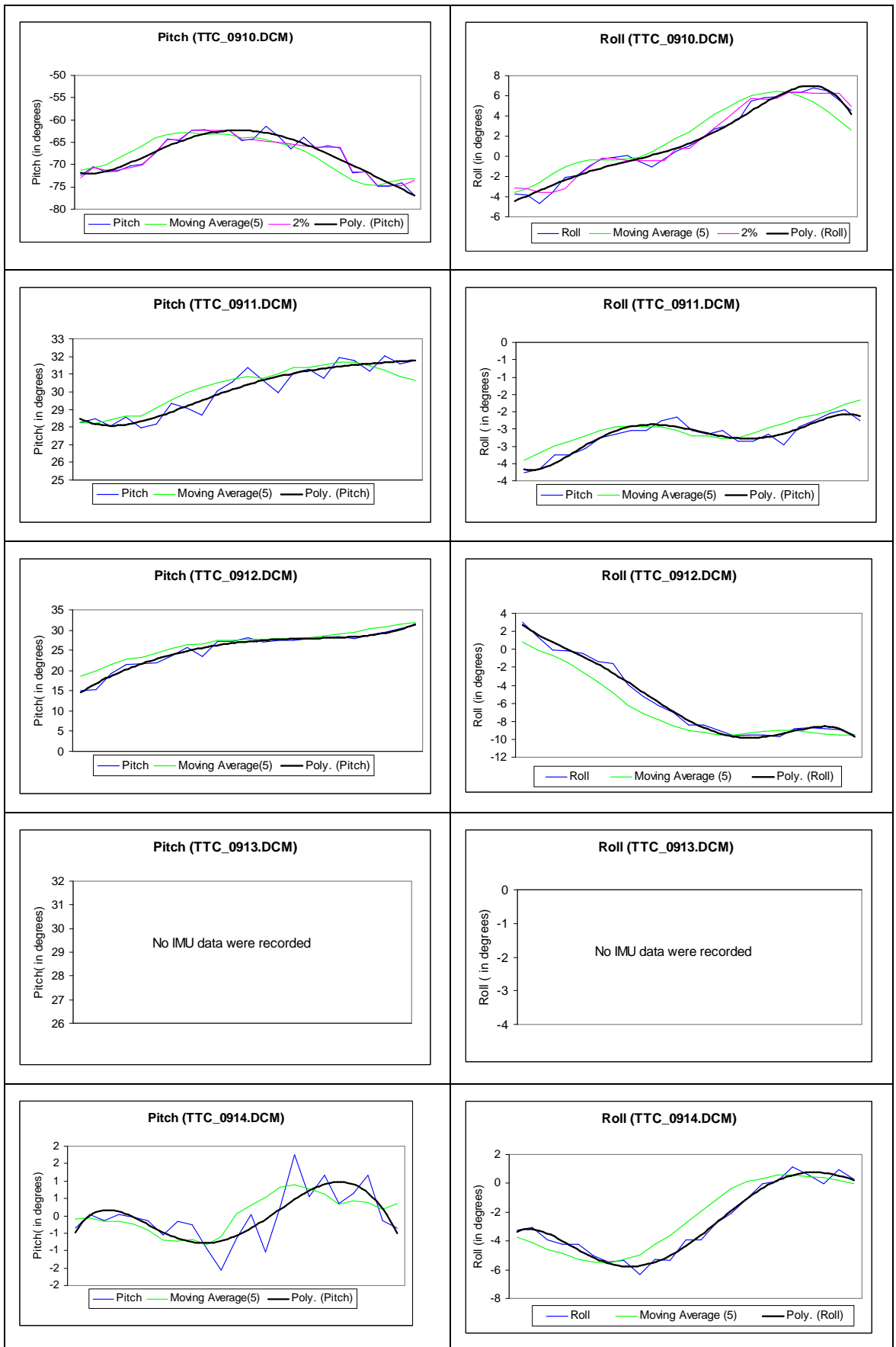


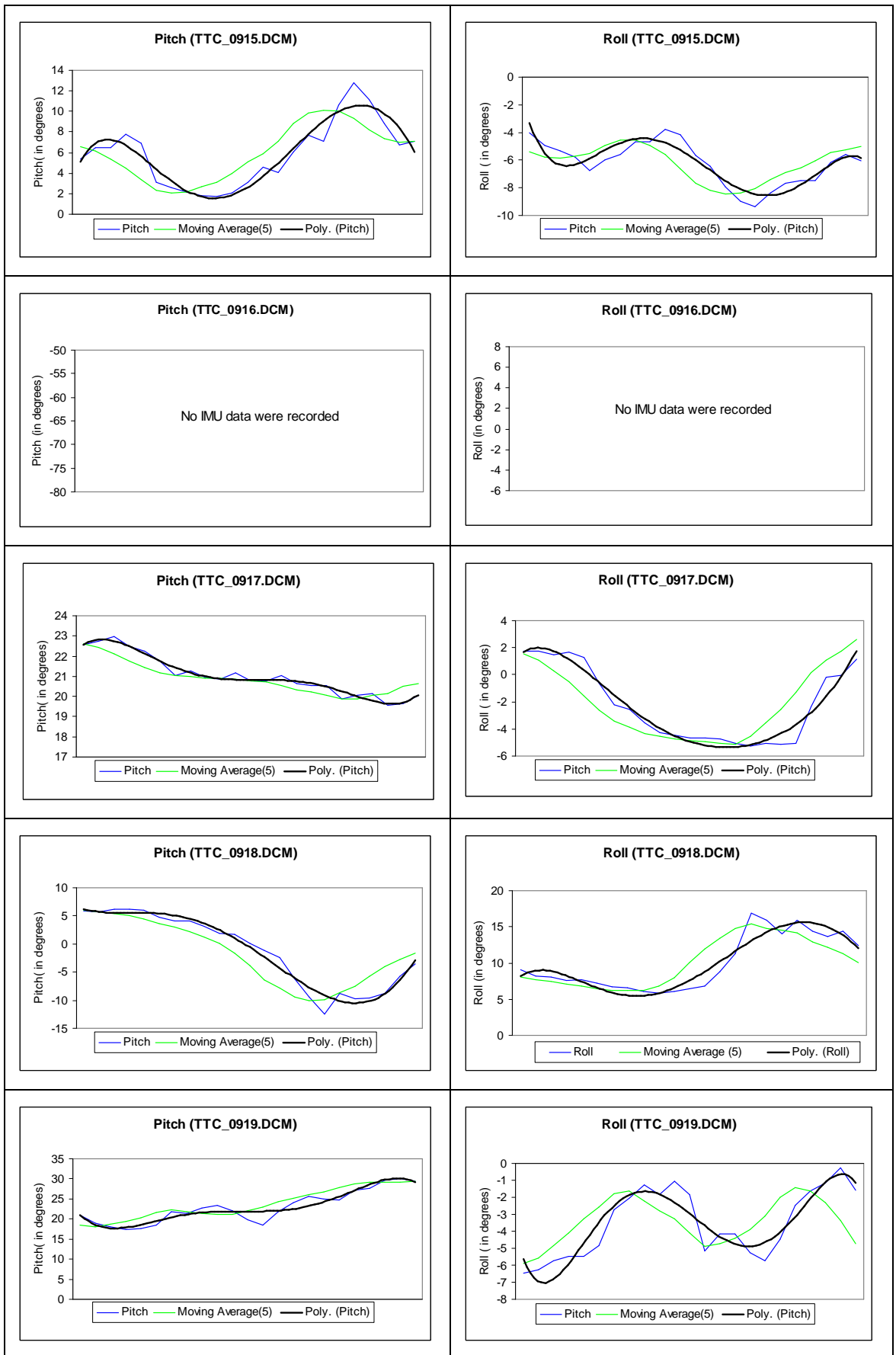
TTC_0926.DCM
July 25, 2008
Unable to be corrected

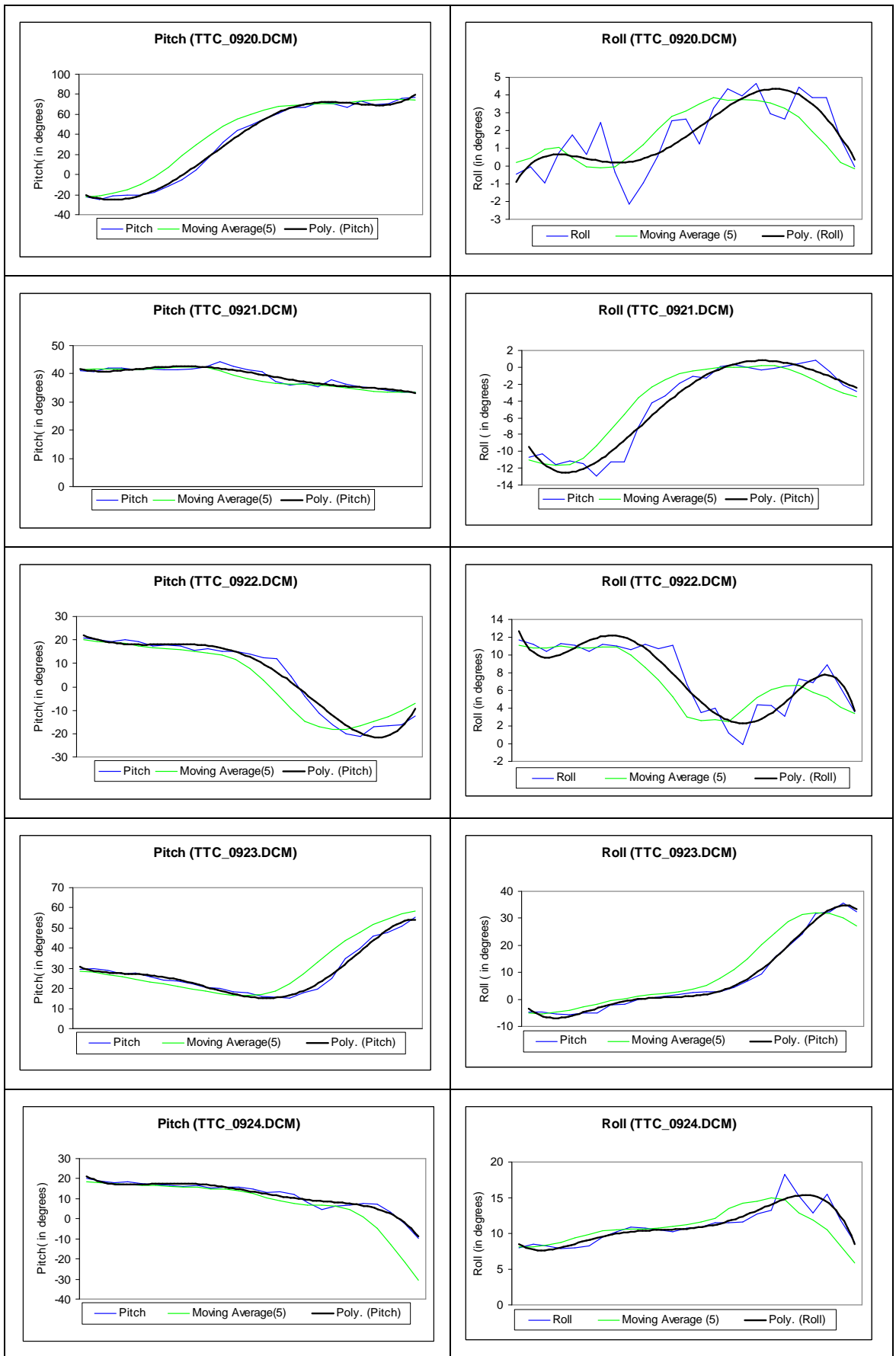
INTENDED BLANK

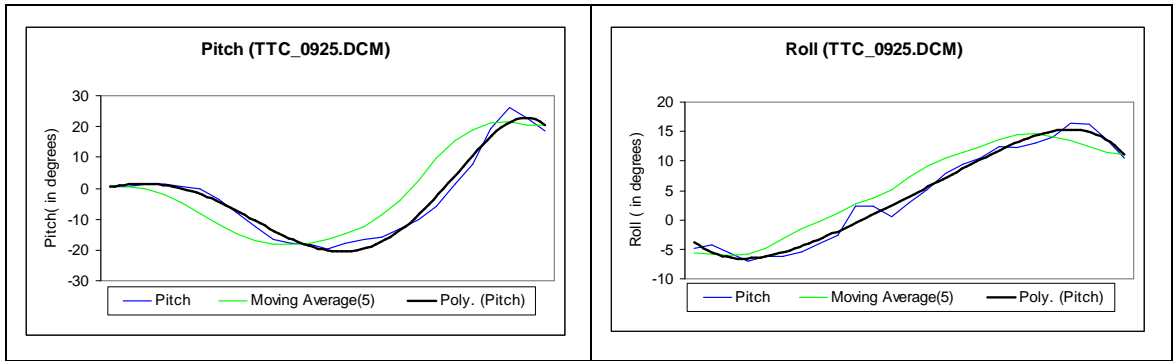
Note: The image that unable to be corrected is because of the IMU or GPS or bothe data were missing.

Appendix D: IMU Data (Process Data)



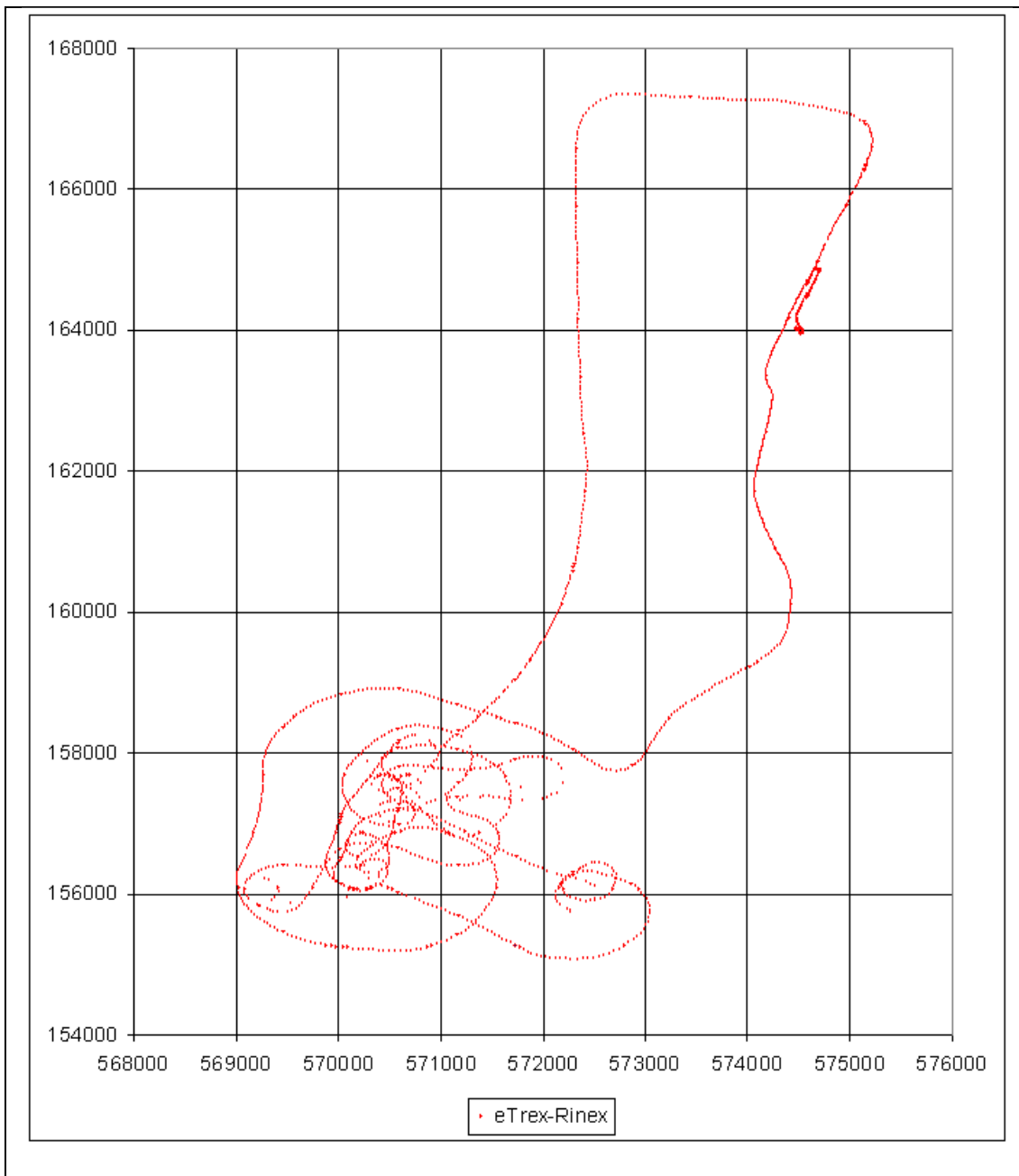






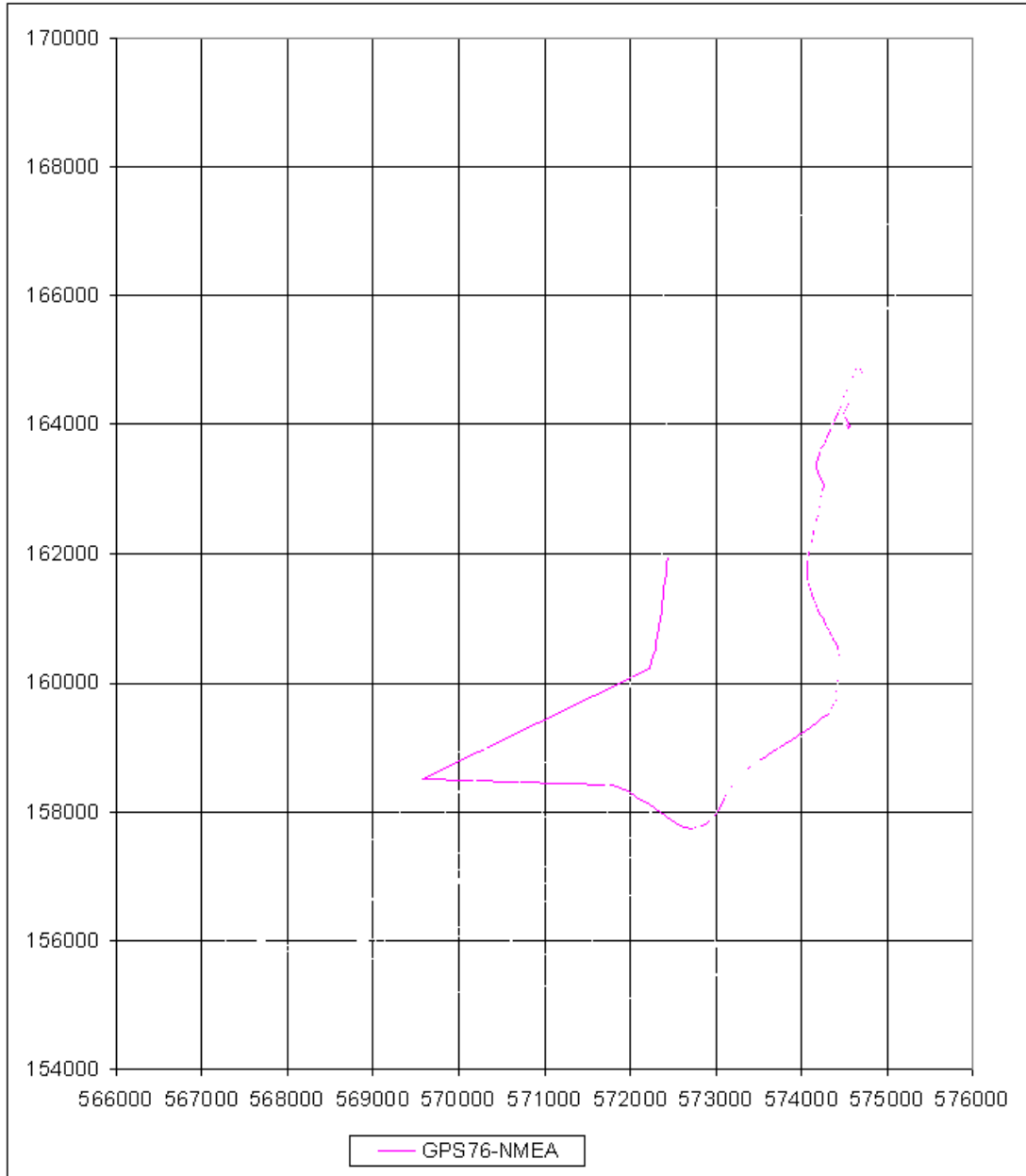
Appendix E: GPS DATA

Trajectory of flight test undertaken on July 25, 2008 using Garmin eTrex GPS.



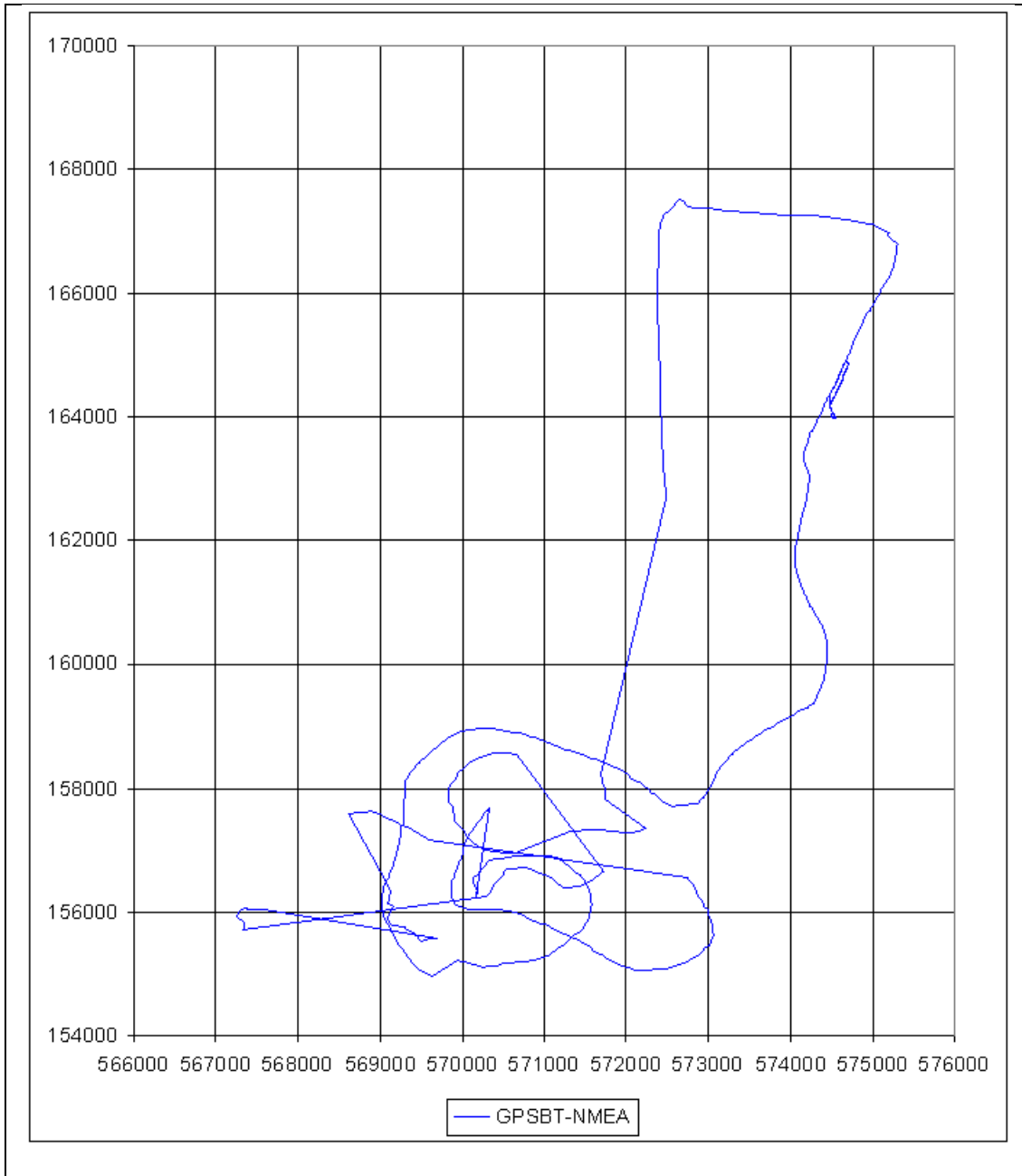
Note: The vertical axis is referring to the north direction while the horizontal axis is referred to the easting direction in OSGB36 (OSTN02) coordinates system.

Trajectory of flight test undertaken on July 25, 2008 using Garmin 76 GPS.



Note: The vertical axis is referring to the north direction while the horizontal axis is referred to the easting direction in OSGB36 (OSTN02) coordinates system.


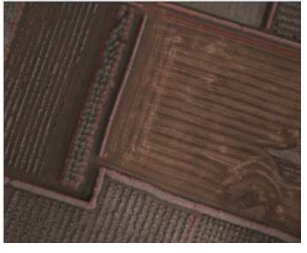


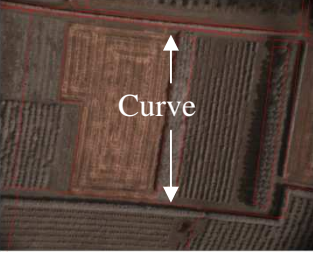
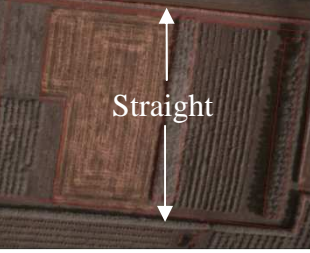




**Trajectory of flight test undertaken on July 25, 2008 using wireless bluetooth
GPS**



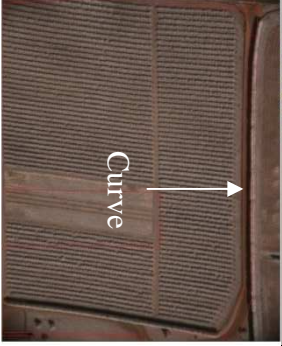




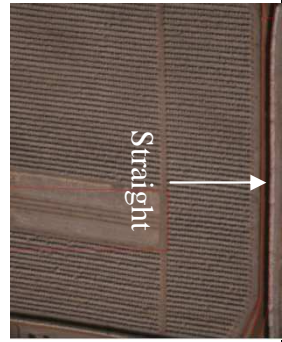
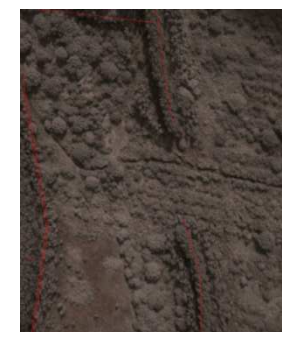


Note: The vertical axis is referring to the north direction while the horizontal axis is referred to the easting direction in OSGB36 (OSTN02) coordinates system.

Appendix F: Corrected Images

Pincushion Correction

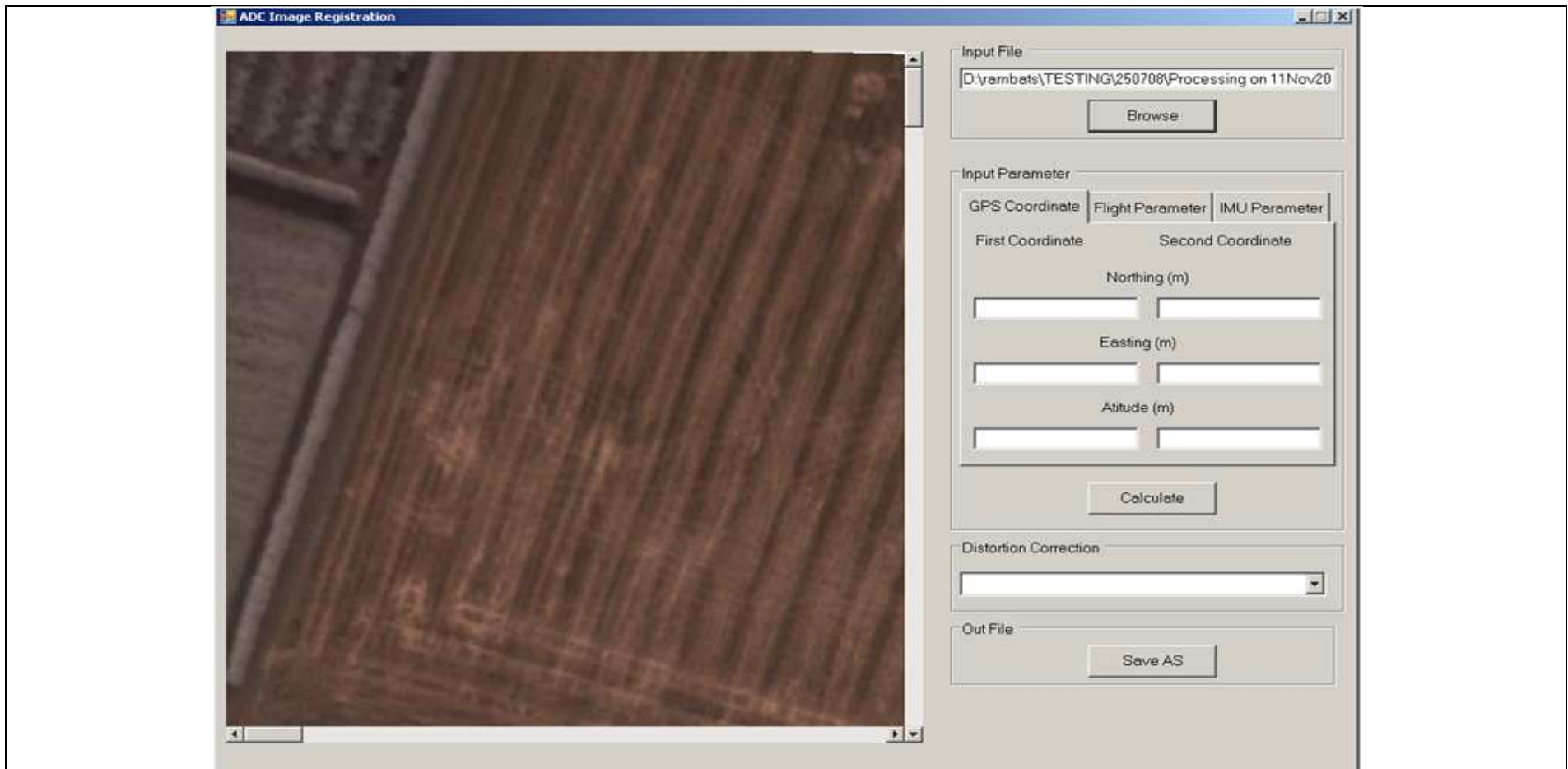
ID	BEFORE Original Image / Uncorrected	AFTER Pincushion (Corrected)
TTC_0911..DCM		
TTC_0912..DCM		
TTC_0914..DCM		
TTC_0915..DCM		
TTC_0917..DCM		

TTC_0927..DCM	TTC_0925..DCM	TTC_0922..DCM	TTC_0921..DCM	TTC_0918..DCM
				
				

Appendix G: Microsoft Visual Studio (Visual Basic)

Programming Scripts Listing

Snapshot of the user interface.



'NOTE: The following procedure is develop to assist the image
'correction process. The description of each programm script is given
'as comments. The image correction process includes:

```
' i -Pincushion Correction  
' ii -Tilt Correction  
' iii -Oblique Correction  
' iv -Rotation
```

```
Imports System  
Imports System.IO  
Imports System.Data  
Imports System.Windows.Forms  
Imports System.Drawing  
Imports System.Collections  
Imports System.Object  
Imports System.Array  
Imports System.Drawing.Drawing2D.Matrix  
Imports System.Drawing.Imaging.PixelFormat  
Imports System.Drawing.Point  
Imports System.Drawing.Drawing2D.GraphicsPath  
Imports System.Drawing.Imaging  
Imports System.Windows.Forms.Control  
Imports System.Windows.Forms.ScrollBar  
Imports System.Windows.Forms.HScrollBar  
Imports System.Windows.Forms.VScrollBar  
Imports System.Drawing.Color  
Imports System.Runtime.InteropServices  
Imports System.Math
```

```
PublicClass FrmMain  
Inherits System.Windows.Forms.Form  
#Region"Declaration"  
Public InFile AsString  
Public OutFile AsString  
Dim N1 AsDouble  
Dim N2 AsDouble  
Dim E1 AsDouble  
Dim E2 AsDouble  
Dim Z1 AsDouble  
Dim Z2 AsDouble  
Dim FL AsDouble  
Dim ALT AsDouble  
Dim MAXE AsDouble  
Dim MINE AsDouble  
Dim ROLL AsDouble  
Dim PITCH AsDouble  
Dim YAW AsDouble  
Dim HEAD AsDouble  
Dim Photo As Bitmap  
Dim PixelCOL AsInteger  
Dim PixelROW AsInteger  
Dim DotInch AsInteger  
Dim RRoll(2, 2) AsDouble  
Dim RPitch(2, 2) AsDouble  
Dim RYaw(2, 2) AsDouble  
Dim YAWDEG AsDouble  
Dim SC AsDouble
```

```

Dim ScanPara AsDouble
Dim NDist AsDouble
Dim RP(2, 2) AsDouble
Dim MM(2, 2) AsDouble
Dim HEADRAD AsDouble
'Dim YAWDEG As Double
Dim DEG AsDouble
Dim DIRECT AsDouble
#EndRegion
#Region"Windows Form Designer generated code "

PublicSubNew()
MyBase.New()

'This call is required by the Windows Form Designer.
    InitializeComponent()

'Add any initialization after the InitializeComponent() call

EndSub

'Form overrides dispose to clean up the component list.
ProtectedOverloadsOverridesSub Dispose(ByVal disposing AsBoolean)
If disposing Then
IfNot (components IsNothing) Then
        components.Dispose()
EndIf
EndIf
MyBase.Dispose(disposing)
EndSub

'Required by the Windows Form Designer
Private components As System.ComponentModel.IContainer

'NOTE: The following procedure is required by the Windows Form Designer
'It can be modified using the Windows Form Designer.
'Do not modify it using the code editor.
FriendWithEvents PictureBox As System.Windows.Forms.PictureBox
FriendWithEvents TabControll As System.Windows.Forms.TabControl
FriendWithEvents GroupBoxInputFile As System.Windows.Forms.GroupBox
FriendWithEvents GroupBoxIPara As System.Windows.Forms.GroupBox
FriendWithEvents TabGPS As System.Windows.Forms.TabPage
FriendWithEvents TabFlight As System.Windows.Forms.TabPage
FriendWithEvents TabImu As System.Windows.Forms.TabPage
FriendWithEvents Label3 As System.Windows.Forms.Label
FriendWithEvents Label2 As System.Windows.Forms.Label
FriendWithEvents Label11 As System.Windows.Forms.Label
FriendWithEvents Label14 As System.Windows.Forms.Label
FriendWithEvents Label15 As System.Windows.Forms.Label
FriendWithEvents BtnBrowse As System.Windows.Forms.Button
FriendWithEvents BtnCal As System.Windows.Forms.Button
FriendWithEvents Label16 As System.Windows.Forms.Label
FriendWithEvents Label17 As System.Windows.Forms.Label
FriendWithEvents Label18 As System.Windows.Forms.Label
FriendWithEvents Label19 As System.Windows.Forms.Label
FriendWithEvents Label110 As System.Windows.Forms.Label

```

```

FriendWithEvents Label11 As System.Windows.Forms.Label
FriendWithEvents Label12 As System.Windows.Forms.Label
FriendWithEvents GroupBox1 As System.Windows.Forms.GroupBox
FriendWithEvents hScrollBar1 As System.Windows.Forms.HScrollBar
FriendWithEvents vScrollBar1 As System.Windows.Forms.VScrollBar
FriendWithEvents TxtFile As System.Windows.Forms.TextBox
FriendWithEvents TxtN1 As System.Windows.Forms.TextBox
FriendWithEvents TxtE1 As System.Windows.Forms.TextBox
FriendWithEvents TxtZ1 As System.Windows.Forms.TextBox
FriendWithEvents TxtN2 As System.Windows.Forms.TextBox
FriendWithEvents TxtE2 As System.Windows.Forms.TextBox
FriendWithEvents TxtZ2 As System.Windows.Forms.TextBox
FriendWithEvents TxtMinE As System.Windows.Forms.TextBox
FriendWithEvents TxtMaxE As System.Windows.Forms.TextBox
FriendWithEvents TxtAlt As System.Windows.Forms.TextBox
FriendWithEvents TxtFL As System.Windows.Forms.TextBox
FriendWithEvents TxtHead As System.Windows.Forms.TextBox
FriendWithEvents TxtPitch As System.Windows.Forms.TextBox
FriendWithEvents TxtRoll As System.Windows.Forms.TextBox
FriendWithEvents ComboBox1 As System.Windows.Forms.ComboBox
FriendWithEvents GroupBox2 As System.Windows.Forms.GroupBox
FriendWithEvents BtnSaveAS As System.Windows.Forms.Button
<System.Diagnostics.DebuggerStepThrough(>>PrivateSub
InitializeComponent()
Me.PicImage = New System.Windows.Forms.PictureBox
Me.TxtFile = New System.Windows.Forms.TextBox
Me.BtnBrowse = New System.Windows.Forms.Button
Me.GroupBoxInputFile = New System.Windows.Forms.GroupBox
Me.GroupBoxIPara = New System.Windows.Forms.GroupBox
Me.BtnCal = New System.Windows.Forms.Button
Me.TabControl1 = New System.Windows.Forms.TabControl
Me.TabGPS = New System.Windows.Forms.TabPage
Me.Label5 = New System.Windows.Forms.Label
Me.Label4 = New System.Windows.Forms.Label
Me.Label11 = New System.Windows.Forms.Label
Me.Label2 = New System.Windows.Forms.Label
Me.TxtN1 = New System.Windows.Forms.TextBox
Me.Label3 = New System.Windows.Forms.Label
Me.TxtE1 = New System.Windows.Forms.TextBox
Me.TxtZ1 = New System.Windows.Forms.TextBox
Me.TxtN2 = New System.Windows.Forms.TextBox
Me.TxtE2 = New System.Windows.Forms.TextBox
Me.TxtZ2 = New System.Windows.Forms.TextBox
Me.TabFlight = New System.Windows.Forms.TabPage
Me.TxtMinE = New System.Windows.Forms.TextBox
Me.Label9 = New System.Windows.Forms.Label
Me.TxtMaxE = New System.Windows.Forms.TextBox
Me.Label8 = New System.Windows.Forms.Label
Me.TxtAlt = New System.Windows.Forms.TextBox
Me.Label7 = New System.Windows.Forms.Label
Me.TxtFL = New System.Windows.Forms.TextBox
Me.Label6 = New System.Windows.Forms.Label
Me.TabImu = New System.Windows.Forms.TabPage
Me.TxtHead = New System.Windows.Forms.TextBox
Me.TxtPitch = New System.Windows.Forms.TextBox
Me.Label12 = New System.Windows.Forms.Label
Me.Label11 = New System.Windows.Forms.Label

```

```

Me.TxtRoll = New System.Windows.Forms.TextBox
Me.Label10 = New System.Windows.Forms.Label
Me.GroupBox1 = New System.Windows.Forms.GroupBox
Me.BtnSaveAS = New System.Windows.Forms.Button
Me.hScrollBar1 = New System.Windows.Forms.HScrollBar
Me.vScrollBar1 = New System.Windows.Forms.VScrollBar
Me.ComboBox1 = New System.Windows.Forms.ComboBox
Me.GroupBox2 = New System.Windows.Forms.GroupBox
Me.GroupBoxInputFile.SuspendLayout()
Me.GroupBoxIPara.SuspendLayout()
Me.TabControll1.SuspendLayout()
Me.TabGPS.SuspendLayout()
Me.TabFlight.SuspendLayout()
Me.TabImu.SuspendLayout()
Me.GroupBox1.SuspendLayout()
Me.GroupBox2.SuspendLayout()
Me.SuspendLayout()
'
'PicImage
'
Me.PicImage.Location = New System.Drawing.Point(8, 24)
Me.PicImage.Name = "PicImage"
Me.PicImage.Size = New System.Drawing.Size(608, 680)
Me.PicImage.TabIndex = 0
Me.PicImage.TabStop = False
'
'TxtFile
'
Me.TxtFile.Font = New System.Drawing.Font("Microsoft Sans Serif",
9.75!, System.Drawing.FontStyle.Regular,
System.Drawing.GraphicsUnit.Point, CType(0, Byte))
Me.TxtFile.Location = New System.Drawing.Point(8, 24)
Me.TxtFile.Name = "TxtFile"
Me.TxtFile.Size = New System.Drawing.Size(328, 22)
Me.TxtFile.TabIndex = 1
Me.TxtFile.Text = ""
'
'BtnBrowse
'
Me.BtnBrowse.Location = New System.Drawing.Point(120, 56)
Me.BtnBrowse.Name = "BtnBrowse"
Me.BtnBrowse.Size = New System.Drawing.Size(112, 32)
Me.BtnBrowse.TabIndex = 3
Me.BtnBrowse.Text = "Browse"
'
'GroupBoxInputFile
'
Me.GroupBoxInputFile.Controls.Add(Me.TxtFile)
Me.GroupBoxInputFile.Controls.Add(Me.BtnBrowse)
Me.GroupBoxInputFile.Location = New System.Drawing.Point(640, 16)
Me.GroupBoxInputFile.Name = "GroupBoxInputFile"
Me.GroupBoxInputFile.Size = New System.Drawing.Size(344, 96)
Me.GroupBoxInputFile.TabIndex = 4
Me.GroupBoxInputFile.TabStop = False
Me.GroupBoxInputFile.Text = "Input File"
'
'GroupBoxIPara

```

```

'
Me.GroupBoxIPara.Controls.Add(Me.BtnCal)
Me.GroupBoxIPara.Controls.Add(Me.TabControll1)
Me.GroupBoxIPara.Location = New System.Drawing.Point(640, 136)
Me.GroupBoxIPara.Name = "GroupBoxIPara"
Me.GroupBoxIPara.Size = New System.Drawing.Size(344, 360)
Me.GroupBoxIPara.TabIndex = 5
Me.GroupBoxIPara.TabStop = False
Me.GroupBoxIPara.Text = "Input Parameter"
'
'BtnCal
'
Me.BtnCal.Location = New System.Drawing.Point(120, 312)
Me.BtnCal.Name = "BtnCal"
Me.BtnCal.Size = New System.Drawing.Size(112, 32)
Me.BtnCal.TabIndex = 1
Me.BtnCal.Text = "Calculate"
'
'TabControll1
'
Me.TabControll1.Controls.Add(Me.TabGPS)
Me.TabControll1.Controls.Add(Me.TabFlight)
Me.TabControll1.Controls.Add(Me.TabImu)
Me.TabControll1.ItemSize = New System.Drawing.Size(109, 30)
Me.TabControll1.Location = New System.Drawing.Point(8, 24)
Me.TabControll1.Multiline = True
Me.TabControll1.Name = "TabControll1"
Me.TabControll1.RightToLeft = System.Windows.Forms.RightToLeft.No
Me.TabControll1.SelectedIndex = 0
Me.TabControll1.Size = New System.Drawing.Size(328, 272)
Me.TabControll1.TabIndex = 0
Me.TabControll1.Tag = ""
'
'TabGPS
'
Me.TabGPS.Controls.Add(Me.Label5)
Me.TabGPS.Controls.Add(Me.Label4)
Me.TabGPS.Controls.Add(Me.Label1)
Me.TabGPS.Controls.Add(Me.Label2)
Me.TabGPS.Controls.Add(Me.TxtN1)
Me.TabGPS.Controls.Add(Me.Label3)
Me.TabGPS.Controls.Add(Me.TxtE1)
Me.TabGPS.Controls.Add(Me.TxtZ1)
Me.TabGPS.Controls.Add(Me.TxtN2)
Me.TabGPS.Controls.Add(Me.TxtE2)
Me.TabGPS.Controls.Add(Me.TxtZ2)
Me.TabGPS.Location = New System.Drawing.Point(4, 34)
Me.TabGPS.Name = "TabGPS"
Me.TabGPS.Size = New System.Drawing.Size(320, 234)
Me.TabGPS.TabIndex = 0
Me.TabGPS.Text = "GPS Coordinate"
'
'Label5
'
Me.Label5.Location = New System.Drawing.Point(168, 8)
Me.Label5.Name = "Label5"
Me.Label5.Size = New System.Drawing.Size(144, 24)

```

```

Me.Label5.TabIndex = 10
Me.Label5.Text = "Second Coordinate"
'
'Label4
'
Me.Label4.Location = New System.Drawing.Point(80, 168)
Me.Label4.Name = "Label4"
Me.Label4.Size = New System.Drawing.Size(144, 24)
Me.Label4.TabIndex = 9
Me.Label4.Text = "Atitude (m)"
Me.Label4.TextAlign = System.Drawing.ContentAlignment.MiddleCenter
'
'Label1
'
Me.Label1.Font = New System.Drawing.Font("Microsoft Sans Serif", 9.75!,
System.Drawing.FontStyle.Regular, System.Drawing.GraphicsUnit.Point,
CType(0, Byte))
Me.Label1.Location = New System.Drawing.Point(8, 8)
Me.Label1.Name = "Label1"
Me.Label1.Size = New System.Drawing.Size(144, 24)
Me.Label1.TabIndex = 6
Me.Label1.Text = "First Coordinate"
'
'Label2
'
Me.Label2.Font = New System.Drawing.Font("Microsoft Sans Serif", 9.75!,
System.Drawing.FontStyle.Regular, System.Drawing.GraphicsUnit.Point,
CType(0, Byte))
Me.Label2.Location = New System.Drawing.Point(88, 40)
Me.Label2.Name = "Label2"
Me.Label2.Size = New System.Drawing.Size(144, 24)
Me.Label2.TabIndex = 7
Me.Label2.Text = "Northing (m)"
Me.Label2.TextAlign = System.Drawing.ContentAlignment.MiddleCenter
'
'TxtN1
'
Me.TxtN1.Font = New System.Drawing.Font("Microsoft Sans Serif", 9.75!,
System.Drawing.FontStyle.Regular, System.Drawing.GraphicsUnit.Point,
CType(0, Byte))
Me.TxtN1.Location = New System.Drawing.Point(8, 72)
Me.TxtN1.Name = "TxtN1"
Me.TxtN1.Size = New System.Drawing.Size(144, 22)
Me.TxtN1.TabIndex = 0
Me.TxtN1.Text = ""
'
'Label3
'
Me.Label3.Font = New System.Drawing.Font("Microsoft Sans Serif", 9.75!,
System.Drawing.FontStyle.Regular, System.Drawing.GraphicsUnit.Point,
CType(0, Byte))
Me.Label3.Location = New System.Drawing.Point(80, 104)
Me.Label3.Name = "Label3"
Me.Label3.Size = New System.Drawing.Size(144, 24)
Me.Label3.TabIndex = 8
Me.Label3.Text = "Easting (m)"
Me.Label3.TextAlign = System.Drawing.ContentAlignment.MiddleCenter

```

```

'
'TxtE1
'
Me.TxtE1.Font = New System.Drawing.Font("Microsoft Sans Serif", 9.75!,
System.Drawing.FontStyle.Regular, System.Drawing.GraphicsUnit.Point,
CType(0, Byte))
Me.TxtE1.Location = New System.Drawing.Point(8, 136)
Me.TxtE1.Name = "TxtE1"
Me.TxtE1.Size = New System.Drawing.Size(144, 22)
Me.TxtE1.TabIndex = 1
Me.TxtE1.Text = ""
'
'TxtZ1
'
Me.TxtZ1.Font = New System.Drawing.Font("Microsoft Sans Serif", 9.75!,
System.Drawing.FontStyle.Regular, System.Drawing.GraphicsUnit.Point,
CType(0, Byte))
Me.TxtZ1.Location = New System.Drawing.Point(8, 200)
Me.TxtZ1.Name = "TxtZ1"
Me.TxtZ1.Size = New System.Drawing.Size(144, 22)
Me.TxtZ1.TabIndex = 2
Me.TxtZ1.Text = ""
'
'TxtN2
'
Me.TxtN2.Font = New System.Drawing.Font("Microsoft Sans Serif", 9.75!,
System.Drawing.FontStyle.Regular, System.Drawing.GraphicsUnit.Point,
CType(0, Byte))
Me.TxtN2.Location = New System.Drawing.Point(168, 72)
Me.TxtN2.Name = "TxtN2"
Me.TxtN2.Size = New System.Drawing.Size(144, 22)
Me.TxtN2.TabIndex = 3
Me.TxtN2.Text = ""
'
'TxtE2
'
Me.TxtE2.Font = New System.Drawing.Font("Microsoft Sans Serif", 9.75!,
System.Drawing.FontStyle.Regular, System.Drawing.GraphicsUnit.Point,
CType(0, Byte))
Me.TxtE2.Location = New System.Drawing.Point(168, 136)
Me.TxtE2.Name = "TxtE2"
Me.TxtE2.Size = New System.Drawing.Size(144, 22)
Me.TxtE2.TabIndex = 4
Me.TxtE2.Text = ""
'
'TxtZ2
'
Me.TxtZ2.Font = New System.Drawing.Font("Microsoft Sans Serif", 9.75!,
System.Drawing.FontStyle.Regular, System.Drawing.GraphicsUnit.Point,
CType(0, Byte))
Me.TxtZ2.Location = New System.Drawing.Point(168, 200)
Me.TxtZ2.Name = "TxtZ2"
Me.TxtZ2.Size = New System.Drawing.Size(144, 22)
Me.TxtZ2.TabIndex = 5
Me.TxtZ2.Text = ""
'
'TabFlight

```

```

'
Me.TabFlight.Controls.Add(Me.TxtMinE)
Me.TabFlight.Controls.Add(Me.Label9)
Me.TabFlight.Controls.Add(Me.TxtMaxE)
Me.TabFlight.Controls.Add(Me.Label8)
Me.TabFlight.Controls.Add(Me.TxtAlt)
Me.TabFlight.Controls.Add(Me.Label7)
Me.TabFlight.Controls.Add(Me.TxtFL)
Me.TabFlight.Controls.Add(Me.Label6)
Me.TabFlight.Location = New System.Drawing.Point(4, 34)
Me.TabFlight.Name = "TabFlight"
Me.TabFlight.Size = New System.Drawing.Size(320, 234)
Me.TabFlight.TabIndex = 1
Me.TabFlight.Text = "Flight Parameter"
'
'TxtMinE
'
Me.TxtMinE.Location = New System.Drawing.Point(176, 104)
Me.TxtMinE.Name = "TxtMinE"
Me.TxtMinE.Size = New System.Drawing.Size(136, 22)
Me.TxtMinE.TabIndex = 7
Me.TxtMinE.Text = ""
'
'Label9
'
Me.Label9.Location = New System.Drawing.Point(176, 72)
Me.Label9.Name = "Label9"
Me.Label9.Size = New System.Drawing.Size(136, 24)
Me.Label9.TabIndex = 6
Me.Label9.Text = "Min. Elevation (m)"
'
'TxtMaxE
'
Me.TxtMaxE.Location = New System.Drawing.Point(176, 40)
Me.TxtMaxE.Name = "TxtMaxE"
Me.TxtMaxE.Size = New System.Drawing.Size(136, 22)
Me.TxtMaxE.TabIndex = 5
Me.TxtMaxE.Text = ""
'
'Label8
'
Me.Label8.Location = New System.Drawing.Point(176, 8)
Me.Label8.Name = "Label8"
Me.Label8.Size = New System.Drawing.Size(120, 24)
Me.Label8.TabIndex = 4
Me.Label8.Text = "Max. Elevation (m)"
'
'TxtAlt
'
Me.TxtAlt.Location = New System.Drawing.Point(8, 104)
Me.TxtAlt.Name = "TxtAlt"
Me.TxtAlt.Size = New System.Drawing.Size(136, 22)
Me.TxtAlt.TabIndex = 3
Me.TxtAlt.Text = ""
'
'Label7
'

```



```

Me.Label7.Location = New System.Drawing.Point(8, 72)
Me.Label7.Name = "Label7"
Me.Label7.Size = New System.Drawing.Size(136, 24)
Me.Label7.TabIndex = 2
Me.Label7.Text = "Altitude (m)"
'
'TxtFL
'
Me.TxtFL.Location = New System.Drawing.Point(8, 40)
Me.TxtFL.Name = "TxtFL"
Me.TxtFL.Size = New System.Drawing.Size(136, 22)
Me.TxtFL.TabIndex = 1
Me.TxtFL.Text = ""
'
'Label6
'
Me.Label6.Location = New System.Drawing.Point(8, 8)
Me.Label6.Name = "Label6"
Me.Label6.Size = New System.Drawing.Size(120, 24)
Me.Label6.TabIndex = 0
Me.Label6.Text = "Focal Lenght (mm)"
'
'TabImu
'
Me.TabImu.Controls.Add(Me.TxtHead)
Me.TabImu.Controls.Add(Me.TxtPitch)
Me.TabImu.Controls.Add(Me.Label12)
Me.TabImu.Controls.Add(Me.Label11)
Me.TabImu.Controls.Add(Me.TxtRoll)
Me.TabImu.Controls.Add(Me.Label10)
Me.TabImu.Location = New System.Drawing.Point(4, 34)
Me.TabImu.Name = "TabImu"
Me.TabImu.Size = New System.Drawing.Size(320, 234)
Me.TabImu.TabIndex = 2
Me.TabImu.Text = "IMU Parameter"
'
'TxtHead
'
Me.TxtHead.Location = New System.Drawing.Point(8, 168)
Me.TxtHead.Name = "TxtHead"
Me.TxtHead.Size = New System.Drawing.Size(128, 22)
Me.TxtHead.TabIndex = 5
Me.TxtHead.Text = ""
'
'TxtPitch
'
Me.TxtPitch.Location = New System.Drawing.Point(8, 104)
Me.TxtPitch.Name = "TxtPitch"
Me.TxtPitch.Size = New System.Drawing.Size(128, 22)
Me.TxtPitch.TabIndex = 4
Me.TxtPitch.Text = ""
'
'Label12
'
Me.Label12.Location = New System.Drawing.Point(8, 136)
Me.Label12.Name = "Label12"
Me.Label12.Size = New System.Drawing.Size(128, 24)

```

```

Me.Label12.TabIndex = 3
Me.Label12.Text = "Heading (dd.mmss)"
'
'Label11
'
Me.Label11.Location = New System.Drawing.Point(8, 72)
Me.Label11.Name = "Label11"
Me.Label11.Size = New System.Drawing.Size(128, 24)
Me.Label11.TabIndex = 2
Me.Label11.Text = "Pitch (in degree)"
'
'TxtRoll
'
Me.TxtRoll.Location = New System.Drawing.Point(8, 40)
Me.TxtRoll.Name = "TxtRoll"
Me.TxtRoll.Size = New System.Drawing.Size(128, 22)
Me.TxtRoll.TabIndex = 1
Me.TxtRoll.Text = ""
'
'Label10
'
Me.Label10.Location = New System.Drawing.Point(8, 8)
Me.Label10.Name = "Label10"
Me.Label10.Size = New System.Drawing.Size(128, 24)
Me.Label10.TabIndex = 0
Me.Label10.Text = "Roll (in degree)"
'
'GroupBox1
'
Me.GroupBox1.Controls.Add(Me.BtnSaveAS)
Me.GroupBox1.Location = New System.Drawing.Point(640, 584)
Me.GroupBox1.Name = "GroupBox1"
Me.GroupBox1.Size = New System.Drawing.Size(336, 64)
Me.GroupBox1.TabIndex = 6
Me.GroupBox1.TabStop = False
Me.GroupBox1.Text = "Out File"
'
'BtnSaveAS
'
Me.BtnSaveAS.Location = New System.Drawing.Point(120, 24)
Me.BtnSaveAS.Name = "BtnSaveAS"
Me.BtnSaveAS.Size = New System.Drawing.Size(112, 32)
Me.BtnSaveAS.TabIndex = 1
Me.BtnSaveAS.Text = "Save AS"
'
'hScrollBar1
'
Me.hScrollBar1.Location = New System.Drawing.Point(0, 0)
Me.hScrollBar1.Name = "hScrollBar1"
Me.hScrollBar1.TabIndex = 0
'
'vScrollBar1
'
Me.vScrollBar1.Location = New System.Drawing.Point(0, 0)
Me.vScrollBar1.Name = "vScrollBar1"
Me.vScrollBar1.TabIndex = 0
'

```

```

'ComboBox1
'
Me.ComboBox1.DropDownStyle =
System.Windows.Forms.ComboBoxStyle.DropDownList
Me.ComboBox1.Items.AddRange(NewObject() {"Pincushion", "Vertical",
"Tilt", "Oblique", "Rotate", "Scale", "Scale1"})
Me.ComboBox1.Location = New System.Drawing.Point(8, 32)
Me.ComboBox1.Name = "ComboBox1"
Me.ComboBox1.Size = New System.Drawing.Size(320, 24)
Me.ComboBox1.TabIndex = 0
'
'GroupBox2
'
Me.GroupBox2.Controls.Add(Me.ComboBox1)
Me.GroupBox2.Location = New System.Drawing.Point(640, 504)
Me.GroupBox2.Name = "GroupBox2"
Me.GroupBox2.Size = New System.Drawing.Size(344, 72)
Me.GroupBox2.TabIndex = 8
Me.GroupBox2.TabStop = False
Me.GroupBox2.Text = "Distortion Correction"
'
'FrmMain
'
Me.AutoScaleBaseSize = New System.Drawing.Size(6, 15)
Me.AutoScroll = True
Me.ClientSize = New System.Drawing.Size(992, 734)
Me.Controls.Add(Me.GroupBox2)
Me.Controls.Add(Me.GroupBox1)
Me.Controls.Add(Me.GroupBoxIPara)
Me.Controls.Add(Me.GroupBoxInputFile)
Me.Controls.Add(Me.PicImage)
Me.Font = New System.Drawing.Font("Microsoft Sans Serif", 9.75!,
System.Drawing.FontStyle.Regular, System.Drawing.GraphicsUnit.Point,
CType(0, Byte))
Me.MaximizeBox = False
Me.Name = "FrmMain"
Me.Text = "ADC Image Registration"
Me.GroupBoxInputFile.ResumeLayout(False)
Me.GroupBoxIPara.ResumeLayout(False)
Me.TabControl1.ResumeLayout(False)
Me.TabGPS.ResumeLayout(False)
Me.TabFlight.ResumeLayout(False)
Me.TabImu.ResumeLayout(False)
Me.GroupBox1.ResumeLayout(False)
Me.GroupBox2.ResumeLayout(False)
Me.ResumeLayout(False)

EndSub

#EndRegion
#Region "Initialization"
Private m_operations As Collection
PrivateEnum WarpOperations
    Pincushion
    Vertical
    Tilt
    Oblique

```

```

        Rotate
        Scale
        Scale1
    EndEnum
    PrivateSub form1_load(ByVal sender As System.Object, ByVal e As
System.EventArgs) Handles MyBase.Load
        m_operations = New Collection
        m_operations.Add(WarpOperations.Pincushion, "Pincushion")
        m_operations.Add(WarpOperations.Vertical, "Vertical")
        m_operations.Add(WarpOperations.Tilt, "Tilt")
        m_operations.Add(WarpOperations.Oblique, "Oblique")
        m_operations.Add(WarpOperations.Rotate, "Rotate")
        m_operations.Add(WarpOperations.Scale, "Scale")
        m_operations.Add(WarpOperations.Scale1, "Scale1")
    EndSub
    #EndRegion
    #Region "Input Data"
    PublicSub Input_String()
    Dim N1_str AsString
    Dim N2_str AsString
    Dim E1_str AsString
    Dim E2_str AsString
    Dim Z1_str AsString
    Dim Z2_str AsString
    Dim ALT_str AsString
    Dim FL_str AsString
    Dim MAXE_str AsString
    Dim MINE_str AsString
    Dim Roll_str AsString
    Dim Pitch_str AsString
    Dim Head_str AsString
        InFile = Me.TxtFile.Text
        N1_str = Me.TxtN1.Text : E1_str = Me.TxtE1.Text : Z1_str =
Me.TxtZ1.Text
        N2_str = Me.TxtN2.Text : E2_str = Me.TxtE2.Text : Z2_str =
Me.TxtZ2.Text
        FL_str = Me.TxtFL.Text : ALT_str = Me.TxtAlt.Text : MAXE_str =
Me.TxtMaxE.Text : MINE_str = Me.TxtMinE.Text
        Roll_str = Me.TxtRoll.Text : Pitch_str = Me.TxtPitch.Text :
Head_str = Me.TxtHead.Text
    Try
        N1 = System.Convert.ToDouble(N1_str)
        N2 = System.Convert.ToDouble(N2_str)
        E1 = System.Convert.ToDouble(E1_str)
        E2 = System.Convert.ToDouble(E2_str)
        Z1 = System.Convert.ToDouble(Z1_str)
        Z2 = System.Convert.ToDouble(Z2_str)
        FL = System.Convert.ToDouble(FL_str)
        ALT = System.Convert.ToDouble(ALT_str)
        MAXE = System.Convert.ToDouble(MAXE_str)
        MINE = System.Convert.ToDouble(MINE_str)
        ROLL = System.Convert.ToDouble(Roll_str)
        PITCH = System.Convert.ToDouble(Pitch_str)
        HEAD = System.Convert.ToDouble(Head_str)
    Catch exception As System.OverflowException
        System.Console.WriteLine( _
"Overflow in String-to-Double conversion.")

```

```

Catch exception As System.FormatException
    System.Console.WriteLine( _
"The string is not formatted as a Double.")
Catch exception As System.ArgumentException
    System.Console.WriteLine("The string is null.")
EndTry

EndSub
#EndRegion
#Region "Grasp an Image & Image Info"
PrivateSub BtnBrowse_Click(ByVal sender As System.Object, ByVal e As
System.EventArgs) Handles BtnBrowse.Click
Dim dlgOpen AsNew OpenFileDialog
Dim Result AsInteger
    dlgOpen.Title = "Load Image"
    dlgOpen.Filter = "JPEG Files (*.jpg,*.jpeg)|*.jpg;*.jpeg|Bitmap
Files (*.bmp)|*.bmp"& _
"|PCX Files (*.pcx)|*.pcx|PNG Files (*.png)|*.png"& _
"|GIF Files (*.gif)|*.gif"& _
"|Wireless Bitmap Files (*.wbm, *.wbmp)|*.wbm;*.wbmp"& _
"|TIFF Files (*.tif, *.tiff)|*.tif;*.tiff"& _
"|All Image
Files|*.bmp;*.jpg;*.jpeg;*.pcx;*.png;*.gif;*.wbm;*.wbmp;*.tif;*.tiff"
    dlgOpen.FilterIndex = 9
    Result = dlgOpen.ShowDialog()
If Result <> DialogResult.Cancel Then
    InFile = dlgOpen.FileName
Me.TxtFile.Text = InFile
    Photo = Image.FromFile(InFile)
    PicImage.Image = CType(Photo, Image)
Me.DisplayScrollBars() 'ADD SCROLL BAR
Me.SetScrollBarValues() 'SET SCROLL BAR MOVEMENT
EndIf

    PixelCOL = Photo.Width
    PixelROW = Photo.Height
    DotInch = Photo.VerticalResolution
Dim PixCenRow AsDouble
Dim PixCenCol AsDouble
    PixCenRow = PixelROW / 2 : PixCenCol = PixelCOL / 2
Dim ScanPara AsDouble
    ScanPara = CType(DotInch, Double) / 0.0254
Dim NDist AsDouble
Dim SC AsDouble
    NDist = ScanPara / SC
EndSub
#EndRegion
#Region "Calculating Process"
PrivateSub BtnCal_Click(ByVal sender As System.Object, ByVal e As
System.EventArgs) Handles BtnCal.Click
'Setup-UP an Initail Value
    RRoll(0, 0) = ROLL / 180.0 * System.Math.PI
    RPitch(0, 0) = ROLL / 180.0 * System.Math.PI
    HEADRAD = DDMMSSSTORAD(HEAD) : DIRECT = BRG(N1, N2, E1, E2) :
RYaw(0, 0) = Math.Abs(DIRECT - HEAD)
    YAWDEG = RADTODEG(RYaw(0, 0))
'MsgBox(RRoll, , "RRoll")

```

```

'Matrix Preparation
'Dim SC As Double
Dim FL1 AsDouble
    FL1 = FL / 1000 : SC = 1 / (FL1 / ALT)
Dim CROLL(2, 2) AsDouble'defines a matrix ROLL with dimensions (3x3)
Dim CPITCH(2, 2) AsDouble'defines a matrix PITCH with dimensions (3x3)
Dim CYAW(2, 2) AsDouble'defines a matrix YAW with dimensions (3x3)
    CROLL(0, 0) = 1.0 : CROLL(0, 1) = 0.0 : CROLL(0, 2) = 0.0
    CROLL(1, 0) = 0.0 : CROLL(1, 1) = Math.Cos(RRoll(0, 0)) :
CROLL(1, 2) = Math.Sin(RRoll(0, 0))
    CROLL(2, 0) = 0.0 : CROLL(2, 1) = -1 * Math.Sin(RRoll(0, 0)) :
CROLL(2, 2) = Math.Cos(RRoll(0, 0))
    CPITCH(0, 0) = Math.Cos(RPitch(0, 0)) : CPITCH(0, 1) = 0.0 :
CPITCH(0, 2) = -1 * Math.Sin(RPitch(0, 0))
    CPITCH(1, 0) = 0.0 : CPITCH(1, 1) = 1.0 : CPITCH(1, 2) = 0.0
    CPITCH(2, 0) = Math.Sin(RPitch(0, 0)) : CPITCH(2, 1) = 0.0 :
CPITCH(2, 2) = Math.Cos(RPitch(0, 0))
    CYAW(0, 0) = Math.Cos(RYaw(0, 0)) : CYAW(0, 1) =
Math.Sin(RYaw(0, 0)) : CYAW(0, 2) = 0.0
    CYAW(1, 0) = -1 * Math.Sin(RYaw(0, 0)) : CYAW(1, 1) =
Math.Cos(RYaw(0, 0)) : CYAW(1, 2) = 0.0
    CYAW(2, 0) = 0.0 : CYAW(2, 1) = 0.0 : CYAW(2, 2) = 1.0
    RP = MatLib.Multiply(CROLL, CPITCH)
    MM = MatLib.Multiply(RP, CYAW)
    MsgBox(YAWDEG, , "YAW")
    MsgBox(SC, , "CALCULATE SCALE")
    MsgBox(MatLib.PrintMat(MM), , "Combination Matrix")
    MsgBox(PixelCOL & " x " & PixelROW, , "Col & Row")
    MsgBox(DotInch, , "DotPerInch")
    MsgBox(ScanPara, , "Scan Parameter")
    MsgBox(NDist, , "Nature Distance")

EndSub
#EndRegion
#Region"Transform Image"
PrivateSub ComboBox1_SelectedIndexChanged(ByVal sender As
System.Object, ByVal e As System.EventArgs) Handles
ComboBox1.SelectedIndexChanged
Me.Cursor = Cursors.WaitCursor
    Application.DoEvents()
'Select Distortion
Dim warp_op As WarpOperations =
DirectCast(m_operations(ComboBox1.Text), WarpOperations)
'Transform Image
Dim bm_src As Bitmap = DirectCast(PicImage.Image.Clone(), Bitmap)
Dim bm_dest AsNew Bitmap(PixelCOL, PixelROW)
    TransformImage(bm_src, bm_dest, warp_op)
'Display Result
    PicImage.Image = bm_dest
    bm_src.Dispose()
Me.Cursor = Cursors.Default
EndSub

#EndRegion
#Region"ScrollBars"
PrivateSub Form1_Resize(ByVal sender AsObject, ByVal e As
System.EventArgs) HandlesMyBase.Resize

```

```

' If the PictureBox has an image, see if it needs
' scrollbars and refresh the image.
IfNot (PicImage.Image IsNothing) Then
Me.DisplayScrollBars()
Me.SetScrollBarValues()
Me.Refresh()
EndIf
EndSub

PublicSub DisplayScrollBars()
' If the image is wider than the PictureBox, show the HScrollBar.
hScrollBar1.Dock = DockStyle.Bottom
vScrollBar1.Dock = DockStyle.Right
If PicImage.Width < PicImage.Image.Width Then
PicImage.Controls.Add(hScrollBar1)
EndIf
If PicImage.Height < PicImage.Image.Height Then
PicImage.Controls.Add(vScrollBar1)
EndIf
EndSub
PrivateSub HandleScroll(ByVal sender As [Object], ByVal se As
ScrollEventArgs) _
Handles vScrollBar1.Scroll, hScrollBar1.Scroll
' Create a graphics object and draw a portion
' of the image in the PictureBox.
Dim g As Graphics = PicImage.CreateGraphics()

g.DrawImage(PicImage.Image, New Rectangle(0, 0, PicImage.Right
- vScrollBar1.Width, _
PicImage.Bottom - hScrollBar1.Height), _
New Rectangle(hScrollBar1.Value, vScrollBar1.Value, PicImage.Right -
vScrollBar1.Width, _
PicImage.Bottom - hScrollBar1.Height), GraphicsUnit.Pixel)

PicImage.Update()
EndSub
PublicSub SetScrollBarValues()
' Set the Maximum, Minimum, LargeChange and SmallChange properties.
Me.vScrollBar1.Minimum = 0
Me.hScrollBar1.Minimum = 0

' If the offset does not make the Maximum less than zero, set its
value.
IfMe.PicImage.Image.Size.Width - PicImage.ClientSize.Width > 0 Then
Me.hScrollBar1.Maximum = Me.PicImage.Image.Size.Width - _
PicImage.ClientSize.Width
EndIf
' If the VScrollBar is visible, adjust the Maximum of the
' HScrollBar to account for the width of the VScrollBar.
IfMe.vScrollBar1.Visible Then
Me.hScrollBar1.Maximum += Me.vScrollBar1.Width
EndIf
Me.hScrollBar1.LargeChange = Me.hScrollBar1.Maximum / 10
Me.hScrollBar1.SmallChange = Me.hScrollBar1.Maximum / 20
' Adjust the Maximum value to make the raw Maximum value attainable by
user interaction.
Me.hScrollBar1.Maximum += Me.hScrollBar1.LargeChange

```

```

' If the offset does not make the Maximum less than zero, set its
value.
IfMe.PicImage.Image.Size.Height - PicImage.ClientSize.Height > 0 Then
Me.vScrollBar1.Maximum = Me.PicImage.Image.Size.Height - _
    PicImage.ClientSize.Height
EndIf
' If the HScrollBar is visible, adjust the Maximum of the
' VScrollBar to account for the width of the HScrollBar.
IfMe.hScrollBar1.Visible Then
Me.vScrollBar1.Maximum += Me.hScrollBar1.Height
EndIf
Me.vScrollBar1.LargeChange = Me.vScrollBar1.Maximum / 10
Me.vScrollBar1.SmallChange = Me.vScrollBar1.Maximum / 20
' Adjust the Maximum value to make the raw Maximum value attainable by
user interaction.
Me.vScrollBar1.Maximum += Me.vScrollBar1.LargeChange
EndSub
#EndRegion
#Region "Subroutine"
#Region "    SubTransform"
' Transform the image.
PrivateSub TransformImage(ByVal bm_src As Bitmap, ByVal _
    bm_dest As Bitmap, ByVal warp_op As WarpOperations)
' Find image information.
Dim xmid AsDouble = bm_dest.Width / 2
Dim ymid AsDouble = bm_dest.Height / 2
Dim rmax AsDouble = bm_dest.Width * 0.75

Dim ix_max AsInteger = bm_src.Width - 2
Dim iy_max AsInteger = bm_src.Height - 2

' Generate a result for each output pixel.
Dim x0 AsDouble
Dim y0 AsDouble
For y1 AsInteger = 0 To bm_dest.Height - 1
For x1 AsInteger = 0 To bm_dest.Width - 1
' Map back to the source image.
    MapPixel(warp_op, xmid, ymid, rmax, x1, y1, x0, y0)

' Interpolate to get the result pixel's value.
' Find the next smaller integral position.
Dim ix0 AsInteger = CInt(Int(x0))
Dim iy0 AsInteger = CInt(Int(y0))

' See if this is out of bounds.
If (ix0 < 0) Or (ix0 > ix_max) Or _
    (iy0 < 0) Or (iy0 > iy_max) Then
' The point is outside the image. Use white.
    bm_dest.SetPixel(x1, y1, Color.White)
Else
' The point lies within the image.
' Calculate its value.
Dim dx0 AsDouble = x0 - ix0
Dim dy0 AsDouble = y0 - iy0
Dim dx1 AsDouble = 1 - dx0
Dim dy1 AsDouble = 1 - dy0

```



```

' Get the colors of the surrounding pixels.
Dim color00 As Color = bm_src.GetPixel(ix0, _
    iy0)
Dim color01 As Color = bm_src.GetPixel(ix0, _
    iy0 + 1)
Dim color10 As Color = bm_src.GetPixel(ix0 _
    + 1, iy0)
Dim color11 As Color = bm_src.GetPixel(ix0 _
    + 1, iy0 + 1)

' Compute the weighted average.
Dim r AsInteger = CInt( _
    color00.R * dx1 * dy1 + color01.R * dx1 _
    * dy0 + _
    color10.R * dx0 * dy1 + color11.R * dx0 _
    * dy0 _
    )
Dim g AsInteger = CInt( _
    color00.G * dx1 * dy1 + color01.G * dx1 _
    * dy0 + _
    color10.G * dx0 * dy1 + color11.G * dx0 _
    * dy0 _
    )
Dim b AsInteger = CInt( _
    color00.B * dx1 * dy1 + color01.B * dx1 _
    * dy0 + _
    color10.B * dx0 * dy1 + color11.B * dx0 _
    * dy0 _
    )
    bm_dest.SetPixel(x1, y1, _
        Color.FromArgb(255, r, g, b))
EndIf
Next x1
Next y1
EndSub
#EndRegion
#Region "    SubMap Pixel"
' Map the output pixel (x1, y1) back to the input pixel
' (x0, y0).
PrivateSub MapPixel(ByVal warp_op As WarpOperations, ByVal _
    xmid AsDouble, ByVal ymid AsDouble, ByVal rmax As _
    Double, ByVal x1 AsInteger, ByVal y1 AsInteger, ByRef _
    x0 AsDouble, ByRef y0 AsDouble)
Dim dx AsDouble
Dim dy AsDouble
Dim r1 AsDouble
Dim r2 AsDouble
Dim theta AsDouble
Dim Rolla AsDouble
Dim Pitcha AsDouble
Dim H AsDouble = 11968.50394
Dim ymax AsDouble = PixelROW
'Dim dyG As Double
'Dim dxG As Double
'Dim kyG As Double
'Dim kxG As Double

```

'Oblique

Dim SD AsDouble = 368039.1267

'Process on 11/11/08, the input data

'Pitcha = -0.070831279 : Rolla = 0 '0.060650192'TTC_0911
'Pitcha = 0.063413629 : Rolla = 0 '-0.288779269'TTC_0913
'Pitcha = -0.08683013 : Rolla = 0.0 ' - 0.334303274'TTC_0914
'Pitcha = 0.12260938 : Rolla = 0 '.268198928 ' TTC_0915
'Pitcha = 0.217893449 : Rolla = 0 '-0.877191574
 Pitcha = 0.623955208 : Rolla = 0 '-0.097738438
'Pitcha = 0.146956723 : Rolla = 0 '0.026965337
'Pitcha = 1.27409 : Rolla=-0.05236
'Pitcha = 1.047198 : Rolla = -0.05236
'Pitcha = 0.645772 : Rolla = 0.0
'Pitcha = 0.366519 : Rolla = 0.069813
'Pitcha = 0.244346 : Rolla = 0.034907
'Pitcha = -0.244346 : Rolla = -0.401426
'Pitcha = -0.314159 : Rolla = -0.314159
'Pitcha = -0.366519 : Rolla = -0.244346
'Pitcha = -0.20944 : Rolla = -0.174533
'Pitcha = -0.10472 : Rolla = -0.087266
'Pitcha = -0.05236 : Rolla = 0.017453
'Pitcha = -0.15708 : Rolla = 0.017453
'Pitcha = -0.226893 : Rolla = 0.0
'Pitcha = 1.186824 : Rolla = 0.087266
'Pitcha = 1.169371 : Rolla = 0.05236
'Pitcha = 0.244346 : Rolla = -0.558505
'Pitcha = 0.122173 : Rolla = -0.610865
'Pitcha = 0.017453 : Rolla = -0.506145
'Pitcha = 0.017453 : Rolla = -0.383972
'Pitcha = 0.10472 : Rolla = 0.0
'Pitcha = 0.279253 : Rolla = 0.174533
'Pitcha = 0.122173 : Rolla = 0.226893
'Pitcha = 0.331613 : Rolla = 0.366519
'Pitcha = 0.820305 : Rolla = 0.15708
'Pitcha = 0.959931 : Rolla = 0.139626
'Pitcha = 0.383972 : Rolla = 0.10472
'Pitcha = 0.471239 : Rolla = 0.069813
'Pitcha = 0.349066 : Rolla = -0.017453
'Pitcha = 0.418879 : Rolla = -0.034907

Dim flenght AsDouble = 1270

'Dim kroll As Double

'Dim kpitch As Double

'Dim FY As Double

'Dim tx As Double

'Dim FX As Double

'Dim ty As Double

Dim k AsDouble

'Dim xx2 As Double

'Dim yy2 As Double

SelectCase warp_op

Case WarpOperations.Pincushion

 dx = x1 - xmid

 dy = y1 - ymid

 r1 = Sqrt((dx * dx + dy * dy) / 1500) '1000

If r1 = 0 Then

```

        x0 = xmid
        y0 = ymid
Else
        r2 = (rmax / 2 * (1 / (1 - r1 / rmax) - 1)) / 0.6
'Scale Image into: 683 x 783
        x0 = (dx * r2 / r1 + xmid)
        y0 = (dy * r2 / r1 + ymid)
EndIf
'*****
Case WarpOperations.Vertical
        x0 = x1 * Cos(Pitcha) + y1 * Sin(Pitcha)
        y0 = x1 * Sin(Rolla) + y1 * Cos(Rolla) + Sin(Rolla) *
Cos(Pitcha)

'*****
Case WarpOperations.Oblique
        dx = x1 - xmid 'current pixel position (x)
        dy = y1 - ymid 'current pixel position (y)

'Dim Flenght As Double = 2360.189 '2438.4
Dim LK AsDouble
        LK = SD / System.Math.Sin(Pitcha)
'MsgBox(LK, , "Lk")
Dim KPP AsDouble
        KPP = SD / System.Math.Tan(Pitcha)
'MsgBox(KPP, , "KPP")
Dim PPn AsDouble
        PPn = SD * System.Math.Tan(Pitcha)
'MsgBox(PPn, , "PPn")
Dim Kn AsDouble
        Kn = KPP + PPn
'MsgBox(Kn, , "Kn")
Dim VD AsDouble
Dim Lambda AsDouble
Dim KP AsDouble
Dim BETA1 AsDouble
Dim DELTAX AsDouble
If dy < 0 Then
        VD = PPn + Abs(dy)
Else
        VD = PPn - Abs(dy)
EndIf
        Lambda = Atan(dx / VD)
        KP = Kn * System.Math.Tan(Lambda)
        BETA1 = Atan(KP / LK)
        DELTAX = dy * System.Math.Tan(BETA1)
'##### For Y coordinate placement #####
Dim dyn AsDouble = xmid + PPn
Dim Ln AsDouble = Sqrt(flenght * flenght + PPn * PPn)
Dim m AsDouble = Atan(PPn / flenght)
Dim mprime AsDouble = Atan(dy / flenght)
Dim delm AsDouble = m - mprime
'Dim DELTAY As Double = VD * System.Math.Tan(Pitcha)
Dim dynew AsDouble = VD * System.Math.Tan(Pitcha) *
System.Math.Tan(delm)
Dim Hprime AsDouble = H / Sin(Pitcha)
Dim Fprime AsDouble = flenght / Sin(Pitcha)

```

```

Dim deltax AsDouble = dy * Cos(Pitcha)
'#####
'If dy >= 0 Then

        x0 = x1 + DELTAX
If dy = 0 Then
        y0 = y1
Else
        y0 = y1 * deltax / dy ' dyn - dynew + (dy ^ 2 *
Cos(Pitcha) ^ 2 / (147388 * SD))
EndIf

'Else
'    x0 = (x1 + DELTAX)
'    y0 = y1 'dyn - dynew + (dy * Cos(Pitcha) / (147388))
'End If

'*****
Case WarpOperations.Tilt
        dx = x1 - xmid
        dy = y1 - ymid
        r1 = Sqrt(dx * dx + dy * dy)
If r1 = 0 Then
        x0 = xmid
        y0 = ymid
Else
'Determine the radius if the image is horizontal
        r2 = Sqrt(((dy / Cos(Pitcha)) ^ 2) + ((dx /
Cos(Rolla)) ^ 2))

        k = r1 / r2
        theta = Atan(dy / dx) 'Determine the angle of the
radius

        x0 = x1 + (k * Cos(theta)) + (k * Sin(theta)) + (k
* Cos(Pitcha))
        y0 = y1 + (k * Cos(theta)) - (k * Sin(theta)) + (k
* Cos(Rolla))
EndIf
'*****
Case WarpOperations.Rotate

        dx = (x1 - xmid)
        dy = (y1 - ymid)
        r1 = Sqrt(dx * dx + dy * dy)
        theta = Atan(dy / dx)
Dim rangle AsDouble
        rangle = 1.570796327
If r1 = 0 Then
        x0 = xmid
        y0 = ymid
Else
        x0 = x1 + (r1 * Cos(theta + rangle)) 'Rotated by
Yaw Angle
        y0 = y1 + (r1 * Sin(theta + rangle)) 'obtained from
GPS

```

```

EndIf

'*****
Case WarpOperations.Scale
    dx = (x1 - xmid)
    dy = (y1 - ymid)
    r1 = Sqrt(dx * dx + dy * dy)
If x0 = 0 Then
    x0 = xmid
    y0 = ymid
Else
'ty = System.Math.Atan(dy / flenght)
'FY = dy / Sin(ty)
'tx = System.Math.Atan(dx / flenght)
'FX = dx / Cos(tx)
    x0 = x1 * 1
    y0 = y1 * 0.6
EndIf
'*****
Case WarpOperations.Scale1
    dx = x1 - xmid
    dy = y1 - ymid
Dim LOP AsDouble
Dim LOR AsDouble
    LOP = 512 * System.Math.Tan(Pitcha) 'L TO O FOR PITCH
    LOR = 640 * System.Math.Tan(Rolla) 'L TO O FOR ROLL
Dim LKP AsDouble
Dim LKR AsDouble
    LKP = Sqrt((LOP * LOP) + (512 * 512)) 'L TO K FOR PITCH
    LKR = Sqrt((LOR * LOR) + (640 * 640)) 'L TO K FOR ROLL
Dim KNP AsDouble
Dim KNR AsDouble
    KNP = LKP * System.Math.Acos(Pitcha) 'K TO N FOR PITCH
    KNR = LKR * System.Math.Acos(Rolla) 'K TO N FOR ROLL
Dim ONP AsDouble
Dim ONR AsDouble
    ONP = KNP - 512 'O TO N FOR PITCH
    ONR = KNR - 640 'O TO N FOR ROLL
Dim DXNEWP AsDouble
Dim DYNEWR AsDouble
If dy < 0 Then
    DXNEWP = KNP * (dx / (ONP - Abs(dy)))
Else
    DXNEWP = KNP * (dx / (ONP + Abs(dy)))
EndIf
If dx < 0 Then
    DYNEWR = KNR * (dy / (ONR - Abs(dx)))
Else
    DYNEWR = KNR * (dy / (ONR + Abs(dx)))
EndIf
    x0 = DXNEWP
    y0 = dy 'DYNEWR

EndSelect
EndSub
#EndRegion
#Region " SubCalculate Bearing"

```

```

PublicFunction BRG(ByVal N1 AsDouble, ByVal N2 AsDouble, ByVal E1
AsDouble, ByVal E2 AsDouble)
Dim LAT AsDouble
Dim DIP AsDouble
Dim SUD AsDouble
Dim BRG1 AsDouble
    LAT = N2 - N1                'Latitude
    DIP = E2 - E1                'Dipature
    SUD = Math.Atan2(LAT, DIP)   'Angle
If (LAT > 0 And DIP > 0) Then
    BRG1 = 90 - SUD
ElseIf (LAT < 0 And DIP > 0) Then
    BRG1 = 90 + SUD
ElseIf (LAT < 0 And DIP < 0) Then
    BRG1 = 270 - SUD
Else
    BRG1 = 270 + SUD
EndIf
Return BRG1
EndFunction
#EndRegion
#Region "    SubRadian"
Function DDMSSTORAD(ByVal HEAD AsDouble)
Dim DD AsInteger
Dim MM AsInteger
Dim SS AsInteger
Dim DEG AsDouble
Dim RAD AsDouble
    DD = CInt(HEAD)
    MM = CInt((HEAD - DD) * 100)
    SS = CInt((((HEAD - DD) * 100) - MM) * 100)
    DEG = (DD + (MM / 60) + (SS / 3600))
    RAD = DEG / 180.0 * System.Math.PI
Return RAD
EndFunction
#EndRegion
#Region "    SubDegree"
'To convert radians to degree, min, sec
Function RADTODEG(ByVal X AsDouble)
Dim DEG AsDouble
    DEG = X * 180.0 / System.Math.PI
Return DEG
EndFunction
#EndRegion
#Region "    Sub SaveAS"
PrivateSub BtnSaveAS_Click(ByVal sender As System.Object, ByVal e As
System.EventArgs) Handles BtnSaveAS.Click
' Displays a SaveFileDialog so the user can save the Image
' assigned to Button SaveAS.
Dim dlgSave AsNew SaveFileDialog
    dlgSave.Title = "SaveAS"
    dlgSave.Filter = "Jpeg Image|*.jpg|Bitmap Image|*.bmp|Gif
Image|*.gif|Tiff Image|*.tif"
    dlgSave.ShowDialog()
' If the file name is not an empty string open it for saving.
If dlgSave.FileName <> ""Then
' Saves the Image via a FileStream created by the OpenFile method.

```

```

Dim fs As System.IO.FileStream = CType _
    (dlgSave.OpenFile(), System.IO.FileStream)
' Saves the Image in the appropriate ImageFormat based upon the
' file type selected in the dialog box.
' NOTE that the FilterIndex property is one-based.
Dim bm AsNew Bitmap(PicImage.Image.Width, PicImage.Image.Height)
Dim gr As Graphics = Graphics.FromImage(bm)
    gr.DrawImage(PicImage.Image, 0, 0, bm.Width, bm.Height)

SelectCase dlgSave.FilterIndex
Case 1
    bm.Save(fs,
System.Drawing.Imaging.ImageFormat.Jpeg)

Case 2
    bm.Save(fs, _
        System.Drawing.Imaging.ImageFormat.Bmp)

Case 3
    bm.Save(fs, _
        System.Drawing.Imaging.ImageFormat.Gif)

Case 4
    bm.Save(fs, _
        System.Drawing.Imaging.ImageFormat.Tiff)

EndSelect

    fs.Close()

EndIf
EndSub
#EndRegion
#EndRegion
EndClass

```